UNIVERSIDADE D
COIMBRA

Marco Calzà

Buracos negros primordiais como laboratórios para nova física

Tese no âmbito do Doutoramento em Física, Física Nuclear e das Partículas orientada pelo Professor Doutor João Pedro Trancoso Gomes Rosa e apresentada ao Departamento de Física da Faculdade de Ciências e Tecnologia da Universidade de Coimbra.

Janeiro de 2024

Faculty of Sciences and Technology,
University of Coimbra

UNIVERSIDADE D
COIMBRA

Marco Calzà

Primordial Black Holes as Laboratories for New Physics

January 2024

A quelle creature che come lo spaziotempo,
piú profonda, irrimediabile e distruttiva é la vertigine,
piú sanno splendere!

Abstract

We show that light Primordial Black Holes (PBHs) develop non-negligible spins through Hawking emission of a large number of Axion-Like Particles (ALPs) (typically referred to as the axiverse and predicted in string theory compactifications) and their spin distributions could be measured by future gamma-ray observatories yielding a probe of the total number of light scalars in the fundamental theory, which is independent of how these interact with Standard Model (SM) particles.
In this scenario, we show also that a heavy axion may trigger superradiant instabilities, and study the coupled dynamics of superradiance and evaporation finding that the BH mass-spin distribution should follow the superradiance threshold condition if a superradiant cloud forms. Furthermore, we show that the decay of the heavy axions within the superradiant cloud into photon pairs may lead to a distinctive line in the black hole's emission spectrum.
Motivated by the string axiverse scenario, we propose three distance-independent methods to infer the mass and the spin of PBHs. Namely, for energies tested in colliders, we propose methods suitable in the case of low Black Hole (BH) spin ($0 \lesssim \tilde{a} \lesssim 0.5$) and one for high BH spin ($\tilde{a} \gtrsim 0.6$) and based on the energy of specific features of the photon Hawking spectrum. The third method extends the possibility of measuring the mass and the spin of PBHs to temperatures typical of Beyond the Standard Model (BSM) physics and is independent of the interaction of the new physics with the SM since it relies on a multi-messenger approach where the primary emitted photons and neutrinos are simultaneously measured. In this context, we also show how the evolution of a PBH reveals information about the underlying theory of particle physics, namely the particle content of the theory at a characteristic energy.
Finally, we study a regular rotating BH, described by the Kerr-black-bounce metric, evaporating under the Hawking emission of a single scalar field, and

compare the results with a Kerr black hole evaporating under the same conditions. We show how the combined contributions of the changes in the Gray-Body Factors (GBFs), the surface gravity and therefore the temperature affect the lifetime, evolution, and primary scalar emission of the Kerr black bounce. We also briefly comment on the possibility of investigating the beyond-the-horizon structure of a black hole by exploiting its Hawking emission.

Keywords: primordial black holes; Hawking evaporation; superradiant instabilities; beyond the standard model of particle physics

Resumo

Nesta tese mostramos que os buracos negros primordiais leves desenvolvem valores substanciais de spin através da emissão por efeito de Hawking de um grande número de espécies de axiões (conjunto conhecido como o "axiverso" e previsto pela teoria de cordas) e que a sua distribuição em termos de valores de spin poderá ser medida por futuros telescópios de raios-gama, constituindo uma forma de testar o número de partículas escalares leves na teoria fundamental, que é independente da forma como estas interagem com as partículas do Modelo Padrão. Neste cenário, demonstramos também que um axião pesado pode desencadear uma instabilidade superradiante, e estudamos a dinâmica acoplada da superradiância e da evaporação, concluindo que a distribuição de massa e spin dos buracos negros deve seguir o limite da condição de superradiância caso ocorra a formação de nuvens superradiantes. Para além disso, mostramos que o decaimento dos axiões pesados numa nuvem superradiante em pares de fotões origina uma linha característica no espectro de emissão de um buraco negro. Motivados pelo cenário do axiverso da teoria de cordas, propomos três métodos independentes da distância para determinar a massa e o spin de buracos negros primordiais. Em particular, para energias já testadas em aceleradores propomos métodos apropriados aos regimes de baixo spin ($0<\sim<0.5$) e de spin elevado (ã>0.6) e baseados na energia de características específicas do espectro de emissão de Hawking electromagnético. O terceiro médodo estende a possibilidade de medir a massa e o spin de buracos negros primordiais a temperaturas típicas da física para além do Modelo Padrão. Este método é independente das possíveis interações entre as novas partículas e as partículas conhecidas uma vez que é baseado numa abordagem multi-mensageiro, em que os espectros primários de fotões e neutrinos são medidos em simultâneo. Neste contexto, mostramos igualmente como a evolução de um buraco negro primordial pode revelar informação sobre

a física de partículas subjacente, nomeadamente o conteúdo de partículas da teoria em cada escala de massa. Finalmente, estudamos um buraco negro regular em rotação, descrito pela métrica de um "Kerr black-bounce", evaporando através da emissão de Hawking de um único campo escalar, comparando com os resultados obtidos para um buraco negro de Kerr nas mesmas condições. Mostramos como a combinação das alterações nos factores de "corpo cinzento", na gravidade superficial e, portanto, na temperatura influenciam o tempo de vida, a evolução e o espectro de emissão escalar primário do Kerr black-bounce. Também discutimos brevemente a possibilidade de investigar a estrutura para além do horizonte de um buraco negro através da exploração do seu espectro de emissão de Hawking.

Palavras-chave: buracos negros primordiais; evaporação de Hawking; instabilidade superradiante; física de partículas para além do modelo padrão;

Contents

1 Introduction **1**

2 Notions of QFT in curved spacetime **5**

2.1 Quantum fields and curved spacetime 5

2.2 Examples of generally covariant field equations 7

3 The tetrad formalism **9**

3.1 The importance of tetrad in curved spacetime 10

3.2 A more formal introduction to tetrad formalism 15

3.3 Dirac Equation in curved spacetime 21

3.4 The spin tetrads 24

3.5 The Newman-Penrose tetrad 26

4 Perturbations of the Kerr metric **29**

4.1 The Newman-Penrose formalism 29

4.2 Explicit example: the electromagnetic perturbation (s=1) . . . 33

4.3 General case: The Teukolsky equation 36

4.3.1 Numerical computation of gray-body factors 41

5 Hawking radiation **45**

5.1 The Bogoliubov transformations 46

5.2 The Unruh effect 48

5.3 The Hawking effect 50

5.4 Black hole emission spectra 52

5.4.1 Black Hole primary emission 52

5.4.2 Black Hole secondary emission 53

5.5 BH evaporation 56

5.5.1 Standard Evolution Scenario 61

5.6 BH superradiance 62
5.6.1 Basics of black hole superradiance 66

6 A look at Beyond the Standard Model physics 73
6.1 SUperSYmmetric (SUSY) extensions of the SM 74
6.2 Kaluza-Klein (KK) theories 77
6.3 QCD Axion 83
6.4 The Axiverse: Axion-Like Particles 88
6.5 Hidden Sector 89

7 Evaporating PBHs, the string axiverse, and hot dark radiation 91
7.1 Introduction 91
7.2 PBHs evaporation in the Axiverse 93
7.3 The hot dark radiation 96
7.4 Detectability 97
7.5 Conclusions 99

8 Superradiance, Hawking evaporation, and the string axiverse 101
8.1 Introduction 101
8.2 Superradiant instabilities for evaporating PBHs 103
8.2.1 A toy model 103
8.2.2 Realistic string axiverse scenarios 111
8.3 Direct detection of superradiant axion clouds 117
8.4 Discussion and conclusions 121

9 Determining the mass and spin of light PBHs with Hawking radiation 127
9.1 Low spin PBHs 128
9.1.1 Hawking spectra for $5 \times 10^7 < M < 10^{12}$ kg and $0 < \tilde{a} < 0.5$ 129
9.1.2 Low mass range ($5 \times 10^7 - 2.5 \times 10^{10}$ kg) 136
9.1.3 Intermediate mass range ($2.5 \times 10^{10} - 5 \times 10^{11}$ kg) . . . 138
9.1.4 High mass range ($5 \times 10^{11} - 10^{12}$ kg) 140
9.1.5 Conclusion 142
9.2 High spin PBHs 144
9.2.1 The Hawking spectrum 146

9.2.2 PBH mass and spin determination 148
9.2.3 Conclusion 155

10 Evaporating Kerr black holes as probes of new physics 157
10.1 BSM physics and Hawking evaporation 158
10.1.1 Multi-messenger detection of evaporating PBHs 163

11 Probing the metric structure using the Hawking emission 167
11.1 Introduction 167
11.2 Kerr-black-bounce metric 169
11.3 Scalar perturbations and evolution 171
11.3.1 Numerical method 173
11.4 Results 175
11.5 Conclusions 181

12 Conclusions 183

Appendices 185

A Double check using BlackHawk 187

B Contribution of different modes to the Hawking spectrum 191

C Secondary photon emission spectrum 193

1 Introduction

Primordial Black Holes (PBHs) are hypothetical black holes formed in the early universe from the direct collapse of density fluctuations in the primordial plasma. They were first suggested in 1967 by Zel'dovich and his student Novikov in the contest of hot cosmological model [1] and later proposed by Hawking [2] who also studied their production mechanisms. Their formation in the early universe has been intensely studied in the last decades and a plethora of different production mechanisms has been proposed. PBHs are promising candidates for addressing many open questions in physics such as, but not only, the dark matter problem, the dynamics of galaxy formation, and supermassive black hole formation. Insight and constraints on the nature of PBHs may be achieved by many proposed experiments that are nowadays in different stages of development. These include presently gravitational wave detectors, space-based telescopes, sky surveys, very large arrays, fast radio bursts observatories, MeV-GeV-TeV gamma-ray telescopes and observatories, Cherenkov telescopes, and neutrinos observatories. Moreover, the study of BH physics received two important boosts in the last years: the detection of binary mergers through gravitational waves [3] and the first images of supermassive BH shadow [4–10].

In this vibrant context, we exploit light PBHs as laboratories for new physics. We use the term new physics in a broad sense and, even if we will mainly consider physics Beyond the Standard Model (BSM) of particle physics, we will also show how it is possible to investigate local solutions beyond vacuum General Relativity (GR).

This thesis is organized as follows: chapters 2 to 6 contain a review of the concepts used in the original part which is presented in chapters 7 to 11. The original contribution of this thesis can also be found in the articles [11–16], mostly written in collaboration with my thesis supervisor, Prof. João Rosa,

but including also a single author paper and collaborations with Prof. John March-Russell (U. Oxford, UK) and MSc student Filipe Serrano. These articles are a part of my production which includes also [17–21] mostly written in collaboration with my friend Dr. Lorenzo Sebastiani and my MSc supervisor Prof. Massimiliano Rinaldi, but including collaborations with Prof. Orlando Luongo (U. Rome, IT) and Dr. Alessandro Casalino.

In chapter 2 we present a synthetic introduction to quantum field theory in curved spacetime together with examples. Chapter 3 contains an informal introduction to the concept of tetrads outlining the practical example of how to extend spinors to curved spacetime. Subsequently, a more formal presentation of the tetrad formalism is given together with some examples of useful tetrad, namely, the spin tetrad and the Newman-Penrose tetrad. In Chapter 4 we discuss the so-called Newman-Penrose formalism leading to the unification of different quantum field equations in the so-called Teukolsky equation, for the case of a Kerr spacetime. We also describe a numerical procedure to solve the scattering problem of quantum fields in such a spacetime. In Chapter 5, we discuss Hawking radiation through Bogoliubov transformations. We show that the concept of vacuum is not generally invariant, and derive the Unruh and Hawking effects in (1+1)-dimensions. Here we also outline the theoretical aspects of BH evaporation, emission and superradiance. In Chapter 6, we give some examples of extensions of the Standard Model (SM) such SUperSYmmetry (SUSY), Kaluza-Klein (KK) theories, QCD axions, Axion Like Particles (ALPs), and the Hidden Sector (HS). Chapter 7 is based on [11] and there we show that PBHs develop non-negligible spins through Hawking emission of a large number of ALPs, and that hot, MeV-TeV, axions would be a smoking gun for evaporating PBHs. In Chapter 8, which reports the results of [12], we study the coupled dynamics of superradiance, triggered by heavy axion, and evaporation, in the scenario described in the previous chapter. We show that once the superradiant threshold is crossed, superradiance processes dominate the evolution for the majority of the remaining PBH lifetime. Furthermore, we show that the decay of the heavy axions within the superradiant cloud into photon pairs may lead to a distinctive line in the black hole's emission spectrum. Chapter 9 is divided into two sections, each of which contains the major results of [13], and [14] respectively. We analyze distance independent methods to infer the mass and spin of light PBHs using their Hawking radiation spectrum. Motivated by the scenario of Chapter 7, we analyze the low

and high range of the adimensional BH spin parameter. Chapter 10 is based on [15] and shows how BSM physics affects the last stages in the evolution of a BH, and how with a multi-messenger approach it may be possible to accurately measure the mass and spin of a PBH from its Hawking photon and neutrino primary emission spectra, independently from any putative interactions between the new degrees of freedom and the SM particles, as well as from the Earth-PBH distance. In Chapter 11 we investigate local solutions beyond the one of vacuum General Relativity. We compare the evolution, under the emission of a single scalar field, of a BH described by the Kerr metric and a regular black hole described by the black-bounce metric. We show that there are differences in the gray-body factors, temperatures, and primary emissivity and comment on the possibility of investigating the beyond-the-horizon structure of a black hole by exploiting its Hawking emission. This chapter is based on [16]. Finally, we summarize our main conclusions in chapter 12.
We use units of $G = c = \hbar = k_B = 1$ and a metric signature given by $(-+++)$ if not otherwise specified.

2 Notions of QFT in curved spacetime

This chapter briefly synthesizes the lines of thought leading to the formulation of Quantum Field Theory in curved spacetime, outlining the limits of validity of such a theory. The second part of the chapter is devoted to some examples of generally covariant quantum field Equations of Motion (EoMs).

2.1 Quantum fields and curved spacetime

The Physics of the 20^{th} century has been characterized by radical changes of paradigm leading to the quantum theories and the theories of relativity. The rejection of the Galilean group as the group of symmetries of spacetime and its substitution with the Lorentz group, as suggested by Maxwell's equations, led Albert Einstein to formulate its special theory of relativity. Later the equivalence principle forced Einstein to further enlarge this group to the invariance under diffeomorphisms (or general linear invariance) and formulate the theory of General Relativity (GR). On the other hand, the contribution of many physicists led to abandoning the deterministic paradigm of classical physics and adopting the probabilistic one of quantum mechanics. In fact, a key concept of the first formulations of quantum mechanics was the wavefunction and its probabilistic interpretation. These quantum theories were not compatible with special relativity since they are a quantized version of Galilean mechanics and respecting the mass-shell equation $E = p^2/2m$. The development of equations respecting the special relativistic mass-shell relation, $E = \sqrt{p^2c^2 + m^2c^4}$, forced the community to abandon the interpretation in terms of wavefunctions in favor of a new one in which the central concept is the quantum field. The theory emerging is known as Quantum Field Theory (QFT) and it is one of

the most successful theories ever developed. In this context, several distinct relativistic equations describe massive or massless fields of different spin. The simplest is certainly the Klein-Gordon (KG) equation, obtained as a sort of squared Schrödinger equation by imposing the relativistic mass shell equation. Table 2.1 reports a list of relativistic field equations.

Spin	Name	Equation
0	Klein-Gordon	$(\partial_a \partial^a - m^2)\psi = 0$
1/2	Dirac	$(i\gamma^a \partial_a - m)\psi = 0$
1	Proca	$(\partial_a \partial^a + m^2)B^n = 0$
3/2	Rarita-Schwinger	$(\epsilon^{akpn}\gamma_5\gamma_k\partial_p - im\sigma^{an})\psi_n = 0$
s	Joos-Weinberg	$(i^{2s}\gamma^{a_1 \dots a_{2s}}\partial_{a_1} \dots \partial_{a_{2s}} + m^{2s})\psi = 0$

Table 2.1: Collection of relativistic quantum equations for different spin.

The milestone around which GR is built is the equivalence principle. As a consequence, it is always possible to locally find a Minkowskian observer, i.e. an observer who does not describe spacetime as curved, but rather as a Minkowski spacetime. This observer is the one in free fall (it belongs to the family of free-falling frames), who does not experiment any accelerations and for which the laws of special relativity hold. Such an observer will describe the quantum fields according to QFT with the above-mentioned field equations. Since the goal is to extend the validity of QFT to any curved spacetime, it seems natural to induce a mapping between the flat Minkowskian spacetime and any curved spacetime that allows us to write more general field equations. In a more refined way, one can say that we aim to pass from the Lorentz invariance of the equations in Tab. 2.1 to a generally covariant formulation of these (the latter reducing to the former only in the case of flat spacetime).
The generally covariant extension of QFT takes usually the name of QFT in curved spacetime. In this theory, spacetime is a fixed background, not perturbed by the presence of matter fields, and on which fields dynamically evolve. Adopting a metaphoric allegory it is possible to imagine the metric as a background stage on which the actors, in the form of the fields, play their role. This approximation ignores the back-reaction that fields may have on the structure of spacetime. In fact, the field energy density, giving an active contribution to the stress-energy tensor T_{mn} in the Einstein equations, changes the structure of the metric itself. Nevertheless, spacetime is a very stiff material, ensuring

that non-negligible modifications to its structure have to be imputed to very large energy densities. Almost the entire set of applications that will follow in this thesis lies in the fruitful approximation of QFT in curved spacetime. Nevertheless, it is important to keep in mind that the approximation is valid if fields are small perturbations. Nonetheless, any quantitative change in a phenomenon implies a qualitative change in the landscape in which it is embedded (Hegel). Some examples of quantitative changes that cause crossing the line of validity of QFT in curved spacetime and imply changes in the landscape (the theory describing the phenomenon) are represented by the last instants of a BH evaporation or in the first instants of the Universe. These cases lie in the realm of Quantum Gravity (QG) which is beyond the scope of this thesis.

2.2 Examples of generally covariant field equations

Let us now sketch a few examples of the general covariant generalization of the field equations of motion. We will consider only the Klein-Gordon and Dirac fields, namely $s = 0, \frac{1}{2}$.
The minimally coupled Klein-Gordon equation is characterized by a scalar function ψ, a scalar quantity m, and the only non-scalar components are the derivatives. Scalar quantities are by definition generally invariant. The derivatives are 4-vectors in a Minkowskian spacetime and need to be modified. The partial derivatives ∂_μ take into account the variation of a quantity with respect to the position, but, in a curved spacetime, the vector basis changes with respect to the position. A derivative operator that takes into account the variation of the basis with respect to the position is the covariant derivative $\nabla_\mu := \partial_\mu + \Gamma^\nu_{\mu\rho}$, where $\Gamma^\nu_{\mu\rho}$ is the affine connection that in a Riemannian theory (metric compatible and torsionless) reduces to the Christoffel symbols. Here, the indices of the connection contracts according to the field types the covariant derivative is acting on. Finally, the minimally coupled Klein-Gordon equation in curved spacetime reads

$$(\nabla_\mu \nabla^\mu - m^2)\psi = (\nabla_\mu \partial^\mu - m^2)\psi = 0. \tag{2.1}$$

The general covariant formulation of the Dirac equation is a more involved task. The gamma matrices need to respect the Clifford algebra of a curved spacetime and ψ is a spinor, transforming, under the Lorentz group, according

to the spinor representation. This problem is overcome by taking advantage of the fact that we can formulate the Dirac equation in flat spacetime and with the use of the tetrad formalism and the spin connection $\omega_\mu^{mn} = e_\nu^m \partial_\mu e^{\nu n} + e_\nu^m \Gamma^\nu_{\rho\mu} e^{\rho n}$ we can connect different patches of spacetime. We denoted with Greek letters the spacetime indices and with Latin letters the spin indices. The covariant derivative of a spinor in such a formalism reads $\nabla_\mu = \partial_\mu - \frac{i}{4}\omega_\mu^{mn}\sigma_{mn}$ where $\sigma_{mn} = i\gamma_{mn} = \frac{1}{2}[\gamma_m, \gamma_n]$. The Dirac equation in curved spacetime reads

$$(i\gamma^m e_m^\mu \nabla_\mu - m)\psi = 0. \tag{2.2}$$

The tetrad formalism is described in the next chapter where it is also used to justify (2.2) and it will also play a central role in chapter 3.
One can notice that both equations are explicitly solvable once the metric tensor is fixed. This statement remains true also in the cases of Proca, Rarita-Schwinger, or Joos-Weinberg generally covariant equations.

3 The tetrad formalism

The first question to address when introducing a new formalism is the motivation to do so, especially since GR works well in the good old coordinates formalism. The answer in this case is three-fold. First, and probably the least interesting, for a utilitarian scope: much of the literature in GR is written in this formalism (and it is so for the next two reasons). Secondly, as it will soon become evident, this is a natural way to describe spin-$\frac{1}{2}$ particles in GR and in general produces remarkable simplifications in the description of quantum fields in curved spacetime. Finally, because physics is more evident, it is possible to overcome the deformation of coordinates in curved spacetime and work in locally inertial frames. Moreover, the tetrad formalism allows us to express physics in a more intuitive frame, emphasizing desired characteristics, and obtaining great simplification.

The term tetrad comes from the Latin tetras and has its origin in the ancient Greek word $\tau\varepsilon\tau\rho\alpha\varsigma$, which means grouped by four. Usually, a tetrad is denoted as e^{μ}_{m} and it is also called Vierbein from the German "four legs". The letter e is chosen because in German this is the first letter of the word unity: Einheit. However, since physicists interested in QFT in curved spacetime also developed theories with more than four dimensions sometimes e^{μ}_{m} is called Vielebein, or n-Bein (Viele being the German word for many). Finally, mathematicians being less constrained by dimensionality more rationally call it simply field frame.

The first section of this chapter proposes an informal introduction to this formalism which outlines the practical example of how to extend the concept of spinor to a general curved spacetime. The second section contains a more formal presentation of the tetrad formalism. Subsequently, some examples of useful tetrad are given in the form of the spin tetrad and the Newman-Penrose tetrad.

3.1 The importance of tetrad in curved spacetime

In Minkowski spacetime (from now on denoted as $\mathbb{M}^4$) a spinor transforms as a spin-$\frac{1}{2}$ object, according to the spinorial representation of of the Lorentz group. In order to proceed and mathematically write the line above some definitions and conventions need to be outlined:

- The metric of $\mathbb{M}^4$ is denoted as η_{mn} and the convention on its sign is $(-+++)$.

- A Lorentz transformation Λ is a transformation which leaves invariant the metric tensor of $\mathbb{M}^4$:

$$\Lambda^q_m \Lambda^p_n \eta_{pq} = \eta_{mn}. \tag{3.1}$$

- The gamma matrices are 4×4 matrices respecting the Clifford algebra [22–24] of $\mathbb{M}^4$:

$$\mathcal{M}_{4\times 4} \ni \gamma^m | \{\gamma^m, \gamma^n\} = 2\eta^{mn} \otimes \mathbb{I}_4 \tag{3.2}$$

  where $\mathbb{I}_\mathbb{n}$ is the $\mathbb{n} \times \mathbb{n}$ identity matrix. The chosen Dirac representation is the one in which γ^0 is anti-symmetric and γ^i with $i = 1, 2, 3$ are hermitian:

$$\gamma^0 = \begin{pmatrix} \mathbb{I}_2 & 0 \\ 0 & -\mathbb{I}_2 \end{pmatrix} \quad ; \quad \gamma^i = \begin{pmatrix} 0 & \sigma^i \\ -\sigma^i & 0 \end{pmatrix} \tag{3.3}$$

  where σ^i are the Pauli matrices.

- The generators of the Lorentz group then read

$$L^{mn} = \frac{1}{2}\gamma^{mn} \tag{3.4}$$

  where $\gamma^{mn} = \frac{1}{2}[\gamma^m, \gamma^n]$. A tedious calculation may convince the reader that L^{mn} do commute correctly according to the rules of the Lorentz group.

Then a spinor under the action of a Lorentz transformation:

$$\psi(x) \to \psi'(x') = S(\Lambda)\psi(x') \tag{3.5}$$

where $x' = \Lambda x$ and $S(\Lambda) = e^{\frac{1}{4}\gamma^{mn}\lambda_{mn}}$ is the spinorial representation of the element of the Lorentz group with λ_{mn} the anti-symmetric infinitesimal Lorentz transformation. (Spinorial and Minkowskian indices have been omitted in (3.5) for simplicity).

How is it possible to generalize the concept of spinor to a curved spacetime? Let us start with denoting the manifold of GR with $\mathbb{E}^4$. In this manifold the static metric η_{mn} is substituted by the more dynamic $g_{\mu\nu}$. Here, Latin letters denote Minkowskian indices, i.e. indices belonging to the space $\mathbb{M}^4$, while Greek letters denote spacetime indices, belonging to $\mathbb{E}^4$.

The equivalence principle ensures that at each point of spacetime, it is possible to construct a local inertial frame, where the spacetime metric reduces to the Minkowskian one. This is the free-falling coordinate system, in which no acceleration is measured. One can build the local inertial frame by choosing a specific event in spacetime and considering the coordinate transformation such that the metric tensor $g^{\mu\nu}$ reduces to η^{mn}. A general coordinate transformation reads

$$x^m \to x'^{\mathfrak{m}}(x^m) \quad ; \quad g_{\mu\nu} \to g'_{\mathfrak{mn}} = A^{\mu}_{\mathfrak{m}} A^{\nu}_{\mathfrak{n}} g_{\mu\nu} \tag{3.6}$$

where $A^{\mu}_{\mathfrak{m}} = \frac{\partial x^{\mu}}{\partial x'^{\mathfrak{m}}}$ are the matrices of the partial derivatives of the coordinate transformation and x^{μ}, $x'^{\mathfrak{m}}$ are sets of coordinates. The equivalence principle ensures that at each point of spacetime, there exists $A^{\mu}_{\mathfrak{m}}{=}A^{\mu}_{m}$ such that $g'_{\mathfrak{mn}} = \eta_{mn}$. The limitation of this approach resides in its local nature: at each point of $\mathbb{E}^4$ the matrices A^{μ}_{m} will change. For example, in the presence of a spherical gravitational source, each value of the radial coordinate possesses a free-falling observer with a different acceleration with respect an observer standing still at a fixed position in the field. Each different radial value corresponds to a different class of inertial observers and so different A^{μ}_{m}. If the gradient of acceleration of the free-falling frame vanishes then A^{μ}_{m} gains a general role.

In order to have a general transformation mapping locally between $\mathbb{E}^4$ and $\mathbb{M}^4$ and valid at each spacetime point one needs to construct something similar to $\eta_{mn} = A^{\mu}_{m} A^{\mu}_{n} g_{\mu\nu}$, and such that

$$\eta_{mn} = e^{\mu}_{m} e^{\nu}_{n} g_{\mu\nu} \tag{3.7}$$

is valid everywhere. The operations represent a generalization of the concept of change of basis, in which the coordinate basis changes continuously in moving

from one point to another. This new particular basis is called tetrad (or tetrad-base, tetrad-frame), $\tau_m(x^\mu) = (\tau_0, \tau_1, \tau_2, \tau_3)$ and the indices are called tetrad indices. In order to achieve the goal, at each point in spacetime τ_m takes the values such that the metric induced by the local coordinates is the one of the local inertial frames. This means that the metric induced by the tensor product of the tetrad basis, which is in general called tetrad metric, is the one of Minkowski.

$$\tau_m \tau_n = \eta_{mn}. \tag{3.8}$$

One can notice that there is a parallelism between coordinates and change of bases, and tetrad-bases and Vierbein. This operation should not be mistaken for coordinates changes since the objects e^μ_m are not built as matrices of partial derivatives, which may not exist in general. Only in trivial cases or at a local level does the interpretation as coordinate transformation hold.
It is possible to raise and lower indices by manipulating separately spacetime and Minkowskian (or tetrad) indices using the spacetime and Minkowski (or tetrad) metrics, respectively:

$$e^{m\mu} = \eta^{mn} e^\mu_n \quad ; \quad e^\mu_n = \eta_{np} e^{p\mu} \quad ; \quad e_{\mu m} = g_{\mu\nu} e^\nu_m \quad ; \quad e^m_\nu = g_{\nu\mu} e^{\mu m}. \tag{3.9}$$

Whenever thinking about symmetries in GR, one always mentions local coordinate invariance. The tetrad formalism helps in remembering a forgotten symmetry, local Lorentz invariance. This is explicit because a Lorenz transformation carried out at a particular spacetime point on a Vierbein leaves the Minkowski metric unchanged. Explicitly:

$$\begin{aligned} e^\mu_m e^\nu_n g_{\mu\nu} &= \eta_{mn} \\ &= \Lambda^p_m \Lambda^k_n \eta_{pk} \\ &= \Lambda^p_m \Lambda^k_n e^\mu_p e^\nu_k g_{\mu\nu} \\ &= (\Lambda^p_m e^\mu_p)(\Lambda^k_n e^\nu_k) g_{\mu\nu} \\ &= \tilde{e}^\mu_m \tilde{e}^\nu_n g_{\mu\nu}, \end{aligned}$$

making it clear that any Lorentz transformation of the frame field gives the frame field itself.

$$\Lambda^p_m e^\mu_p = \tilde{e}^\mu_m = e^\mu_m. \tag{3.10}$$

Furthermore, since Λ^p_m is in general a local function of the position, $\Lambda^p_m = \Lambda^p_m(x)$, then

$$\eta_{mn} = \Lambda^p_m(x)\Lambda^k_n(x)e^\mu_p e^\nu_k g_{\mu\nu}. \tag{3.11}$$

In other words, the general local invariance of $\mathbb{M}^4$ is inherited by $\mathbb{E}^4$ as a local Lorentz invariance.

It is now possible to answer the question about a spinor in GR. Given the tetrad formalism where the tetrad metric is the Minkowskian one, a spinor is an object that transforms under the spinorial representation of the Lorenz group under the action of local Lorentz transformations.

Now, to better understand the meaning of (2.2) let us introduce the concept of derivative in this new formalism.

In the coordinate formalism of GR, the concept of differentiation was connected to the covariant derivative. The simple derivative was not sufficient. It was necessary to take into account not only how a quantity changes by changing the coordinates value, but also how the quantity changes because of changes in the spacetime structure in changing the value of the "rigid" coordinate system. For this reason, it was necessary to introduce the metric connection (under the hypothesis of a torsion-free and metric-compatible theory of gravity) in the form of the Christoffel symbols.

In the tetrad formalism, we need to do something similar. In order to define a covariant derivative one needs to take into account how a quantity changes upon changing the values of the tetrad basis and how a quantity changes because of a modification of the basis itself. This is done with the aid of the tetrad connection, also called the spin connection.

Let us do it considering the Vielbein which has a spacetime and a Lorentz index. Under coordinate transformation, it transforms as a 4-vector (tensor). Under Lorentz transformation, it transforms as a Lorentz vector (tensor). So, if one wants to consistently build something like $\nabla_\nu e^\mu_m$, one has to ensure that this object transforms as a (1,1) tensor and a Lorentz vector. Since GR is both metric compatible and torsion-free, it would be nice if the properties of ∇_ν were consistent with the idea that the spacetime metric is associated with a

symmetric connection. (This is not necessary, just convenient!)

$$\begin{aligned} 0 &= \nabla_\nu g_{\rho\kappa} \\ &= \nabla_\nu (e^m_\rho e^n_\kappa \eta_{mn}) \\ &= e^m_\rho e^n_\kappa \nabla_\nu [\eta_{mn}] + e^m_\rho \eta_{mn} \nabla_\nu [e^n_\kappa] + e^n_\kappa \eta_{mn} \nabla_\nu [e^m_\rho]. \end{aligned}$$

The first term is identically 0 since η_{mn} is a Lorentz tensor but a spacetime scalar. So for the metric compatibility to hold, we must have

$$\nabla_\nu e^\mu_m = 0. \tag{3.12}$$

The standard covariant derivative of the Vierbein is composed of the partial derivative and connection (Christoffel symbols) but this is not enough to ensure that (3.12) holds. We are not taking into account the local indices, namely we are not considering how the local Lorenzian bases are changing. We can use simple linear algebra, add a new piece, denoted by ω and known as the spin connection or tetrad frame connection, for accounting the Minkowskian index ignored, and guarantee that (3.12) is verified. Thus

$$\nabla_\nu e^m_\mu = \partial_\nu e^m_\mu - \Gamma^\rho_{\nu\mu} e^m_\rho + \omega^m_{n\nu} e^n_\mu. \tag{3.13}$$

Solving for the spin connection:

$$\omega^m_{n\nu} = -e_{n\mu} \partial_\nu e^{\mu m} - e_{n\mu} \Gamma^\mu_{\nu\rho} e^{\rho m}. \tag{3.14}$$

The tetrad formalism introduces a local inertial coordinate system at each point of the curved manifold. The spin connection relates a vector located at one point with components in the local basis at that point, with the one at another point with a new local basis. The new covariant derivative will now take into account: the bare variations of the quantity, the variations of the rulers with which we measure it, and the variation in the definition of the local Lorentz frame. Using the spin connection for defining a Riemann tensor as in differential geometry, one obtains

$$R_{mn\rho\kappa} = \partial_m \omega_{n\rho\kappa} - \partial_n \omega_{m\rho\kappa} + \omega_m{}^\sigma{}_\rho \omega_{m\sigma\kappa} + \omega_n{}^\sigma{}_\rho \omega_{m\sigma\kappa}, \tag{3.15}$$

which is antisymmetric under the exchange of $m \leftrightarrow n$ and $\rho \leftrightarrow \kappa$ but does not seem to share anything with the conventional Riemann tensor. Nonetheless, it is possible to demonstrate that given the choices of metric compatibility and vanishing torsion

$$R_{\mu\nu\rho\kappa} = e^m_\mu e^n_\nu R_{mn\rho\kappa} \tag{3.16}$$

the explicit calculation is straightforward but long and tedious and can be found in books introducing differential forms [25, 26].

Now we can have an intuitive idea of why in the covariant derivative of a spinor (2.2) only the spin connection and no affine connection is present: the spinor does not carry any spacetime or Minkowskian indices, but only spinorial ones. In fact, it transforms according to the spinorial representation under the action of a Lorentz transformation. Certainly, the covariant derivative of a spinor has to transform as a spacetime vector times a spinor. Thus, the partial derivatives of a spinor do not correctly transform under a Lorentz transformation and require the addition of a second piece to behave correctly. This second piece cannot be the only $\omega^m_{n\nu}$ as in (3.12) since $\partial_n\psi + \omega^m_{n\nu}\psi$ is clearly wrong, because of the indices in its second term. Moreover, nothing suggested that the covariant derivative of a Vierbein should be the same for a spinor. If we want to have the covariant derivative of a spinor, we need to consider also the rules of the parallel transport for spinors (as for example done in (7.7) of [27]). This derivation is proposed in section (3.3) after a more formal introduction to the tetrad formalism.

3.2 A more formal introduction to tetrad formalism

This section takes many thoughts and follow the formalis of [28]. A tetrad $\tau_m(x) = (\tau_0(x), \tau_1(x), \tau_2(x), \tau_3(x))$ is a set of axes at each point of spacetime. Each component $\tau_0, \tau_1, \tau_2, \tau_3$ is itself a four-vector and for this reason sometime in the following formulas a contraction/scalar inner product is understood. In the previous section, we outlined a particular choice called an orthonormal tetrad, in which the axes formed a local inertial frame at each point of spacetime. This choice was made explicit by Eq. (3.8) which in the general case may be rewritten as

$$\tau_m\tau_n = \Theta_{mn} \tag{3.17}$$

and Θ_{mn} takes the name of tetrad metric. If $\Theta_{mn} = \eta_{mn}$ we are back to the orthonormal tetrad. In general, the choice of a specific tetrad is taken to emphasize characteristics and obtain simplifications of specific problems. Some examples of useful tetrads, which will be later considered, are the spin tetrads and the null tetrads.

Given a coordinate frame defining the metric through $\mathbb{e}_\mu \mathbb{e}_\nu = g_{\mu\nu}$ one can define the Vierbein as the transformation matrix between tetrad and coordinate frames according to

$$\mathbb{e}_\mu = e^m_\mu \tau_m \quad ; \quad \tau_m = e^\mu_m \mathbb{e}_\mu. \tag{3.18}$$

It is also valid that

$$e^m_\mu e^\mu_n = \delta^m_n \quad ; \quad e^m_\mu e^\nu_m = \delta^\nu_\mu, \tag{3.19}$$

and

$$e^\mu_m e_{n\mu} = \eta_{mn} \quad ; \quad e^m_\mu e_{m\mu} = g_{\mu\nu}. \tag{3.20}$$

This way

$$g_{\mu\nu} = \Theta_{mn} e^m_\mu e^n_\mu, \tag{3.21}$$

and one recovers

$$ds^2 = \mathbb{e}_\mu \mathbb{e}_\nu dx^\mu dx^\nu = g_{\mu\nu} dx^\mu dx^\nu = \Theta_{mn} e^m_\mu e^n_\nu dx^\mu dx^\nu. \tag{3.22}$$

In order to define what to call a tetrad vector/tensor we need a set of transformations preserving some interesting properties, such as, for example, a set of transformations acting on τ and leaving Θ_{mn} unchanged. This is certainly an arbitrary choice but for what concerns the orthonormal, spin, and Newman-Penrose tetrads, and more in general for what concerns most applications in the field of physics, this choice is a quite standard one: the tetrad transformations are the Lorentz transformations $\tau_m \to \tau'_m = \Lambda^n_m \tau_n$. For such cases, it holds that

$$\Theta'_{mn} = \tau'_m \tau'_n = \Lambda^q_m \tau_q \Lambda^p_n \tau_n = \Lambda^q_m \Lambda^p_n \Theta_{qp} = \Theta_{mn}. \tag{3.23}$$

Note that the Lorentz transformation may change for distinct points in spacetime and therefore Λ^q_m is a dynamical object.

In this framework, it is possible to define a tetrad vector $V_m = (V_0, V_1, V_2, V_3)$ as the object that under a Lorentz transformation transforms as $V_m \to V'_m =$

$\Lambda^n_m V_n$. More generally for a tetrad tensor we have:

$$V'^{m_1\cdots}_{n_1\cdots} = \Lambda^{m_1}_{q_1}\cdots\Lambda^{p_1}_{n_1}\cdots V^{q_1\cdots}_{p_1\cdots} \tag{3.24}$$

Raising and lowering the indices of a tetrad vector is an operation mediated by the tetrad metric Θ_{mn} in the very same way that in a coordinate frame, it was mediated by the coordinate metric $g_{\mu\nu}$. In fact, it is valid that

$$\delta^n_k = \Theta_{km}\Theta^{mn}, \tag{3.25}$$

$$V^m = \Theta^{mn}V_n \quad ; \quad V_m = \Theta_{mn}V^n, \tag{3.26}$$

$$\tau^m = \Theta^{mn}\tau_n \quad ; \quad \tau^m\tau_n = \delta^m_n \quad ; \quad \tau^m\tau^n = \Theta^{mn}. \tag{3.27}$$

It is possible to go from tetrad to coordinate component description of a vector/tensor using the Vierbein:

$$V_\mu = e^m_\mu V_m \quad ; \quad V_m = e^\mu_m V_\mu. \tag{3.28}$$

This ensures that the scalar product is unchanged in the two formalisms and it is possible to define the invariant concept of abstract vector

$$\mathbf{V} = \tau_m V^m = \mathbb{e}_\mu V^\mu, \tag{3.29}$$

$$\mathbf{V}\cdot\mathbf{U} = V^m U_m = V^\mu U_\mu. \tag{3.30}$$

It is worth now making a clear distinction between vector/tensor nomenclature and definition:

- Coordinate vector: is denoted with Greek indices and changes under spacetime coordinate transformations without changing the spacetime structure. It does not change under tetrad transformations and is therefore a tetrad scalar.

- Tetrad vector: is denoted by Latin indices and changes accordingly under tetrad transformations. It is not influenced by coordinate transformations and so it is a coordinate scalar.

- Abstract vector: denoted with a bold font, it is the abstract idea of

vector, and does not change changing the formalism of its description. It is therefore both a coordinate and tetrad scalar

In analogy with the coordinate partial derivatives, it is possible to define the tetrad formalism counterparts, namely the directional derivatives along the axes τ_m, which we may call directed derivatives:

$$\partial_m = \tau_m \boldsymbol{\partial} = \tau_m \mathbb{e}^\mu \partial_\mu = e^\mu_m \partial_\mu. \tag{3.31}$$

These operators do not satisfy the Schwartz theorem, in fact:

$$\begin{aligned}[\partial_m, \partial_n] &= [e^\mu_m \partial_\mu, e^\nu_n \partial_\nu] \\ &= e^\mu_m \partial_\mu [e^\nu_n] \partial_\nu - e^\nu_n \partial_\nu [e^\mu_m] \partial_\mu \\ &= (d^q_{mn} - d^q_{nm}) \partial_q \end{aligned} \tag{3.32}$$

where

$$d_{qmn} = -\Theta_{qk} e^k_\kappa e^\nu_n \partial_\nu [e^\kappa_m] = \Theta_{qk} e^\mu_m e^\nu_n \partial_\nu [e^k_\mu] \tag{3.33}$$

with $d_{qmn} = \Theta_{qk} d^k_{mn}$.
The tetrad covariant derivative is obtained through a straightforward process, similar to its coordinates counterpart. The requirement for a tetrad covariant derivative operator is to generate tetrad vectors/tensors. In the case of a scalar function it is effortless since $\partial_m \Phi$ is a tetrad vector, so the tetrad covariant derivative of a scalar function is just the tetrad derivative

$$\nabla_m \Phi = \partial_m \Phi. \tag{3.34}$$

The derivative of a tetrad vector is not as simple since $\partial_m V^m$ is not a tetrad tensor (it does not transform correctly under Lorentz transformations). The same situation occurred in the coordinates frame and led to the introduction of the Christoffel symbols. Let us consider this known situation to find a possible way out of our problem. The derivative of an abstract vector is a coordinate tensor and reads

$$\begin{aligned}\partial_\nu \mathbf{V} &= \partial_\nu (\mathbb{e}_\mu V^\mu) \\ &= V^\mu \partial_\nu (\mathbb{e}_\mu) + \mathbb{e}_\mu \partial_\nu (V^\mu).\end{aligned}$$

By the definition of the affine connection

$$\Gamma^{\rho}_{\nu\mu}\mathbb{e}_{\rho} := \partial_{\nu}(\mathbb{e}_{\mu}). \tag{3.35}$$

It is then possible to define the coordinates, covariant derivative of a vector

$$\nabla_{\nu}V^{\mu} = \partial_{\nu}V^{\mu} + \Gamma^{\mu}_{\nu\rho}V^{\rho}. \tag{3.36}$$

In a free-torsion theory, the commutator of two coordinate covariant derivatives vanishes and the connection is symmetric with respect to the exchange of the lower indices. As we have seen in the previous section another desirable feature of the theory is also to be metric compatible. In this case, the affine connection reduces to the Christoffel symbols.
Let us now perform the same steps in the tetrad formalism in order to define the tetrad covariant derivative of a vector and the tetrad connection.

$$\begin{aligned}\partial_n \mathbf{V} &= \partial_n(\tau_m V^m) \\ &= V^m\partial_n(\tau_m) + \tau_m\partial_n(V^m),\end{aligned}$$

$$\Gamma^{p}_{nm}\tau_p := \partial_n(\tau_m), \tag{3.37}$$

$$\nabla_n V^m = \partial_n V^m + \Gamma^m_{np}V^p. \tag{3.38}$$

The extension to contravariant vectors is quite trivial. There is a little abuse of notation in the precedent section where the tetrad connection was denoted with ω. Here the letter with which it is denoted is changed to underline the parallelism between the two connections. The relation between the two connections can be calculated considering

$$\begin{aligned}\Gamma^{\kappa}_{\mu\nu}\mathbb{e}_{\kappa} &= \partial_{\nu}\mathbb{e}_{\mu} \\ &= \partial_{\nu}(e^m_{\mu}\tau_m) \\ &= \tau_m\partial_{\nu}(e^m_{\mu}) + e^m_{\mu}\partial_{\nu}(\tau_m) \\ &= e^m_{\mu}e^n_{\nu}(d^p_{mn} + \Gamma^p_{mn})\tau_p\end{aligned}$$

and reads

$$\Gamma_{pmn} + d_{pmn} = e^{\rho}_p e^{\mu}_m e^{\nu}_n \Gamma_{\rho\mu\nu} \tag{3.39}$$

where the indices of the connections are raised and lowered using the respective metrics. It is possible to use the symmetry of the coordinate connection together with (3.39) to obtain the relation that the tetrad connection needs to respect for a vanishing torsion tensor,

$$\Gamma_{pmn} + d_{pmn} = \Gamma_{pnm} + d_{pnm}. \tag{3.40}$$

If the tetrad metric is constant, and this is the case for orthonormal, spin, and null tetrads, the tetrad connection is antisymmetric, and it holds

$$\begin{aligned} 0 &= \partial_p(\Theta_{mn}) \\ &= \partial_p(\tau_m \tau_n) \\ &= \tau_m \partial_p(\tau_n) + \tau_n \partial_p(\tau_m) \\ &= \Gamma_{mnp} + \Gamma_{nmp}. \end{aligned}$$

In Riemannian differential geometry, once the connection is known, it is possible to calculate the Riemann tensor which in the tetrad frame reads:

$$R_{qpmn} = \partial_q \Gamma_{mnp} - \partial_p \Gamma_{mnq} + \Gamma^a_{mp}\Gamma_{anq} - \Gamma^a_{mq}\Gamma_{anp} + (\Gamma^a_{qp} + \Gamma^a_{pq})\Gamma_{mna}. \tag{3.41}$$

The symmetries of the tetrad frame Riemann tensor are the same as its coordinate frame counterpart, being

$$R_{qpmn} = R_{mnqp}, \tag{3.42}$$

$$R_{qpmn} = -R_{pqmn}, \tag{3.43}$$

$$R_{qpmn} = -R_{qpnm} \tag{3.44}$$

$$R_{qpmn} + R_{qmnp} + R_{qnpm} = 0, \tag{3.45}$$

$$\nabla_a R_{qpmn} + \nabla_q R_{pamn} + \nabla_p R_{aqmn} = 0. \tag{3.46}$$

All the building blocks of GR have now been defined in the new formalism and it is possible to write the GR equation of motion in the tetrad formalism

$$G_{mn} = 8\pi G T_{mn} \tag{3.47}$$

where the Einstein tensor is

$$G_{mn} = R_{mn} - \frac{1}{2}R, \tag{3.48}$$

and the Ricci scalar and tensor are

$$R = \Theta^{mn} R_{mn}, \tag{3.49}$$

$$R_{mn} = \Theta^{qp} R_{mqnp}. \tag{3.50}$$

Finally, metric compatibility ensures the covariant conservation of the Einstein tensor and therefore the conservation of the energy-momentum tensor,

$$\nabla^m G_{mn} = 0, \tag{3.51}$$

$$\nabla^m T_{mn} = 0. \tag{3.52}$$

One could also consider mixed coordinate-tetrad objects such as the coordinates covariant derivative of a tetrad vector (or the tetrad derivative of a coordinate vector)

$$\nabla_\alpha V_m = e^a_\alpha \nabla_a V_m = \partial_a V_m - \Gamma^n_{m\alpha} V_n \tag{3.53}$$

where

$$\Gamma^m_{n\alpha} = e^a_\alpha \Gamma^m_{na}$$

and $\Gamma_{mn\alpha} = \Theta_{mp}\Gamma^p_{n\alpha}$. It is also valid that:

$$\Gamma_{mn\kappa} = -e^p_\kappa d_{mnp} + e^\mu_m e^\nu_n \Gamma_{\mu\nu\kappa} \tag{3.54}$$

so that we may rewrite the Riemann tensor and so on in a mixed coordinate-tetrad frame.

3.3 Dirac Equation in curved spacetime

We now have all the elements to derive the Dirac equation in curved spacetime. We restart where we left off in section 2.1: $\Theta_{mn} = \eta_{mn}$ and for building the covariant derivative of a spinor field we want to consider the parallel transport of a spinor. Let us consider formerly a coordinate or spacetime vector V^μ and

a local or Lorentzian or Minkowskian vector V^m and analyze their parallel transport from x to $x + dx$

$$V^\mu(x \to x + dx) = V^\mu(x) - \Gamma^\mu_{\nu\rho}(x)V^\rho(x)dx^\nu, \tag{3.55}$$

$$V^m(x \to x + dx) = V^m(x) - \omega^m_{\nu p}(x)V^p(x)dx^\nu. \tag{3.56}$$

In (3.55) Γ is the usual affine connection defining the parallel transport of a vector on the manifold, while in (3.56) ω needs to involve both the affine connection and the Vierbein since it has to relate the local inertial coordinates of x to the one of $x + dx$. Meanwhile, it must hold true that

$$V^\mu(x) = e^\mu_m(x)V^m(x), \tag{3.57}$$

$$V^\mu(x \to x + dx) = e^\mu_m(x \to x + dx)V^m(x \to x + dx). \tag{3.58}$$

The expansion at the first order $e^\mu_m(x \to x+dx) \sim e^\mu_m(x)+\partial_\nu e^\mu_m(x)dx^\nu$ is valid since the considered displacement is infinitesimal. Inserting this expansion and (3.56) into (3.58) and again keeping only the linear terms in dx we have

$$\begin{aligned} V^\mu(x \to x + dx) &= e^\mu_m(x)V^m(x \to x + dx) + \partial_\nu e^\mu_m(x)dx^\nu V^m(x \to x + dx) \\ &= e^\mu_m(x)V^m(x) - e^\mu_m(x)\omega^m_{\nu p}(x)V^p(x)dx^\nu + \partial_\nu e^\mu_m(x)dx^\nu V^m(x) \\ &= e^\mu_m(x)V^m(x) - \left[e^\mu_m(x)\omega^m_{\nu p}(x) + \partial_\nu e^\mu_p(x)\right] V^p(x)dx^\nu \\ &= e^\mu_m(x)V^m(x) - \left[e^\mu_m(x)\omega^m_{\nu p}(x) + \partial_\nu e^\mu_p(x)\right] e^p_\rho V^\rho(x)dx^\nu \end{aligned} \tag{3.59}$$

and using (3.55) we can identify

$$\Gamma^\mu_{\nu\rho} = \left[e^\mu_m(x)\omega^m_{\nu p}(x) + \partial_\nu e^\mu_p(x)\right] e^p_\rho \tag{3.60}$$

from which it is not hard to find (3.14). It is easy to convince ourselves that the spin connection needs to be anti-symmetric with respect to the Lorentz indices if we want a metric-compatible theory (namely a theory preserving the magnitude of a vector when parallel transported):

$$V^m(x)V_m(x) = V^m(x + dx)V_m(x + dx) \quad \Rightarrow \quad \omega_{mn\nu} = -\omega_{nm\nu}. \tag{3.61}$$

Equivalently one can consider a metric compatible theory, therefore $\Gamma^{\mu}_{\nu\rho}$ are the Christoffel symbols and we have

$$0 = \nabla_\mu \eta_{mn} = \partial_\mu \eta_{mn} - \omega^p_{\mu m}\eta_{pn} - \omega^p_{\mu n}\eta_{mp} = -\omega_{\mu mn} - \omega_{\mu nm}. \tag{3.62}$$

We can now consider the parallel transport of a spinor. A priori we do not know how it behaves when parallel transported, so we introduce the most general linear transformation

$$\psi(x \to x + dx) = \psi(x) - \Omega_\nu(x)\psi(x)dx^\nu \tag{3.63}$$

where Ω_ν is a suitable connection having a consistent number of indices. To find the explicit form of Ω_ν we can consider the parallel transport of a known quantity: the scalar $S = \bar{\psi}\psi$ and a vector $V^m = \bar{\psi}\gamma^m\psi$. From (3.63) we have

$$S(x \to x + dx) = S(x) - \bar{\psi}(x)(\gamma^0\Omega^\dagger_n(x)\gamma^0 + \Omega_n(x))\psi dx^\nu \tag{3.64}$$

and to ensure the invariance of the scalar when parallel transported we need to have

$$\gamma^0\Omega^\dagger_\nu\gamma^0 = -\Omega_\nu. \tag{3.65}$$

Analogously, the vector is parallel transported correctly when:

$$[\gamma^m, \Omega_\nu] = \omega^m_{n\nu}\gamma^n. \tag{3.66}$$

Using those last two equations and some algebraic calculations one can conclude that

$$\Omega_\nu = \frac{1}{8}\omega_{mn\nu}[\gamma^m, \gamma^n] = \frac{1}{4}\omega_{mn\nu}\gamma^{mn} = -\frac{i}{4}\omega_{mn\nu}\sigma^{mn}. \tag{3.67}$$

Thus,

$$\nabla_\mu\psi = (\partial_\mu - \frac{i}{4}\omega_{mn\mu}\sigma^{mn})\psi. \tag{3.68}$$

To prove that it transforms correctly one can perform a Lorentz transformation and a coordinate transformation (or have a look at Weinberg's books [29–31] where he does it).

In the tetrad formalism, it is fairly simple to obtain the curved spacetime

representation of the Clifford algebra

$$2g^{\mu\nu} \otimes \mathbb{I}_4 = \{e^{\mu}_m \gamma^m, e^{\nu}_n \gamma^n\} = \{\gamma^\mu, \gamma^\nu\} \tag{3.69}$$

and one can generalize $(i\gamma^m \partial_m - m)\psi = 0$ by taking $\gamma^m \to e^{\mu}_m \gamma^\mu$ and $\partial_m \to \nabla_\mu$. This justifies Eq. (2.2).

3.4 The spin tetrads

In section (2.1), we outlined explicitly the orthonormal tetrad, i.e. the one for which the tetrad metric is the Minkowski metric

$$\Theta_{mn} = \eta_{mn} = \begin{pmatrix} -1 & 0 & 0 & 0 \\ 0 & 1 & 0 & 0 \\ 0 & 0 & 1 & 0 \\ 0 & 0 & 0 & 1 \end{pmatrix}. \tag{3.70}$$

Let us now consider a different tetrad system.
GR is a classical theory, nevertheless, it encodes spin properties in the behavior of classical waves, such as electromagnetic or gravitational waves. Moreover, to each quantum field and related particles, is associated with a spin. A legitimate question may then be if there exists a way to project objects into their spin components. The answer is clearly yes and involves the spin tetrad.
Spin describes how objects transform if rotated around a preferred axis. In the case of electromagnetic and gravitational waves, this axis is the one along which they propagate. The values of the possible spins (or helicities since they are massless particles) are ± 1 and ± 2, respectively. For simplicity let us say that the direction of propagation of the wave is along the z-axis of the orthonormal tetrad $(\tau_t, \tau_x, \tau_y, \tau_z)$. It is now possible to define the spin tetrad as $(\tau_t, \tau_z, \tau_+, \tau_-)$ where

$$\tau_+ = \frac{1}{\sqrt{2}}(\tau_x + i\tau_y) \tag{3.71}$$

$$\tau_- = \frac{1}{\sqrt{2}}(\tau_x - i\tau_y) \tag{3.72}$$

are called the spin axes. It is not difficult to verify that

$$\tau_+ \cdot \tau_- = \tau_- \cdot \tau_+ = 1 \tag{3.73}$$

as well as

$$\tau_+ \cdot \tau_+ = \tau_- \cdot \tau_- = 0. \tag{3.74}$$

The non-vanishing components of the tetrad metrics are the diagonal components $\tau_t^2 = \Theta_{tt}$ and $\tau_z^2 = \Theta_{zz}$ and the off-diagonal components $\tau_+\tau_- = \Theta_{+-}$ and $\tau_-\tau_+ = \Theta_{-+}$. The spin tetrad metric reads

$$\Theta_{mn} = \begin{pmatrix} -1 & 0 & 0 & 0 \\ 0 & 1 & 0 & 0 \\ 0 & 0 & 0 & 1 \\ 0 & 0 & 1 & 0 \end{pmatrix}. \tag{3.75}$$

One can notice that under a counterclockwise rotation of an angle θ around the z-axes, the spin axes $\tau_\pm$ transforms as

$$\tau_\pm = e^{\mp i\theta}\tau_\pm. \tag{3.76}$$

It is also possible to say that $\tau_\pm$ possesses a spin ± 1. To better motivate this last sentence let us remember that an object of spin s is an object that behaves under a rotation of an angle θ according to $e^{-is\theta}$. In this way, scalar objects are unaffected by rotation, and spin-$\frac{1}{2}$ objects return to the same configuration after a 4π rotation while just a π rotation is needed for spin-2 objects. The components of a tetrad tensor inherit the spin properties of the bases and a general tensor reads

$$V_{mn} = \begin{pmatrix} V_{tt} & V_{tz} & V_{t+} & V_{t-} \\ V_{zt} & V_{zz} & V_{z+} & V_{z-} \\ V_{+t} & V_{+z} & V_{++} & V_{+-} \\ V_{-t} & V_{-z} & V_{-+} & V_{--} \end{pmatrix}. \tag{3.77}$$

Each entry of V_{mn}will have a spin given by the number of plus/minus in its subscript, that is

$$\begin{aligned} s = -2: &\quad V_{--} \\ s = -1: &\quad V_{t-}, V_{z-}, V_{-t}, V_{-z} \\ s = 0 \;\; : &\quad V_{tt}, V_{zz}, V_{tz}, V_{zt}, V_{+-}, V_{-+} \\ s = 1 \;\; : &\quad V_{t+}, V_{z+}, V_{+t}, V_{+z} \\ s = 2 \;\; : &\quad V_{++} \end{aligned}$$

3.5 The Newman-Penrose tetrad

A Newman-Penrose (NP) tetrad $(\tau_v, \tau_u, \tau_+, \tau_-)$ is a double null tetrad. It is built along the ingoing and outgoing light-like directions v and u and the complex light-like vectors of the spin tetrad $\tau_\pm$. In terms of the orthonormal tetrad denoted with $(\tau_t, \tau_x, \tau_y, \tau_z)$ it reads

$$\tau_v = \frac{1}{\sqrt{2}}(\tau_t + \tau_z) \tag{3.78}$$

$$\tau_u = \frac{1}{\sqrt{2}}(\tau_t - \tau_z) \tag{3.79}$$

$$\tau_+ = \frac{1}{\sqrt{2}}(\tau_x + i\tau_y) \tag{3.80}$$

$$\tau_- = \frac{1}{\sqrt{2}}(\tau_x - i\tau_y) \tag{3.81}$$

or equivalently

$$\begin{pmatrix} \tau_v \\ \tau_u \\ \tau_+ \\ \tau_- \end{pmatrix} = \frac{1}{\sqrt{2}} \begin{pmatrix} 1 & 0 & 0 & 1 \\ 1 & 0 & 0 & -1 \\ 0 & 1 & i & 0 \\ 0 & 1 & -i & 0 \end{pmatrix} \begin{pmatrix} \tau_t \\ \tau_x \\ \tau_y \\ \tau_z \end{pmatrix}. \tag{3.82}$$

It is easy to verify that

$$\tau_v \cdot \tau_v = \tau_u \cdot \tau_u = \tau_+ \cdot \tau_+ = \tau_- \cdot \tau_- = 0, \tag{3.83}$$

$$\tau_v \cdot \tau_u = \tau_u \cdot \tau_v = -1, \tag{3.84}$$

$$\tau_+ \cdot \tau_- = \tau_- \cdot \tau_+ = 1, \tag{3.85}$$

and all other products vanish. Thus, the NP tetrad metric reads

$$\Theta_{mn} = \begin{pmatrix} 0 & -1 & 0 & 0 \\ -1 & 0 & 0 & 0 \\ 0 & 0 & 0 & 1 \\ 0 & 0 & 1 & 0 \end{pmatrix}. \tag{3.86}$$

This tetrad will play a central role in the next chapter. It will allow us to develop the Newman-Penrose formalism through which it is possible to condense field equations of different spin into a single master equation if the background metric is the Kerr one.

4 Perturbations of the Kerr metric

In this chapter, we make use of concepts developed in the previous one and show how in the formalism provided by Newman and Penrose, the adoption of a double null tetrad implies the unification of quantum field equations in the so-called Teukolsky equation in the case of a Kerr spacetime. We provide an explicit example for the case of the electromagnetic field which is then generalized to an arbitrary spin-s field. We also describe a numerical procedure to solve the scattering problem of quantum fields in the Kerr spacetime.

4.1 The Newman-Penrose formalism

We aim to describe fields of different spin propagating at the speed of light in a spacetime described by a vacuum solution of GR (propagating in the vacuum). Intuitively, we need to find a way to gather together in a smart way 3 different concepts: different spin, speed of light, and vacuum. The concept of spin seems well represented in the NP tetrad given the + and − components. The same can be said for the speed of light, since in the NP tetrad the u and v components are in-going and out-going light-like surfaces. For what concerns GR in a vacuum the key object is the Weyl tensor C_{mnpq}. Let us see what happens when combining those ingredients.
The energy-momentum tensor vanishes in a vacuum. Therefore the Einstein and Ricci tensor and the Ricci scalar also vanish. The Einstein equations in vacuum read $R_{\mu\nu} = g^{\rho\sigma} R_{\mu\rho\sigma\nu} = R^{\rho}_{\mu\rho\nu} = 0$. Thus, the trace of the Riemann tensor is forced to vanish and the surviving part of this tensor is trace-free. In this case, we have that $C_{\mu\nu\rho\sigma} = R_{\mu\nu\rho\sigma}$ where the Weyl tensor $C_{\mu\nu\rho\sigma}$ is the trace-less part of the Riemann tensor. $C_{\mu\nu\rho\sigma}$ encodes all the gravitational phenomena in vacuum such as gravitational radiation, waves, tidal forces, and so on. The equation of motion for the Weyl tensor reads $C^{\rho}_{\mu\rho\nu} = 0$ everywhere

in spacetime, with or without the presence of mass-energy. The Riemann tensor possesses up to 20 degrees of freedom of which only 10 survive in the Weyl tensor. More precisely, the symmetries that the Wayl tensor inherited from the Riemann tensor such as the cyclic first Bianchi identity, together with it being trace-free, makes it is possible to show that some components vanish while others remain related, leaving us with ten degrees of freedom. We can classify the non-vanishing components of the Weyl tensor according to their spin-s behavior

$$\begin{aligned}
s = -2: &\quad C_{u-u-} \\
s = -1: &\quad C_{+-u-}, C_{uvu-} \\
s = 0 \;\; : &\quad C_{uvuv}, C_{uv+-}, C_{+-+-}, C_{v+-u} \\
s = 1 \;\; : &\quad C_{vuv+}, C_{-+v+} \\
s = 2 \;\; : &\quad C_{v+v+}
\end{aligned}$$

The representation of a vector/tensor component with the NP tetrad always introduces complex scalars possessing therefore 2 degrees of freedom each. As a consequence the 10 components above are not linearly independent and we have:

$$\begin{aligned}
s = -2: &\quad \psi_{-2} = C_{u-u-} \\
s = -1: &\quad \psi_{-1} = C_{+-u-} = C_{uvu-} \\
s = 0 \;\; : &\quad \psi_0 = C_{v+-u} = \frac{1}{2}(C_{uvuv} + C_{uv+-}) = \frac{1}{2}(C_{+-+-} + C_{uv+-}), \\
s = 1 \;\; : &\quad \psi_1 = C_{vuv+} = C_{-+v+} \\
s = 2 \;\; : &\quad \psi_2 = C_{v+v+}
\end{aligned}$$

The 10 degrees of freedom of the Weyl tensor are encoded in 5 complex components labeled with ψ_s according to their spin-s behavior.

The interesting quantities are hence:

$$\begin{aligned}
s = -2: &\quad C_{u-u-} = C_{\mu\nu\sigma\rho} e_u^\mu e_-^\nu e_u^\sigma e_-^\rho = \psi_{-2} \\
s = -1: &\quad C_{+-u-} = C_{\mu\nu\sigma\rho} e_+^\mu e_-^\nu e_u^\sigma e_+^\rho = \psi_{-1} \\
s = 0 \;\; : &\quad C_{v+-u} = C_{\mu\nu\sigma\rho} e_v^\mu e_+^\nu e_u^\sigma e_-^\rho = \psi_0 \\
s = 1 \;\; : &\quad C_{-+v+} = C_{\mu\nu\sigma\rho} e_-^\mu e_+^\nu e_v^\sigma e_+^\rho = \psi_1 \\
s = 2 \;\; : &\quad C_{v+v+} = C_{\mu\nu\sigma\rho} e_u^\mu e_+^\nu e_v^\sigma e_+^\rho = \psi_2
\end{aligned}$$

where $C_{\mu\nu\sigma\rho}$ is the usual spacetime Weyl tensor and e_u^μ is the part of the Vielbein e_α^μ for which $\alpha = u$ or $\alpha = 1$. In four dimensions e_u^a is then a vector of four components and we have that $e_u^a = (\tau_u)^a$. A similar argument on the other components of the Vierbein leads to

$$\begin{aligned}
s = -2: &\quad C_{u-u-} = C_{\mu\nu\sigma\rho} (\tau_u)^\mu (\tau_-)^\nu (\tau_u)^\sigma (\tau_-)^\rho = \psi_{-2} \\
s = -1: &\quad C_{+-u-} = C_{\mu\nu\sigma\rho} (\tau_+)^\mu (\tau_-)^\nu (\tau_u)^\sigma (\tau_+)^\rho = \psi_{-1} \\
s = 0 \;\; : &\quad C_{v+-u} = C_{\mu\nu\sigma\rho} (\tau_v)^\mu (\tau_+)^\nu (\tau_u)^\sigma (\tau_-)^\rho = \psi_0 \\
s = 1 \;\; : &\quad C_{-+v+} = C_{\mu\nu\sigma\rho} (\tau_-)^\mu (\tau_+)^\nu (\tau_v)^\sigma (\tau_+)^\rho = \psi_1 \\
s = 2 \;\; : &\quad C_{v+v+} = C_{\mu\nu\sigma\rho} (\tau_u)^\mu (\tau_+)^\nu (\tau_v)^\sigma (\tau_+)^\rho = \psi_2.
\end{aligned}$$

For a better comparison with the existing literature on this topic, let us now rewrite the relevant quantities in the notation first introduced in the original article of Newman and Penrose [32]:

- The tetrad basis $(\tau_v, \tau_u, \tau_+, \tau_-)$ is renamed $(\mathfrak{l}, \mathfrak{n}, \mathfrak{m}, \bar{\mathfrak{m}})$ and we have

$$\begin{aligned}
&\mathfrak{l}^2 = \mathfrak{n}^2 = \mathfrak{m}^2 = \bar{\mathfrak{m}}^2 = 0 \\
&\mathfrak{l} \cdot \mathfrak{m} = \mathfrak{l} \cdot \bar{\mathfrak{m}} = \mathfrak{n} \cdot \mathfrak{m} = \mathfrak{n} \cdot \bar{\mathfrak{m}} = 0 \\
&\mathfrak{l} \cdot \mathfrak{n} = \mathfrak{m} \cdot \bar{\mathfrak{m}} = 1 \\
&g^{mn} = \mathfrak{l}^m \mathfrak{m}^n + \mathfrak{n}^m \mathfrak{l}^n + \mathfrak{m}^m \bar{\mathfrak{m}}^n + \bar{\mathfrak{m}}^m \mathfrak{m}^n
\end{aligned}$$

- The directive derivatives will be denoted by

$$\mathbb{D} = \nabla_{\mathfrak{l}} = \partial_v, \quad \mathbb{\Delta} = \nabla_{\mathfrak{n}} = \partial_u, \quad \mathfrak{\delta} = \nabla_{\mathfrak{m}} = \partial_+, \quad \bar{\mathfrak{\delta}} = \nabla_{\bar{\mathfrak{m}}} = \partial_-$$

- The convention on the scalars of the Weyl is not ψ_s but ψ_{s+2} so that

$$\psi_{-2} \to \psi_0, \quad \psi_{-1} \to \psi_1, \quad \psi_0 \to \psi_2, \quad \psi_1 \to \psi_3, \quad \psi_2 \to \psi_4,$$

- The decomposition of the Weyl into the five complex scalars then reads

$$\begin{aligned}
\psi_0 &= -C_{\mu\nu\sigma\rho}\mathfrak{l}^\mu\mathfrak{m}^\nu\mathfrak{l}^\sigma\mathfrak{m}^\rho \\
\psi_1 &= -C_{\mu\nu\sigma\rho}\mathfrak{l}^\mu\mathfrak{n}^\nu\mathfrak{l}^\sigma\mathfrak{m}^\rho \\
\psi_2 &= -C_{\mu\nu\sigma\rho}\mathfrak{l}^\mu\mathfrak{m}^\nu\bar{\mathfrak{m}}^\sigma\mathfrak{n}^\rho \\
\psi_3 &= -C_{\mu\nu\sigma\rho}\mathfrak{l}^\mu\mathfrak{n}^\nu\bar{\mathfrak{m}}^\sigma\mathfrak{n}^\rho \\
\psi_4 &= -C_{\mu\nu\sigma\rho}\mathfrak{n}^\mu\bar{\mathfrak{m}}^\nu\mathfrak{n}^\sigma\bar{\mathfrak{m}}^\rho
\end{aligned}$$

- The non-vanishing components of the tetrad connection are grouped into 12 objects called spin coefficient:

$$\begin{aligned}
\kappa = \Gamma_{131} \quad &, \quad \pi = -\Gamma_{241} \quad , \quad \epsilon = \frac{1}{2}(\Gamma_{121} - \Gamma_{341}) \\
\varrho = \Gamma_{134} \quad &, \quad \lambda = -\Gamma_{244} \quad , \quad \alpha = \frac{1}{2}(\Gamma_{124} - \Gamma_{344}) \\
\sigma = \Gamma_{133} \quad &, \quad \mu = -\Gamma_{243} \quad , \quad \beta = \frac{1}{2}(\Gamma_{123} - \Gamma_{343}) \\
\nu = \Gamma_{-242} \quad &, \quad \tau = \Gamma_{123} \quad , \quad \gamma = \frac{1}{2}(\Gamma_{122} - \Gamma_{342})
\end{aligned} \tag{4.1}$$

It is possible to write the Weyl tensor as the linear combination

$$\begin{aligned}
\frac{1}{4}C_{\mu\nu\sigma\rho} =& \psi_0 V_{\mu\nu}V_{\sigma\rho} - \psi_1(V_{\mu\nu}W_{\sigma\rho} + W_{\mu\nu}V_{\sigma\rho}) \\
&- \psi_2(U_{\mu\nu}V_{\sigma\rho} + V_{\mu\nu}U_{\sigma\rho} + W_{\mu\nu}W_{\sigma\rho}) \\
&- \psi_3(U_{\mu\nu}W_{\sigma\rho} + W_{\mu\nu}U_{\sigma\rho}) - \psi_4 U_{\mu\nu}U_{\sigma\rho} + c.c.
\end{aligned} \tag{4.2}$$

Where $U_{\mu\nu} = \mathfrak{l}_{[\mu}\mathfrak{m}_{\nu]}$, $V_{\mu\nu} = \bar{\mathfrak{m}}_{[\mu}\mathfrak{n}_{\nu]}$, $W_{\mu\nu} = \mathfrak{l}_{[\mu}\mathfrak{n}_{\nu]} - \bar{\mathfrak{m}}_{[\mu}\mathfrak{n}_{\nu]}$.
The study of the Weyl tensor and its complexified version led to Petrov's classification of vacuum spacetimes [33] (1954). The very same classification was also independently discovered by Felix Pirani in 1957. Black hole solutions are "type D" spacetimes in Petrov's classification, for which

$$\kappa = \sigma = \nu = \lambda = 0 \tag{4.3}$$

and

$$C_{\mu\nu\sigma[\rho}\mathfrak{l}_{\kappa]}\mathfrak{l}^{\nu}\mathfrak{l}^{\sigma} = C_{\mu\nu\sigma[\rho}\mathfrak{n}_{\kappa]}\mathfrak{n}^{\nu}\mathfrak{n}^{\sigma} = 0 \tag{4.4}$$

implying

$$\psi_0 = \psi_1 = \psi_3 = \psi_4 = 0 \tag{4.5}$$

This topic has been extensively studied by William Morris Kinnersley in his PhD thesis [34, 35] which was inspired by [36]. He found the explicit representation of the NP tetrad basis for D-type spacetimes (Namely, spacetime with two double principal null directions). A rotating black hole is described by the Kerr solution which is a Petrov D-type solution, and in Boyer-Lindquist coordinates (t, r, θ, φ) reads

$$\begin{aligned} ds^2 = &\left(1 - \frac{2Mr}{\Sigma}\right) dt^2 + \frac{4Mar\sin^2\theta}{\Sigma} dt d\varphi + \\ &- \frac{\Sigma}{\Delta} dr^2 - \Sigma d\theta^2 - \left(r^2 + a^2 + \frac{2Ma^2 r\sin^2\theta}{\Sigma}\right)\sin^2\theta d\varphi^2, \end{aligned} \tag{4.6}$$

where M is the hole mass, $a = J/M$ is the BH angular momentum, $\Delta = r^2 + a^2 - 2Mr$, and $\Sigma = r^2 a^2 \cos^2\theta$. This solution has an inner Cauchy horizon and an outer event horizon at $r = r_{\pm}$ ($\Delta(r_{\pm}) = 0$). For a spacetime described by the Kerr metric, we than have

$$\mathfrak{l} = \left(\frac{r^2 + a^2}{\Delta}, 1, 0, \frac{a}{\Delta}\right) \tag{4.7}$$

$$\mathfrak{n} = \frac{1}{2\rho^2}\left(r^2 + a^2, -\Delta, 0, a\right) \tag{4.8}$$

$$\mathfrak{m} = \frac{1}{2\bar{\rho}^2}\left(ia\sin\theta, 0, 1, i\csc\theta\right) \tag{4.9}$$

where $\bar{\rho} = r + ia\cos\theta$, and $\rho^2 = |\bar{\rho}|^2 = \bar{\rho}\bar{\rho}^*$.

4.2 Explicit example: the electromagnetic perturbation (s=1)

In the NP formalism, the Kinnersley tetrads, in particular the tetrad of the Kerr metric, opens the possibility of studying the general relativistic fields equations conveniently, being able to condense them into a single separable master equation: the Teukolsky equation. This section contains as an example

the derivation of the Teukolsky equation in the case of the spin-1 field. The general case is discussed in the next section. Let us now study explicitly the electromagnetic radiation in the NP formalism. Maxwell equations in vacuum read

$$\nabla_m F^{mn} = 0 \quad , \quad F_{[mn;p]} = \nabla_{[p} F_{mn]} = \nabla_p (\frac{1}{2} \epsilon_{mnuv} F^{uv}) = 0 \tag{4.10}$$

The 6 degrees of freedom of the electromagnetic tensor can be written in terms of the 3 complex NP scalars

$$\phi_0 = F_{\mu\nu} \mathfrak{l}^\mu \mathfrak{m}^\nu \quad , \quad \phi_1 = \frac{1}{2} F_{\mu\nu} (\mathfrak{l}^\mu \mathfrak{n}^\nu + \bar{\mathfrak{m}}^\mu \mathfrak{m}^\nu) \quad , \quad \phi_2 = F_{\mu\nu} \bar{\mathfrak{m}}^\mu \mathfrak{n}^\nu \tag{4.11}$$

Maxwell equations in the Kerr background then read

$$\mathbb{D}\phi_2 - \bar{\delta}\phi_1 = -\lambda\phi_0 + 2\pi\phi_1 + (\varrho - 2\epsilon)\phi_2 \tag{4.12}$$

$$\mathbb{\Delta}\phi_1 - \delta\phi_2 = \nu\phi_0 - 2\mu\phi_1 + (2\beta - \tau)\phi_2 \tag{4.13}$$

$$\mathbb{D}\phi_1 - \bar{\delta}\phi_0 = (\pi - 2\alpha)\phi_0 - 2\rho\phi_1 + \kappa\phi_2 \tag{4.14}$$

$$\mathbb{\Delta}\phi_0 - \delta\phi_1 = (2\gamma - \mu)\phi_0 - 2\tau\phi_1 + \sigma\phi_2). \tag{4.15}$$

The choice of the Kinnersley tetrad then guarantees that $\kappa = \sigma = \lambda = \nu = 0$, and therefore after explicit substitution of the spin coefficients,

$$\left(\mathbb{D} + \frac{1}{\bar{\rho}^*}\right)\phi_2 = \left(\bar{\mathfrak{\delta}} + \frac{2ia\sin\theta}{\sqrt{2}\bar{\rho}^{*2}}\right)\phi_2 \tag{4.16}$$

$$\left(\mathbb{\Delta} - \frac{\Delta}{\rho^2\bar{\rho}^*}\right)\phi_1 = \left(\mathfrak{\delta} + \frac{1}{\sqrt{2}\bar{\rho}}\left(\cot\theta - \frac{ia\sin\theta}{\bar{\rho}^*}\right)\right)\phi_2 \tag{4.17}$$

$$\left(\mathbb{D} + \frac{2}{\bar{\rho}^*}\right)\phi_1 = \left(\bar{\mathfrak{\delta}} + \frac{1}{\sqrt{2}\bar{\rho}^*}\left(\cot\theta - \frac{ia\sin\theta}{\bar{\rho}^*}\right)\right)\phi_0 \tag{4.18}$$

$$\left(\mathbb{\Delta} - \frac{\Delta}{\rho^2}\left(\frac{1}{\bar{\rho}^*} - \frac{2(r-M)}{\Delta}\right)\right)\phi_0 = \left(\mathfrak{\delta} + \frac{2ia\sin\theta}{\sqrt{2}\bar{\rho}\bar{\rho}^*}\right)\phi_1. \tag{4.19}$$

The stationarity and axial symmetry of the Kerr metric allow for a wave decomposition of the form $\phi_j \sim e^{-i\omega t} e^{im\varphi}$. Therefore, the differential operators $\mathbb{D}, \mathbb{\Delta}, \mathfrak{\delta}$, and $\bar{\mathfrak{\delta}}$ must involve the radial coordinate and the remaining angular coordinate. One can verify that $\mathbb{D}$ and $\mathbb{\Delta}$ are radial operators and δ and $\bar{\delta}$ are

angular operators. In fact,

$$\mathbb{D} = \mathcal{D}_0, \quad \mathbb{\Delta} = -\frac{\Delta}{2\rho^2}\mathcal{D}_0^\dagger, \quad \mathfrak{d} = \frac{1}{\sqrt{2}\bar{\rho}}\mathcal{L}_0^\dagger, \quad \bar{\mathfrak{d}} = \frac{1}{\sqrt{2}\bar{\rho}^*}\mathcal{L}_0$$

where

$$\mathcal{D}_n = \partial_r + 2n\frac{r-M}{\Delta} - \frac{iK}{\Delta} \qquad \mathcal{D}_n^\dagger = \partial_r + 2n\frac{r-M}{\Delta} + \frac{iK}{\Delta} \tag{4.20}$$

$$\mathcal{L}_n = \partial_\theta + n\cot\theta - Q \qquad \mathcal{L}_n^\dagger = \partial_\theta + n\cot\theta + Q \tag{4.21}$$

and $K = (r^2 + a^2)\omega - ma$, $Q = a\omega\sin\theta - m\cot\theta$.
Useful properties of the operators $\mathcal{D}_n$ and $\mathcal{L}_n$ valid for any integer number n, p, and q are

$$\mathcal{D}_n\Delta = \Delta\mathcal{D}_{n-1} \tag{4.22}$$

$$\mathcal{L}_n\sin\theta = \sin\theta\mathcal{L}n + 1 \tag{4.23}$$

$$\left(\mathcal{D}_n + \frac{q}{\bar{\rho}^*}\right)\frac{1}{\bar{\rho^*}^p} = \frac{1}{\bar{\rho^*}^p}\left(\mathcal{D}_n + \frac{q-p}{\bar{\rho}^*}\right) \tag{4.24}$$

$$\left(\mathcal{L}_n + \frac{iaq\sin\theta}{\bar{\rho}^*}\right)\frac{1}{\bar{\rho^*}^p} = \frac{1}{\bar{\rho^*}^p}\left(\mathcal{L}_n + \frac{i(q-p)a\sin\theta}{\bar{\rho}^*}\right) \tag{4.25}$$

$$\left(\mathcal{D}_n + \frac{q}{\bar{\rho}^*}\right)\left(\mathcal{L}_n + \frac{iaq\sin\theta}{\bar{\rho}^*}\right) = \left(\mathcal{L}_n + \frac{iaq\sin\theta}{\bar{\rho}^*}\right)\left(\mathcal{D}_n + \frac{q}{\bar{\rho}^*}\right) \tag{4.26}$$

$$\tag{4.27}$$

Defining

$$\Phi_0 = \phi_0, \qquad \Phi_1 = \sqrt{2}\bar{\rho}^*\phi_1, \qquad \Phi_2 = 2\bar{\rho^*}^2\phi_2 \tag{4.28}$$

it is possible to rewrite Maxwell's equations as

$$\left(\mathcal{D}_0 - \frac{1}{\bar{\rho}^*}\right)\Phi_2 = \left(\mathcal{L}_0 + \frac{ia\sin\theta}{\bar{\rho}^*}\right)\Phi_1 \tag{4.29}$$

$$\Delta\left(\mathcal{D}_0^\dagger + \frac{1}{\bar{\rho}^*}\right)\Phi_1 = \left(\mathcal{L}_1^\dagger - \frac{ia\sin\theta}{\bar{\rho}^*}\right)\Phi_2 \tag{4.30}$$

$$\left(\mathcal{D}_0 + \frac{1}{\bar{\rho}^*}\right)\Phi_1 = \left(\mathcal{L}_0 - \frac{ia\sin\theta}{\bar{\rho}^*}\right)\Phi_0 \tag{4.31}$$

$$\Delta\left(\mathcal{D}_0^\dagger - \frac{1}{\bar{\rho}^*}\right)\Phi_0 = \left(\mathcal{L}_0^\dagger + \frac{ia\sin\theta}{\bar{\rho}^*}\right)\Phi_1. \tag{4.32}$$

After some manipulation, exploiting the properties of the differential operators, it is possible to gain further simplification by eliminating Φ_1, and obtaining

$$\left(\Delta\mathcal{D}_1\mathcal{D}_1^\dagger + \mathcal{L}_0^\dagger\mathcal{L}_1 + 2i\omega(r + ia\cos\theta)\right)\Phi_0 = 0 \tag{4.33}$$

$$\left(\Delta\mathcal{D}_0^\dagger\mathcal{D}_0 + \mathcal{L}_0\mathcal{L}_1^\dagger - 2i\omega(r + ia\cos\theta)\right)\Phi_2 = 0 \tag{4.34}$$

The two quantities Φ_0 and Φ_2 are related to the spin ±1 components of the Maxwell tensor (the same way ψ were related to the spin of components of the Weyl tensor). It is then reasonable to separate the radial and angular variables as $\Phi_0 = R_{+1}(r)S_{+1}(\theta)$ and $\Phi_2 = R_{-1}(r)S_{-1}(\theta)$ such that

$$\left(\Delta\mathcal{D}_0\mathcal{D}_0^\dagger + 2i\omega r\right)\Delta R_{+1} = \lambda\Delta R_{+1} \tag{4.35}$$

$$\left(\Delta\mathcal{D}_0^\dagger\mathcal{D}_0 - 2i\omega r\right)R_{-1} = \hat{\lambda}R_{-1} \tag{4.36}$$

$$\left(\mathcal{L}_0^\dagger\mathcal{L}_1 - 2a\omega\cos\theta\right)S_{+1} = -\hat{\lambda}S_{+1} \tag{4.37}$$

$$\left(\mathcal{L}_0\mathcal{L}_1^\dagger + 2a\omega\cos\theta\right)S_{-1} = -\hat{\lambda}S_{-1} \tag{4.38}$$

where $\hat{\lambda}$ is the separation constant, which must be real. One may also obtain the equations relating spin plus and minus functions called Teukolsky-Starobinsky identities. Equations (4.33) and (4.34) can be rewritten as special cases ($s = \pm1$) of

$$\begin{aligned}&\frac{1}{\Delta^s}\partial_r(\Delta^{s+1}\partial_r\Upsilon_s) + \frac{1}{\sin\theta}\partial_\theta(\sin\theta\partial_\theta\Upsilon_s) - \left(\frac{(r^2+a^2)^2}{\Delta} - a^2\sin^2\theta\right)\partial_t^2 + \\ &- \frac{4Mar}{\Delta}\partial_t\partial_\varphi\Upsilon_s - \left(\frac{a^2}{\Delta} - \frac{1}{\sin^2\theta}\right)\partial_\varphi^2\Upsilon_s + 2s\left(\frac{M(r^2-a^2)}{\Delta} - r - ia\cos\theta\right)\partial_t\Upsilon_s + \\ &+ 2s\left(\frac{a(r-M)}{\Delta} + \frac{i\cos\theta}{\sin^2\theta}\right)\partial_\varphi\Upsilon_s - (s^2\cot^2\theta - s)\Upsilon_s = 0\end{aligned} \tag{4.39}$$

[37–41], where $\Upsilon_s = e^{-i\omega t}e^{im\varphi}\upsilon_s(r,\theta)$ and $\upsilon_s = R_s(r)S_s(\theta)$ with υ_{+1} and υ_{-1} corresponding to Φ_0 and Φ_2 respectively.

4.3 General case: The Teukolsky equation

The line of reasoning employed in the previous section can be extended to any value of the field spin. The electromagnetic and gravitational perturbations

are rigorously discussed in [37–41]. The calculations for the spin-1/2 field are described in [38,42–46]. It has to be noticed that prior to these studies the NP formalism had been applied to the spin-1/2 field without deriving the master equation in [47], while [48] considered the spin-1 case reaching a single second order partial differential equation which they considered non-separable. In the case of a scalar field, the NP scalar is the field itself [49,50]. Finally, references for the Rarita-Schinger perturbation in the Kerr background can be found in [51–59] and considerations regarding different spin fields can be found in several textbooks and articles [60–64].

Despite the different equations governing the dynamics of massless (test) fields in curved spacetime, in the case of the Kerr metric a unified description can be obtained with the aid of the Newman-Penrose (NP) formalism [32, 35, 36], and one can condense all these equations into the so-called Teukolsky master equation, which in Boyer-Lindquist coordinates reads exactly as (4.39), where the functions Υ_s encode the NP scalars, obtained by contraction of the original tensor fields with the Kinnersley tetrad null vectors [35]. This equation thus encodes the dynamics of Klein-Gordon scalar fields ($s = 0$), Weyl fermions ($s = \pm 1/2$), vector fields ($s = \pm 1$), Rarita-Schwinger fields ($s = 3/2$) and gravitational perturbations ($s = \pm 2$) in the massless limit. Moreover, the Teukolsky equation can be solved by the separation of variables, with the NP scalars admitting a mode decomposition of the form:

$$\Upsilon_s = \sum e^{-i\omega t} e^{im\varphi} S_s(\theta) R_s(r) \ , \tag{4.40}$$

where ω is the perturbation frequency, m is the azimuthal angular momentum quantum number. Υ_s represents a general perturbation of spin s and it is defined by the NP-scalars relative to the respective perturbation. Namely, the NP-scalars involved in the definition of Υ_s are ϕ, $\chi_{0,1}$, $\phi_{0,2}$, $\Omega_{0,3}$, $\psi_{0,4}$ for spin 0, 1/2, 1, 3/2, 2 respectively and they compine according to Tab. 4.1 in the definition of Υ_s.

Υ_s	s
ϕ	0
χ_0	+1/2
$\rho^{-1}\chi_1$	-1/2
ϕ_0	+1
$\rho^{-2}\phi_2$	-1
Ω_0	+3/2
$\rho^{-3}\Omega_3$	-3/2
ψ_0	+2
$\rho^{-4}\psi_4$	-2

Table 4.1: Newman-Penrose scalars.

The angular functions $S_s(\theta)$ are the so-called spin-weighted spheroidal harmonics, which satisfy the equation [65–68]

$$\frac{1}{\sin\theta}\partial_\theta\left(\sin\theta\ \ \partial_\theta S_s\right) + \left(a^2\omega^2\cos^2\theta - \frac{m^2}{\sin^2\theta} - 2a\omega s\cos\theta + \right. \tag{4.41}$$
$$\left. -\frac{2ms\cos\theta}{\sin^2\theta} - s^2\cot^2\theta + s + {}_sA_l^m\right) S_s = 0\ .$$

These functions reduce to scalar spherical harmonics for $s = 0$ and $a = 0$, and generalize conventional spin-weighted spherical harmonics to the more general case of axial symmetry. ${}_sA_l^m = {}_sA_l^m(a\omega)$ are the eigenvalues of (4.41) and cannot be expressed analytically in terms of the spherical angular momentum quantum numbers l, m. Nevertheless, for $a\omega \ll 1$ they can be computed using a perturbative expansion [68], yielding:

$$\begin{aligned}
{}_sA_l^m(a\omega) &= l(l+1) - s(s+1) - a\omega\frac{2ms^2}{l(l+1)} \\
&+ (a\omega)^2\left\{\frac{2}{3}\left[1 + \frac{3m^2 - l(l+1)}{(2l-1)(2l+3)}\right] - \frac{2s^2}{l(l+1)}\frac{3m^2 - l(l+1)}{(2l-1)(2l+3)}\right. \\
&+ \left. 2s^2\left[\frac{(l^2-s^2)(l^2-m^2)}{l^3(2l-1)(2l+1)} - \frac{[(l+1)^2-m^2][(l+1)^2-s^2]}{(l+1)^3(2l+1)(2l+3)}\right]\right\} \\
&+ \mathcal{O}\left[(a\omega)^3\right]\ .
\end{aligned} \tag{4.42}$$

The functions R_s are the radial part of the NP scalars and satisfy the radial

equation

$$\Delta^{-s}\partial_r(\Delta^{s+1}\partial_r R_s)+((K^2-2is(r-M)K)\Delta^{-1}+4is\omega r-{}_sQ_l^m)R_s=0\ , \quad (4.43)$$

where ${}_sQ_l^m={}_sA_l^m+a^2\omega^2-2a\omega m$ and $K=(r^2+a^2)\omega-ma$. These functions take the following form far away and near the BH horizon:

$$R_s\sim R_s^{in}\frac{e^{-i\omega r_*}}{r}+R_s^{out}\frac{e^{i\omega r_*}}{r^{2s+1}}\ , \quad r\gg r_+ \quad (4.44)$$

$$R_s\sim R_s^{hole}\Delta^{-s}e^{-ikr_*}\ , \quad r\sim r_+ \quad (4.45)$$

where r_* is the tortoise coordinate, defined via $dr_*/dr=(r^2+a^2)/\Delta$, and we have imposed in-going boundary conditions at the horizon such that we have no outgoing radiation from the black hole. We note that the solutions R_s and R_{-s} for the same spin are, in general, distinct, but are nevertheless related through the Teukolsky-Starobinsky identities [69, 71–74] that can be derived from the original field equations:

$$\Delta^s(\mathcal{D}^\dagger)^{2s}\Delta^s R_s=C_s^*R_{-s}\ , \quad (4.46)$$

$$(\mathcal{D})^{2s}R_{-s}=C_sR_s\ , \quad (4.47)$$

where $\mathcal{D}=\partial_r-i\frac{K}{\Delta}$. The Starobinsky constants C_s (omitting the l,m quantum numbers for simplicity) for the fields of interest are given by:

$$C_0^2=1 \quad (4.48)$$

$$C_{1/2}^2=Q_{1/2}+\frac{1}{4} \quad (4.49)$$

$$C_1^2=Q_1^2+-4a^2\omega^2-2a\omega m \quad (4.50)$$

$$C_{3/2}^2=\left(Q_{3/2}+\frac{3}{4}\right)\left(Q_{3/2}+\frac{1}{4}\right)-16a^2\omega^2\left(Q_{3/2}-\frac{7}{4}\right)+16am\omega\left(Q_{3/2}-\frac{3}{4}\right) \quad (4.51)$$

$$|C_2|^2=(Q_2^2+4a\omega m-4a^2\omega^2)((Q_2-2)^2+36a\omega m-36a^2\omega^2)+ \quad (4.52)$$
$$+(2Q_2-1)(96a^2\omega^2-48a\omega m)+144\omega^2(M^2-a^2)\ .$$

Note that $C_0, C_{1/2}, C_1$, and $C_{3/2}$ are real, while C_2 is complex.
Through the redefinition $Y_s=\Delta^{s/2}(r^2+a^a)^{1/2}R_s$ we may also write (4.43) in

a Schrödinger-like form:

$$(\partial^2_{r_*} - V(r_*))Y_s = 0 \ , \tag{4.53}$$

where the effective potential $V = {}_sV^m_l$ vanishes both at the horizon, where $r_* \to -\infty$, and at infinity, for $r_* \to +\infty$. The form of Eq. (4.53) guarantees that the Wronskian does not change if calculated at different radial positions. In particular, there is a conserved current:

$$\left[Y^*_{-s}\partial_{\tilde{r}}Y_s - Y_s\partial_{\tilde{r}}Y^*_{-s}\right]_{r=r_+} = \left[Y^*_{-s}\partial_{\tilde{r}}Y_s - Y_s\partial_{\tilde{r}}Y^*_{-s}\right]_{r=\infty} . \tag{4.54}$$

Substituting the asymptotic and near-horizon solutions in the Teukolsky-Starobinsky identities yields the relations between $R_{+|s|}$ and $R_{-|s|}$, while (4.54) yields an energy conservation law.

It is possible to investigate the scattering problem. Namely, to radially send a wave from infinity to the event horizon and calculate what is scattered back to infinity due to the potential V, and what is transmitted and falls into the event horizon. This way one obtains the transmission coefficient for each (l, m)-mode of the wave with spin s as a function of the energy of the wave for a given spin of the BH. It is worth noticing that the computed transmission coefficient has to be the same if one imagines the reverse scattering problem in which a wave emerges from the event horizon and is scattered back and transmitted to infinity. As we will explain in the next chapter, this is the picture that an observer at infinity would draw by observing an evaporating BH. In the wave scattering problem, the transmission coefficient is given by the ratio between the energy flux into the BH horizon and the incoming energy flux at infinity:

$$\Gamma = \frac{dE_{hole}/dt}{dE_{in}/dt} \ . \tag{4.55}$$

These energy fluxes can be computed from the form of the energy-momentum tensor for each field as described in [38,40,70]. As said, this transmission coefficient depends on the frequency, spin, and angular momentum quantum numbers of each field mode, as well as on the BH spin parameter, $\Gamma = {}_s\Gamma^l_m(a, \omega)$. In the context of Hawking emission, it usually takes the name of gray-body factor, since it quantifies the filtering of field modes by the BH effective potential as they propagate away from the event horizon.

4.3.1 Numerical computation of gray-body factors

Transmission coefficients can be computed analytically only under very stringent approximations [71–73, 75–80], so numerical methods are in general required to compute them for different wave modes. Here, we will use a shooting method similar to the one employed in i.e. [70] and first used to calculate the quasi-normal modes of the Schwarzschild black hole by Chandrasekhar and Detweiler in 1975 [81]. The first step is to write Eq. (4.43) in terms of the re-scaled radial coordinate $x = (r - r_+)/r_+$:

$$x^2(x+\tau)^2\partial_x^2 R(x) + (s+1)(2x+\tau)x(x+\tau)\partial_x R(x) + V(x)R(x) = 0 \ , \quad (4.56)$$

where the effective radial potential can be written as:

$$V(x) = k^2 - is(2x+\tau)k + (4is\omega(x+1) - Q_s^{l,m})x(x+\tau) \ , \quad (4.57)$$

where $k = (2-\tau)(\omega - m\Omega_H)r_+ + x(x+2)\omega r_+$, Ω_H is the angular velocity of the black hole horizon and $\tau = (r_+ - r_-)/r_+$. Imposing ingoing boundary conditions at the horizon, the near-horizon solutions of Eq. (4.56) can then be expressed in a Taylor expansion [70, 82] of the form

$$R(x) = x^{-s-i\varpi/\tau}\sum_{n=0}^{\infty} a_n x^n, \quad (4.58)$$

where $\varpi = (2-\tau)(\omega - m\Omega_H)r_+$ and the coefficients a_n can be determined by substituting the power series (4.58) into (4.56) and solving iteratively the resulting algebraic equations. The near-horizon solution is then used as a boundary condition for numerically integrating the radial Teukolsky equation up to large distances, where the general form of the solution is known and reads:

$$R(x) \to \frac{{}_sR_{in}^{lm}}{r_+}\frac{e^{-i\bar{\omega}x}}{x} + \frac{{}_sR_{out}^{lm}}{r_+^{2s+1}}\frac{e^{i\bar{\omega}x}}{x^{2s+1}} \ , \quad (4.59)$$

where $\bar{\omega} = \omega r_+$. It is then possible to extract the coefficient ${}_sR_{in}^{lm}(\omega)$ in order to evaluate the transmission coefficient. The normalization of the scattering problem is set by i.e. $a_0 = 1$ which is equivalent to

$$|{}_sR_{hole}^{lm}|^2 = (2r_+)^{2s}(a^2 - M^2)^2 \ . \quad (4.60)$$

This then yields the transmission coefficients for the different spin fields:

$$\Gamma_0^{lm} = \frac{\varpi}{\bar{\omega}} |_0 R_{in}^{lm}|^{-2} \tag{4.61}$$

$$\Gamma_{1/2}^{lm} = \tau |_{1/2} R_{in}^{lm}|^{-2} \tag{4.62}$$

$$\Gamma_1^{lm} = \frac{\tau^2 \bar{\omega}}{\varpi} |_1 R_{in}^{lm}|^{-2} \tag{4.63}$$

$$\Gamma_{3/2}^{lm} = \frac{\tau^3 \bar{\omega}^2}{(\varpi^2 + \tau^2/16)} |_{3/2} R_{in}^{lm}|^{-2} \tag{4.64}$$

$$\Gamma_2^{lm} = \frac{\tau^4 \bar{\omega}^3}{\varpi(\varpi^2 + \tau^2/4)} |_2 R_{in}^{lm}|^{-}2 \ , \tag{4.65}$$

or, in a more compact way,

$$\Gamma_s^{lm} = \delta_s |_s R_{in}^{lm}|^{-2} \tag{4.66}$$

with

$$\delta_s = -ie^{i\pi s} \bar{\omega}^{(2s-1)} \left(\frac{1}{2}\right)^{1-2s} \frac{\Gamma(1 - s + i2\frac{\varpi}{\tau})}{\Gamma(s + i2\frac{\varpi}{\tau})} \tau \ . \tag{4.67}$$

We applied this method and numerically calculated the Γ_s^{lm} for the different values of the spin of the field up to the modes $l = 4$ ($l = 7/2$) included for bosons (fermions) by solving (4.56) with $Q_s^{l,m}$ and (4.58) up to the fifth order, for different values of the BH spin by taking 600 equally distributed points between $\omega r_+ = 0$ and $\omega r_+ = 2.4$. This maximum frequency is sufficiently large so that all relevant transmission coefficients for our calculations are already close to unity. In addition, higher frequency modes are Boltzmann-suppressed in the calculation of the Hawking emission spectra as we will see in the next chapter.

It has to be noted that the gray-body factors are computed for massless fields. In principle, this can also be done for massive fields, but given that the emission of particles with masses, m, above the Hawking temperature (see next chapter) $T_H = \kappa/2\pi \simeq 1\,\mathrm{GeV}(10^{10}\mathrm{kg}/M)$ is exponentially suppressed we will work in the approximation where particles are considered massless for $T_H > m$ and are otherwise absent from the emission spectrum.

In chapter 9, Fig. 9.18 shows some examples of gray-body factors for a spin-1 massless field as a function of $\bar{\omega}$. Fig. 9.18 also shows that the transmission coefficient is negative when $\omega < m\Omega_H$. Only bosons are characterized by the possibility of having negative transmission coefficients that we can interpret

as stimulated emission. The phenomenon takes the name of superradiance and may lead to instabilities as it is discussed in the next chapter.

5 Hawking radiation

In curved spacetime, different observers do not necessarily agree in their definition of what is the quantum vacuum state, i.e. the state with the lowest possible energy. This is due to the use of different time coordinates to perform the separation between the positive and negative frequency modes that underlie the field quantization procedure. While in flat Minkowski space, all inertial observers perform this mode separation in an equivalent way due to Lorentz invariance, in spacetime manifolds that include regions with non-negligible curvature, particularly event horizons, this is typically not the case.

In particular, Hawking showed in 1974 [83,84] that a stationary (and therefore non-inertial) observer standing far away from a BH horizon will measure an outgoing flux of particles with a nearly thermal spectrum if the associated quantum field is in the vacuum state as defined by an observer freely falling into the BH, or equivalently the vacuum state as defined in the asymptotic past well before the collapsing matter formed the BH. He took into account the collapse of gas and the consequent formation of an event horizon and counted the accessible frequencies before and after the formation of the horizon. This Hawking radiation is, therefore, a purely gravitational effect, such that a BH essentially emits all the particle degrees of freedom related to the temperature characterizing the radiation, called Hawking temperature, $T_H \simeq M_P^2/8\pi M$, where $M_P = \sqrt{\hbar c/G} \sim 2.17645 \times 10^{-8}$ kg is the Plank mass, for a slowly rotating BH. In practice, all the particle species with masses below the Hawking temperature are emitted. In this process only the BH and the Hawking radiation are involved, so, imposing the conservation of the energy one concludes that the radiation is emitted at the expense of the mass and angular momentum of the BH (as measured by an asymptotic observer), thus leading to its evaporation.

This chapter does not follow Hawking's original idea. Nonetheless, we will de-

rive the Hawking radiation using the Bogoliubov transformations. We will see that the concept of vacuum is not generally invariant, and define the Unruh and Hawking effects in (1+1)-dimensions. We will outline the theoretical aspects of BH evaporation, emission, and superradiance.

5.1 The Bogoliubov transformations

As said, different observers in curved spacetime do not necessarily agree on the definition of the quantum vacuum state, i.e. the state with the lowest possible energy. This is due to the use of different proper time definitions they will adopt in performing the separation between positive and negative frequency modes, a procedure at the base of the field quantization process. In Minkowski spacetime the Lorentz transformations ensure that all inertial observers perform this mode separation equivalently, writing the creation operators of one observer as a linear combination of creation operators of another observer (and the same holds true for the annihilation operators). This is not the case if accelerations are involved or if spacetime has a non-negligible curvature.
The elements of the proper, orthocronous Lorentz group $SO^+(1,3)$ link inertial observers describing the manifold according to the Minkowski metric. Given two inertial observers, Alice and Bob, we want to describe their creation and annihilation operators in the simplest relativistic quantum theory: a massless and minimally coupled scalar field. The difference in the two descriptions lies in how the Lorentz transformations change the operators. Elements of $SO^+(1,3)$ do not change the sign of the frequencies associated with creation/annihilation operators used for defining the quantum field. As a result, the annihilation operators of Bob correspond to a linear combination of the annihilation operators of Alice, and vice versa

$$\hat{b}_{\vec{k}'} = \int \hat{a}_{\vec{k}} n_{\vec{k},\vec{k}'} d^3k, \tag{5.1}$$

$$\hat{a}_{\vec{k}} = \int \hat{b}_{\vec{k}'} n^*_{\vec{k}',\vec{k}} d^3k', \tag{5.2}$$

and the very same can be said about the creation operators. This implies that Alice and Bob will agree on the vacuum definition:

$$\hat{b}_{\vec{k}'}|0\rangle = \hat{a}_{\vec{k}}|0\rangle = 0. \tag{5.3}$$

Let us now consider two observers experimenting with different acceleration in a Minkowskian spacetime or locally equivalently to two observers in different positions in a gravitational field. Such observers are linked by transformations belonging to a group much larger than $SO^+(1,3)$: the general linear group, $GL(1,3)$. One may reproduce the previous steps: considering a minimally coupled massless scalar field for Alice and Bob, and writing the creation/annihilation operators of one observer as a linear combination of creation/annihilation operators of the other. As a result, one finds that the elements of $GL(1,3)$ may map positive frequencies into negative and vice versa. This means that in general the creation/annihilation operators of one observer are given by a linear combination of both creation and annihilation operators of the other according to:

$$\hat{b}_{\vec{k}'} = \int \left(\hat{a}_{\vec{k}} A^*_{\vec{k},\vec{k}'} - \hat{a}^\dagger_{\vec{k}} B^*_{\vec{k},\vec{k}'} \right) d^3k \tag{5.4}$$

$$\hat{a}_{\vec{k}} = \int \left(\hat{b}_{\vec{k}'} A_{\vec{k},\vec{k}'} + \hat{b}^\dagger_{\vec{k}'} B^*_{\vec{k},\vec{k}'} \right) d^3k'. \tag{5.5}$$

These are the famous Bogoliubov transformations and entail a profound consequence: Alice and Bob will disagree on the vacuum definition! They will be defined respectively as:

$$|0_A\rangle : \quad \hat{a}_{\vec{k}} |0_A\rangle = 0 \quad \forall \vec{k} \tag{5.6}$$

$$|0_B\rangle : \quad \hat{b}_{\vec{k}'} |0_B\rangle = 0 \quad \forall \vec{k}' \tag{5.7}$$

and we have that:

$$\langle 0_A | \hat{b}_{\vec{k}'} \hat{b}^\dagger_{\vec{k}'} | 0_A \rangle = \int |B_{\vec{k},\vec{k}'}|^2 d^3k \tag{5.8}$$

$$\langle 0_B | \hat{a}_{\vec{k}} \hat{a}^\dagger_{\vec{k}} | 0_B \rangle = \int |A_{\vec{k},\vec{k}'}|^2 d^3k'. \tag{5.9}$$

In a more refined way, it is possible to say that the concept of vacuum is not generally covariant.
The normalization of the operators imposes that

$$[\hat{a}_{\vec{k}}, \hat{a}^\dagger_{\vec{k}'}] = \delta^3(\vec{k} - \vec{k}') \tag{5.10}$$

and implies the normalization of the Bogoliubov coefficients:

$$\delta^3(\vec{k}-\vec{k}') = \int \left(A_{\vec{k},\vec{k}''} A^*_{\vec{k}',\vec{k}''} + B^*_{\vec{k},\vec{k}''} B_{\vec{k}',\vec{k}''} \right) d^3k'' \tag{5.11}$$

5.2 The Unruh effect

Let us consider a $1+1$ flat spacetime in which we have an inertial observer, and a Rindler observer, i.e. an observer moving at a constant acceleration α with respect to the inertial one. The line elements of the two observers read

$$ds^2 = -dT^2 + dX^2 \tag{5.12}$$

$$ds^2 = e^{2x\alpha}(-dt^2 + dx^2). \tag{5.13}$$

These two line elements are related by a conformal transformation so that the consequent massless, minimally coupled Klein-Gordon equation is given by

$$(-\partial_T^2 - \partial_X^2)\phi = (-\partial_t^2 + \partial_x^2)\phi = 0. \tag{5.14}$$

It is possible to write the field in terms of plane waves for the two observers

$$\phi = \int \frac{d\Omega}{2\pi}(\hat{a}_\Omega f_\Omega + \hat{a}^\dagger_\Omega f^*_\Omega) \tag{5.15}$$

$$\phi = \int \frac{d\omega}{2\pi}(\hat{b}_\omega g_\omega + \hat{b}^\dagger_\omega g^*_\omega), \tag{5.16}$$

where

$$f_\Omega = \frac{e^{i(-\Omega T + KX)}}{\sqrt{4\pi\Omega}} = \frac{e^{-i\Omega(T-X)}}{\sqrt{4\pi\Omega}} = \frac{e^{-i\Omega U}}{\sqrt{4\pi\Omega}} \tag{5.17}$$

$$g_\omega = \frac{e^{i(-\omega t + kx)}}{\sqrt{4\pi\omega}} = \frac{e^{-i\omega(t-x)}}{\sqrt{4\pi\omega}} = \frac{e^{-i\omega u}}{\sqrt{4\pi\omega}}, \tag{5.18}$$

since $\Omega = K$ and $\omega = k$. It is understood that all the considerations regarding the Bogoliubov transformations hold, in particular

$$g_\omega = \int_0^\infty d\Omega(A_{\omega\Omega} f_\Omega + B_{\omega\Omega} f^*_\Omega) = \int_0^\infty \frac{d\Omega}{\sqrt{4\pi\Omega}}(A_{\omega\Omega} e^{-i\Omega U} + B_{\omega\Omega} e^{i\Omega U}) = g_\omega(U) \tag{5.19}$$

It is possible to express this last quantity as a Fourier transform

$$g_\omega(U) = \frac{1}{2\pi}\int_0^\infty \tilde{g}_\omega(-W)e^{iWU}dW + \frac{1}{2\pi}\int_0^\infty \tilde{g}_\omega(W)e^{-iWU}dW \qquad (5.20)$$

and identify $A_{\omega\Omega} = \sqrt{\frac{\Omega}{\pi}}\tilde{g}_\omega(\Omega)$ and $B_{\omega\Omega} = \sqrt{\frac{\Omega}{\pi}}\tilde{g}_\omega(-\Omega)$.
Considering the line elements in light-cone coordinates $ds^2 = dUdV = e^{2x\alpha}(dudv)$ it is easy to obtain

$$U = -\alpha^{-1}e^{\alpha u} \quad ; \quad u = \alpha^{-1}ln[-\alpha U] \qquad (5.21)$$

and the relations

$$g_\omega(U) = \frac{1}{\sqrt{4\pi\omega}}e^{-i\frac{\omega}{\alpha}ln[-\alpha U]} \quad if \quad U < 0, \qquad (5.22)$$

$$g_\omega(U) = 0 \quad if \quad U > 0, \qquad (5.23)$$

hold.
Using the inverse Fourier transformation one has

$$\tilde{g}_\omega(-\Omega) = \int_{-\infty}^{\infty} g_\omega(U)e^{-i\Omega U}dU = \frac{1}{\sqrt{4\pi\omega}}\int_{-\infty}^{0} e^{-i\frac{\omega}{\alpha}ln[-\alpha U]}e^{-i\Omega U}dU \qquad (5.24)$$

It is possible to solve this integral by exploiting the residue theorem and the fact that the logarithmic function of a complex argument is multi-valued, obtaining:

$$\tilde{g}_\omega(-\Omega) = -e^{-\frac{\omega}{\alpha}\pi}\tilde{g}_\omega(\Omega) \qquad (5.25)$$

Eq (5.25) allows to set the important relation $A_{\omega\Omega} = -B_{\omega\Omega}e^{\frac{\omega}{\alpha}\pi}$.
Using Eqs. (5.8) and (5.11) one then arrives at

$$\langle 0_A|\hat{b}_{\vec{k}'}\hat{b}^\dagger_{\vec{k}'}|0_A\rangle = \langle\hat{N}_b\rangle = \int |B_{\vec{k},\vec{k}'}|^2 d^3\vec{k} = \frac{\delta^3(0)}{(e^{2\frac{\omega}{\alpha}\pi}-1)}. \qquad (5.26)$$

Equation (5.26) represents the number of particles that one observer measures when the other measures the vacuum. This is a divergent quantity due to the presence of a δ. This is a sign that we are considering an infinite volume space. The constant and meaningful quantity is the particle number density

that takes the value

$$n_b = \frac{1}{(e^{2\frac{\omega}{\alpha}\pi} - 1)}. \tag{5.27}$$

Equation (5.27) represents manifestly a Bose-Einstein statistics corresponding to a thermal bath at the Unruh temperature:

$$T_U = \frac{\alpha}{2\pi} = \frac{\hbar\alpha}{2\pi c k_B}. \tag{5.28}$$

It is possible to obtain the number density of the Fermi-Dirac statistics by imposing anti-commutation relations in the definition of the Bogoliubov transformations.

To underline the relation between the Unruh and Hawking effects it is worth emphasizing that the acceleration of the Rindler observer causes the formation of an apparent horizon the closer to the observer the higher the magnitude of the acceleration.

5.3 The Hawking effect

Let us consider the non-flat situation where a BH is present, and let us analyze the $(1+1)$ dimensions case. We aim to explore how an observer at an infinite distance will regard the vacuum defined by an observer free-falling near the horizon. For this reason, we consider the $(1+1)$ Schwarzschild geometry with Schwarzschild radius in Planck units, $r_S = 2M$

$$ds^2 = -\left(1 - \frac{r_S}{r}\right) dt^2 + \left(1 - \frac{r_S}{r}\right)^{-1} dr^2 \tag{5.29}$$

and we rewrite it into two different coordinate systems: the tortoise coordinates are good for describing an observer at a fixed radial position

$$ds^2 = \left(1 - \frac{r_S}{r}\right)(-dt^2 + dx^2) \xrightarrow{r\to\infty} (-dt^2 + dx^2) \tag{5.30}$$

where $dx = (1 - r_S/r)$, and the Kruskal coordinates are good for describing a free-falling observer

$$ds^2 = \frac{r_s}{r} e^{1-\frac{r}{r_S}}(-dT^2 + dX^2) \xrightarrow{r\to r_S} (-dT^2 + dX^2), \tag{5.31}$$

where

$$\begin{aligned} v = t + x \quad &, \quad u = t - x \\ V = \kappa^{-1} e^{\kappa v} \quad &, \quad U = -\kappa^{-1} e^{-\kappa u} \\ T = U + V \quad &, \quad X = V - U \end{aligned}$$

and $\kappa = (2r_S)^{-1}$ is the surface gravity of the black hole, the acceleration that an observer would experiment while standing still arbitrarily close to the event horizon.

The related Klein-Gordon massless, minimally coupled equations will read identically to (5.14). Performing the same steps as we did for the Unruh effect one reaches very similar conclusions. There is only a significant difference concerning the light-cone coordinates "u" and "U" that will differ from (5.21) and read

$$U = -\kappa^{-1} e^{\kappa u} \quad ; \quad u = \kappa^{-1} ln[-\kappa U] \tag{5.32}$$

One therefore concludes that (5.27) and (5.28) are modified and give a Bose-Einstein distribution at a Hawking temperature:

$$n = \frac{1}{(e^{2\frac{\omega}{\kappa}\pi} - 1)}. \tag{5.33}$$

$$T_H = \frac{\kappa}{2\pi} = \frac{\hbar\kappa}{2\pi c k_B} \simeq 1 \text{ GeV} \left(\frac{10^{10}\text{kg}}{M} \right). \tag{5.34}$$

Similar reasoning leads to writing the Hawking temperature of a Kerr BH as

$$T_H = \frac{1}{(2 + (\sqrt{1 - \tilde{a}})^{-1})} \frac{M_P^2}{8\pi M}, \tag{5.35}$$

where M_P is the Planck mass and $\tilde{a} = J/M^2$ is the dimensionless spin parameter of the BH. Note that Hawking's original derivation [83, 84] takes into account the gravitational collapse of a massive star into a black hole and the dynamical evolution of field modes through the whole spacetime and reaches the same results presented above.

5.4 Black hole emission spectra

In this section, we outline the methodologies adopted for computing the primary and secondary components of the spectra emitted by a BH. The primary component of the spectrum is the one given by the particles directly emitted by the black hole due to Hawking radiation, while the secondary component results from all the processes the particles may undergo after being emitted and which produce further particles. We consider different methods for computing the secondary component according to the energies of the emitted particles and therefore to the mass of the PBH. We have, in particular, used the BlackHawk [93–96] code to determine the secondary photon spectrum. It makes use of Hazma [97] and PYTHIA [98, 99] codes for low and high-energy primary particles. For low-temperature PBHs ($\lesssim$ 20 MeV), we employ the semi-analytical method described in [100] to compute the secondary spectrum which is dominated by the electron Final State Radiation (FSR). These methods rely on different approximations and have different ranges of validity, which we discuss in each case. When taking into account the very energetic emission coming from light PBHs, we decided not to consider the approximation given in [101] for calculating the secondary component. In fact, to compute the secondary emission [101] extends the known particle physics to energies beyond the ones tested in colliders. This procedure may be spoiled by the presence of new physics at these energies which may lead to different fragmentation processes and different spectra. Therefore, we assumed an agnostic position and based our considerations at those energies only on the primary component.

5.4.1 Black Hole primary emission

As already discussed there are differences in the quantum vacuum definition by a near horizon free-falling observer and a distant observer at rest in the BH frame. In principle, such differences should lead to a perfect thermal flux described by equation (5.33). However, the presence of a gravitational potential will filter differently the different modes of the fields. As a result, a net nearly-thermal flux at infinity emerges. For a Kerr BH with dimensionless spin parameter $\tilde{a}$ and angular velocity at the horizon Ω_H, a particle species i with

spin s is emitted at a differential rate [87, 88, 102]:

$$\frac{d^2N_{P,i}}{dtdE_i} = \frac{1}{2\pi}\sum_{l,m}\frac{\Gamma^s_{l,m}(\omega)}{e^{2\pi k/\kappa}\pm 1}\ , \tag{5.36}$$

where P stands for primary, $\omega = E_i$ is the mode frequency (in natural units), $\Gamma^s_{l,m}$ are the transmission coefficients or gray-body factors discussed in 5.4 encoding the deviations from a black-body spectrum for each (l,m)-mode in a spheroidal wave decomposition, $k = \omega - m\Omega$ and $\kappa = \sqrt{1-\tilde{a}^2}/2r_+$ is the surface gravity of the Kerr BH with event horizon at r_+. The reader may have noticed that in (5.36) the angle defining the line of sight between the Earth and the BH is not explicitly mentioned. If one considers a Schwarzschild BH this does not represent a problem since the spherical symmetry of the problem. This holds true as an approximation in the case of slow rotation of the BH, but it is otherwise not true. In fact, a Kerr BH being axially symmetric shows a non-trivial dependence on the angular variable θ inherited from the angular part of the field equations. In fact, the angular differential emission rate is given by [42, 103–107]:

$$\frac{d^2N_{P,i}}{dtdE_i d\Omega} = \frac{1}{4\pi}\sum_{l,m}\frac{\Gamma^s_{l,m}}{e^{2\pi k/\kappa}\pm 1}(|S^{-s}_{l,m}(\theta)|^2 + |S^s_{l,m}(\theta)|^2)\ , \tag{5.37}$$

where $d\Omega$ is the infinitesimal solid angle element.

5.4.2 Black Hole secondary emission

It is worth noticing that among the plethora of emitted particles, we are interested in the ones that may reach the Earth, and be used as a probe, namely, the stable and uncharged components of the SM, the photons, and the neutrino. For the scope of this thesis, in the next chapters, we will consider the neutrinos spectrum only in relation to energies beyond the SM for which we will consider only the primary emitted neutrinos. Therefore, we will not discuss the secondary component of the neutrino spectrum and focus only on the secondary component of the photon spectrum. An evaporating PBH emits several different charged particles that radiate photons as they travel away from the PBH. Photons also result from the decay of unstable particles, like neutral pions. These photons are naturally less energetic than those emitted directly

by the Hawking effect, but nevertheless yield a very significant contribution to the total photon spectrum, in some cases a few orders of magnitude above the intensity of primary emission. The full spectrum can then be obtained by convoluting the primary emission rate in Eq. (5.36) with the number of photons radiated by each charged/unstable primary particle. This is, generically, a non-trivial procedure that has to be performed using numerical tools, particularly in the case of quarks and gluons that hadronize as they move away from the PBH, for Hawking temperatures roughly exceeding the QCD deconfinement temperature Λ_{QCD}.

We have chosen to use the publicly available BlackHawk code for numerical calculations of the secondary spectrum. In fact, this code gives the full photon spectrum for a given PBH mass and spin, and we have checked that the primary component yields results in agreement with our independent calculation. We must note that the latest version of BlackHawk relies on two different particle physics codes to compute the number of photons radiated by primary particles: Hazma for primary particle energies below a few GeV and PYTHIA for energies > 5 GeV.

Let us note that the PBH primary emission has a near blackbody shape, implying that peak emission occurs for energies about five times larger than the Hawking temperature. In particular, a PBH with temperature $T_H \sim 1$ GeV emits more intensely particles with an energy ~ 5 GeV. Taking into account that the Hawking temperature is given by (5.35) and that for the PBHs away from extremality the first multiplicative factor is close to unity, we conclude that the use of PYTHIA is appropriate for PBH masses $\lesssim 10^{10}$ kg ($T_H \gtrsim 1$ GeV). We note that PYTHIA offers the possibility of extending its operative range via extrapolation tables. However, as described in [100], this may lead to unreliable spectra. In particular, a comparison of the PYTHIA extrapolated spectra with the ones obtained using Hazma, for $M > 2.5 \times 10^{10}$ kg, reveals the failure of the former method in describing physical features such as neutral pion decay, $\pi^0 \to \gamma\gamma$, which should yield a symmetric emission peaked at energies corresponding to half of the pion's mass that is not well reproduced by the PYTHIA-based spectra. The contribution of pion decay to the photon spectrum is significant for PBH masses in the range $2.5 \times 10^{10} - 10^{11}$ kg ($T_H \sim 100 - 400$ MeV) since for lighter PBHs it is overcome by other secondary photon sources, while for heavier PBHs primary pion emission is Boltzmann-suppressed.

For these reasons, we employ PYTHIA for PBH masses $M = 5\times10^7 - 2.5\times10^{10}$ kg (*low mass range*). We considered a lower bound in masses in the use of PITHYA since it corresponds to a higher bound on the energies at roughly 1 TeV ensuring us to operate within tested particle physics. For the interval $M = 2.5 \times 10^{10} - 5 \times 10^{11}$ kg (*intermediate mass range*) we use Hazma. In principle, Hazma can be used also for higher BH masse. Nonetheless, for such masses, it is also possible to perform a semi-analytical computation that we can perform ab initio and which is in agreement with Hazma. In both cases, PITHYA and Hazma are implemented through the BlackHawk code.
For PBH masses $M = 5 \times 10^{11} - 10^{12}$ kg (*high mass range*), for which the Hawking temperature $T_H \lesssim 20$ MeV, we have chosen to use the semi-analytical method considered in [100], since secondary emission is in this case fully dominated by electron FSR, with no muons, pions, or QCD degrees of freedom being significantly emitted by the PBHs. In this case, the secondary photon spectrum is given by convoluting the primary electron and positron spectrum given in Eq. (5.36) with the Altarelli-Parisi splitting functions at leading order in the electromagnetic fine-structure constant α_{EM} [108, 109]:

$$\frac{d^2N^{FSR}_{S,\gamma}}{dtdE_\gamma} = \sum_{i=e^\pm,\mu^\pm,\pi^\pm} \int dE_i \frac{d^2N_{P,i}}{dtdE_i}\frac{dN^{FSR}_i}{dE_\gamma}, \tag{5.38}$$

where for completeness we have also included the (sub-dominant) contributions from muons and charged pions and:

$$\frac{dN^{FSR}_i}{dE_\gamma} = \frac{\alpha_{EM}}{\pi Q_i} P_{i\to i\gamma}(x) \log\left(\frac{1-x}{\mu_i^2} - 1\right), \tag{5.39}$$

$$P_{i\to i\gamma}(x) = \begin{cases} \frac{1+(1-x)^2}{x} & \text{for } i = e^\pm,\, \mu^\pm \\ \frac{2(1-x)}{x} & \text{for } i = \pi^\pm \end{cases}, \tag{5.40}$$

with $x = E_\gamma/E_i$, $\mu_i = m_i/2E_i$. With these analytical expressions for the splitting functions, we have computed the convolution integrals numerically for the *high mass range*, using the primary emission spectrum given in Eq. (5.36) for the corresponding particles.
It is possible to extend the validity range of the above calculation by taking into account the π^0 double photon decay, which is non-negligible for $M \lesssim 5 \times 10^{11}$

kg as done and described in [100, 110]

$$\frac{d^2N_{\gamma,tot}}{dtdE_\gamma} = \frac{d^2N_{P,\gamma}}{dtdE_\gamma} + \frac{d^2N^{FSR}_{S,\gamma}}{dtdE_\gamma} + \frac{d^2N^{decay}_{S,\gamma}}{dtdE_\gamma}. \tag{5.41}$$

Here P and S stand for primary and secondary. The third term on the right-hand side of Eq. (5.41) is given by the decay of the neutral pion and reads:

$$\frac{d^2N^{decay}_{S,\gamma}}{dtdE_\gamma} = 2\int dE_\pi \frac{d^2N_{P,\pi}}{dtdE_\pi}\frac{dN^{decay}_{\pi}}{dE_\gamma} \ , \tag{5.42}$$

with

$$\frac{dN^{decay}_{\pi}}{dE_\gamma} = \frac{\Theta(E_\gamma - E^-_\pi)\Theta(E^+_\pi - E_\gamma)}{E^+_\pi - E^-_\pi} \tag{5.43}$$

where Θ is the Heaviside step function and $E^\pm_\pi = (E_\pi \pm \sqrt{E^2_\pi - m^2_\pi})/2$. Nonetheless, given the proximity of the pion rest mass and the Λ_{QCD} energy we preferred to leave the treatment of these temperatures to the fully coputational treatment of Hazma.

5.5 BH evaporation

In the previous chapter, we described the emission of field quanta in the Hawking radiation. If one enforces the conservation of energy one must conclude that such emission comes at the expense of both the BH mass and angular momentum. Following the procedure described in [87–89] and later in [90–92] it is possible to compute how much energy and angular momentum is extracted by each field mode (l,m) by spin s. Therefore, summing over all (l,m)-modes we obtain the rates of mass and angular momentum loss due to a specific field of spin-s, f_s, and g_s respectively:

$$\begin{pmatrix} f_s \\ g_s \end{pmatrix} = \sum_{l,m} \frac{1}{2\pi}\int_0^\infty dx \frac{{}^s\Gamma_{i,l,m}}{e^{2\pi k/\kappa} \pm 1} \begin{pmatrix} x \\ m\tilde{a}^{-1} \end{pmatrix} \ , \tag{5.44}$$

where $x = \omega M$ and we removed the dependence on the BH mass. Tab. 5.1 reports the numerically calculated values for functions f_s and g_s, while Tab. 5.2 contains the parameters obtained by fitting the functions f_s and g_s to 11^{th} order polynomials in the BH spin $\tilde{a}$, of for different values of field spin s. Since we are working in the massless approximation one may notice that the inte-

gral in (5.44) spans all energies going from 0 to infinity. As discussed later in this section, we will take into account the field mass by considering or not the presence of a specific field in the set of fields characterizing the evaporation of the BH at a fixed temperature.

If one sums over all the particle degrees of freedom accessible at the temperature of the BH one has the functions determining the PBH mass and spin evolution $\mathcal{F} \equiv -M^2 dM/dt$ and $\mathcal{G} \equiv -(M/\tilde{a}) dJ/dt$

$$\begin{pmatrix} \mathcal{F} \\ \mathcal{G} \end{pmatrix} = \begin{pmatrix} n_0 f_0 + n_{1/2} f_{1/2} + n_1 f_1 + n_{3/2} f_{3/2} + n_2 f_2 \\ n_0 g_0 + n_{1/2} g_{1/2} + n_1 g_1 + n_{3/2} g_{3/2} + n_2 g_2 \end{pmatrix} \tag{5.45}$$

$$= \sum_{i,l,m} \frac{1}{2\pi} \int_0^\infty dx \frac{{}^s\Gamma_{i,l,m}}{e^{2\pi k/\kappa} \pm 1} \begin{pmatrix} x \\ m\tilde{a}^{-1} \end{pmatrix} , \tag{5.46}$$

where the sum is taken over all particle species i and angular momentum quantum numbers (l, m). The upper/lower sign corresponds to fermion/boson fields. The function

$$\mathcal{H} = \frac{\mathcal{G}}{\mathcal{F}} - 2 = \frac{d \log \tilde{a}}{d \log M} \tag{5.47}$$

determines whether a black hole spins up or down during its evolution, taking into account the relative magnitude of mass and angular momentum loss rates. If there is a value $\tilde{a}_*$ for which $\mathcal{H}(\tilde{a}_*) = 0$, the PBH spin parameter will tend to this stable value provided that $\partial_{\tilde{a}} \mathcal{H}|_{\tilde{a}=\tilde{a}_*} > 0$. We note that for $\partial_{\tilde{a}} \mathcal{H}|_{\tilde{a}=\tilde{a}_*} \leq 0$ the equilibrium point is unstable but that we will not find such cases in our analysis.

	0.01	0.05	0.1	0.2	0.3	0.4	0.5	0.6	0.7	0.8	0.9	0.99
f_0	0.74430	0.74379	0.74147	0.73465	0.72231	0.70627	0.69355	0.68482	0.69459	0.74344	0.90670	1.4560
g_0	0.88855	0.89241	0.90250	0.94359	1.0139	1.1172	1.2630	1.4610	1.7336	2.1278	2.7718	4.0601
$f_{1/2}$	0.81855	0.82241	0.83449	0.88342	0.96719	1.0897	1.2584	1.4868	1.8033	2.2774	3.1405	5.7833
$g_{1/2}$	6.1615	6.1649	6.1755	6.2200	6.3011	6.4312	6.6326	6.9464	7.4535	8.3381	10.155	15.814
f_1	0.33660	0.34118	0.35812	0.42661	0.55259	0.75756	1.0799	1.5937	2.4492	4.0048	7.4779	20.422
g_1	4.7947	4.8188	4.8947	5.2063	5.7571	6.6030	7.8449	9.6683	12.444	17.011	26.181	55.619
$f_{3/2}$	0.11928	0.12295	0.13473	0.18692	0.29425	0.49710	0.87951	1.6252	3.1834	6.8426	17.951	84.731
$g_{3/2}$	2.5020	2.5336	2.6337	3.0573	3.8540	5.1931	7.4021	11.138	17.858	31.400	65.895	229.37
f_2	0.03839	0.04034	0.04674	0.07725	0.11493	0.31100	0.68446	1.5700	3.8965	10.833	40.703	347.04
g_2	1.0620	1.0865	1.1650	1.5128	2.2296	3.5968	6.2251	11.522	23.144	51.845	153.14	928.81

Table 5.1: Values of function $f_s, g_s \times 10^{-4}$ for different values of field spin s and BH spin $\tilde{a}$.

(Achtung: in all the cases except for scalars we include a factor 2 taking into account for polarizations.)

	a^0	a^1	a^2	a^3	a^4	a^5	a^6	a^7	a^8	a^9	a^{10}	a^{11}
f_0	0.0000744823	-7.9450910^{-6}	0.000329669	−0.00672486	0.0645755	−0.353005	1.17705	−2.47588	3.29814	−2.69579	1.23215	−0.24076
g_0	0.0000888287	7.4789510^{-7}	0.000206934	−0.00186151	0.0188198	−0.100836	+0.319985	−0.625436	0.756088	−0.544549	0.210135	−0.0322118
$f_{1/2}$	0.0000817794	8.8508210^{-6}	−0.000181004	0.00582245	−0.0534605	0.294113	−1.02201	2.30006	−3.34177	3.02372	−1.54858	0.342845
$g_{1/2}$	0.000616017	0.0000176332	−0.000540316	0.0116003	−0.106459	0.586036	−2.03652	4.58378	−6.66062	6.02769	−3.0877	0.683813
f_1	0.0000333334	0.0000452634	−0.00153258	0.0298044	−0.273873	1.50836	−5.24818	11.8294	−17.2174	15.6098	−8.01207	1.77801
g_1	0.000478811	0.0000832772	−0.00221346	0.054893	−0.504852	2.78695	−9.72044	21.9753	−32.0963	29.2156	−15.0625	3.35922
$f_{3/2}$	9.6163610^{-6}	0.00034063	−0.012991	0.224003	−2.05757	11.3067	−39.2688	88.3115	−128.196	115.866	−59.2568	13.0944
$g_{3/2}$	0.000245139	0.000731022	−0.0268967	0.480786	−4.41566	24.2742	−84.3201	189.673	−275.417	249.019	−127.414	28.1733
f_2	-8.9818610^{-6}	0.00190075	−0.0732876	1.2513	−11.5062	63.288	−220.082	495.602	−720.415	651.964	−333.81	73.8225
g_2	0.0000784163	0.00410679	−0.157523	2.70426	−24.8713	136.867	−476.233	1073.34	−1562.	1415.7	−726.213	160.979

Table 5.2: Values of linear fit parameters of f_s, g_s times for different values of field spin s and BH spin $\tilde{a}$.

(Achtung: in all the cases except for scalars we include a factor 2 taking into account for polarizations.)

It is of extreme interest to focus on the single field h_s functions stating the contribution to each field to the definition of an asymptotic value of $\tilde{a}$

$$h_s = \frac{g_s}{f_s} - 2 \tag{5.48}$$

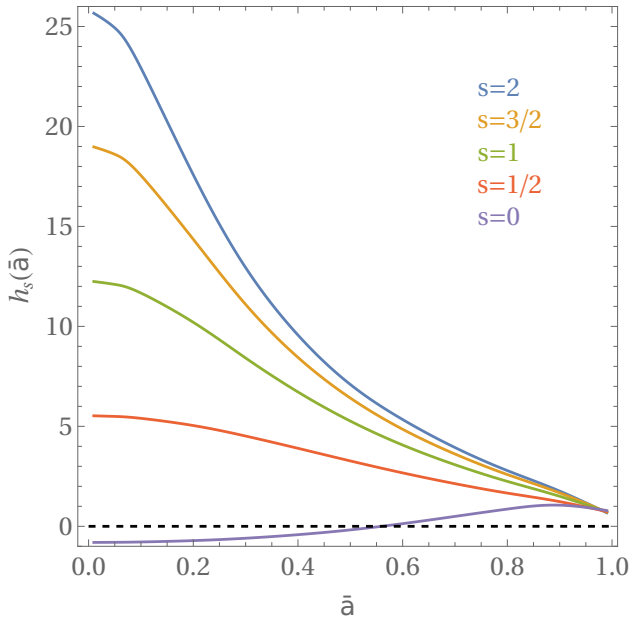

Figure 5.1: h_s functions computed from the data in Tab. (5.1).

Notice that only the scalar field possesses a value such that $h_0(\tilde{a}_*) = 0$ and it is $\tilde{a}_* \sim 0.555$. This result is in agreement with what was found in [90–92]. The scalar field is in fact the only field that can be emitted without taking away angular momentum from the BH if it is emitted in the $l = m = 0$ mode which is dominant for low BH spin. The differential equations governing the PBH spin and mass evolution can be written in terms of dimensionless variables useful for numerical integration:

$$y = -\ln \tilde{a}, \qquad z = -\ln M/M_i, \qquad \tau = -M_i^{-3} t \ , \tag{5.49}$$

such that

$$z'(y) = \frac{1}{\mathcal{H}} \ , \qquad \tau'(y) = \frac{e^{-3z(y)}}{\mathcal{H}\mathcal{F}} \ , \tag{5.50}$$

and M_i is the initial BH mass, with initial conditions $z(t_0) = 0$, $\tau(t_0) = 0$.

5.5.1 Standard Evolution Scenario

The evolution described by equations (5.49), (5.50) forces the BH to change its mass and spin resulting in a temporal evolution (an increase) of the BH temperature. The increasing temperature will cause the BH to be able to directly emit heavier and heavier degrees of freedom. As already mentioned we computed gray-body factors for massless fields, and given that the emission of particles with masses, m, above the Hawking temperature is exponentially suppressed we will work in the approximation where particles are considered massless for $T_H > m$ and are otherwise absent from the set of particles causing the BH evaporation.

In this way, the functions $\mathcal{F}$ and $\mathcal{G}$ are step functions of the BH temperature and it is possible to build a code evolving the BH between particle mass thresholds with (5.49), and (5.50). The masses of the SM particles are taken from the Particle Data Group (PDG) [111, 112] and are reported in Tab. 5.3.

Particle	m (MeV)	Spin
$\mathcal{G}$	0	2
γ	0	1
$\nu, \bar{\nu}$	~ 0	1/2
$e, \bar{e}$	0.511	1/2
$\mu, \bar{\mu}$	106	1/2
π^0	135	1
$\pi^{\pm}$	140	1
$u, \bar{u}$	336	1/2
$d, \bar{d}$	340	1/2
$s, \bar{s}$	486	1/2
g	550	1
$c, \bar{c}$	1550	1/2
$\tau, \bar{\tau}$	1777	1/2
$b, \bar{b}$	4730	1/2
$W^{\pm}$	80000	1
Z^0	91200	1
H^0	125000	0
$t, \bar{t}$	177000	1/2

Table 5.3: Particle content of the Standard Evolution Scenario.

One should note that the only hadrons with mass below the QCD scale, $\Lambda_{QCD} \simeq 200 - 300$ MeV, are pions (π^0 and $\pi^{\pm}$), these being the only hadronic

states included directly in the BH emission spectrum. Temperatures above the QCD scale allow for the direct emission of elementary quarks and gluons that subsequently hadronize. For such temperatures, pions are not emitted as effective degrees of freedom. Following [101, 113–121], we have considered the effective quark and gluon QCD masses given in [112], taking these as threshold values above which each particle is included in the PBH emission spectrum. We note that our results do not change significantly if we consider other values for the effective quark and gluon masses given in the literature, such as in [122].
It is possible to rapidly count the total number of Degrees of Freedom (DoF) of the SM plus the massless spin-2 graviton. The Higgs is the only scalar field present, corresponds to a complex doublet, and therefore has 4 DoF. There are 15 spin-1/2 Weyl fermions (quarks and leptons) in each of the 3 families giving a total of 90 DoF. The gauge bosons contribute with 12×2 DoF: the photon, 8 gluons, $W^{\pm}$, and Z^0. The total amounts to 120 DoF.

5.6 BH superradiance

Superradiance occurs each time a wave scatters off a target and emerges enhanced, having extracted energy from the target. This phenomenon can occur both at the classical and quantum levels.
Superradiant amplification leads to the extraction of energy from BHs, and can also lead to instabilities. The instabilities are caused by the establishment of a chain of events leading the system to undergo superradiant extraction numerous times, exponentially increasing the wave amplitude. If the field modes suffering the superradiant instability carry angular momentum it results in the extraction of rotational energy from the BH, spinning it down.
There exist many alternative ways to trigger the chain of instability. An intriguing one is represented by black hole fission processes. A BH cluster, due to its spatial configuration, may reach a criticality point causing an exponential amplification of an incoming wave in a fashion similar to the familiar nuclear fission processes. A graphical representation of this phenomenon is proposed in Fig.5.2.

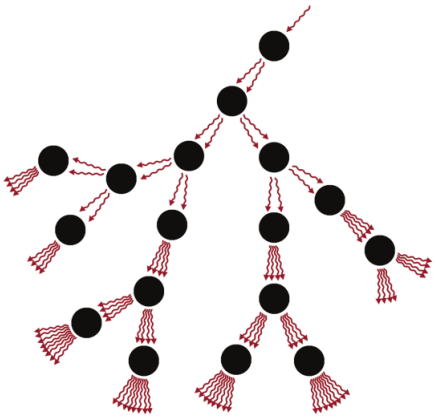

Figure 5.2: Representation of a BH fission process (taken from [123]).

However, it can be demonstrated that fission-like processes do not occur for Kerr BH clusters. The reason is straightforward, the entire cluster would have to be contained in its own Schwarzschild radius [89].
An alternative and generic way to establish a superradiant instability regime in rotating BHs is provided by any possible confinement of an incoming wave. A representation of this idea is depicted in Fig.5.3: an incoming pulse is superradiantly amplified by a BH and a reflecting mirror, of any source forces the wave to scatter numerous times, giving rise to an exponentially increasing amplitude. These kinds of superradiant instabilities are called BH bombs.

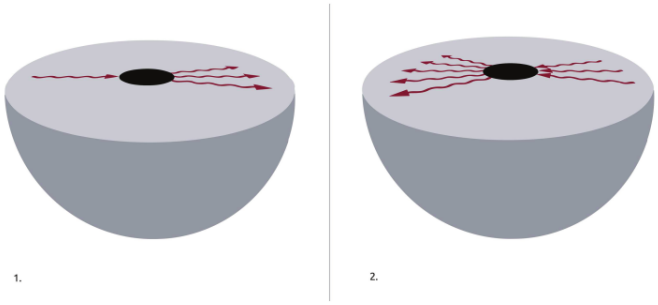

Figure 5.3: Scheme of a confined rotating BH, and how an initially small fluctuation grows by successive reflections at the confining wall and amplifications (taken from [123]).

The nature of the reflecting mirror does not play an essential role for the instability to occur. Various solutions can be considered, some more feasible, others just regarded as Gedankenexperiments. Nevertheless, it is worth mentioning them. In the following list are reported the most cited ones from the more speculative to the more plausible:

- An unlikely scenario is provided by surrounding a spinning BH with a perfectly reflecting mirror. Any initial fluctuation grows exponentially, leading to an increasing field density and pressure inside the mirror. The exponentially increasing pressure eventually disrupts the confining mirror, leading to an "explosion". [123–126].

- In general relativity, Anti-de Sitter (AdS) space is a maximally symmetric vacuum solution of Einstein's equations with negative cosmological constant Λ. It corresponds to a negative vacuum energy density and positive pressure. Mathematically it is a maximally symmetric Lorentzian manifold with constant negative scalar curvature and can be regarded as the Lorentzian analog of the hyperbolic space. Similarly, the Minkowski space and the de Sitter space are the analogs of the Euclidean space and the elliptical space, respectively.
  A crucial feature of AdS spacetime is that no time-like geodesic and thus particle can reach the spatial infinity of the manifold. For this reason, a BH in AdS background can be looked at as a confined system [127–130], producing the phenomenon of the BH-bomb.

- BH may be surrounded by ionized matter in the form of thin or thick accretion disks unequally distributed around the BH. This plasma is a good low-frequency ElectroMagnetic (EM) wave reflector [131–133] and may play the role of the mirror [134]. This geometrical configuration disfavors the non-directional low angular eigenvalue instability modes [135, 136] but does not suppress all possible instabilities. However, absorption effects at the mirror could erase any sign of superradiant instabilities [136]. In an optimistic setup, the EM wave is amplified by $\sim 1\%$ each time that it interacts with the BH [89].

- Eventually, we consider the presence of a massive bosonic field. It naturally confines low-frequency radiation due to the coupling generated by the gravitational attraction between the field and black hole masses

$M\mu$. In this sense, it is possible to say that "Nature provides its own mirror" [123,125,126]. Superradiant instabilities triggered by massive bosons are relevant only when the gravitational coupling $M\mu_i \lesssim 1$, where μ_i is the physical mass of the fields and $i = S, V, T$ identifies the scalar, vector, and tensor fields, respectively. This means that for BHs in the Solar mass range, only ultra-light bosonic fields with masses below 10^{-10} eV can trigger superradiant instabilities.

The equations for scalar and vectorial massive fields in curved spacetime are known (the massive Klein-Gordon and Proca equations). Superradiant instabilities for the scalar perturbations have a relatively extensive history. The spin-1 field, however, has been investigated only more recently due to some technical difficulties in separating the equation in a system of coupled differential equations. This problem has been overcome only recently [137, 138]. Massive tensor fields cannot be trivially coupled to gravity. Due to the works of Fierz and Pauli [139] the related equation is known at the linear level, being the unique ghost-free and tachyon-free equation preserving Lorenz invariance describing the five polarizations of a massive spin-2 field on a flat background. There is also a more general theory called massive gravity that has been used to study superradiant instabilities [140].

Despite the differences in the equation governing a massive spin-0, spin-1, and spin-2 field in curved spacetime, it is possible to portray a unified picture describing the superradiant instability of massive bosonic fields, around a spinning BH. There exists a set of quasi-bound states satisfying the superradiance condition $\omega_R < m\Omega_H$. These states are localized at a distance from the BH governed by the Compton wavelength μ^{-1} (more precisely given by the gravitational Bohr radius) and decay exponentially at large distances. For $M\mu < 1$ the spectrum of these modes resembles a Hydrogen-like structure for the real part of the frequency,

$$\omega_R \sim \mu \left(1 - \frac{(M\mu)^2}{(l+s+1+n)^2}\right) \tag{5.51}$$

The imaginary part giving rise to the instability will scale as the real component minus a factor $m\Omega_H$,

$$\omega_I \sim (\omega_R - m\Omega_H). \tag{5.52}$$

5.6.1 Basics of black hole superradiance

To corroborate the above-mentioned equations (5.51) and (5.52) we proceed as in [141]. We begin by discussing the basic dynamical features of BH superradiance neglecting the effects of Hawking emission. Consider then a massive scalar field minimally coupled to gravity, of mass μ, described the action:

$$S = \int d^4x\sqrt{-g}\ \left(\frac{1}{2}g^{\mu\nu}\partial_\mu\Phi\partial_\nu\Phi - \frac{1}{2}\mu^2\Phi^2\right)\ , \tag{5.53}$$

The massive scalar field in a Kerr background reads

$$(\nabla_\mu\nabla^\mu - \mu^2)\Phi = 0 \tag{5.54}$$

which choosing the Kerr metric (4.6) becomes

$$\begin{aligned} &\frac{\left(r^2+a^2\right)^2 - a^2\sin^2\theta}{\Delta\Sigma}\partial_t^2\Phi - \frac{1}{\Sigma}\partial_r\left(\Delta\partial_r\Phi\right) - \frac{1}{\Sigma\sin\theta}\partial_\theta\left(\sin\theta\partial_\theta\Phi\right) \\ - \ &\frac{\Delta - a^2\sin^2\theta}{\Sigma\Delta\sin^2\theta}\partial_\varphi^2\Phi + \frac{2a}{\Delta\Sigma}2Mr\partial_t\partial_\varphi\Phi + \mu^2\Phi = 0\ , \end{aligned} \tag{5.55}$$

which, in the massless limit, reduces to the Teukolsky equation (4.39) for $s = 0$. Let us call it massive (scalar) Teukolsky equation.
Separating the variables, as reported in [50], $\Phi = R(r)S(\theta)e^{im\phi}e^{-i\omega t}$, one finds that $S(\theta)$ is an oblate spheroidal harmonic obeying (4.41) at $s = 0$ and ω^2 substituted by $(\omega^2 - \mu^2)$, namely:

$$\frac{1}{\sin\theta}\partial_\theta\left(\sin\theta\ \ \partial_\theta S_s\right) + \left(a^2(\omega^2-\mu^2)\cos^2\theta - \frac{m^2}{\sin^2\theta} + \lambda_l^m\right)S_s = 0\ . \tag{5.56}$$

Therefore, λ_{lm} is given by Eq. (4.42) at $s = 0$ and ω^2 substituted by $(\omega^2 - \mu^2)$. The radial part $R(r)$ satisfies

$$\Delta\frac{d}{dr}\left(\Delta\frac{dR}{dr}\right) + \left[a^2m^2 - 4Mram\omega + (r^2+a^2)^2\omega^2 - (\mu^2r^2 + \lambda_{lm} + \omega^2a^2)\Delta\right]R = 0. \tag{5.57}$$

This equation can be recast in a Schrödinger-like form using the tortoise coordinates r_*, such that $dr_* = dr\,(r^2a^2)/\Delta$ and defining $\psi = \sqrt{r^2+a^2}R$:

$$\frac{d^2\psi}{dr_*} + (\omega^2 - V(\omega))\psi = 0, \tag{5.58}$$

where

$$V(\omega) = \frac{\Delta\mu^2}{r^2+a^2} + \frac{4Mram\omega - a^2m^2 + \Delta(\lambda_{lm} + (\omega^2-\mu^2)a^2)}{(r^2+a^2)^2} + \frac{\Delta(3r^2-4Mr+a^2)}{(r^2+a^2)^3} - \frac{3\Delta^2 r^2}{(r^2+a^2)^4}. \tag{5.59}$$

The potential (see Fig. 5.4) reaches $V_\infty = \mu^2$ when $r_* \to +\infty$ and is rising from a well where $V < \mu^2$. However, the values of V are not distant from the asymptotic value as $r \gtrsim 1/\mu$. Following the potential in the in-going radial direction after the well, we encounter a barrier peaked at $r \sim M$. Beyond the centrifugal barrier there is the ergoregion and reaching the horizon, for $r_* \to -\infty$ the potential reaches the asymptotic value $V_+ = 2m\Omega_H\omega - m^2\Omega_H^2$. Inside the potential well, if the energy of the mode is less than the mass of the field ($\mu > \omega$), it is possible to establish bound states characterized by an exponential suppression of the field at a large distance from the horizon. Otherwise, if the energy of the mode exceeds the mass of the field, the modes are called normal modes and are characterized by a fixed amplitude at an infinite distance from the horizon.

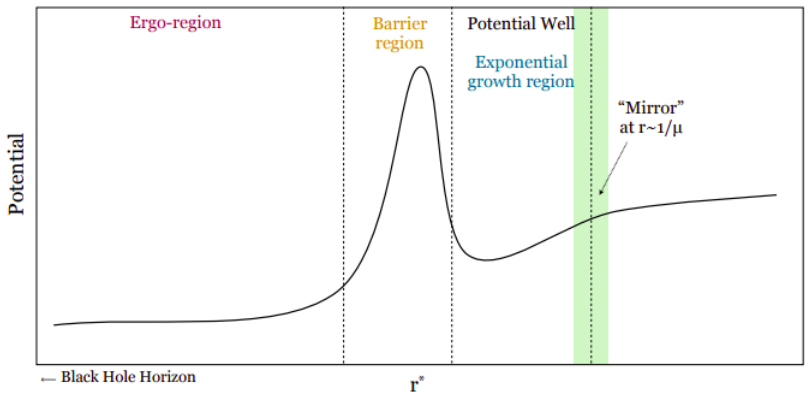

Figure 5.4: Graphical representation of the potential experienced by a massive scalar field in the Kerr geometry (taken from [142]).

Eq. (5.58) is not a self-adjoint eigenvalue problem since the potential depends explicitly on ω if $a \neq 0$. For this reason, it is possible to have a non-zero imaginary part in the frequency of the bound states. Bound states having an imaginary frequency component are called quasi-bound states (in analogy nor-

mal modes having an imaginary frequency component are called quasi-normal modes) and, over time, can be exponentially suppressed or have exponential growth.
Near the horizon, one has

$$\omega^2 - V(\omega, r) \xrightarrow{r \to r_+} \omega^2 - V_+ = (\omega - m\Omega_H)^2 = k_+^2. \tag{5.60}$$

Therefore, the general wavefunction solution at the horizon reads $e^{\pm ik_+ r_*}$. Imposing pure in-going waves at the horizon leaves us with $e^{-ik_+ r_*}$. At infinity, one finds

$$\omega^2 - V(\omega, r) \xrightarrow{r \to \infty} \omega^2 - V_\infty = \omega^2 - \mu^2 = k_\infty^2 \tag{5.61}$$

The appropriate boundary conditions at infinity are given by the exponential decay of ψ since we want the state to be bound. Therefore, the appropriate form of the wavefunction at infinity is $\sim e^{-\sqrt{\mu^2 - \omega^2} r_*}$.
The quasi-bound states in the superradiant regime, $\omega < m\Omega_H$, is characterized by a positive imaginary part of the frequency giving origin to an exponential growth in time of the mode amplitude, since $\Phi = R(r)\Theta(\theta)e^{im\phi}e^{-i\omega t}$.
We can physically break down the events as follows: some modes of a boson field can undergo a stimulated emission called superradiance and, if the field is massive, these modes can be trapped in a gravitational potential well and therefore amplified exponentially. This last process is mathematically described by a positive imaginary part of ω.
We can obtain a quantitative expression for the imaginary part of the frequency through analytical calculations both in the limits $M\mu \ll 1$ [143] and $M\mu \gg 1$ [50]. In the latter case one has that the coupling is such that superradiance is exponentially suppressed. In the case $M\mu \ll 1$, one can use Starobinsky's matching procedure [75]. This method is based on dividing the exterior of the black hole into two distinct and overlapping regions. A near horizon region $\omega r_+ x \ll l$ and a far region $x \gg 1$ where $x = (r - r_+)/r_+$. In

these regions, it is possible to analytically solve the radial equation, obtaining

$$\begin{aligned} R_{near}(x) &= A\left(\frac{x}{x+\tau}\right)^{-i\varpi\tau} {}_2F_1(l+1,-l,1-2i\varpi,-x/\tau) \\ &\Big\downarrow x \gg \tau \\ &\sim A\Gamma(1-2i\varpi)\left[\frac{\Gamma(2l+1)}{\Gamma(l+1)\Gamma(l+1-2i\varpi)}\left(\frac{x}{\tau}\right)^{l}\right. \\ &\left.+\frac{\Gamma(-2l-1)}{\Gamma(-l)\Gamma(-l-2i\varpi)}\left(\frac{x}{\tau}\right)^{-l-1}\right] \end{aligned} \tag{5.62}$$

$$\begin{aligned} R_{far}(x) &= Bx^l e^{r_+qx} U(l+1-\nu,2l+2,2qr_+x) \\ &\Big\downarrow r_+q \ll 1 \\ &\sim B\frac{\pi}{\sin((2l+2)\pi)}\left[\frac{x^l}{\Gamma(-l-\nu)\Gamma(2l+2)}+\frac{(2qr_+\tau)^{-(2l+1)}x^{-l-1}}{\Gamma(l+1-\nu)\Gamma(-2l)}\right] \end{aligned} \tag{5.63}$$

where ${}_2F_1$ and U are the hypergeometric and the confluent hypergeometric functions, respectively, $q=\sqrt{\mu^2-\omega^2}$, $\nu=\frac{2-\tau}{2}\frac{\omega^2-q^2}{q}r_+$ and τ, ϖ are defined as in the previous section. In the overlapping region, $1 \ll x \ll l/(\omega r_+)$, the two equations must coincide, defining the condition:

$$\frac{\Gamma(-l-\nu)\Gamma(2l+2)}{\Gamma(l+1-\nu)\Gamma(-2l)} = -(2qr_+\tau)^{2l+1}\frac{\Gamma(-2l-1)\Gamma(l+1)\Gamma(l+1-2i\varpi)}{\Gamma(-l)\Gamma(2l+1)\Gamma(-l-2i\varpi)} \tag{5.64}$$

To leading order the r.h.s. of (5.64) vanishes since $qr_+ \ll 1$ and it is valid

$$\frac{\Gamma(-l-\nu)\Gamma(2l+2)}{\Gamma(l+1-\nu)\Gamma(-2l)} = 0, \tag{5.65}$$

which can be satisfied by a diverging $\Gamma(l+1-\nu)$. This situation is verified each time the argument of the Γ is a negative integer and leads to the condition

$$\nu_0 = n_r + l + 1 \tag{5.66}$$

where $n_r \in \mathbb{N}$. Using the definition of ν it is then possible to obtain the Hydrogen-like spectrum typical of massive fields in a gravitational potential already introduced in Eq. (5.51).

To determine whether a mode exhibits a superradiant behavior, we have to

obtain the imaginary part of the bound state frequency. For this we need to compute the leading correction from the non-zero value of the r.h.s. of (5.64). After some algebra one obtains

$$\omega_I = -\varpi \frac{1}{2r_+} C_{ln} (\mu M)^{4l+5} \left(\frac{r_+ - r_-}{r_+ + r_-} \right)^{2l+1} \tag{5.67}$$

where

$$C_{ln} = \frac{4^{2+2}}{(l+1+n_r)^{2l+4}} \frac{(2l+1+n_r)!}{n_r!} \frac{l!}{(2l+1)!(2l)!} \prod_{j=1}^{l} (j^2 + 16(\varpi M)^2) \tag{5.68}$$

Since $\varpi \propto (\omega - m\Omega) \simeq (\omega_R - m\Omega)$ we obtain an imaginary part of the frequency of the form (5.52).

Moreover, from (5.67), we can infer that the lowest angular momentum modes will have the largest values for the imaginary part of the frequency in this regime. So the leading superradiant mode has $l = m = 1$.

Numerical methods are also applied in the determination of the spectrum of superradiant scalar massive modes [145].

Similar approaches are also investigated in the case of a vector field, leading to similar results, as reported in [82, 144]. One may notice that amplification of boson waves occurs also in the case of massless particles. In fact, the gray-body factors are negative in the low-frequency regime for bosonic modes with positive azimuthal quantum number m. In the nearly extremal cases, our massless gray-body factor displays a superradiant regime matching the one reported in the literature, having a maximal amplification of 0.356%, 4.4%, 138% for scalar, vector, and tensor bosons respectively.

To summarize, (5.57) admits quasi-bound state solutions with complex frequencies $\omega = \omega_R + i\omega_I$, such that $\omega_R < \mu$ and the field is trapped in the BH gravitational well [50, 82, 123, 141, 143, 145–152]. It is worth defining the dimensionless mass coupling

$$\alpha = \frac{\mu M}{M_P^2} \tag{5.69}$$

where for clarity we explicitly included the missing Planck mass factor. In the non-relativistic limit, α is small, and the real part of the quasi-bound state

spectrum approaches a Hydrogen-like form

$$\omega_R = \mu\left(1 - \frac{\alpha^2}{2n^2}\right) \tag{5.70}$$

as a consequence of the fact that when written in the Schrödinger-like form (5.58) the potential is Coulomb-like $V(r) \simeq -\alpha/r$ at large distances from the event horizon.

The imaginary part, ω_I, reflects the instability of the bound-states (hence the use of the prefix "quasi-"), with $\omega_I < 0$ corresponding to a decay or absorption of the scalar field by the BH, and $\omega_I > 0$ to an exponential amplification of the field and of the associated particle number. For $\alpha \ll 1$, one finds an approximate analytical expression (5.67) that can be rearranged as:

$$\begin{aligned}\omega_I = &-\frac{1}{2}\Big(\frac{l!}{(2l+1)!(2l)!}\Big)^2 \frac{(l+n)!}{(n-l-1)!}\frac{4^{2l+2}}{n^{2l+4}}\times \\ &\times \prod_{k=1}^{l}\Big(k^2 + 16\Big(\frac{M(\omega_R - m\Omega_H)}{\tau}\Big)^2\Big)\Big(\frac{\omega_R - m\Omega_H}{\tau}\Big)\alpha^{4l+5}\Big(\frac{r_+ - r_-}{r_+ + r_-}\Big)^{2l+1}\end{aligned} \tag{5.71}$$

The superradiant instability occurs when $\omega_R < m\Omega_H$ ($\alpha < \tilde{a}/4$ if $\tilde{a} \ll 1$), and leads to the production of particles forming a bound superradiant cloud around the spinning BH. The fastest growing mode is the 2p-state ($l = m = 1$):

$$\omega_I = -\frac{1}{12}\Big(1 + 16\Big(M\frac{\omega_R - \Omega_H}{\tau}\Big)^2\Big)\Big(\frac{\omega_R - \Omega_H}{\tau}\Big)\alpha^9\Big(\frac{r_+ - r_-}{r_+ + r_-}\Big)^3 \tag{5.72}$$

The "2p-state" grows exponentially faster with respect to the other modes and the number of particles in the state will grow even faster since the number of particles $N \propto \Phi^2$. Thus, we may neglect any other modes when considering the dynamics of superradiance (neglecting self-interactions). Given that each particle produced by superradiance carries spin and mass, enforcing the energy and angular momentum conservation yields the variation in the mass and spin of the BH:

$$\frac{dM}{dt} = -\mu\frac{dN}{dt}\ , \qquad \frac{dJ}{dt} = -\frac{dN}{dt}\ , \tag{5.73}$$

such that the dimensionless spin parameter evolves according to:

$$\frac{d\tilde{a}}{dt} = -\frac{1}{M^2}(1 - 2\tilde{a}\alpha)\frac{dN}{dt} \simeq -\frac{M_P^2}{M^2}\frac{dN}{dt}\ , \tag{5.74}$$

where in the last step we considered the limit $\alpha \ll 1$. The number of particles within the superradiant cloud then follows:

$$\frac{dN}{dt} = \Gamma_s(M, \tilde{a}, \mu)N \tag{5.75}$$

where $\Gamma_s = 2\omega_I$. It is useful to note that, for slowly rotating BHs:

$$\Gamma_s \simeq \frac{1}{24}(\tilde{a} - 4\alpha)\alpha^8\mu \tag{5.76}$$

Strictly speaking, the instability growth rates are computed assuming a fixed BH mass and spin parameter, but since $\mu \ll M$ and $M \gg 1(M_P)$ in the regime we will be interested in in our future discussion, we may take this as a good approximation.

6 A look at Beyond the Standard Model physics

The particle content of Nature, namely the number of existing quantum fields, drastically influences the evolution of a BH in many aspects. It is possible to understand from the previous chapter that the number of fields and their characteristics in the underlying theory of particle physics is related to the lifetime and the time evolution of the parameters of the BH. For example, as we will see in next chapter the emission of a large number of scalar bosons drastically alters the adimensional spin parameter time evolution. In this way, due to their characteristic temperatures, one can use light PBHs as a test bench for particle physics Beyond the Standard Model (BSM). Moreover, elementary bosons are observed to be either massless or with masses in the range of the 100 GeV and the superradiant condition $\mu_i M < 1$ sets the relevant superradiant-produced boson mass for a given BH mass. In the case of 100 GeV bosons it corresponds to BHs with $M \sim 10^{-21} M_\odot$ (10^9) kg. Such light BHs could have formed in the early universe as PBHs [1, 2, 153, 154] and are promising as dark-matter candidates [155, 156]. However, the directly observed black holes possess masses of the order of solar masses for which the relevant boson mass range has to be ultra-light. In addition, also PBHs may have masses of several Solar masses. For these reasons, it is significant for the scope of the thesis to understand the main extensions of the Standard Model (SM) predicting new light and many particles. In the following, we give some examples of such extensions, considering supersymmetric extensions of the SM, Kaluza-Klein theories, QCD axions and Axion Like Particles (ALPs), and Hidden Sector (HS).

6.1 SUperSYmmetric (SUSY) extensions of the SM

Providing a description of supersymmetric theories in a few pages represents a nearly impossible task. Alternatively, I prefer to focus on the main SUSY motivations to establish some foundational concepts and be able to identify the new bosons candidates in the simplest supersymmetric scenario.
What follows represents a collection of notions taken from the introductory papers/notes [157–160] and from [31,161–163]. The SM describes a world made of a particle zoo divided into two families: bosons that mediate interactions and fermions that constitute matter. It naturally raise one question about this sharp dichotomy Nature chooses and whether there is a symmetry relating these two sectors, providing a unified description of interactions and matter.
Besides these speculative reasons, much more theoretical and well-justified motivations exist. Modern physics possesses two well-studied symmetry groups:

- The Poincaré group produced by the semidirect product of the proper orthochronous Lorentz group $SO^+(1,3)$ with the continuous group of translations $R^{1,3}$. It is known as the spacetime symmetry group.
- The internal symmetries group is given by intrinsic characteristics of particles interacting with each other. This group is obtained by the direct product of the groups describing the electromagnetic, nuclear weak and strong interactions, and reads, $SU(3) \times SU(2) \times U(1)$.

Is there a way to combine these symmetries in a non-trivial manner? This question can be placed in a more mathematical way considering the generators of the respective Lie algebras: is there a way to prevent the commutation relations between generators of internal and spacetime symmetries from being not identically 0? An answer came in 1967 with the no-go theorem of Coleman and Mandula: no! [164]
A way to circumvent this statement can be found within the hypothesis of the theorem itself. In fact, it only takes into account Lie algebras and commutation relations. Relaxing this hypothesis with the introduction of graded Lie algebras gives the opportunity to consider also the fermionic anti-commutation relations giving rise to a set of non-trivially behaving operators. The structure of the resulting group is restricted by the theorem of Haag-Łopuszański-Sohnius [165], which represents an extended version of the Coleman-Mandula

theorem considering also anti-commutators.
The simplest case is when the graded Lie algebra is given by the direct sum of just two Lie algebras. In this case, two new operators are introduced Q and $\bar{Q}$. Their non-trivial anti-commutation relations are

$$\{Q_a, \bar{Q}_b\} = 2\gamma^{\mu}_{ab} P_{\mu}, \tag{6.1}$$

$$\{Q_a, P_{\mu}\} = 0, \tag{6.2}$$

$$\{Q_a, M^{\mu\nu}\} = \sigma^{\mu\nu}_{a,b} Q^b, \tag{6.3}$$

where P and M are the generators of translations and Lorentz transformations, $\bar{Q} = Q^{\dagger}\gamma_0$, and $\sigma^{\mu\nu} = \frac{i}{4}[\gamma^{\mu}, \gamma^{\nu}]$. We adopt the convention of Greek for spacetime indices and Latin for spinorial ones.
The Q generators commute with the internal symmetry generators leaving unchanged the charges of a particle. The way they commute/anti-commute with spacetime symmetries indicates that they transform fermions into bosons and vice-versa, according to

$$Q|fermion\rangle = |boson\rangle \quad , \quad Q|boson\rangle = |fermion\rangle. \tag{6.4}$$

In this way, each component of the SM gains a superpartner completely identical but for its spin. This symmetry, called supersymmetry, is extremely useful in solving the hierarchy problem, i.e. the 16 orders of magnitude of fine-tuning required between the bare mass of the Higgs boson and its first correction at the Planck scale cut off, for obtaining the physically measured mass of the Higgs itself. The superpartner contribution provides corrections of the opposite sign cancelling the fine-tuning at all orders if SUSY is exact.
Another motivation for SUSY is the fact that in the SM the renormalized electromagnetic, weak, and strong coupling constants reach similar values at a scale of the order 10^{16} GeV but do not unify exactly. If supersymmetry is included just above the weak scale, these forces naturally unify at $M_U \approx 2\ 10^{16}$ GeV. This behavior is a hint in favor of SUSY Grand Unified Theories (GUT).
Within the above-described framework, it is possible to have elementary bosons in the mass range of the respective fermion in the SM, from the eV to a scale of 100 GeV. It is, however, worth noticing that if SUSY exists, it must be a broken symmetry of Nature since no superpartner has yet been experimentally

observed. The superpartners must be heavier than their counterparts, and the LHC has generically set constraints on their masses above the TeV scale.
These theories are attractive because they also yield appealing candidates for Dark Matter (DM) in the form of Weakly Interacting Massive Particles (WIMP). In general, in SUSY models, not all the allowed renormalizable couplings conserve the baryon and lepton numbers. Experimental data tested the conservation of lepton and baryon numbers in an accurate way, constraining these couplings to be very small. R-parity is an additional symmetry that forbids these couplings. It is given by $P = (-1)^{3B+L+2s}$, where B, L, and s are the baryon number, the lepton number, and the spin respectively. R-parity takes the value +1 for standard model particles while -1 for the superpartners. If R-parity is preserved, the heavier superpartners may decay into standard model particles and other SUSY particles, but the lightest supersymmetric particle (LSP) is prevented from decaying and is stable. For this reason, the LSP is a good DM candidate. An example of a WIMP candidate that arises is the so-called lightest neutralino. It is an admixture of the superpartners of the B, W_3, H_1, H_2 bosons, called bino, wino, and Higgsino, denoted with a tilde. The neutralino is a linear combination of the fields:

$$\chi = N_{11}\tilde{B} + N_{12}\tilde{W}_3 + N_{13}\tilde{H}_1 + N_{14}\tilde{H}_2 \tag{6.5}$$

In the above formula N_{ij} are the coefficients of the linear combination. Typically this superposition has 4 mass eigenstates. As a heavy and stable particle, the lightest neutralino represents an excellent candidate for cold dark matter. Moreover, it is expected to be produced thermally in the early Universe and to be non-relativistic at the present epoch. Its mass is roughly $10 - 10^4$ GeV and its self-annihilation rate and elastic scattering off nuclei are studied in detail [166]. In future chapters, we will consider the Minimal Supersymmetric Standard Model (MSSM) which adds 128 DoF to the 120 of the SM plus the graviton. The MSSM DoF that we will consider in addition to the SM and the graviton are:

- 4 scalar DoF comes from the extra DoF from the Higgs sector which in the MSSM is formed by two complex doublets (Higgs up and down, H_1 and H_2 above).

- 90 scalar DoF super-partners of the Wyel fermions (squarks, sleptons).

- 4 spin-1/2 fermions (8 DoF) super-partner of the Higgs (Highsinos).
- 12 spin-1/2 (24 DoF) fermions super-partner of the gauge bosons g, W, B (gluino, wino, bino).
- 2 spin-3/2 DoF, the super-partner of the graviton (gravitino).

To be consistent with the observed physics supersymmetry has to be spontaneously broken and the SUSY braking mechanism must make the superpartners heavier than the SM particles. For example, in chapter 10, for simplicity, we will consider that all the superpartners have the same mass in a range of masses not tested by colliders i.e. 5 TeV.

6.2 Kaluza-Klein (KK) theories

The first idea that the world may have more than four dimensions is due to Kaluza (1921) and his efforts to construct a theory unifying Einstein's theory of general relativity and Maxwell's theory of electromagnetism. Klein's contribution was to develop a connection with the quantum theory and add the hypothesis that the extra dimension was microscopically small.
The essential idea of this theory is to postulate one extra compactified space dimension and introduce nothing but pure gravity having a (1 + 4)-dimensional version of general relativity. It turns out that the 5-dimensional gravity manifests in our observable (1 + 3)-dimensional spacetime as a gravitational, an electromagnetic, and a scalar field or in the language of particle physics as a spin-2 graviton, a spin-1 photon, and a spin-0 boson.
This theory represents a version of general relativity in 5D. For this reason, the theory possesses more degrees of freedom than standard general relativity, and it needs additional constraints. Such constraints can be identified in the two conditions physically aiming to explain why the 5^{th} dimension is not perceived. Mathematically these conditions state that the 5^{th} dimension has a closed topology and a compact size (as the one of a circle). The former means that the 5D topology can be written as $M^4 \times S^1$, where M^4 is the standard spacetime Minkowskian topology and S^1 is the one of a circle. The closure of the extra dimension topology introduces periodicity allowing for Fourier decomposition. These constraints are in agreement with the so-called cylinder condition consisting of setting all partial derivatives of the metric tensor with

respect to the 5^{th} coordinate to zero.
The cylinder condition and the coordinate choice (in gravitational jargon) or gauge choice (in particle physics jargon) together with the 5-dimensional general relativity-like equation in vacuum turn out to provide the right equations of motion for gravity and electromagnetism once the scalar field is taken to be constant.
Let us consider a generic 5×5 metric tensor

$$g_{\alpha\beta} = \begin{pmatrix} g_{\mu\nu} & g_{\mu 5} \\ g_{5\nu} & g_{55} \end{pmatrix}. \tag{6.6}$$

It possesses 15 degrees of freedom. We assumed the convention that Greek indices (α, β, γ, ...) denote curved indices, while Latin indices (a, b, c, ...) denote flat indices. Letters from the beginning of both alphabets (a, b, c, ... and α, β, γ, ...) indicate general 5D indices, from the middle of the alphabets denote the four dimensions of standard general relativity (m, n, ... and μ, ν, ... = 1, 2, 3, 4) while letters from the bottom of the alphabets (s, t, ... and σ, τ, ...) indicate the compactified extra space dimensions. The cylinder condition reads

$$\partial_5 g_{\alpha\beta} = 0, \tag{6.7}$$

and a smart gauge choice leads to a metric tensor of the form

$$g_{\alpha\beta} = \begin{pmatrix} g_{\mu\nu} - \kappa\Phi^2 A_\mu A_\nu & -\kappa\Phi^2 A_\mu \\ -\kappa\Phi^2 A_\nu & -\Phi^2 \end{pmatrix}. \tag{6.8}$$

At this time, with the underlying assumption of a metric variational approach, it is possible to build the 5D Ricci scalar and tensor, as well as the Einstein tensor, thus yielding the 5D field equations

$$R_{\alpha\beta} - \frac{1}{2} R g_{\alpha\beta} = G_{\alpha\beta} = kT_{\alpha\beta} \tag{6.9}$$

where k is an appropriate 5D coupling constant and $T_{\alpha\beta}$ is an unknown 5D stress-energy tensor. The vacuum version of (6.9) reduces to

$$G_{\alpha\beta} = 0, \tag{6.10}$$

or equivalently

$$R_{\alpha\beta} = 0. \tag{6.11}$$

An explicit calculation then leads to:

$$G_{\mu\nu} = \frac{\kappa^2\Phi^2}{2}T_{\mu\nu} \tag{6.12}$$

$$\nabla^\mu F_{\mu\nu} = -3\frac{\nabla^\mu\Phi}{\Phi}F_{\mu\nu} \tag{6.13}$$

$$g^{\mu\nu}\nabla_\mu\nabla_\nu\Phi = -\frac{\kappa^2\Phi^3}{4}F_{\mu\nu}F^{\mu\nu} \tag{6.14}$$

$$\tag{6.15}$$

where $T_{\mu\nu}$ is the energy-momentum tensor for an electromagnetic field given by

$$T_{\mu\nu} = \frac{(g_{\mu\nu}F_{\lambda\xi}F^{\lambda\xi}/4 - F^\xi_\mu F_{\nu\xi})}{2} \tag{6.16}$$

and $F^{\mu\nu}$ is the usual field strength of the electromagnetic field.
It is straightforward to see that taking $g_{55} = -\Phi^2 = -1$ equations (6.12), (6.13) reduce to the Einstein and Maxwell equations in 4D and (6.14) defines the electromagnetic gauge.

$$G_{\mu\nu} = \frac{\kappa^2}{2}T_{\mu\nu}, \tag{6.17}$$

$$\nabla^\mu F_{\mu\nu} = 0, \tag{6.18}$$

$$F^{\mu\nu}F_{\mu\nu} = 0. \tag{6.19}$$

One can notice that in the absence of the electromagnetic field, the set of equations describes only gravitational vacuum solutions of a Universe with no matter or energy content and consequently flat. The unique deviations from a 4D flat metric come from the electromagnetic sector implying that $g_{\mu\nu} = \eta_{\mu\nu}$. In this way (6.8) becomes:

$$g_{\alpha\beta} = \begin{pmatrix} \eta_{\mu\nu} - \kappa\Phi^2 A_\mu A_\nu & -\kappa\Phi^2 A_\mu \\ -\kappa\Phi^2 A_\nu & -\Phi^2 \end{pmatrix}. \tag{6.20}$$

It is possible to summarize what has been done in a more refined fashion by saying that starting from a gravitational 5D action of the form

$$S_G = -k \int d^5 x R^{(5)} \sqrt{-g^{(5)}}, \tag{6.21}$$

we to obtain the effective 4D action

$$S_{eff} = -\kappa \int d^4 x R^{(4)} \sqrt{-g} - \int d^4 x \frac{1}{4} F_{\mu\nu} F^{\mu\nu} \tag{6.22}$$

under the assumptions of cylinder constraint, appropriate gauge, and constancy of the scalar component.
The further step is to introduce a five-dimensional fermion field and look at its effective manifestation in the non-compact (3+1)-dimensions. The mathematics involved requires a certain familiarity with the Dirac equation and action in curved spacetime. This means being familiar with the Vielebein, the spin connection, and so on. In the following pages, I will give a brief synthesis since this is not the main topic of this chapter.

- The spin space of a 5-dimensional spacetime is 4-dimensional, so the spinorial representation remains the familiar one having four indices.

- The gamma matrices need to satisfy a Clifford algebra for a 5D curved spacetime metric tensor

  $$\{\tilde{\gamma}_\alpha, \tilde{\gamma}_\beta\} = g_{\alpha\beta} \times I_{4\times 4}.$$

  A 5^{th} gamma matrix needs to be introduced even in a flat 5D manifold. It is easy to verify that

  $$\gamma_5 = \gamma_1 \gamma_2 \gamma_3 \gamma_4$$

  is the one desired if $\gamma_{1,2,3,4}$ are the usual Dirac matrices, since

  $$\{\gamma_a, \gamma_b\} = \eta_{ab} \times I_{4\times 4}.$$

  To obtain the curved version one invokes the vielbein defined as

  $$e_a^\alpha e_b^\beta \eta^{ab} = g^{\alpha\beta}$$

  and defines $\tilde{\gamma}_\alpha = e_\alpha^a \gamma_a$.

- Spinors are orientable objects. If transported along a line in a curved spacetime it is important that their transport takes place in a parallel way to guarantee a proper definition of differentiation. For this reason, one introduces the covariant derivative

$$D_\alpha = (\partial_\alpha - \frac{i}{2}\omega_\alpha^{cd} S_{cd}),$$

where $S_{cd} = \frac{i}{4}[\gamma_c, \gamma_d]$ and $\omega_\alpha^{cd} = e_\beta^c \Gamma_{\delta\alpha}^\beta e^{\delta d} + e_\beta^c \partial_\alpha e^{\beta d}$ is called spin connection. As seen in previous chapters.

We may then generalize the massless Dirac action in 4D

$$\int d^4x (i\bar{\psi}\gamma^\mu \partial_\mu \psi + h.c.), \tag{6.23}$$

to the 5D in curved spacetime

$$S_D = \int d^5x \sqrt{g^{(5)}} (i\bar{\psi}\tilde{\gamma}^\alpha D_\alpha \psi + h.c.), \tag{6.24}$$

and by the explicit definition of the momentum operator $p_\alpha = i\partial_\alpha$, we obtain

$$S_D = \int d^5x \sqrt{g^{(5)}} (\bar{\psi}\tilde{\gamma}^\alpha (p_\alpha + \frac{1}{2}\omega_\alpha^{cd} S_{cd})\psi + h.c.). \tag{6.25}$$

An explicit calculation of the Vielbein and the invariant volume considering the metric tensor given in (6.20) with $\Phi^2 = -1$ leads to

$$S_D = \int d^5x (\bar{\psi}(\gamma^m (p_m + \frac{p_5}{\sqrt{\kappa}} A_m) + \gamma^5 p_5 + \tilde{\gamma}^\alpha \frac{1}{2}\omega_\alpha^{cd} S_{cd})\psi + h.c.). \tag{6.26}$$

One may ignore the last term of Eq. (6.26), since it can be decomposed into a null term and a negligible term describing an extremely small coupling with gravity, thus obtaining

$$S_D = \int d^5x (\bar{\psi}(\gamma^m (p_m + \frac{p_5}{\sqrt{\kappa}} A_m) + \gamma^5 p_5)\psi + h.c.). \tag{6.27}$$

It is now easy to recognize the arising charge and mass from the motion in the extra dimension and identify them as

$$q = \frac{p_5}{\sqrt{\kappa}} \quad \text{, and} \tag{6.28}$$

$$m = p_5. \tag{6.29}$$

Integrating in the 5^{th} dimension

$$S_{Deff} = 2\pi R \int d^4x (\bar{\psi}(\gamma^m(p_m + qA_m) + \gamma^5 m)\psi + h.c.). \tag{6.30}$$

The 5^{th} dimension is such that $x^5 = x^5 + 2\pi R$ so the Fourier expansion of a spinor ψ, periodic in x^5 can be made, and will have the coefficients depending on x^μ,

$$\psi = \sum_n \psi(x^\mu) Y_n(x^5) \tag{6.31}$$

where $-\partial_5^2 Y_n = \frac{n^2}{R^2} Y_n$, so that $Y_n(x^5) = \frac{1}{\sqrt{2\pi R}} e^{-ix^5 \frac{n}{R}}$. Now substituting the spinor Fourier expansion in the general 5D Dirac action differentiating with respect x^5 where possible and subsequently integrating one obtains

$$S_{Deff} = 2\pi R \sum_n \int d^4x (\bar{\psi}_n(\gamma^m(p_m + \frac{n}{R\sqrt{\kappa}} A_m) + \gamma^5 \frac{n}{R})\psi_n + h.c.). \tag{6.32}$$

It is trivial to deduce that

$$q_n = \frac{n}{R\sqrt{\kappa}} \tag{6.33}$$

$$m_n = \frac{n}{R} \tag{6.34}$$

These are called Kaluza-Klein states, and for a four-dimensional observer, they appear as a series of states, known as the Kaluza-Klein tower. All states in the tower share the same quantum numbers except for the electric charge [1] and the mass. These quantities increase proportionally as one climbs the tower. The proportionality depends on the radius of the 5^{th} dimension.
The zero-mode has no dependence on the 5^{th} dimension and so has a vanishing mass. It is followed by the tower of massive modes, the lightest of which is

[1] In more realistic extra-dimensional models, the photon corresponds to the zero mode of a 5-dimensional gauge field and not from the metric, in which case all states in the KK tower of 5D fields share the same electric charge.

called the Lightest Kaluza-Klein Particle (LKP). The SM fields correspond to the $n = 0$ modes of the towers, one for each 5^{th} dimensional field. The chirality of fermionic zero-modes is realized by imposing an additional discrete symmetry (i.e. a reflection) on the compact extra-dimension, known as an orbifold, under which the 5D fields are either even or odd. Momentum conservation along the compact extra-dimension, which would result in the conservation of the KK-number n, is then broken by the orbifold discrete symmetry, nevertheless preserving a conserved KK-parity. Modes in the tower are allowed to decay if respecting the KK-parity $P = (-1)^n$, and as in the case of R-parity in supersymmetric theories, the LKP is stable. Kolb and Slansky in 1984 [167] first studied the LKP as a DM candidate. The LKP has since been reconsidered in the framework of universal extra dimensions. Servant and Tait [168, 169] calculated the relic density of the LKP. They found that if the LKP is to account for the observed DM quantity, its mass range should span between 900 and 1200 GeV. The LKP annihilation cross-section was calculated in [168, 169].

6.3 QCD Axion

The vacuum structure of non-Abelian theories, and in particular of QCD, is topologically non-trivial. This is at the base of the so-called strong CP-problem. In principle, all pieces of Lagrangian of dimension 4, renormalizable, unitary, and Lorentz invariant have the same right to be introduced in the definition of the Lagrangian density of a specific theory. The contraction of the field strength with its dual is often neglected. The reason is that it can be written as a total derivative and does not affect the equation of motion and the Feynman rules. However, this term can produce physical consequences if we consider non-perturbative effects. In QCD this term reads

$$\mathcal{L}_\theta = \theta \frac{g}{32\pi^2} G^{a\ \mu\nu} \tilde{G}^a_{\mu\nu}, \tag{6.35}$$

where $G^{a\ \mu\nu}$ is the field strength, $\tilde{G}^a_{\mu\nu} = \frac{1}{2}\epsilon_{\mu\nu\sigma\rho} G^{a\ \sigma\rho}$ (where $\epsilon_{\mu\nu\sigma\rho}$ is the totally asymmetric symbol) is its dual, and a is the color index.
It is not hard to show that

$$G^{a\ \mu\nu} \tilde{G}^a_{\mu\nu} = 2\partial^\mu J^{CS}_\mu \tag{6.36}$$

where $J^{CS}_\mu = \epsilon^{\mu\nu\sigma\rho} A^a_\nu \left(G^a_{\sigma\rho} - \frac{1}{3} f^{abc} A^b_\rho A^c_\sigma \right)$, A^a_μ is the gauge field and f^{abc} are the structure constants of the symmetry group.
Let us consider a Wick rotation in which $t \to it$ in order not to work in a Minkowskian spacetime but in a 4-dimensional Euclidean one. The contribution to the action of (6.35) reads

$$S_E^{G\tilde{G}} \sim \int G^{a\ \mu\nu} \tilde{G}^a_{\mu\nu} d^4x = \int 2\partial^\mu J^{CS}_\mu d^4x = \oint_{S^3} J^{CS}_\mu d^3x, \tag{6.37}$$

where S^3 is the 3-sphere at the boundary of the 4-dimensional Euclidean spacetime. It is thus understandable why the contribution of such a term was neglected at a classical level, not contributing to the equations of motion.
However, since we are interested in a quantum field formulation of the theory, we have to consider the mean values of observables calculated through path integrals. In Euclidean spacetime, these integrals over the configurations of the fields are weighted by the factor $\exp[-S_E]$. For this reason, the contribution of the $G\tilde{G}$ term can be non-vanishing only if the integral (6.37) converges. This integral certainly converges for a field strength vanishing at infinity rapidly enough. This condition can be fulfilled trivially by requiring the gauge field to vanish at infinity rapidly enough, having so a vanishing current. However, it is equally possible to consider a gauge field at infinity given by a gauge transformation depending solely on the angular variable of the Euclidean spacetime Ω. Such a transformation is called pure gauge transformation:

$$A^\mu|_{r\to\infty} = -\frac{i}{g}(V(\Omega))V^\dagger(\Omega). \tag{6.38}$$

In this case the integral (6.37) reads:

$$S_E^{G\tilde{G}} \sim \oint_{S^3} (V(\Omega))V^\dagger(\Omega)(V(\Omega))V^\dagger(\Omega)(V(\Omega))V^\dagger(\Omega) d^3x. \tag{6.39}$$

This integral is the one defining the Pontryagin index or winding number. This quantity is counting how many times the map $V(\Omega) : S^3 \to SU(3)$, is wrapping up the elements of the gauge group while going across the 3-sphere. This must be an integer number. Configurations possessing different winding numbers cannot be recast into one another by a continuous transformation. In such a case, the vacuum configurations are topologically distinct, and between one vacuum configuration and the other, there are non-vacuum states. This

vacuum configuration is far from trivial. At a classical level once a vacuum configuration is chosen, the system will stay there, but at the quantum level, there is the possibility of tunneling between one vacuum and another. Thus, in the general case, the integral (6.39) will provide a non-vanishing contribution depending on the number of topologically non-trivial configurations.
In the case of an abelian theory, the gauge group is so simple that on the 3-sphere there is space enough to be recast always in the trivial configuration. Namely, for abelian theories, there is only one vacuum configuration. For this reason, in QED the term $F\tilde{F}$ is neglected also at the quantum level. As we just saw, in the case of non-Abelian gauge theories there exist configurations allowing this term to obtain a finite action. These configurations are called instantons [170]. Due to the existence of instantons, we must consider the vacuum structure of a quantum field theory in an unusual way called the theta vacuum. Such a vacuum structure is periodic and there exist different ground states, one for each non-trivial configuration. Instantons are the quasi-particles associated with the tunneling of the field from one vacuum into another. Instantons give a physical contribution modifying the vacuum energy which will be a periodic function of θ. An approximation of this term is

$$E(\theta) = m_\pi^2 f_\pi^2 \sqrt{1 - \frac{4 m_u m_d}{(m_u + m_d)^2} \sin^2 \frac{\theta}{2}} \tag{6.40}$$

where m_π and f_π are the pion mass and decay constant determining the confinement scale of QCD, Λ_{QCD}, and m_u and m_d are the up and down quark mass respectively.
Historically, these solutions were involved as a resolution of the old $U(1)_A$-problem of QCD [171,172] the resolution of which generates another problem: the strong CP-problem.
In interacting quantum theory, the bare θ term does not represent a physical quantity. The pre-factor of the $G\tilde{G}$ piece of the Lagrangian receives an additional contribution. The origin of this contribution is due to the triangular anomaly in performing the chiral rotation of the Yukawa phases of the quark masses. The physical term will read

$$\bar{\theta} = \theta + \arg[\det[M_q]], \tag{6.41}$$

where M_q is the matrix of quark masses. Therefore the QCD Lagrangian reads

$$\mathcal{L}_{QCD} = \sum_q \bar{\psi}_q(iD - m_q)\psi_q - GG - \bar{\theta}\frac{g}{32\pi}G\tilde{G}, \tag{6.42}$$

It is possible to show that the $G\tilde{G}$ piece of the Lagrangian violates the CP symmetry. In fact, this term yields an electric dipole moment for the neutron given by:

$$|d_n| = 3.6 \times 10^{-16}\bar{\theta}, \tag{6.43}$$

while experimental measurements [173] constrain $|d_n| < 2.9 \times 10^{-26}$, requiring $\bar{\theta} \lesssim 10^{-10}$. Such a constraint represents a fine-tuning problem since (6.41) states that this parameter is composed of two terms belonging to unrelated sectors of particle physics: θ having a pure QCD origin and $\arg[\det[M_q]]$ which has a weak origin due to the Higgs mechanism.

An elegant and attractive solution to the strong CP-problem was proposed by Peccei and Quinn [174–177]. The idea is to introduce a dynamical quantity mimicking the $\bar{\theta}$ parameter and taking a zero value in the minimum energy configuration. Shortly time after the proposal, it was suggested that this dynamical variable should be identified as a light spin-zero particle, called the axion [178, 179].

It is in fact possible to equip the SM with an additional field, called the axion field, enjoying a $U(1)_{PQ}$ global symmetry, i.e. a symmetry that is spontaneously broken at some high scale, and the axion is the resulting Goldstone boson mode. This symmetry is also broken by the axial anomaly so that the axion acquires interactions with gluons through the triangular anomaly, which generates the desired axion potential.

This then motivates the introduction of a new piece of Lagrangian describing the axion field:

$$\mathcal{L}_a = \frac{1}{2}\partial_\mu a(x)\partial^\mu a(x) + \frac{a(x)}{f_a}\frac{g}{32\pi^2}G^{a\ \mu\nu}\tilde{G}^a_{\mu\nu} \tag{6.44}$$

In Eq.(6.44) $a(x)$ is the axion field and f_a is an energy scale called axion decay constant corresponding to the scale at which the PQ symmetry is spontaneously broken.

The CP violating term in the full Lagrangian reads

$$\mathcal{L}_{eff} = \left(\bar{\theta} + \frac{a(x)}{f_a}\right) \frac{g}{32\pi^2} G^{a\ \mu\nu} \tilde{G}^a_{\mu\nu}. \tag{6.45}$$

We then see that the effective theta-term becomes a dynamical field, with a periodic potential that results from QCD instanton effects as in Eq. (6.40). Defining the physical axion field as $a_P = a - \langle a \rangle = \bar{\theta} f_a + a$, The axion potential is given by:

$$V_{eff}(a_P) = m_\pi^2 f_\pi^2 \sqrt{1 - \frac{4 m_u m_d}{(m_u + m_d)^2} \sin^2 \frac{a_P}{2}}. \tag{6.46}$$

A Taylor expansion of Eq. (6.46) around the vacuum expectation value reads

$$V_{eff}(a_P)|_{a_P \sim 0} \sim V_{eff}(0) + \frac{a_P}{f_a} [\partial_{a_P} V_{eff}](0) + \frac{1}{2} \frac{a_P^2}{f_a^2} [\partial^2_{a_P} V_{eff}](0) \tag{6.47}$$

$$\sim 0 + 0 + \frac{1}{2} \frac{a_P^2}{f_a^2} [\partial^2_{a_P} V_{eff}](0). \tag{6.48}$$

From this, we can identify the axion mass:

$$m^2_{a_P} = \frac{[\partial^2_{a_P} V_{eff}](0)}{f_a^2}. \tag{6.49}$$

Exploiting Eq. (6.46) one can obtain an explicit formula for the axions mass:

$$m^2_{a_P} = \frac{m_\pi f_\pi}{f_a} \frac{m_u m_d}{(m_u + m_d)^2} \quad \Rightarrow \quad m_{a_P} \sim (5.91 \pm 0.53)\ \mu\text{eV}\ \left(\frac{10^{12}\ \text{GeV}}{f_a}\right). \tag{6.50}$$

These particles have not been experimentally detected. Therefore, if they exist, they must be extremely light $m_a < 10^{-2}$ eV [180], from astrophysical constraints. This implies that the axion decoupling constant f_a needs to be fixed at remarkably high energies.

It is worth noting that the anomaly giving rise to the interesting axion potential involving gluons also leads in general to a similar axion-photon interaction term (since quarks carry not only the color charge but also the electromagnetic one) that reads:

$$\mathcal{L}_{a\gamma\gamma} = \frac{a(x)}{f_a} \frac{\alpha}{32\pi^2} F^{\mu\nu} \tilde{F}_{\mu\nu}. \tag{6.51}$$

This interaction allows the axions to decay into two photons and the lifetime of an axion is given by

$$\tau_a \sim 3 \times 10^{32} \left(\frac{m_a}{10^{-5}\ \text{eV}} \right)\ \text{Gyr}. \tag{6.52}$$

Considering the allowed axion mass range, we see that their lifetime is larger than the age of the Universe, making them interesting light dark matter candidates.

6.4 The Axiverse: Axion-Like Particles

String theories usually invoke six dimensions in addition to the normal four-dimensional spacetime. In order to reconcile this and the observational evidence the extra dimensions must be compactified as in the KK theory. Therefore, it is somewhat intuitive that any type of field (tensor, vectors, spinor, etc) living in the extra dimensions manifests in spacetime as a scalar field. String theories are usually built through bosonic strings and, to agree with the low-energy observations, fermions must be obtained through supersymmetry. No supersymmetric partner has been observed therefore this symmetry must be broken.

Superstring theory is one of the leading candidates for a fundamental theory combining quantum gravity and the Standard Model (SM) of particle physics. The energy scale at which 'stringy' effects become relevant is, however, unknown, and it may well be too high for these effects to be tested in the foreseeable future. The need for six additional compact spatial dimensions, with unknown size and geometry, and (broken) supersymmetry also leads to a plethora of different low energy theories, making it hard to identify specific signatures of the underlying fundamental theory that could be tested in the laboratory or with astrophysical observations.

There is, however, a fairly generic prediction of string compactifications, if the strong CP problem is solved by the Peccei-Quinn mechanism [174, 178, 179], is the existence of a large number of light pseudoscalar particles in the effective four-dimensional theory [181]. These axion-like particles (ALPs) arise as the zero-modes in the Kaluza-Klein expansion of antisymmetric tensor fields in the underlying string theory, including the Neveu-Schwarz 2-form B_2, existent in all closed string theories, and the Ramond-Ramond p-forms of Type II and

Type 1 string theories [192]. (There are also other ways that ALPs can arise.) Each p-form can give rise to a multitude of ALPs in the 4d theory, as many as the number of homologically inequivalent p-cycles (closed surfaces) in the extra-dimensional manifold. This number is typically large, of the order of 10^2 or even 10^5, simply due to the number of different ways in which a closed surface can be embedded within a six-dimensional compact manifold.
One of these particles can be the strong-CP-problem solving QCD axion, and much like the latter a large fraction of the ALPs are protected at all loop orders by shift symmetries inherited from the gauge symmetries of their parent tensor fields. The generic expectation is therefore that realistic string scenarios exhibit a large number of light or even ultra-light axions, whose exponentially small masses are generated solely by non-perturbative effects. This string axiverse prediction will play a key role in our discussion.

6.5 Hidden Sector

The term Hidden (or dark) Sector (HS) in particle physics denotes a broad container filled with collections of hypothetical and yet-unobserved quantum fields and their corresponding particles. These particles couple weakly to the SM particles, through gravity or by means of new mediators. Examples of hidden particles include the dark photon, sterile neutrino, and axion.
Typically, a new gauge group independent from the SM gauge group characterizes the HS and the HS could be simply a single particle, or contain multiple new particles, dark gauge forces, and more degrees of freedom [182–191]. Commonly string theory provides a rich HS, as, for example, the copy of the SM coming from the gauge group of the heterotic string $E_8 \times E_8$. Similarly, hidden valley models [187] introduce a populated sector that only weakly communicates with the SM.
In Chapter 8 we will consider a model where the HS contains an exact copy of the SM degrees of freedom and all particles in the HS sector have a common mass, 5 TeV. This model is motivated by the Mirror Dark Matter [184] scenario in which an HS copy of the SM communicates with the SM only via small portal couplings and corresponds to the specific model $DS(N, \Lambda_{DS})$ considered in [190, 191], with $N = 1$ and $\Lambda_{DS} = 5$ TeV.

7 Evaporating PBHs, the string axiverse, and hot dark radiation

We show that primordial black holes (PBHs) develop non-negligible spins through Hawking emission of a large number of axion-like particles generically present in string theory compactifications. This is because scalars can be emitted in the monopole mode ($l = 0$), where no angular momentum is removed from the BH, so a sufficiently large number of scalars can compensate for the spin-down produced by fermion, gauge boson, and graviton emission. The resulting characteristic spin distributions for 10^8-10^{12} kg PBHs could potentially be measured by future gamma-ray observatories, provided that the PBH abundance is not too small. This yields a unique probe of the total number of light scalars in the fundamental theory, independent of how weakly they interact with known matter. The present local energy density of hot, MeV-TeV, axions produced by this Hawking emission can possibly exceed $\rho_{\rm CMB}$. Evaporation constraints on PBHs are also somewhat weakened. All these results can be found in [11].

7.1 Introduction

Light string axions can have a wide range of cosmological and astrophysical effects, i.e. steps in the matter power-spectrum, rotation of the CMB polarization, and black hole superradiant instabilities [181, 193]. These effects can yield interesting observational signatures of individual string axions in particular mass ranges, but not of the whole 'string axiverse'. The number of relativistic degrees of freedom during cosmological nucleosynthesis or recombination could, in principle, be sensitive to the total number of light axions below a certain mass scale, but this depends crucially on whether they have

been in thermal equilibrium with SM particles in the early Universe, which given the feebleness of their expected interactions with the latter is rather unlikely.

Here, we propose a new way to probe the total number of ALPs with mass $m <$ few MeV through the spin distribution of primordial black holes (PBHs) that are evaporating today. PBHs [2] can be formed in the early Universe through the gravitational collapse of large overdensities once their scale becomes smaller than the Hubble horizon [153,194]. These could be generated by a plethora of different mechanisms, eg, non-standard inflation scenarios, curvaton models, or bubble collisions in cosmological phase transitions, spanning a wide range of masses. PBHs may account for at least a fraction of the dark matter in the Universe, which has sparked a renewed interest in this subject, alongside the recent detection of gravitational waves from a population of astrophysical BH binaries (see i.e. [156] for a recent review).

Here we will be interested in small PBHs born with masses around 10^{12}-10^{13} kg, which are evaporating today. Although Hawking evaporation generically spins down a BH, an exception is the emission of light scalar particles, as first pointed out by Taylor, Chambers, and Hiscock (TCH) [90–92], since these are the only type of particle that can be emitted in the monopole ($l = 0$) mode. Scalar emission may therefore reduce a BH's mass without reducing its angular momentum, therefore increasing its dimensionless spin parameter $\tilde{a} = J/M^2$ (we set $G = \hbar = c = k_B = 1$). In fact, TCH showed a BH evaporating solely through scalar emission would asymptote to a configuration with $\tilde{a} \simeq 0.555$, and that at least 32 light scalars could compensate the BH spin down through the emission of photons, neutrinos, and gravitons.

Given the large number of ALPs expected in realistic string compactifications, this motivates exploring the spin evolution of PBHs in this context. We will assume that Hawking emission is the only mechanism that affects the PBH spin, an assumption that we will critically review at the end of our discussion. In the simplest scenario of PBH formation where large density fluctuations are generated on super-horizon scales and reenter the Hubble horizon during the radiation era, the nearly spherical collapse endows the BHs with only a small spin, at the few percent level [195–197]. There are, however, several possible scenarios where PBHs could be born with much larger spins, i.e. formation during an early matter-dominated epoch [198]. We will be agnostic about such initial conditions, since as we will show any natal spin is erased once a PBH

has evaporated significantly *unless* a substantial number of light scalar fields is emitted. Appendix A is related to this chapter and discusses a calculation performed with BlackHawk validating our results.

7.2 PBHs evaporation in the Axiverse

To determine the evolution of PBHs we follow the formalism of Page [87, 88], where the dynamics of the BH mass and spin are determined by the functions $\mathcal{F} \equiv -M^2 dM/dt$ and $\mathcal{G} \equiv -(M/\tilde{a})dJ/dt$, which removes the dependence on the BH mass.

We include in our numerical calculation an arbitrary number, N_a, of scalars which, for simplicity, we assume to have masses below the initial T_H, which is around the 10 MeV scale for PBHs with a lifetime comparable to the age of the Universe. These are emitted alongside photons, gravitons, neutrinos, and electrons/positrons from the start of our calculation.

In Figure 7.1, we give our result for the present spin of PBHs, $\tilde{a}_0$, as a function of their present mass, M_0, for different numbers of emitted ALPs, assuming an initial spin $\tilde{a} = 0.01$ corresponding to PBH formation in the radiation era. Note that BHs in the given mass range correspond to the evaporated remnants of an initial population of PBHs with comparable masses which are presently at different stages of their evolution. This justifies assuming a common initial spin. We also note that the critical PBH mass for a lifetime matching the age of the Universe of 13.8 Gyr exhibits a weak dependence on the number of different axions emitted, ranging from $5 \times 10^{11}\,\mathrm{kg}$ in the absence of light axions to $\sim 2.7 \times 10^{12}\,\mathrm{kg}$ for $N_a = 1000$, with a $N_a^{1/3}$ scaling for $N_a \gtrsim 10$. While Fig. 1 shows the current snapshot of the PBH Regge plot, it can also be viewed as a time evolution, since heavier BHs have evaporated little and lighter BHs have already lost a significant fraction of their original mass. For $N_a = 0$, PBHs quickly lose their initial spin as they evaporate, as has been the standard lore in the literature. However, the inclusion of many ALPs changes this picture considerably, with $\tilde{a}$ increasing initially due to the emission of the light scalars. For $N_a \lesssim 400$, the spin increases until T_H reaches the threshold for quark and gluon emission, at which point the BH starts to spin down due to the large number of colored spin-1/2 and spin-1 degrees of freedom. For yet larger N_a, which is still plausible in string theories, the BH spin parameter stabilizes at values $\tilde{a}_0 \gtrsim 0.2$ and tending to the critical value

$\tilde{a}_0 \simeq 0.555$ found by TCH for pure scalar emission. Note that, for $N_a \gtrsim 400$, PBHs never spin down completely even including all SM degrees of freedom, since $d\ln\tilde{a}/d\ln M = \mathcal{G}/\mathcal{F} - 2$ has a non-trivial zero.

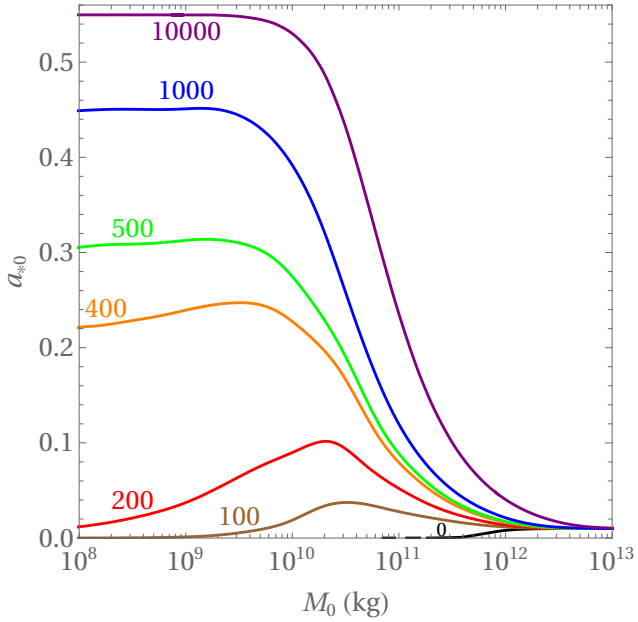

Figure 7.1: Present PBH spin, $\tilde{a}_0$, as a function of their present mass, M_0, for an initial population with spin $\tilde{a} = 0.01$ and varying mass. Curves labeled by the number of light ALPs.

For comparison, we show in Fig. 7.2 the results for an initial population of near-extremal PBHs. Again, we find that even in this case PBHs with masses below $\sim 10^{11}$ kg should have a presently negligible spin for $N_a = 0$, but the inclusion of many light axions halts the BH spin-down or at least delays it considerably until QCD degrees of freedom can be efficiently emitted. Once more we find that for $N_a \gtrsim 400$, $\tilde{a}_0 \gtrsim 0.2$ for light BHs. We note that the slightly oscillatory behavior that can be observed in some of the curves in Fig. 7.2 in the mass range 10^{10}-10^{11}kg is due to the opposing effects of π's and μ's on the spin evolution, with the former contributing to the BH spin-up and the latter spinning the BH down.

Although not shown explicitly, we have found similar spin distributions for intermediate values of the initial spin, with either a 'peak'- or 'plateau'-like shape in the 10^{10}-10^{11} kg (present) BH mass range, where $T_H \sim 0.1$-1 GeV. These are the PBHs that have evaporated essentially through the emission

of non-colored degrees of freedom and for which the effect of the additional axions is more pronounced. A generic feature is thus that PBHs in this mass range should have present spin parameters of at least $\tilde{a}_0 \sim$ few $\times 10^{-2}$, and up to or slightly over ~ 0.5 in the presence of hundreds of light axions so that detecting BHs with such properties would constitute a 'smoking gun' for the string axiverse.

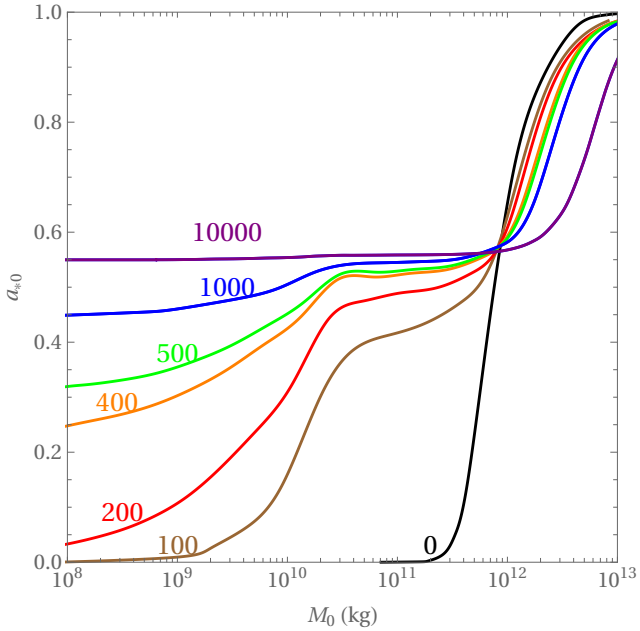

Figure 7.2: As Fig. 1 except initial spin parameter $\tilde{a} = 0.99$.

This conclusion is, of course, based on the assumption that evaporation is the main mechanism driving spin evolution. This is justified in the relevant PBH mass range as, firstly, accretion has been shown to be irrelevant for small PBHs with a lifetime close to the age of the Universe [199] and is also expected to occur in a quasi-spherical regime where a BH cannot efficiently spin up [200]. Secondly, mergers should also be rare events for PBHs in this mass range. Following i.e. [201], two BHs can become gravitationally bound and decouple from the Hubble flow if their physical separation at matter-radiation equality $x < f^{1/3}\bar{x}$, where $\bar{x}$ is the average BH separation at this redshift and f is the PBH fraction of the dark matter density. Given the existing constraints on f for BHs that are evaporating today from the contribution of Hawking radiation to the extra-galactic diffuse gamma-ray background, $f \lesssim 10^{-7}$ [154, 202],

we conclude that only a small fraction of such BHs can become gravitationally bound and subsequently merge. Furthermore, mergers occurring early in the cosmic history will only affect the 'initial' conditions for the subsequent evolution driven essentially by evaporation.

Finally, PBHs in the interesting mass range also suffer from pion superradiant instabilities, where dense clouds of π^0's are produced around the PBHs at the expense of their rotational energy [203]. However, such instabilities are only triggered for large initial spins and remain active for less than $\sim 1\,\mathrm{Gyr}$, before the PBHs have evaporated significantly. Hawking evaporation will thus still determine the final BH spins as assumed in our computation. Superradiant instabilities could also be triggered by other exotic particles, in particular, if there are string axions with masses $\gtrsim$ MeV-GeV and sufficiently long lifetimes (see next chapter), potentially producing characteristic gaps in the primordial black hole mass-spin distribution [12]. This is quite model-dependent and requires a simultaneous study of the evolution of the black holes' mass and spin through both superradiance and Hawking evaporation. We leave this analysis to the next chapter.

The PBH spin distribution found here is, in any case, characteristic of the evaporation process in the presence of many light scalar fields and cannot, to our knowledge, be mimicked by other processes. Thus, observing such a distribution would constitute a unique signature of an underlying theory with a large number of light scalars.

7.3 The hot dark radiation

Note that the presence of many ALPs weakens the limits on the initial f (and somewhat f_0) as, for a given present M_0 a reduced fraction of the total lifetime-integrated BH luminosity goes into photons. Moreover, the past-emitted photons are less energetic than they would have been in the absence of the ALPs as the past BH must be heavier, and thus colder, than in the $N_a = 0$ case. Precise evaluation of the new limits requires a dedicated study which we leave to future work. (For related studies of modified PBH constraints in the context of extra-dimensional and other non-SM theories see [95, 190, 206–208].) We take $f_0 \sim 10^{-7}$ to roughly saturate current bounds[1] [154, 202].

[1] A recent analysis of the 21 cm EDGES signal places a more constraining bound $f < 10^{-9.7}$ [205], but only when assuming a significant X-ray heating of the intergalactic medium

Instead, the BH Hawking luminosity is dominated by a population of hot quasi-blackbody ALPs with mean energy $\sim 2.8T_H$, which are 'dark' with respect to the SM up to possible feeble interactions set by $1/f_a$, where f_a is the appropriate axion 'decay constant'. The integrated flux of ALPs from a single PBH is $\sim 3 \times 10^{22} N_a (10^{10}\ kg/M)$ in the relevant PBH spin range. Unlike the case of greatly-red-shifted dark matter particles and/or axions produced by the Hawking evaporation of micro PBHs in the very early pre-BBN universe [209–212] the axions in our case are hardly red-shifted at all as the relevant Hawking emission is occurring now.

Although extremely challenging to detect, the much higher energies of these axions (and masses too for some of the ALPs) might enable new detection strategies as compared to the standard QCD axion solar flux expected for a given $1/f_a$. Also note that the usual ΔN_{eff} constraints [211–213] on extra relativistic degrees of freedom from BH evaporation derived from observations of BBN, CMB, or structure-formation epochs do not apply as the Hawking emission conversion of PBH mass into relativistic ALPs is dominated by late times and the present local energy density of hot 'dark-radiation' ALPs can potentially exceed ρ_{CMB}. Detection of one or more sub-components of this background of energetic dark axions would be a striking signal for both axiverse physics and the existence of Hawking evaporating PBHs.

7.4 Detectability

Evaporating PBHs in the interesting mass range may in principle be detected through their Hawking photon emission, which includes both primary and secondary photons, i.e. those produced by the decays of the Hawking-emitted particles. The latter dominate the flux for PBHs in the 10^{10}-10^{11} kg mass range [116]. According to [204], a 10^{10} kg PBH could be detectable with Fermi-LAT up to a distance of ~ 200 AU. This compares to the mean distance between PBHs of present mass M_0 accounting for a present fraction f_0 of the local dark matter density $d \simeq 40\,\mathrm{AU}(M_0/10^{10}\mathrm{kg})^{1/3}(10^{-7}/f_0)^{1/3}$.

Planned gamma-ray observatories, i.e. HARPO and e-ASTROGAM, are expected to reach a somewhat better sensitivity than Fermi-LAT in the energy range of 0.1-1GeV [214], although an improvement of a few orders of magnitude

at large redshifts, which is not known. We anyway expect this constraint to be weakened in the axiverse picture given that PBHs at large z are colder than in the standard scenario.

could be required if $f_0 \ll 10^{-7}$, or if a precise measurement of the full photon spectrum, including secondaries, is required for an accurate determination of the PBH mass and spin.

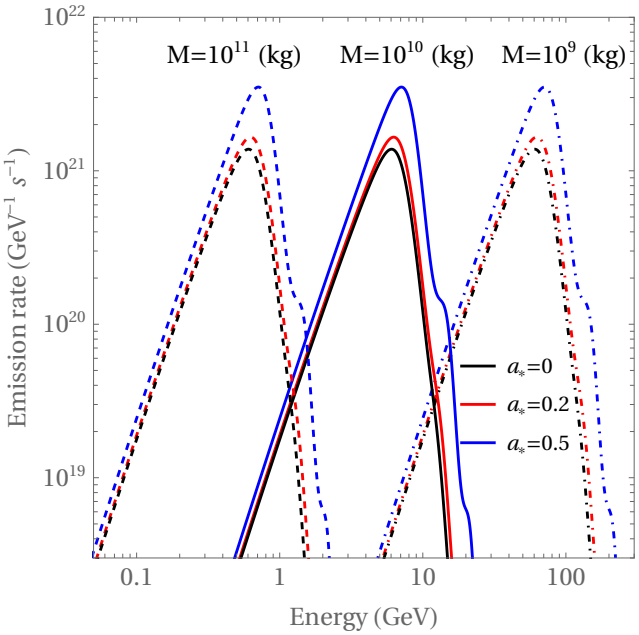

Figure 7.3: Primary photon spectrum for PBHs with $\tilde{a} = 00.2, 0.5$ (black, red, and blue respectively) and $M = 10^{11}, 10^{10}, 10^9$ kg (solid, dashed, and dotted curves, respectively), obtained using Eq. (5.36).

An interesting possibility is that some ALPs could decay into photon pairs after emission. Although this requires f_a's well below the typical GUT scale values of string constructions, such reduced decay constants are possible for some ALPs in warped and large-volume constructions [192, 215, 216]. In this case, such ALPs would contribute to the secondary photon emission, which would encode additional information on the axiverse. The corresponding contribution to the diffuse gamma-ray background could also yield additional constraints on PBHs.

In Fig. 3 we show the primary photon spectrum for different PBH masses and spins, given by (5.36) with $E_\gamma = \omega$.

As one can see, the peak emission is quite sensitive to the PBH spin, while the corresponding energy depends mostly on the PBH mass. A similar effect is obtained for spin-1/2 particles so we expect both the primary and secondary photon spectra to exhibit non-trivial dependences on the PBH mass and spin.

Although we will leave a detailed analysis of the full spectrum for future chapters, this suggests that in principle one can measure PBH spins $\tilde{a}_0 \gtrsim 0.1$ with at least a $\sim 10\%$ precision measurement of the photon spectrum, provided the distance to the PBH can be measured with comparable accuracy through parallax. Note that the time evolution of T_H, and thus photon flux and mean energy, is faster in the presence of many ALPs, than in the $N_a = 0$ case. Given suitable high-precision measurements, this can give confirmation of $N_a \neq 0$.
Moreover, halo PBHs velocities relative to the Earth are 2-3$\times 10^2$ km/s, corresponding roughly to 40-60 AU/yr. Thus the population of bright (for both photons and hot ALPs) 'point source' evaporating PBHs in the solar neighborhood can potentially change every few years, so increasing the chance of detecting BHs at different stages of their evaporation process. This further allows one to fully assess the effects of a large number of axions.

7.5 Conclusions

As one can see in this figure, in the absence of axions ($N_a = 0$, black curves) PBHs lose their spin quite quickly, such that any PBHs with present mass $\lesssim 10^{11}$ kg should have negligible spin, i.e. spin parameters well below the percent level. A drastic change in this picture occurs in the string axiverse for $N_a \gtrsim 100$, with PBHs initially spinning up due to the emission of a large number of light scalars (or spin loss being initially halted for initially near-extremal PBHs). When the PBH mass approaches $\sim 10^{10}$ kg and the corresponding Hawking temperature exceeds the QCD scale, the large number of spin-1/2 and spin-1 degrees of freedom emitted starts counteracting the light scalar emission, effectively spinning down the PBH as it evaporates for $N_a \lesssim 400$. Above this number of light axions, the PBH spin asymptotes to a non-vanishing value, which tends to the critical value $\tilde{a} \simeq 0.555$ originally found in [90–92] for pure scalar emission as $N_a \to \infty$.
Fig. 7.1 and 7.2 shows that, independently of their natal spin, PBHs with present mass $M_0 \lesssim 10^{11}$ kg should have a non-negligible spin in the string axiverse scenario (for $N_a \gtrsim 100$). For the case of initially slowly spinning PBHs, this is particularly relevant, since this spin up due to Hawking emission may render them unstable with respect to superradiant particle creation, namely if the string axiverse includes (as one may expect) heavier axions. As we will analyze in the next chapters, this may have a dramatic effect on the PBH spin

evolution, making the present PBH mass-spin distribution an even more powerful probe of the string axiverse spectrum, with potential directly observable signatures.

In conclusion, detecting evaporating PBHs is, of course, a worthy endeavor to pursue on its own, given what it can tell us about both the early history of the Universe and the nature of semi-classical BHs. Our analysis shows that, in addition, their mass-spin distribution can give a unique probe of beyond the SM physics, which we hope may motivate future efforts in PBH detection.

8 Superradiance, Hawking evaporation, and the string axiverse

In the string axiverse scenario, light primordial black holes may spin up due to the Hawking emission of a large number of light (sub-MeV) axions. We show that this may trigger superradiant instabilities associated with a heavier axion during the black holes' evolution, and study the coupled dynamics of superradiance and evaporation. We find, in particular, that the present black hole mass-spin distribution should follow the superradiance threshold condition for black hole masses below the value at which the superradiant cloud forms, for a given heavy axion mass. Furthermore, we show that the decay of the heavy axions within the superradiant cloud into photon pairs may lead to a distinctive line in the black hole's emission spectrum, superimposed on its electromagnetic Hawking emission. This chapter is based on the results of the original paper [12].

8.1 Introduction

As seen in the previous chapter PBHs naturally develop non-negligible spin parameters through Hawking emission of many light scalar particles naturally emerging from string compactification. This scenario motivates exploring whether this may trigger superradiant instabilities. In particular, in the string axiverse spectrum, there may also exist a number of *heavy axions* ($\mu \gtrsim$ MeV), since the non-perturbative nature of the axion mass generation mechanism only implies that their masses are exponentially suppressed compared to a high mass scale such as the supersymmetry breaking scale. Hence, if the PBHs are born with low spin, the condition for superradiant particle production $\mu < \Omega_H$ will only be satisfied once the PBHs evaporate sufficiently and

spin up due to the emission of *light axions*.

In this work, we thus study the dynamical generation of superradiant heavy axion clouds around PBHs born with mass $\sim 10^{12}$ kg throughout the cosmic history, including both superradiance and Hawking emission. We will show that indeed such clouds may form with two important observational consequences.

First, the formation of superradiant clouds spins down the PBHs faster than evaporation can spin them up. This modifies the present PBH mass-spin distribution such that the lightest PBHs (which have evaporated sufficiently for superradiant clouds to form) saturate the superradiance condition, $\Omega_H \simeq \mu$, while the spins of the heavier PBHs are determined solely by their evaporation stage and, hence, by the number of light axion species.

Second, the decay of the heavy axions into photon pairs leads to a characteristic gamma-ray line in the PBH-axion cloud photon emission spectrum. This is a unique signature since the Hawking emission spectrum (including both primary and secondary photons) evolves as the PBH evaporates, while the line has a fixed energy corresponding to approximately half of the heavy axion's mass.

We begin our discussion by first considering a toy model where a BH evaporates by emitting a single light axion and a superradiant instability is induced by another heavy axion. Although unrealistic, this toy model allows one to understand the basic dynamics of the problem towards exploring a more realistic setup where all Standard Model particles are included in the PBH evaporation process alongside an arbitrary number of light axions. We then compute the PBH photon emission spectrum including primary and secondary Hawking emission as well as heavy axion decay within the superradiant clouds. We summarize our main results and conclusions in the final section.

We note in advance that axion self-interactions are assumed to play a negligible role in the dynamical evolution. This is a good approximation for the large axion decay constants typically predicted in string constructions and that we also take into account when discussing observational prospects of their photon decay.

8.2 Superradiant instabilities for evaporating PBHs

This section[1] contains a toy model in which only 2 types of particles are considered: a massless scalar field, emitted through Hawking radiation, and a 1 GeV scalar field, which induces a superradiant instability. The toy model shows the competition, in the evolution of a BH, between evaporation and superradiance. Subsequently, we propose a more realistic model in which the Hawking radiation is given by the SM particles and an arbitrary number of ALPs.

8.2.1 A toy model

Given the discussion in the previous section, we may now consider the full evolution of a PBH mass and spin taking into account the effects of both superradiance and Hawking evaporation, given by:

$$\frac{dM}{dt} = -\mathcal{F}(\tilde{a})\frac{1}{M^2} - \mu\Gamma_s N \ , \tag{8.1}$$

$$\frac{d\tilde{a}}{dt} = \tilde{a}\frac{1}{M^3}(-\mathcal{G}(\tilde{a}) + 2\mathcal{F}(\tilde{a})) - \frac{1}{M^2}\Gamma_s N \ . \tag{8.2}$$

The equation for dN/dt is givn by (5.75). As previously discussed, we are interested in PBHs with a lifetime close to the age of the Universe, i.e. with an initial mass in the range $5 \times 10^{11} - 10^{12}$ kg, and particularly those born in the radiation era, with initial spins at or below the percent level. Despite their low spins, such PBHs may be superradiantly unstable already at formation, provided there are axions within the string axiverse in the right mass range. In particular, for PBHs with such mass and spin, superradiant instabilities may be triggered for axions with mass $\mu \lesssim 1$ MeV, but the axion mass cannot be too low, since the instability growth rate is proportional to μ^9 as given approximately in Eq. (5.76). Note, furthermore, that a significant amount of spin is only extracted from the PBH once the number of particles within the superradiant cloud $N \sim \tilde{a}M^2 \sim 10^{37}(\tilde{a}/0.01)(M/10^{12}\text{ kg})^2$, requiring $\mathcal{O}(100)$

[1] This section is the fruit of the collaboration with Filipe Serrano which I had the pleasure to follow during his master's thesis project he carried under the supervision of João G. Rosa. For this reason, part of this section may be similar to parts of Filipe's master thesis. I decided to include this section to be able to properly motivate the next section and with the additional motivation that it also contains results to which I originally contributed (i.e. Fig. 8.8) and ideas I helped develop.

e-folds of superradiant amplification. This means that superradiance is only efficient for axions roughly in the 0.1-1 MeV mass range for PBHs born in the radiation era, as illustrated in Fig. 8.1.

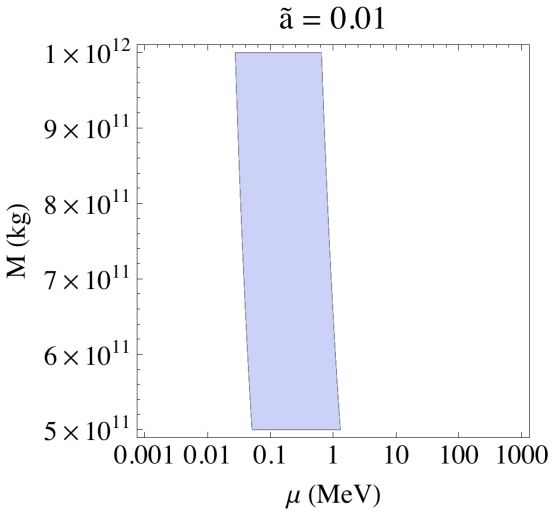

Figure 8.1: Range of the axion masses for which (i) superradiant instabilities are triggered at PBH formation for $\tilde{a}_i = 0.01$ and (ii) the superradiance condition is saturated by the present day ($\Gamma_s > 100\tau_{univ}$, where $\tau_{uni} \simeq 14$ Gyr is the age of the Universe).

Although there may be string theory compactifications including one or possibly more axions in this mass range, this is certainly not a generic expectation, since axion masses are exponentially sensitive to the magnitude of the non-perturbative effects that generate them. The hundreds or even thousands of light axions expected in realistic string compactifications should have masses distributed throughout a wide range of mass scales. Hence, scenarios with an axion in the mass range shown in Fig. 8.1 are certainly possible but not necessarily the most likely, so we will focus our discussion henceforth on scenarios where nearly all axions have masses well below the MeV scale (contributing to the Hawking emission spectrum already at PBH formation), with possibly one extra axion (or more generally another heavy scalar boson[2] above the MeV scale. The latter will not contribute to the initial Hawking spectrum (although it will once the PBH becomes hot enough), nor will it be produced via the

[2]We point out that the Higgs boson has a too large decay width ($\Gamma_H \simeq 3$ MeV) to be produced via superradiant instabilities since the maximum instability growth rate ($\tilde{a} \simeq 1$ and $\alpha \simeq 0.42$) is $\Gamma_s^{\max} \simeq 3 \times 10^{-7} M_P^2/M \simeq 89$ keV [145,148] for $\mu \simeq 125$ GeV (and consequently $M \simeq 10^9$ kg).

superradiant instability until the PBH spin increases sufficiently as a result of evaporation – *a unique feature of the string axiverse*.

To better understand the dynamical interplay between evaporation and superradiance, we start by considering a toy model where a PBH evaporates through the emission of a single light axion (well below the MeV mass scale), while superradiant instabilities may be triggered for a heavy axion of mass $\mu \gg 1$ MeV. Although unrealistic, this will help us identifying the main qualitative features of the problem without the intricacies of adding the Standard Model particles across different mass thresholds.

In Fig. 8.2 we show the PBH spin as a function of its mass considering only the effects of single scalar Hawking emission, obtained by solving numerically Eqs. (8.1) and (8.2) for an initial PBH mass $M_i = 10^{12}$ kg and spin $\tilde{a}_i = 0.01$. In this figure, we also give the curves in the PBH mass-spin plane corresponding to the superradiance threshold $\omega = \Omega_H$ for different heavy axion masses.

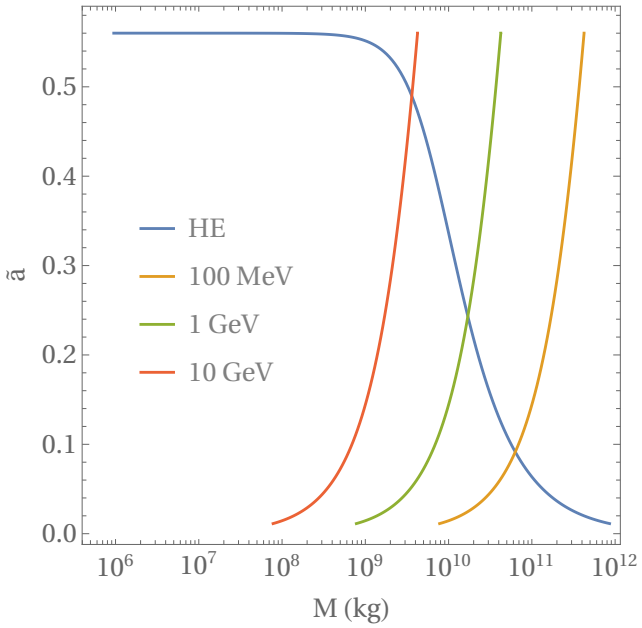

Figure 8.2: PBH Regge trajectory for single-scalar Hawking emission (HE) for $M_i = 10^{12}$ kg and $\tilde{a}_i = 0.01$, and superradiance threshold curves for different heavy axion masses, as labeled.

The dynamics are thus expected to develop as follows. Initially, while the PBH spin is below the superradiance threshold for a given heavy axion mass, the latter is non-superradiant, and any quantum fluctuations in the correspond-

ing field are damped by the PBH. However, light scalar emission through the Hawking effect increases the PBH spin until at some point it crosses the threshold for superradiant heavy axion production. Any subsequent quantum fluctuation in the heavy axion field is then expected to be exponentially amplified via the superradiant instability, leading to the growth of a heavy axion cloud around the PBH.

We note that the timescales for superradiance and Hawking emission above the threshold differ by several orders of magnitude. For instance, as one can see in Fig. 8.2, for $\mu \sim 100$ MeV the superradiance threshold is attained when $\tilde{a} \sim 0.1$ and $M \sim 10^{11}$ kg. Such a PBH will evaporate in $\sim 10^8$ years ($\mathcal{F}(\tilde{a} = 0.1) \sim 10^{-4}$), while the superradiance e-folding time when i.e. the spin exceeds the critical value by 1% is $\sim 10^{-14}$ s. We illustrate this in Fig. 8.3, where we plot the Hawking evaporation and superradiance timescales for a heavy axion with $\mu = 100$ MeV and a given PBH spin, as a function of the PBH mass.

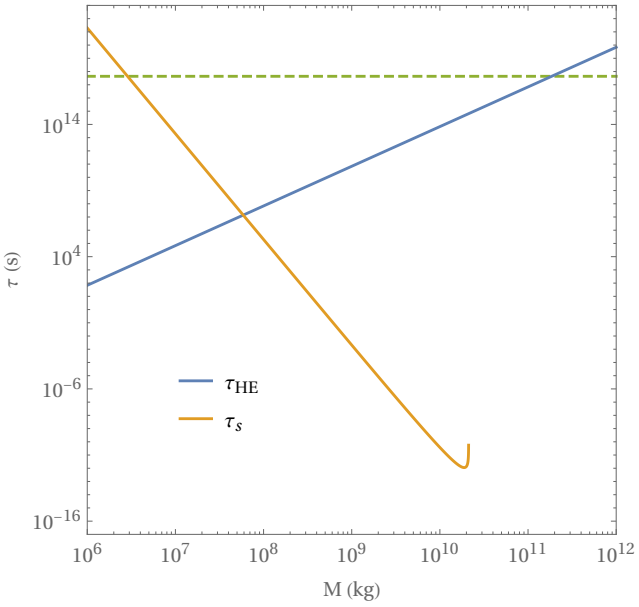

Figure 8.3: Characteristic timescales for Hawking emission (HE), $\tau_{HE} = \mathcal{F}^{-1} M^3/M_P^4$, and superradiance, $\tau_s = 1/\Gamma_s$, for a PBH with $\tilde{a} = 0.3$ and a heavy axion with mass $\mu = 100$ MeV, as a function of the PBH mass. The dashed line corresponds to the age of the Universe.

As one can see in this figure, superradiance is a much faster process for the larger values of the PBH mass, implying that this will be the dominant process

determining the PBH mass and spin after the critical spin value yielding $\omega < \Omega_H$ is reached. This difference in the timescales of the two processes may pose a numerical challenge for solving Eqs. (8.1) and (8.2) alongside $dN/dt = \Gamma_s N$ for the number of particles within the superradiant cloud. Nevertheless, we have found that the numerical tools available in i.e. Mathematica are sufficiently accurate for this purpose. An alternative possibility is to artificially reduce the superradiant growth rate via a tunable multiplicative factor and then extrapolate the obtained results to the realistic case. We find that these two methodologies yield results consistent with each other.

A further numerical difficulty is crossing the superradiance threshold, since N decreases exponentially fast in the non-superradiant regime, thus quickly reaching values below numerical precision before the PBH attains the critical spin value through light scalar Hawking emission. This, however, does not correspond to a realistic approach, since it discards the quantum nature of the heavy axion field. Although the development of superradiant instabilities from quantum field fluctuations has not, to our knowledge, been studied in detail so far, it is widely believed that superradiance will amplify any quantum field fluctuations, quickly increasing the corresponding occupation number in the quasi-bound state, so that a classical description is then sufficient to describe the dynamics.

In fact, Kofman showed [217] that Hawking emission populates not only free states, with $\omega > \mu$, but also quasi-bound states $\omega < \mu$, in a semi-classical calculation similar to the original computation by Hawking. While Kofman's analysis considered only a static BH, so that bound particles produced by Hawking emission are quickly reabsorbed by the BH, in principle it should extend also to the rotating case. The difference for a Kerr BH should reside in the exponential amplification of the bound state occupation number for spin parameters above the superradiance threshold.

In our numerical analysis, we assume this to be the case, and we simulate the effect of bound state quantum emission by first setting $N = 0$ in the differential equations for the PBH mass and spin evolution, Eqs. (8.1) and (8.2), until just after the superradiance threshold is crossed within our numerical precision. We then take the obtained mass and spin values as initial conditions for the subsequent evolution, where we include the heavy axion cloud starting with $N = 1$ (changing this initial value somewhat does not significantly affect our results). In the example shown in Fig. 8.4, we begin with $M_i = 10^{12}$ kg and

$\tilde{a} = 0.01$, while the second part of the simulation including a heavy axion with $\mu = 100$ MeV starts with $M = 6.30 \times 10^{10}$ kg and $\tilde{a} = 0.097$.

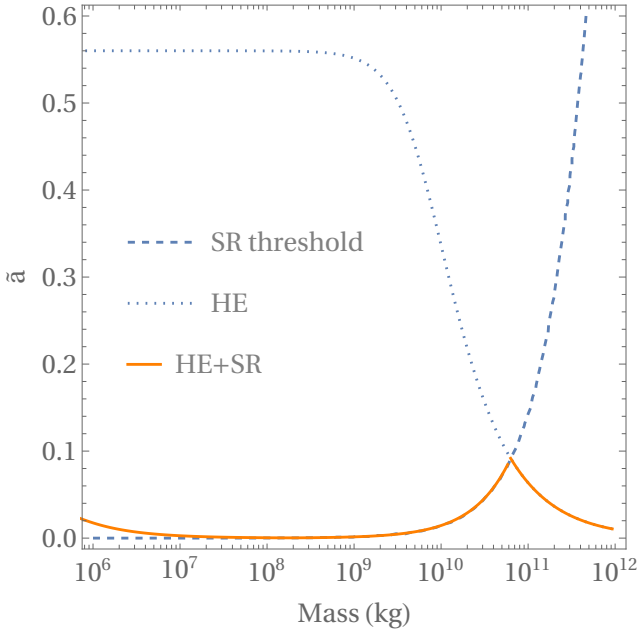

Figure 8.4: Black hole trajectory in the mass-spin "Regge" plane through Hawking emission and superradiance (solid orange curve) for $M_i = 10^{12}$ kg, $\tilde{a}_i = 0.01$ and a heavy axion with mass $\mu = 100$ MeV. Also shown are the trajectory in the absence of superradiance (dotted blue curve) and the superradiance threshold (dashed blue curve).

As one can see in this figure, once the superradiant instability is triggered after the critical spin value is attained, the PBH follows closely the superradiance threshold. This is simply due to the fact that the latter occurs on much shorter timescales, quickly depleting the PBH spin until $\omega = \Omega_H$ and superradiant heavy axion production is halted. However, this condition is never fully attained since Hawking emission continuously spins up the PBH due to light axion emission. To better illustrate this, we show in Fig. 8.5 the time evolution of the PBH spin parameter and of the number of heavy axions in the superradiant cloud for the same example.

This shows that the number of heavy axions produced by superradiance grows exponentially fast after the instability is triggered, quickly decreasing the PBH spin back to close to the critical value. As one can observe in Fig. 8.5, this does not constitute a very significant decrease in the PBH spin, since the su-

perradiant instability is triggered just above the critical value at $\tilde{a} \simeq 4\alpha$. In fact, the number of heavy axions increases only until the superradiant term in Eq. (8.2) becomes comparable to the Hawking emission term.

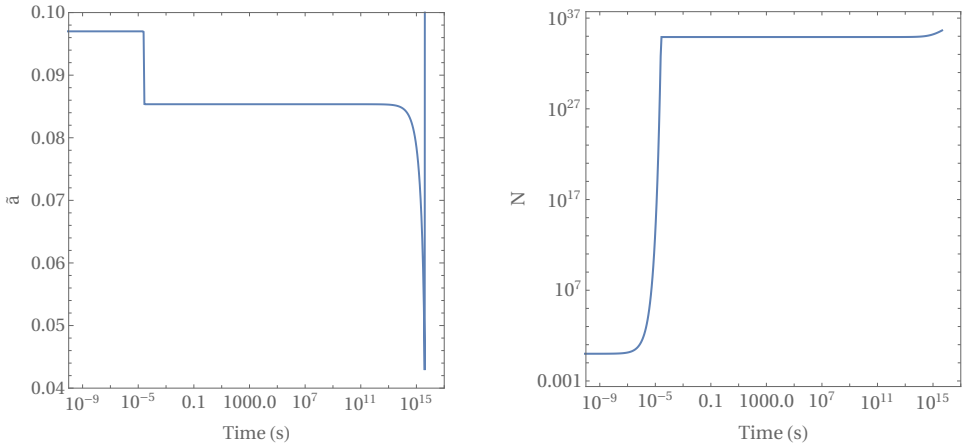

Figure 8.5: Numerical evolution of the PBH spin (left) and number of heavy axions in the superradiant cloud (right) for the same parameters of the example shown in Fig. 8.4. In these plots, time is measured from the onset of the superradiant instability.

At this stage the system reaches a quasi-equilibrium, in which the spin-down effect of superradiance is nearly compensated by the spin-up due to Hawking evaporation. Setting $d\tilde{a}/dt \simeq 0$ and $\tilde{a} \simeq 4\alpha$ in Eq. (8.2) then yields the quasi-equilibrium condition:

$$\Gamma_s = \frac{4\mu(2\mathcal{F}(\tilde{a}) - \mathcal{G}(\tilde{a}))}{N} \tag{8.3}$$

This is analogous to the condition found in [218], although in the latter case, the opposite effect was observed since, in the absence of scalar emission, Hawking evaporation tends to spin down the PBH, leading to reabsorption of the (initially superradiant) cloud in the $\Gamma_s < 0$ regime. In the present case, the cloud remains in the superradiant regime, i.e. with $\Gamma_s > 0$, so that superradiance produces more and more heavy axions within the cloud as evaporation continues to spin up the PBH. Since the product $\Gamma_s N$ is approximately constant, the number of particles grows linearly in this phase at a rate $4\mu(2\mathcal{F} - \mathcal{G})) \simeq 4 \times 10^{19}$ axions per second in this example.

This quasi-equilibrium configuration is maintained only while the number of heavy axions within the superradiant cloud does not change significantly, in

this example up until $\sim 10^{13}$ s. After this, superradiance efficiently spins down the PBH, keeping the spin parameter very close to the critical value.
Despite the large number of heavy axions produced until this stage, superradiance has little effect on the PBH mass, which only begins to decrease after $\sim 10^{15}$ s ($\sim$ 30 Myrs), corresponding to the remaining lifetime of the PBH when the superradiant cloud forms.
The subsequent decrease in the PBH mass has two important effects since it decreases the dimensionless mass coupling $\alpha = \mu M/M_P^2$. First, it lowers the critical spin value for which $\omega = \Omega_H$; second, it damps the superradiance growth rate $\Gamma_s \propto \alpha^8$. The first effect makes the PBH follow a trajectory in the Regge plane corresponding to the superradiance threshold, as observed in Fig. 8.4. This holds while superradiance remains faster than evaporation despite the decreasing PBH mass, i.e. down to masses $\sim 10^7$ kg. This means that in its final hour (literally in this example) the PBH spins up once more as light scalar emission takes over in the last stages of evaporation. Asymptotically the PBH reaches the stable value $\tilde{a}_* = 0.555$ yielding $\mathcal{H}(\tilde{a}_*) = 0$ for pure scalar Hawking emission, as discussed in Section 2. This is not visible in Fig. 8.4, since it is only attained in the very last stages of the PBH evaporation, beyond the reach of the numerical precision of our simulation.
To summarize our findings in this toy model, a PBH formed with a mass $\sim 10^{12}$ kg evaporates through light axion emission and consequently spins up. After nearly $\sim$ 14 billion years, its spin surpasses the critical value for triggering a superradiant instability, producing a cloud of heavy axions around it. For most of its remaining lifetime, the PBH is in a quasi-equilibrium configuration with the heavy axion cloud, with evaporation spinning up the PBH nearly at the same rate superradiance spins it down. In our working example, the PBH remains in this stage for about 30 million years. At the end of its life, its mass starts decreasing and the PBH follows a Regge trajectory along the superradiance threshold up until its very last stages where evaporation once more increases its spin.
We note that once superradiance becomes inefficient the number of heavy axions within the superradiant cloud stabilizes near the maximum possible value:

$$N_{\max} \simeq \tilde{a}_c M_c^2 \ , \tag{8.4}$$

where the subscript 'c' indicates the PBH mass and spin parameter when su-

perradiance is triggered. This corresponds to converting most of the PBH's angular momentum into heavy axions via the superradiant instability (but fueled by the spin-up produced by light scalar Hawking emission). In our example, this yields nearly 10^{36} axions.
Although the critical PBH-mass spin values for superradiance change for different values of the heavy axion mass, we observe the same qualitative behavior for all $\mu >$ few MeV (recalling that in the $0.1 - 1$ MeV mass range superradiance is triggered at PBH formation for $\tilde{a} = 0.01$ as discussed earlier).
Our toy model should be an accurate description when the PBH can emit $N_a \gg 1$ light axions, up to an overall rescaling of the PBH lifetime by a factor $\sim N_a^{1/3}$.

8.2.2 Realistic string axiverse scenarios

With the basic understanding of the main dynamical features of the interplay between superradiance and evaporation in the simplified toy model, we now perform more realistic simulations, with a finite number N_a of light axions in the Hawking emission spectrum alongside all the Standard Model degrees of freedom. As described in Section 2, each particle species is included in the emission spectrum once the Hawking temperature exceeds its mass (or effective mass as in the case of quarks and gluons above the QCD scale).
Given our understanding of the evaporation dynamics in the absence of superradiance, the main difference expected between the toy model and more realistic scenarios is the fact that most Standard Model particles have a non-zero spin, therefore carrying away part of the angular momentum of the BH. This means that Hawking emission is overall less efficient in spinning up the BH, and unless the number of light axions is sufficiently large the BH may actually spin down, as discussed in the previous section. The expectation is therefore that superradiant instabilities can only be triggered above a minimum number of light axion species N_a. This is illustrated in Fig. 8.6, where we show the results of our numerical simulations for different numbers of light axions and a heavy axion with $\mu = 100$ MeV.

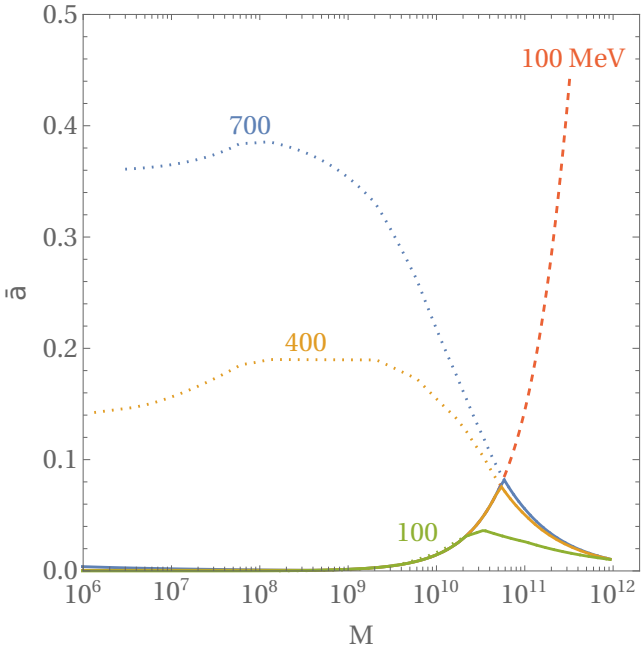

Figure 8.6: Black hole trajectory in the mass-spin "Regge" plane through Hawking emission and superradiance (solid curves) for $M_i = 10^{12}$ kg, $\tilde{a}_i = 0.01$ and a heavy axion with mass $\mu = 100$ MeV, for different values of the number of light axions N_a in the Hawking emission (HE) spectrum, as labeled. Also shown are the trajectory in the absence of superradiance (dotted curves) and the superradiance threshold (dashed curve).

As one can see in this figure, for different numbers of light axions the superradiant instability is triggered for different values of the PBH mass and spin, although converging to those found in the toy model in the limit $N_a \to \infty$. For $N_a \lesssim 100$ the superradiant threshold is not crossed for heavy axions with $\mu \gtrsim 10$ MeV, but since the string axiverse generically predicts hundreds or even thousands of light axions we typically expect instabilities to occur during the PBH evolution if axions in this mass range exist.

As for the toy model, superradiance is initially much faster than Hawking emission in changing the PBH spin, so that after the instability is triggered the PBH follows a trajectory in the Regge plane corresponding to the superradiance threshold $\omega = \Omega_H$ ($\tilde{a} \simeq 4\alpha = 4\mu M/M_P^2$ for slowly rotating PBHs). The main difference in realistic scenarios is the fact that we do not observe a spin up of the PBH for low masses, i.e. at the end of its lifetime, as also clear in the time evolution plots shown in Fig. 8.7, given that Hawking emission is

in this case much less efficient in increasing $\tilde{a}$ than for single scalar emission.

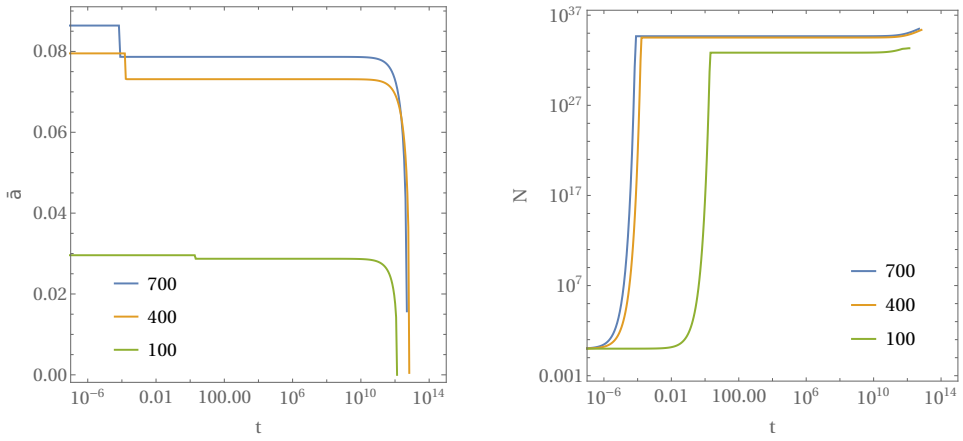

Figure 8.7: Numerical evolution of the PBH spin (left) and number of heavy axions in the superradiant cloud (right) for the same parameters of the example shown in Fig. 8.6. In these plots, time is measured from the onset of the superradiant instability.

Although this may occur when the PBH reaches masses below those that our numerical precision can probe, we may safely conclude that for present PBH masses $\gtrsim 10^6$ kg (lifetime exceeding $\sim$1 s), the PBH distribution in the mass-spin Regge plane should exhibit a single peak at the values $(M_c, \tilde{a}_c)$ at which the instability is triggered and which depend on the string axiverse parameters μ and N_a. In particular, the mass of the heavy axion can be inferred from the superradiance threshold condition:

$$\mu \simeq \frac{M_P^2}{M_c} \frac{\tilde{a}_c}{2(1+\sqrt{1-\tilde{a}_c^2})} \simeq \frac{M_P^2}{4M_c} \tilde{a}_c \ . \tag{8.5}$$

The dependence on the number of light axions, N_a, emitted through the Hawking process is less trivial since it depends on the PBH evaporation dynamics, which has to be computed numerically. In Fig. 8.8 we show the critical spin contours in the (μ, N_a) plane, from which one can determine N_a upon computing μ from Eq. (8.5).

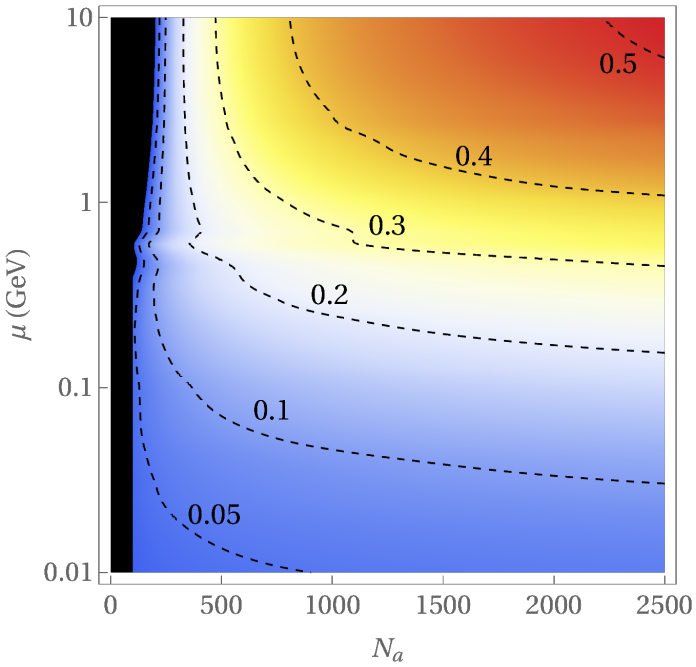

Figure 8.8: Contours of the critical spin parameter $\tilde{a}_c$ at which the superradiant instability is triggered as a function of the number of light axions N_a and the mass of the heavy axion μ. This corresponds to the present maximum spin of PBHs in the range $10^6 - 10^{12}$ kg (slowly rotating at birth). In the black region, no superradiant instabilities are triggered.

We thus find a unique signature of the string axiverse with hundreds of light ($\lesssim$0.1 MeV) axions and a single heavy axion ($\gtrsim$ few MeV), corresponding to a sharply peaked spin distribution as a function of mass, with a nearly linear relation between PBH mass and spin for masses below the peak. Moreover, as shown above, the number of light axions and the mass of the heavy axion can be determined from the position of this peak in the Regge plane, so that the full PBH distribution need not be probed across many orders of magnitude in mass.

This shows that measuring the present mass-spin distribution of PBHs below 10^{12} kg may have a very significant impact on finding (or excluding) new physics. Methodologies to determine both the mass and spin of a PBH from its photon Hawking emission spectrum will be discussed in the next chapters. Although these may be challenging from the experimental perspective, since they require measuring the PBH photon spectrum close to the primary emission peak energy (where the photon flux is lower than for the secondary

component at lower energies), they may be within the reach of future gamma-ray telescopes, as we discuss in Section 8.4.

We note that, in the presence of multiple heavy axions ($>$ few MeV), the first instability to be triggered during the evolution of a PBH corresponds to the lightest of these. The growth of this first heavy axion superradiant cloud will quickly spin down the black hole close to the corresponding superradiant threshold, as we have observed. This will therefore inhibit superradiant instabilities for heavier axions (except in the last fractions of a second of a PBH's lifetime where evaporation may still spin up the PBH). Hence, the shape of the present PBH mass-spin distribution is determined only by the lightest of the heavy axions, being largely insensitive to the existence of other axions.

We also note that our distinction between light axions and the heavy axion refers to the Hawking temperature of $\sim 10^{12}$ kg PBHs at formation. As they evaporate towards their present-day mass, the Hawking temperature of these PBHs increases, such that at some stage the heavy axion can also be efficiently emitted. Since we are considering scenarios with $N_a \gg 1$, the inclusion of one (or even a few) more axion(s) does not significantly change the dynamics, and for simplicity, we have kept N_a fixed throughout the numerical evolution of the PBH mass and spin.

In our numerical simulations we have considered only free axions, i.e. we have neglected the effects of axion self-interactions, which have been analyzed in detail in [219, 220] and also [221] (see also [203, 222–226]). The latter considered superradiant axion production around rotating PBHs, although heavier than the ones considered in the present work so that the effects of Hawking emission could be neglected. Axion self-interactions lead, in particular, to 2-2 scattering processes that populate other superradiant and non-superradiant levels in the "gravitational atom" corresponding to the spectrum of BH-axion quasi-bound states. Some axions are "ionized" in these processes, escaping the BH's gravitational potential, which slows down the growth of the dominant 2p-superradiant cloud and may, in fact, prevent its occupation number from growing beyond a maximum number.

The results obtained in [220, 221] cannot be easily extrapolated to the case of PBHs with a lifetime comparable to the age of the Universe, given how significant a role we have found PBH evaporation to play in the development of superradiant clouds. We may, nevertheless, try to estimate the parametric regimes in which it is a good approximation to neglect the effects of axion self-

interactions, based on the analyses of [220,221]. Since we are mostly interested in the non-relativistic regime, we may consider the effects of the leading non-linear term in the axion potential in the resulting Schrödinger-like equation, which has the Gross-Pitaevskii form:

$$i\frac{\partial\psi}{\partial t} = -\frac{1}{2\mu}\nabla^2\psi - \frac{\alpha}{r}\psi - \frac{\lambda}{8\mu^2}|\psi|^2\psi \ , \tag{8.6}$$

where the axion field $\Phi = (\psi e^{-i\mu t} + \text{c.c.})/\sqrt{2\mu}$ and $\lambda = \mu^2/f_a^2$, with f_a denoting the axion decay constant. In the limit $\lambda \to 0$ this corresponds to a Schrödinger equation for a Coulomb-like potential, yielding a Hydrogen-like spectrum of (quasi-)bound states as previously discussed. Self-interactions may thus play an important role when the non-linear term becomes comparable to the energy eigenvalue of the linear Hamiltonian, i.e. when $\lambda|\psi|^2 \sim \alpha^2\mu^3$ for the 2p-state ($\Phi \sim \alpha f_a$). Since $|\psi|^2$ represents the axion number density, and the 2p-cloud has approximately a toroidal shape with volume $V_{\rm cloud} = 50\pi^2/(\alpha\mu)^3$ (with $(\alpha\mu)^{-1}$ yielding the gravitational Bohr radius) [221,227], we conclude that self-interactions can be neglected for $N \lesssim 50\pi^2/(\alpha\lambda)$. We may then derive a lower bound on f_a by taking the maximum number of heavy axions produced in the 2p-cloud when the superradiant instability is triggered by PBH evaporation, $N_{\rm max} \simeq \tilde{a}_c(M_c/M_P)^2$:

$$f_a \gtrsim \frac{\alpha_c^{3/2}\tilde{a}_c^{1/2}}{\sqrt{50}\pi} \sim 7\times 10^{14}\left(\frac{\tilde{a}_c}{0.1}\right)^2 \ \text{GeV} \tag{8.7}$$

where we recall that the subscript 'c' refers to the PBH parameters when the superradiant instability is triggered by evaporation, with $4\alpha_c \simeq \tilde{a}_c$ in the slowly rotating limit. Since $\tilde{a}_c \lesssim 0.5$, given that Hawking emission cannot spin up a PBH beyond this value (which is only achieved for pure light scalar emission), we conclude that for heavy axions with decay constants above the grand unification scale, $f_a \gtrsim 10^{16}$ GeV, we may safely neglect the effects of self-interactions in the development of superradiant instabilities. Such large decay constants are, in fact, generic for string axions (see i.e. [181]), thus justifying the free-axion approximation in this context.

We note that our dynamical simulations are applicable to any heavy scalar field ($\mu \gtrsim 1$ MeV) and not only axion-like fields, but the above arguments show that only for very feeble self-interactions may the dynamical effects of the latter be neglected. For instance, neutral pions are similar to heavy axions

but interact quite strongly, with $\lambda \simeq 1$, as already analyzed in detail in [203].

8.3 Direct detection of superradiant axion clouds

In the previous section, we have shown that PBH evaporation in the string axiverse may trigger superradiant instabilities for heavy axions due to the emission of hundreds (or even thousands) of light scalar axions and the consequent spin-up of (initially slowly-rotating) PBHs. In addition to the unique imprint, this leaves on the present mass-spin distribution of PBHs with masses $\lesssim 10^{12}$ kg, the formation of superradiant clouds may leave a much more direct observational signature since the produced axions decay into photon pairs. In particular, as we will now describe in detail, an evaporating PBH surrounded by a heavy axion cloud will emit photons as a result of both Hawking emission and heavy axion decay, yielding a unique spectrum.

Hawking emission leads to two types of photons in a PBH emission spectrum. Primary photons are directly emitted by the PBH with a nearly-thermal spectrum (up to the gray-body factors) given by (5.36) [87,88]. In addition, charged particles produced via the Hawking effect also emit photons as they travel away from the PBH, and additional photons also result from the decay of unstable particles like the neutral pion[3]. Such secondary photons are less energetic than their primary counterparts but may nevertheless dominate the emission spectrum at energies below the primary emission peak.

Although the primary spectrum can be computed using semi-analytical methods (computing the gray-body factors numerically as described in Section 8.2), determining the secondary spectrum typically requires numerical methods of convoluting the primary emission rate for each particle species (analogous to Eq. (5.36)) with their corresponding photon emission rate. We have used the publicly available BlackHawk code [93–96] to compute both the primary and secondary emission spectra of PBHs with mass and spin satisfying the superradiance threshold condition $\omega = \Omega_H$, corresponding to the trajectory followed by a PBH after the formation of a heavy axion superradiant cloud of a given mass $\mu \gtrsim 1$ MeV. We have nevertheless checked that our semi-analytical calculation of the primary emission spectrum agrees with the results obtained

[3]The N_a light axions emitted by the PBH also decay into photons, but their lifetime is so long that they typically decay far away from the PBH, so that we do not include their contribution to the Hawking photon emission spectrum.

using this code.

The latest version of BlackHawk uses two well-known particle physics codes to compute the number of photons radiated by primary particles, namely Hazma [98,99] for primary particle energies below a few GeV and PYTHIA [97] for energies > 5 GeV. PYTHIA may operate in an extended range via extrapolation tables, but as reported in [100] this may lead to unreliable spectra due to its failure in describing physical processes as the neutral pion decay, $\pi^0 \to \gamma\gamma$ which should cause a symmetric emission peak centered at half of the pion's mass. We note that the primary emission peak corresponds to photon energies ~ 5 times the Hawking temperature. For this reason, and taking into account the limits of validity of Hazma and PYTHIA, we employ PYTHIA for PBH masses $M < 2.5 \times 10^{10}$ kg, while for $M > 2.5 \times 10^{10}$ kg we use Hazma.

The heavy axions within the superradiant cloud decay into photon pairs with a rate (see i.e. [228, 229]):

$$\Gamma_a = \frac{g_{a\gamma\gamma}^2 \mu^3}{64\pi} \,, \qquad g_{a\gamma\gamma} = \frac{\alpha_{EM}}{2\pi f_a} |\mathcal{C}_{a\gamma\gamma}| \,, \tag{8.8}$$

where $\alpha_{EM} \simeq 1/137$ is the electromagnetic fine structure constant and $\mathcal{C}_{a\gamma\gamma} = \mathcal{O}(1-10)$ is a model-dependent numerical factor (possibly reaching larger values in some axion models (see i.e. [230]). We may write this as:

$$\Gamma_a \simeq 7 \times 10^{-35} |\mathcal{C}_{a\gamma\gamma}|^2 \left(\frac{\mu}{100 \text{ MeV}}\right)^3 \left(\frac{10^{16} \text{ GeV}}{f_a}\right)^2 \text{ eV} \,. \tag{8.9}$$

Note that for the heavier axions, this may exceed the present Hubble rate $H_0 \sim 10^{-33}$ eV, i.e. yield axions with a lifetime shorter than the age of the Universe. However, the heavy axion cloud is only formed after $\simeq 14$ Gyrs, once evaporation spins up the PBH sufficiently to trigger the superradiant instability. It is easy to check that the axion decay rate is always smaller than the PBH evaporation rate when the cloud forms:

$$\frac{\Gamma_a}{\Gamma_{\text{evap}}} = \frac{\alpha_{EM}^2 |\mathcal{C}_{a\gamma\gamma}|^2}{256\pi^3 \mathcal{F}} \left(\frac{M_P}{f_a}\right)^2 \alpha_c^3 \simeq |\mathcal{C}_{a\gamma\gamma}|^2 \left(\frac{10^{-2}}{\mathcal{F}}\right) \left(\frac{10^{16} \text{ GeV}}{f_a}\right)^2 \alpha_c^3 \ll 1 \tag{8.10}$$

since the function characterizing the PBH mass loss rate (see Section 8.2) $\mathcal{F} \gtrsim 10^{-2}$ for $N_a \gtrsim 100$ and, as discussed in the previous section, $f_a \gtrsim 10^{16}$ GeV for string axions, taking also into account that superradiance is triggered for

$\alpha_c < 0.15$ in all axiverse scenarios. This means that axion decay does not play a significant role in the formation and evolution of the superradiant clouds. It may, however, yield an observable signal as we now show. The corresponding photon emission spectrum is given by:

$$\frac{d^2N_{\gamma,a}}{dtdE_\gamma} \simeq 2\Gamma_a N\delta\left(E_\gamma - \frac{\mu}{2}\right) \simeq \frac{2\Gamma_a N}{\sqrt{2\pi}\Delta E} e^{-\frac{(E_\gamma-\mu/2)^2}{2\Delta E^2}} \tag{8.11}$$

since each of the two photons has approximately half of the axion rest energy (up to sub-leading gravitational binding energy corrections) and, in the last step, we have replaced the monochromatic spectrum by a Gaussian function of width ΔE in order to take into account the effects of a detector's resolution. We then obtain for the maximum photon emission rate from the superradiant axion cloud (at $E_\gamma \simeq \mu/2$), considering the maximum number of axions produced in the evolution, as computed in the previous section:

$$\left.\frac{d^2N}{dtdE_\gamma}\right|_{\rm max} \simeq 1.5\times 10^{18}\,|C_{a\gamma\gamma}|^2 \left(\frac{\tilde{a}_c}{0.1}\right)^3 \left(\frac{10^{16}\ {\rm GeV}}{f_a}\right)^2 \left(\frac{\Delta E}{E_\gamma}\right)^{-1}\ {\rm GeV}^{-1}{\rm s}^{-1} \tag{8.12}$$

The energy of the axion line is always smaller than the peak of the primary photon emission spectrum of the PBH since the latter occurs for $E_\gamma \simeq 5T_H \simeq 0.2\alpha^{-1}\mu \gtrsim \mu$. Hence, whether the axion line is detectable depends on the magnitude of the secondary photon emission spectrum from Hawking evaporation. In Fig. 8.9 we give two examples illustrating the effect of a superradiant cloud with heavy axions with $\mu = 100$ MeV and 1 GeV on the emission spectrum of PBHs with three different masses and spins. The heaviest PBH in each case corresponds to a PBH where the heavy axion cloud has just formed (and reached its maximum mass), after evaporating with $N_a = 400$ light axions for nearly the age of the Universe. The other two mass and spin values correspond to subsequent stages of the same PBH as it evaporates further and follows the Regge trajectory given by the superradiance threshold condition $\omega = \Omega_H$ ($\tilde{a} \simeq 4\alpha$) as discussed in the previous section. We note that in practice one would aim to observe three distinct PBHs presently at different stages of the evaporation process (already dressed with a heavy axion cloud), and not the same PBH at different times since the evaporation timescale in this mass range is still very large (~ 1 million years).

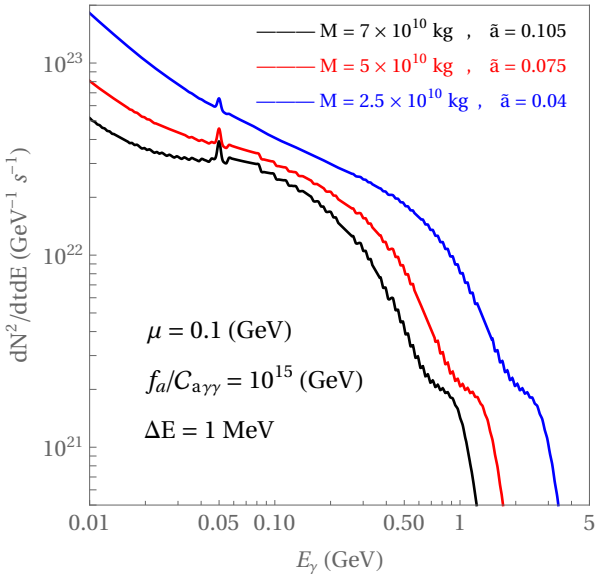

Figure 8.9: Photon emission spectrum of PBHs in the presence of a heavy axion with 100 MeV mass and $f_a/\mathcal{C}_{a\gamma\gamma} = 10^{15}$ GeV ($g_{a\gamma\gamma} \simeq 10^{-18}$ GeV). The heaviest PBH (black curve) corresponds to the mass and spin values at which the superradiant cloud forms, while the red and blue curves correspond to subsequent stages in the latter's evolution (along the superradiance threshold curve). The energy resolution for the axion line is taken to be 1% of the axion mass in each case.

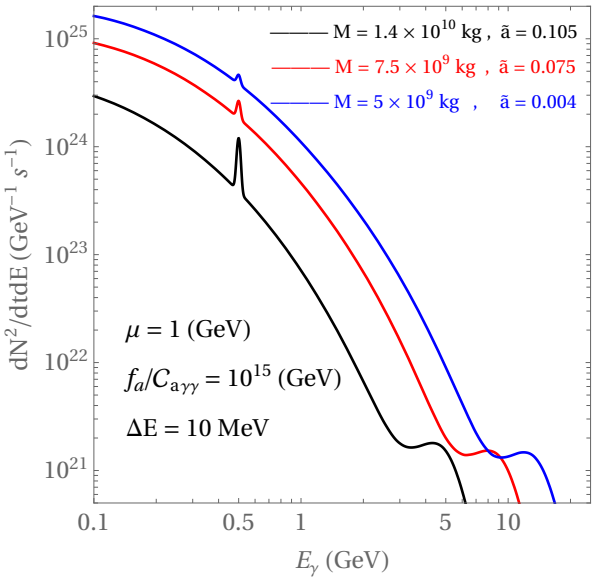

Figure 8.10: Same as Fig.(8.9) but with the heavy axion mass of 1 GeV.

In these examples, we have chosen $f_a = 10^{16}$ GeV and $|C_{a\gamma\gamma}| = 10$ (or equivalently any combination with $g_{a\gamma\gamma} \simeq 10^{-18}$ GeV^{-1}), which maximizes the intensity of the heavy axion line given the constraints obtained from neglecting axion self-interactions discussed above and the typical values of axion decay constants of string compactifications (being also within current experimental constraints [231]). We see that with a $\simeq 2\%$ peak energy resolution the axion line is clearly visible above the secondary photon emission from the PBH evaporation for the PBH mass values considered. Although these examples may be somewhat optimistic, it is quite remarkable that such an axion line is observable for such low values of the axion-photon coupling. Note that in the case of heavier axions, for which the instability is triggered at higher spin values, the axion line is more pronounced as given by Eq. (8.12).
It is worth remarking that detecting a slowly rotating black hole with a mass $\lesssim 10^{11}$ kg, which must in principle be a remnant of the evaporation of a heavier PBH[4], exhibiting a monochromatic line in its electromagnetic emission spectrum would be evidence for the existence not only of a heavy axion but also of hundreds of light axions, as otherwise, it could not have developed a large enough spin to trigger the superradiant instability (recall that for $N_a = 0$ any natal spin is quickly lost, as can be seen in Fig. 7.2).

8.4 Discussion and conclusions

In this work, we have considered the evaporation of PBHs in the context of the string axiverse, following the seminal work of the previous chapter. The generic prediction of hundreds or even thousands of light scalar axions in realistic string scenarios has a tremendous impact on the dynamics of small PBHs since light scalar emission tends to spin up a BH, as opposed to the emission of particles with non-zero spin. This is due to spin-zero particles being the only particles that can be emitted in the spherically symmetric $l = 0$ mode, i.e. without carrying away the BH's angular momentum. As shown in the previous chapter, an initially slowly rotating PBH ($\tilde{a} \lesssim 0.01$) can spin up to values $\tilde{a} \sim 0.1 - 0.5$ for $N_a \gtrsim 100$ light axions.
This increase in a PBH's angular velocity, which for PBHs born with $\sim 10^{12}$ kg occurs on timescales comparable to the age of the Universe, has an impor-

[4] Although there could be more exotic scenarios where light black holes form much later (see i.e. [232]).

tant consequence that we have explored in detail in this work - it may trigger superradiant instabilities. The string axiverse typically includes axions with masses spread out over several orders of magnitude [181], most of which are likely below the MeV scale and hence included in the PBH Hawking emission spectrum for the above-mentioned natal mass range. However, there may be one or more axions with a larger mass, and which can be produced via the superradiant instability once a PBH reaches a critical spin value as a result of evaporation.

The dynamical interplay between Hawking evaporation (with light sub-MeV axions) and the superradiant instability (producing heavy super-MeV axions in clouds gravitationally bound to the PBH) is quite interesting, given in particular the very different timescales of the two particle production processes. As we have shown in this work, once evaporation spins up a PBH above a certain critical spin, the superradiant instability quickly amplifies any quantum fluctuation in the heavy axion field, and the expense of reducing the PBH's spin back to the critical value. On a longer timescale, the PBH continues to spin up due to light axion emission, therefore feeding the superradiant instability and the heavy axion cloud. These two opposing effects keep the PBH-axion cloud system in a quasi-equilibrium state with nearly constant spin for a long time, and as the PBH mass decreases it follows a very simple Regge trajectory (mass-spin plane) corresponding to the superradiance threshold for the heavy axion $\tilde{a} \simeq 4\mu M/M_P^2$.

Towards the end of the PBH's lifetime superradiance becomes less and less efficient in extracting the PBH spin, as a consequence of the decreasing dimensionless mass coupling $\alpha = \mu M/M_P^2$. The number of heavy axions in the cloud stabilizes near the maximum value $N_{\max} \simeq \tilde{a}_c M_c^2$, where the subscript 'c' denotes the PBH parameters when the superradiant instability is triggered, as supported by our numerical simulations. Evaporation then takes over as the main mechanism driving the PBH evolution and therefore increasing its spin for a sufficiently large number of light axions. Numerically, we can only observe this final spin up in the toy model with pure scalar Hawking emission, given that numerical precision limits the considered PBH mass range to $M_0 \gtrsim 10^6$ kg[5] in a toy model with pure scalar emission. This toy model mimics what happens in the limit $N_a \to \infty$.

[5]Such PBHs live less than a second, while our simulations span the age of the Universe, requiring a very large numerical precision.

This thus leads to a striking prediction for the present mass-spin distribution of PBHs in the range $10^6 - 10^{12}$ kg. On the one hand, for the heavier ones that are still spinning up due to light axion emission, the spin parameter should decrease with the mass (the exact function depends on the number of light axion species, N_a). On the other hand, for the lighter PBHs that have already formed a heavy axion cloud, the spin parameter should increase linearly with the PBH mass, along the Regge trajectory corresponding to the superradiance threshold $\tilde{a} \simeq 4\mu M$. This gives a peaked mass-spin distribution (see Fig. 8.6), the mass and spin of the most rapidly rotating PBH depending on the number of light axions, N_a, and the mass of the heavy axion μ (see Fig. 8.8 and associated discussion).

In addition to this indirect signature of the string axiverse, the presence of a superradiant axion cloud can in principle be directly detected as a single emission line on top of the PBH's Hawking emission spectrum, located at approximately half of the heavy axion's mass (since axions decay into photon pairs). Although we have not performed a detailed analysis of the detectability of this axion line, we have shown that its intensity can be comparable to that of the PBH's (secondary) Hawking emission for axion-photon couplings as low as $g_{a\gamma\gamma} \sim 10^{-18}$ GeV, corresponding to axion decay constants of the order of the grand unification scale, $f_a \sim 10^{16}$ GeV, typical of string axions, up to an $\mathcal{O}(10)$ model-dependent coefficient $\mathcal{C}_{a\gamma\gamma}$. This feature is quite unique, since PBHs with different masses and spins, presently at distinct evaporation stages, should exhibit the same axion line despite their different Hawking emission spectra if they have grown a superradiant cloud around them.

Both direct and indirect signatures of the string axiverse depend intrinsically on detecting and accurately measuring a PBH's photon emission spectrum, since in addition to the axion line this allows for a determination of both its mass and spin, as we will see in the following chapters and studied in [11, 13]. In particular, the latter requires determining specific features in the spectrum close to the primary emission peak, where, as illustrated in Fig. 8.9 the emission rate is lower.

Planned gamma-ray telescopes such as AMEGO [233–235] or All-Sky-ASTROGAM [236, 237] missions will reach sensitivities of $\sim 10^{-6}$ MeVcm^{-2}s^{-1} in the MeV-GeV range. The dark matter fraction in the form of PBHs born with $M_i \sim 10^{12}$ kg is currently bound by their contribution to the extra-galactic gamma-ray

background [238]:

$$f_{PBH} < 2 \times 10^{-8} \left(\frac{M_i}{5 \times 10^{11} \text{ kg}} \right)^{3+\epsilon} \tag{8.13}$$

where $\epsilon = 0.1 - 0.4$. Note that the reference value of 5×10^{11} kg corresponds to PBHs with a lifetime equal to the age of the Universe *in the absence of light axions*, whereas in the axiverse scenario PBHs which are currently in the final stages of their evaporation process must have been born with somewhat larger masses $\sim 10^{12}$ kg as previously mentioned. Considering a fiducial value for the Solar System's velocity in the dark matter halo $v = 250$ km/s and for the local dark matter density $\rho_{DM} \simeq 0.4$ GeVcm^{-3}, we obtain a bound on the PBH flux in our astrophysical neighborhood of:

$$F_{PBH} \lesssim 10^6 \left(\frac{M_i}{10^{12} \text{ kg}} \right)^{2+\epsilon} \text{ pc}^{-2}\text{yr}^{-1} \tag{8.14}$$

This means that, within the typical lifetime of a detector of ~ 10 years, we may expect up to one evaporating PBH to come within a distance of $\simeq 30 - 40$ AU of the Earth. The photon energy flux for a PBH at distances of this order is given by:

$$\Phi_\gamma \simeq 3.6 \times 10^{-6} \left(\frac{E_\gamma}{5 \text{ GeV}} \right)^2 \left(\frac{d^2N/dtdE_\gamma}{10^{21} \text{ GeV}^{-1}\text{s}^{-1}} \right) \left(\frac{d}{50 \text{ AU}} \right)^{-2} \text{ MeVcm}^{-2}\text{s}^{-1} \tag{8.15}$$

This means that both primary and secondary Hawking emission from PBHs with $M \lesssim 10^{10}$ kg (i.e. less than 1% of their original mass) could be detectable with planned gamma-ray telescopes if the bounds on their abundance are nearly saturated (i.e. if they give a non-negligible contribution to the extragalactic gamma-ray background. If they are less abundant one will of course require even more sensitive telescopes to detect them, such as the proposed MAST mission [239], with an unprecedentedly large detector area.

An important question also comes out of our analysis in this work − what happens to the heavy axion clouds once the PBHs evaporate away? The analysis of superradiant dark matter production by light PBHs ($< 10^6$ kg) performed in [218] has suggested (although not rigorously proven), that superradiant clouds may survive black hole evaporation as self-gravitating, microscopic boson stars. The main idea is that, as a PBH evaporates, its gravitational po-

tential (which bounds the scalar cloud) decreases in time, first adiabatically (compared to the timescale of the Hydrogen-like wavefunction), but speeding up towards the end of the PBH's lifetime so that the PBH suddenly vanishes - much like a quantum quench. Using the results obtained in [218], we find that PBH evaporation should only become non-adiabatic when the PBH reaches a value:

$$M_* \simeq 7 \times 10^{-5} \left(\frac{0.1}{\tilde{a}_c}\right)^{13/5} \left(\frac{10^{11}\ \mathrm{kg}}{M_c}\right)^{2/5} M_{\mathrm{cloud}}\ , \tag{8.16}$$

where $M_{\mathrm{cloud}} = \mu N$ is the total mass of the axion cloud. This then suggests that the heavy axion field profile should slowly evolve from a superradiant cloud around a PBH to an essentially self-gravitating configuration well before the PBH fully evaporates away. PBH evaporation could thus leave behind microscopic axion stars! Note that the cloud expands from an initial size of a few times the gravitational Bohr radius $\sim 1/M_c\mu^2$ to the much larger size of the self-gravitating configuration, $\sim$few$\times 1/M_{\mathrm{cloud}}\mu^2$, given that the axion cloud only contains, in general, a small fraction of the PBH mass when it forms, i.e. $M_{\mathrm{cloud}} \ll M_c$. Note also that this should result in a rotating boson star by angular momentum conservation, but that these configurations are unstable and end up decaying into non-rotating spherical stars [240–242].

Showing that superradiant clouds may indeed become self-gravitating states requires dedicated numerical simulations, given the intrinsically non-linear nature of the problem, and which are beyond the scope of this work. Nevertheless, it is interesting to speculate about the possibility of directly observing such a transition, since after its final Hawking explosion, a PBH could leave behind a compact object (the "axion star") with a monochromatic gamma-ray spectrum, as computed in the previous section.

This work thus demonstrates the enormous potential of evaporating PBHs as probes of beyond the Standard Model physics and we can only hope that the Universe has been kind enough to provide us with a sufficiently large number of these fascinating compact objects.

9 Determining the mass and spin of light PBHs with Hawking radiation

This chapter is divided into two sections, each of which contains the major results of [13], and [14] respectively.

In the first section, we propose a method to determine the mass and spin of primordial black holes (PBHs) in the mass range $5 \times 10^7 - 10^{12}$ kg (Hawking temperatures ~ 10 MeV -200 GeV), based on measuring the energy of specific features in the photon Hawking emission spectrum, including both primary and secondary components. This is motivated by scenarios where PBHs in this mass range spin up as they evaporate, namely, the string axiverse, where dimensionless spin parameters $\tilde{a} \sim 0.1 - 0.5$ can be achieved through the Hawking emission of hundreds or even thousands of light axion-like particles. Measuring the present PBH mass-spin distribution may thus be an important probe of physics beyond the Standard Model. Since the proposed method relies on the energy of the photons emitted by a given PBH, rather than on the associated flux, it is independent of the PBH-Earth distance and, as a byproduct, can also be used to infer the latter.

We continue and propose in the second section a method to determine the mass and spin of primordial black holes based on measuring the energy and emission rate at the dipolar and quadrupolar peaks in the primary photon Hawking spectrum, applicable for dimensionless spin parameters $\tilde{a} \gtrsim 0.6$. In particular, we show that the ratio between the energies of the two peaks is only a function of the black hole spin, while the ratio between their emission rates depends also on the line-of-sight inclination. The black hole mass and distance from the Earth may then be inferred from the absolute values of the

peak energies and emission rates. This method is relevant for PBHs born with large spin parameters and that at are presently still in the early stages of their evaporation process.

9.1 Low spin PBHs

As we have seen in the previous chapters, in the context of the string axiverse, and potentially other SM extensions with large numbers of light scalars, evaporating PBHs should presently exhibit a non-trivial spin, and measuring the present mass-spin distribution of PBHs at different stages of their lifetime may therefore yield a unique probe of new physics. In our previous work, we showed that the spectrum of primary photons (those directly emitted by the PBH) is sensitive to both the mass and spin of a PBH, such that detecting such photons could allow one to determine both quantities. This, however, relies on the measured photon flux and hence depends also on precise measurements of the PBH-Earth distance. While this may be relatively easy to do with parallax techniques if a PBH is not too far away (which is nevertheless required for detection), it would be better to devise a mass-spin determination method independent of distance measurements. In addition, the observed flux will correspond not only to the primarily emitted photons but also to secondary photons radiated by the other particles that also result from the PBH's evaporation. These result from final state radiation (FSR) of charged particles, particle decays (muons, pions, etc) as well as parton fragmentation processes, and can be more numerous, albeit less energetic, than the primary photons.

In this section, we, therefore, study the full Hawking photon spectra of PBHs with temperatures roughly between 10 MeV and 200 GeV, corresponding to PBH masses from 10^{12} kg down to 5×10^7 kg, respectively, which are significantly evaporating today but are sufficiently cold for us to ignore any contributions from potential new particles with masses above the electroweak scale (The same can be said about next section: we will not consider temperature exceeding the electroweak scale. See i.e. [190, 191] for the effects of new heavy particles on PBH evaporation). We will also ignore photons from ALP decays since string axions typically have large decay constants (above the GUT scale) and therefore very long lifetimes/small decay rates. We employ the publicly available BlackHawk code [93–96] to compute the Hawking spectra of PBHs

with different mass and spin, which uses both PYTHIA [98,99] and Hazma [97] as particle physics codes to determine the secondary photon emission, taking into account the regime of validity of the latter codes described in section 5.4.2. For the heavier (and hence colder) PBHs that cannot effectively emit particles heavier than the electron, we employ semi-analytical tools to determine the secondary photon spectrum resulting mainly from electron FSR following [100].

We identify particular features in the Hawking spectrum and from their energies (and energy ratios) devise a method to determine both the mass and spin of a PBH in the above-mentioned mass range. We will show, in particular, that, with this methodology, one can distinguish an effective Schwarzschild PBH from one that is spinning with $\tilde{a} \simeq 0.1 - 0.5$ as the result of light scalar emission. By using the energy of these features rather than the corresponding photon flux, the method is thus independent of the distance between the observer and the PBH. One can then use the inferred PBH mass and spin to predict the expected photon flux as a function of the Earth-PBH distance, therefore allowing one to determine the latter from the measured flux, alongside potential parallax measurements.

In this section we describe the general characteristics of the photon spectrum, discussing the differences observed for distinct PBH masses and low ($0 < \tilde{a} < 0.6$) spins. The section is further divided into subsections according to the low, intermediate, and high mass ranges described in 5.4.2. We outline our proposed method to determine the PBH mass and spin and discuss the energy resolution requirements for sufficiently precise measurements of these quantities that may allow one to detect the effects of new physics, particularly those of the string axiverse. Finally, we summarize our main conclusions and discuss future prospects. This section is based on the results of [13].

9.1.1 Hawking spectra for $5 \times 10^7 < M < 10^{12}$ kg and $0 < \tilde{a} < 0.5$

Here we show the spectra of PBHs in the three ranges identified in 5.4.2 and obtained through the described methods. We will see that the spectra exhibit different features according to the different ranges. We will identify features of the spectra which will be used in later chapters for the PBH mass and spin determination.

Low mass range $(5 \times 10^7 - 2.5 \times 10^{10}$ kg)

Fig. (9.1) shows the spectra obtained using BlackHawk and PYTHIA, for different PBH masses and spins. As one can clearly observe, the particle emission rate increases with the PBH spin $\tilde{a}$ for fixed mass. This is a generic feature of the emission of particles with non-zero spin like the photon and the many charged fermions contributing to the secondary spectrum in this low-mass/high-temperature range. We note that the opposite behavior is observed for scalar emission, which decreases with $\tilde{a}$ (see i.e. Fig. 2 in [94]).

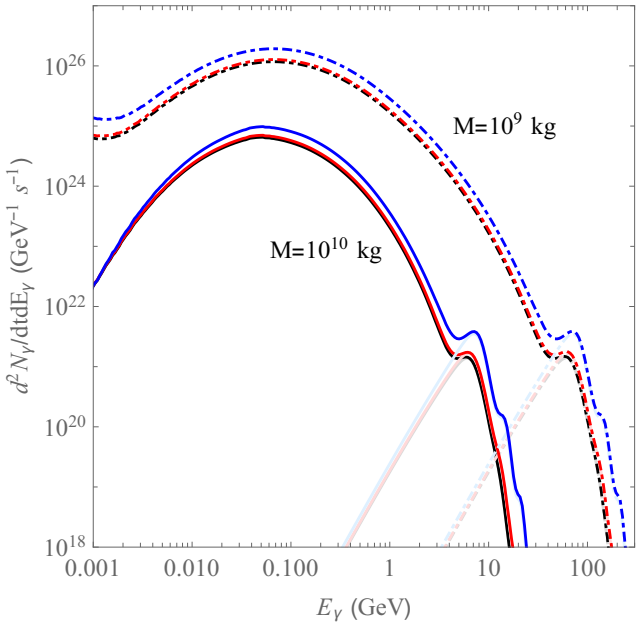

Figure 9.1: Primary (light colors) and total (dark colors) photon emission rates for a PBH of 10^{10} kg (solid lines) and 10^9 kg (dash-dotted lines), for $\tilde{a} = 0, 0.2, 0.5$ (black, red, and blue, respectively). The spectra are obtained using BlackHawk/PYTHIA.

In Fig. 9.1 we can also identify the primary emission peak at about five times the value of the Hawking temperature, while the secondary emission is more intense at lower energies. At the intersection of the secondary and primary emission spectra we can identify a "valley-peak" structure, and the energy of the "valley", E_V, as identified in Fig. 9.2, seems to be quite insensitive to the spin parameter $\tilde{a}$.

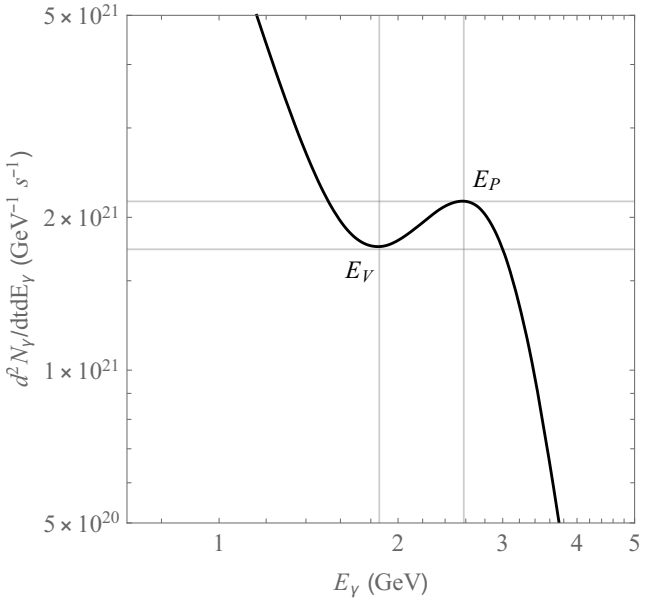

Figure 9.2: Photon spectrum near the primary emission peak for $M = 2.5 \times 10^{10}$ kg and $\tilde{a} = 0$, illustrating the quantities characterizing the "valley-peak" structure.

This is not surprising since the secondary spectrum depends on $\tilde{a}$ essentially through the primary spectrum of charged/unstable particles, which, like the primary photon spectrum, increases with $\tilde{a}$. Therefore, the energy at which they become comparable remains essentially the same for all PBH spins (for a given mass). The energy of the primary emission peak, E_P, is also largely independent of the PBH spin, due to the mild dependence of the Hawking temperature on $\tilde{a}$ away from extremality, although there is a non-negligible spin dependence due to the graybody factors. In the next subsection, we will explore the mass and spin dependence of these two energy values to determine the latter values.

We note that the "bell-shaped" maximum of the secondary spectrum at lower energies, albeit more intense, cannot be used to reliably determine the PBH mass and spin, since its shape is degenerate in these parameters. For instance, we may increase the maximum emission rate and the broadness of the peak by either increasing $\tilde{a}$ or decreasing the PBH mass. Moreover, this bell structure is present in simulations performed using BlackHawk [93, 95, 96] through the hadronization routine PYTHIA [98, 99], but not when employing Hazma [97] or the semi-analytical methods proposed in [100, 116]. For these reasons, we

will ignore this part of the secondary spectrum in our subsequent analysis.

Intermediate mass range ($2.5 \times 10^{10} - 5 \times 10^{11}$ kg)

In this mass range, we have used BlackHawk with Hazma to compute the secondary photon spectrum, particularly given the significant contribution of $\pi^0 \to \gamma\gamma$, as visible in the spectra shown in Fig. 9.3 for $\tilde{a} = 0$.

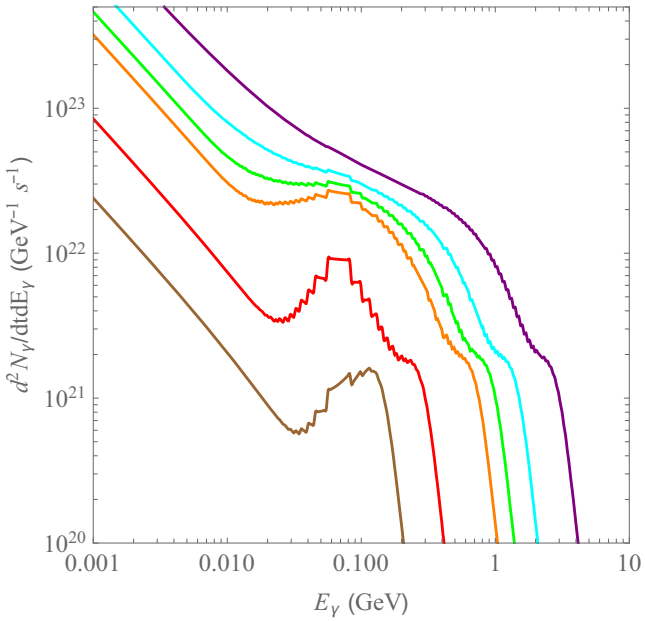

Figure 9.3: Photon spectrum for $\tilde{a} = 0$ PBHs with masses 2.5, 5, 7.5, 10, 25 and 50×10^{10} kg (purple, cyan, green, orange, red and brown, respectively), obtained using BlackHawk/Hazma.

As one can see in this figure, pion decay induces a bump in the secondary spectrum at energies around half the pion mass (~ 0.07 GeV). This feature is less prominent for the PBHs at the boundaries of this mass range since, on the one hand, for the lighter (hotter) ones other secondary emission processes overcome the pion contribution while, on the other hand, for the heavier (colder) ones primary pion emission is suppressed. In Fig. 9.4 we show how the photon spectrum changes with the PBH spin, and as expected we see that the pion contribution decreases with $\tilde{a}$, given that they are spin-0 particles as explained earlier.

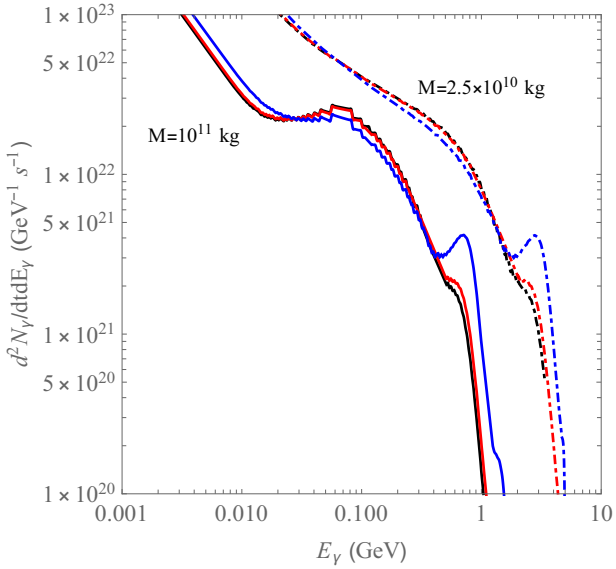

Figure 9.4: Photon spectrum for PBHs with $\tilde{a} = 0, 0.2, 0.5$ (black, red and blue, respectively) and for $M = 2.5 \times 10^{10}$ and 10^{11} kg (dashed-dotted and solid lines, respectively), obtained using BlackHawk/Hazma.

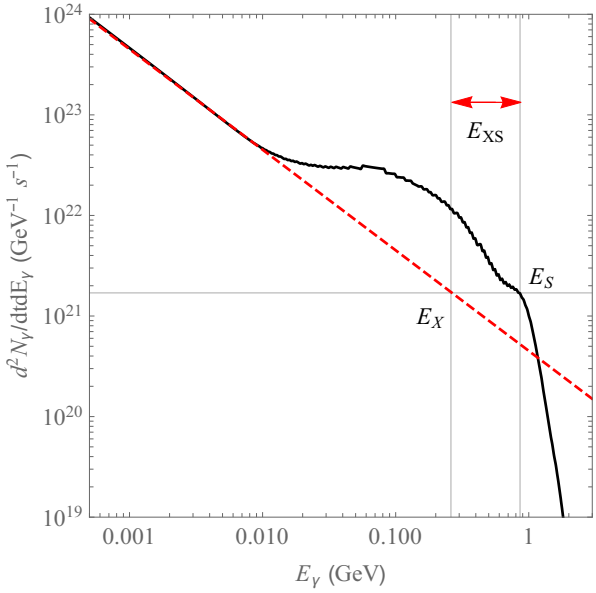

Figure 9.5: Photon spectrum near the primary emission peak for a PBH with $M = 7.5 \times 10^{10}$ kg and $\tilde{a} = 0$, illustrating the "shoulder" feature, the pion "bump" and the fit to the low-energy tail of the secondary spectrum (dashed red line).

A generic feature of the spectra in this mass range is, however, the absence of the "valley-peak" structure identified in the low mass range. Nevertheless, it is possible to characterize these spectra through alternative features that we will later use for mass and spin determination. In particular, we can identify a "shoulder" at the energies at which the primary and secondary photon emission rates become comparable, corresponding to a local maximum of $d^3N_\gamma/dtdE_\gamma^2$ at energy E_S, as shown in Fig. 9.5.
Another feature that we may use to characterize the spectrum is the energy E_X at which the low-energy tail of the secondary spectrum (extrapolated using a power-law fit) would match the emission rate at the "shoulder", in the absence of the pion "bump", as shown in Fig. 9.5. We will examine the mass and spin dependence of these two energy values, as well as their difference $E_{XS} = E_S - E_X$ in the next section.

High mass range ($5 \times 10^{11} - 10^{12}$ kg)

As described above, for these PBHs, we computed the dominant FSR contributions to the secondary spectrum semi-analytically, our results being shown in Figs. 9.6 and 9.7. The pion "bump"'s absence makes the "valley-peak" structure evident as for the low mass PBHs, and we may use the energies E_P and E_V to characterize the spectrum.

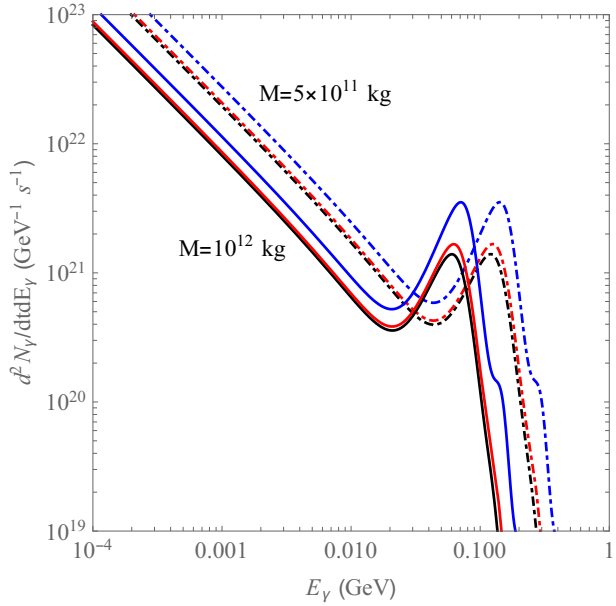

Figure 9.6: Photon spectrum for PBHs with $\tilde{a} = 0, 0.2, 0.5$ (black, red and blue, respectively) and masses of $10^{11}/2.5\times10^{11}$ kg (solid/dashed-dotted lines), obtained using the semi-analytical method.

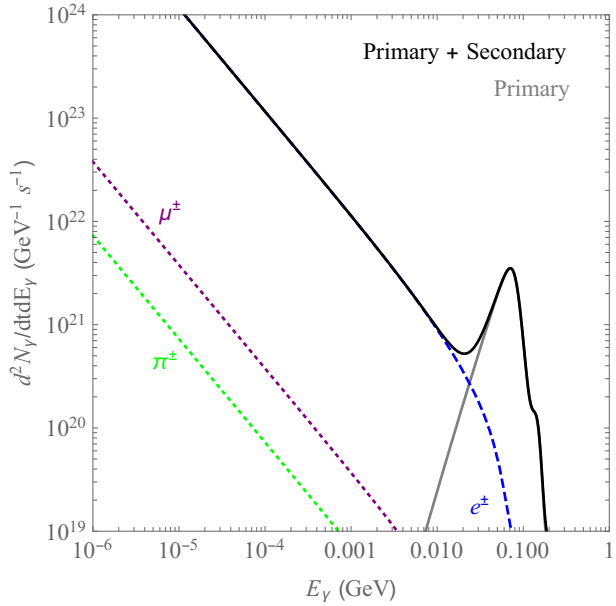

Figure 9.7: Photon spectrum for a PBH with $M = 5 \times 10^{11}$ kg and $\tilde{a} = 0.2$, obtained using the semi-analytical method (black), illustrating the different contributions including primary photons (gray) and secondary photons from electron (blue), muon (purple) and pion (green) FSR.

Recall that PBHs with $M \gtrsim 10^{12}$ kg have not yet lost a significant fraction of their mass and hence could not have spun up due to axion emission. We nevertheless note that the spectrum is qualitatively similar for PBHs that can significantly emit electrons ($T_H \gtrsim m_e/5 \simeq 0.1$ MeV or $M \lesssim 10^{14}$ kg) and is characterized by the same energy values.
We now describe our proposal for determining the mass and spin of a PBH from its photon Hawking emission spectrum using the features identified in the previous section, within the different mass ranges of our analysis.

9.1.2 Low mass range $(5 \times 10^7 - 2.5 \times 10^{10}$ kg)

In Fig. 9.8 we show how the energy E_V depends on the PBH mass for different values of dimensionless spin parameter $\tilde{a}$.

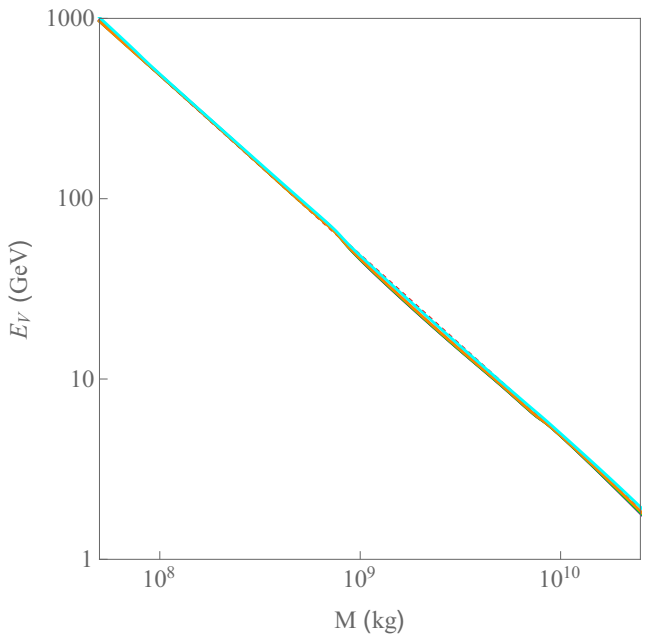

Figure 9.8: Energy of the "valley" as a function of the PBH mass for spin parameters $\tilde{a} = 0, 0.1, 0.2, 0.3, 0.5$ (red, blue, green, orange and cyan, respectively), computed using BlackHawk. The dotted red line yields the best fit curve for E_V given by Eq. (9.1).

We thus find that the "valley" energy E_V exhibits a simple dependence on the PBH mass, with only a very mild dependence on the spin parameter, and is

well fitted by a simple inverse power law:

$$E_V^{(low)} \simeq \frac{4.85 \times 10^{10} \text{ kg}}{M} \text{ GeV} , \tag{9.1}$$

such that a measurement of the "valley" energy can be used to determine the PBH mass with a relative error essentially given by the energy resolution of the detector, $\Delta E/E_V \simeq \Delta M/M$ (up to the mild dependence on $\tilde{a}$).
On the other hand, the primary peak energy, albeit also quite close to a M^{-1} dependence, exhibits a more pronounced dependence on the PBH spin, which is mostly due to the gray-body factors, since as discussed earlier the Hawking temperature is only mildly dependent on this parameter (away from extremality as we are considering). Given the similar mass dependence of both E_P and E_V, we expect their ratio to be largely independent of the PBH mass, therefore isolating the PBH spin dependence of the Hawking spectrum. This is illustrated in Fig. 9.9, where we plot E_P/E_V as a function of the PBH mass for different $\tilde{a}$ values.

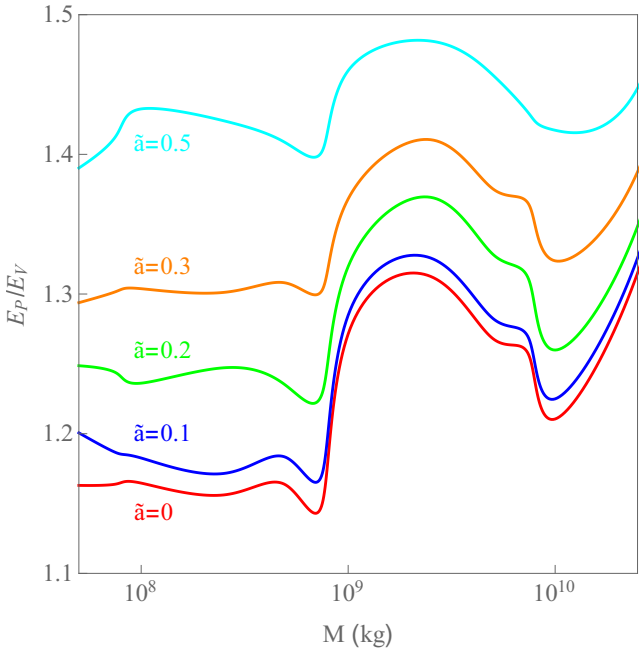

Figure 9.9: Ratio E_P/E_V as a function of the PBH mass computed with BlackHawk/PYTHIA, for $\tilde{a} = 0, 0.1, 0.2, 0.3, 0.5$ (red, blue, green, orange, cyan, respectively).

This figure shows that the ratio E_P/E_V has a non-trivial behavior with the PBH mass, which essentially reflects the number of different SM particle species that are emitted by PBHs with different masses, particularly the effects of quarks and gluons. Nevertheless, this ratio varies by less than 20% for a fixed PBH spin within this mass range. This means that if we determine the PBH mass from a measurement of E_V, a measurement of E_P and of the ratio E_P/E_V can be used to infer the PBH spin. Roughly, we conclude that measuring the energy of these features with a 10% resolution may allow for distinguishing between a slowly rotating PBH ($\tilde{a} \ll 1$) and a PBH with $\tilde{a} \gtrsim 0.2$, i.e. one that has spun up as it evaporated. If $\tilde{a} \lesssim 0.1$, a much better resolution below the few percent level should be required for inferring a non-vanishing rotation.

9.1.3 Intermediate mass range ($2.5 \times 10^{10} - 5 \times 10^{11}$ kg)

In this mass range we will explore the mass and spin dependence of the energy features E_S ("shoulder" energy) and $E_{XS} = E_S - E_X$ identified in the previous section, given the absence of a clear "valley-peak" structure due to pion contamination. Unfortunately, none of these quantities exhibits a clean dependence on either the mass or the spin of PBH, so a precise determination of these quantities does not seem possible with this method. Nevertheless, as shown in Fig. 9.10, E_S is nearly inversely proportional to the PBH mass, although the proportionality constant is somewhat dependent on the PBH spin ($\lesssim$ 20% variation for $\tilde{a} = 0 - 0.5$). This means that a measurement of E_S alone can at most allow us to infer the PBH mass with a $\lesssim$20% error even with infinite energy resolution.

We now turn to the ratio E_{XS}/E_S, which is shown in Fig. 9.11 and exhibits essentially a power-law increase with the PBH mass within this range, despite some minor features. The exact power depends on $\tilde{a}$, making an accurate determination of the PBH spin challenging in this case, taking into account the uncertainty in measuring the PBH mass. In this case, we may nevertheless hope to obtain upper and lower bounds on both quantities depending on the energy resolution of the detector. For the lower PBH masses in this range, one would need to measure E_{XS}/E_S with at least $\sim 5\%$ precision to infer $\tilde{a} \gtrsim 0.2$, while a percent level precision may be required for this towards the upper bound of this mass range.

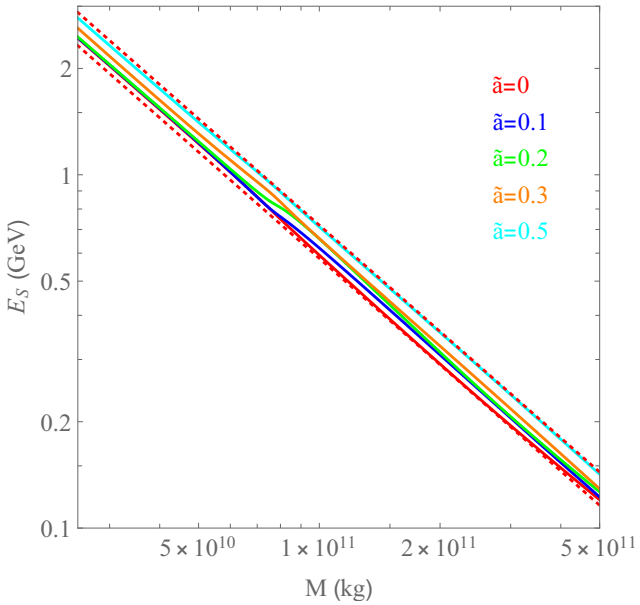

Figure 9.10: "Shoulder" energy E_S as a function of the PBH mass computed using BlackHawk and Hazma, for $\tilde{a} = 0, 0.1, 0.2, 0.3, 0.5$ (red, blue, green, orange and cyan, respectively).

We expect that these uncertainties might be mitigated by including additional features of the Hawking spectrum in the analysis, such as the height and width of the "pion bump", which are sensitive to both the PBH mass and spin as previously discussed (here we mean the height relative to i.e. the primary peak, such that this is independent of the PBH-Earth distance as well). While this may improve the precision with which the mass and spin of a PBH are determined, we will not pursue this any further in this work, given the theoretical uncertainties that could still plague the computation of the Hawking spectrum in this mass range, given in particular the discrepancies we have observed in the spectra obtained using PYTHIA or Hazma alongside BlackHawk. The method proposed for this mass range relies mostly on the primary photon emission (which determines the "shoulder" position to a large extent) and the low-energy tail of the secondary emission, so while it cannot clearly disentangle the mass and spin dependence of the spectrum it is nevertheless robust from the theoretical perspective, and a more thorough analysis of other features is left for future work.

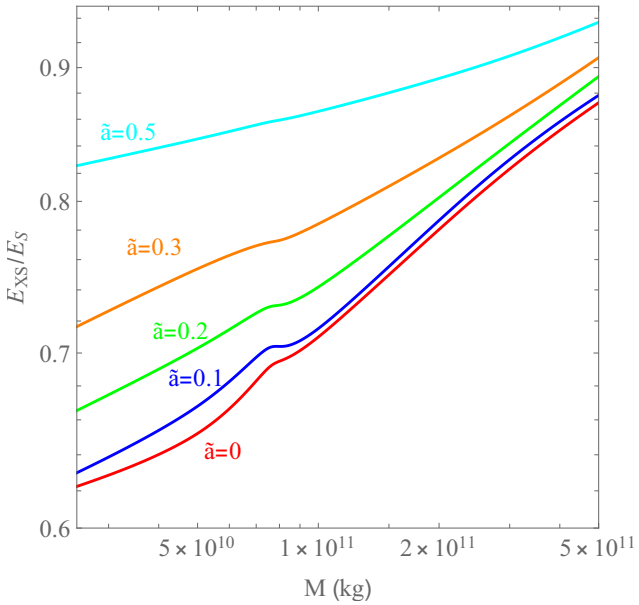

Figure 9.11: Ratio E_{XS}/E_S as a function of the PBH mass computed using BlackHawk/Hazma, for $\tilde{a} = 0, 0.1, 0.2, 0.3, 0.5$ (red, blue, green, orange and cyan, respectively).

9.1.4 High mass range $(5 \times 10^{11} - 10^{12}$ kg)

For masses higher than 5×10^{11} kg, the pion contribution becomes subdominant and the "valley-peak" structure is again well defined, so that we may use the method employed for the low mass range. In Fig. 9.12 we show how E_V and E_P depend on the PBH mass for different values of $\tilde{a}$ in this mass range.

As in the low mass range, E_V is nearly independent of the PBH spin, although its mass dependence deviates slightly from an inverse power law:

$$E_V^{(high)} \simeq \left(\frac{2.5\times10^{10}\ \text{kg}}{M}\right)^{1.05}\ \text{GeV}\ , \tag{9.2}$$

In Fig. 9.13 we plot the ratio E_P/E_V as a function of the PBH mass for different spin values, and in this mass range, we find only a mild dependence on the mass, such that measuring this ratio with a precision of a few percent suffices to distinguish a non-spinning PBH from one that is spinning with $\tilde{a} \gtrsim 0.2$, with around 10% resolution required to measure $\tilde{a} \gtrsim 0.5$.

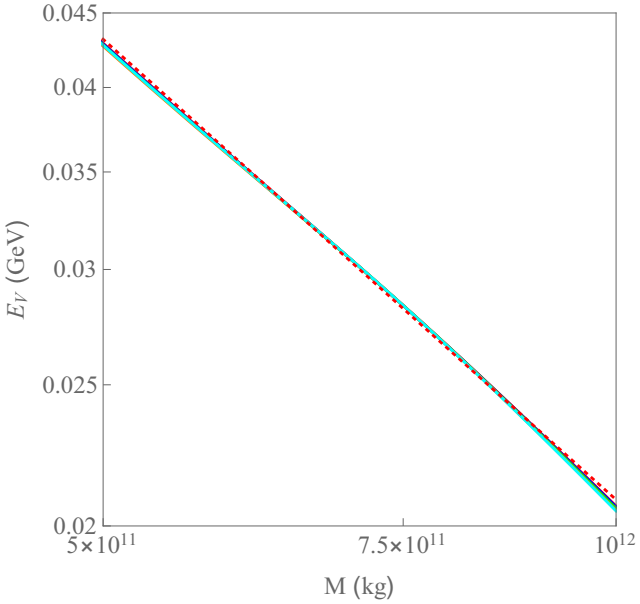

Figure 9.12: "Valley" energy as a function of the PBH mass, computed with the semi-analytical method, for $\tilde{a} = 0, 0.1, 0.2, 0.3, 0.5$ (red, blue, green, orange and cyan, respectively). The dotted red line yields the best-fit curve in Eq. (9.2).

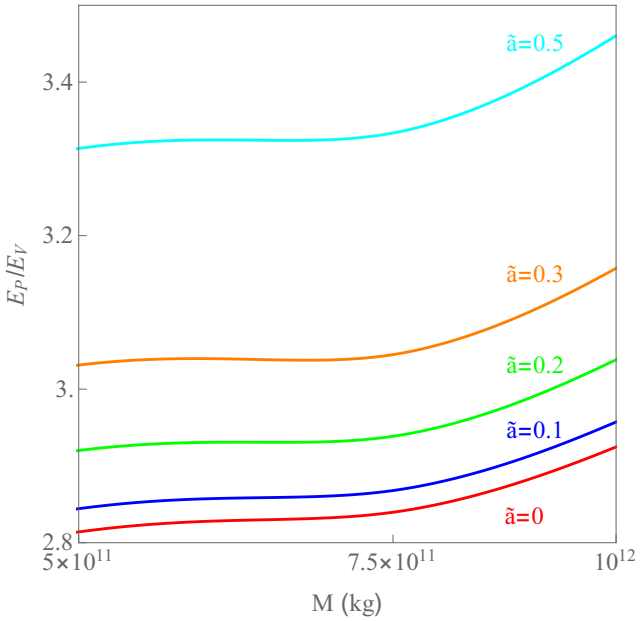

Figure 9.13: Ratio E_P/E_V as a function of the PBH mass, computed using the semi-analytical method, for $\tilde{a} = 0, 0.1, 0.2, 0.3, 0.5$ (red, blue, green, orange and cyan, respectively).

9.1.5 Conclusion

In this work, we have proposed a distance-independent methodology for determining the mass and spin of a PBH from its photon Hawking emission spectrum, including both the primary and secondary emission components. The methods rely on the energy of particular features in the spectrum, in the vicinity of the primary emission peak. For most of the PBH mass range considered ($5 \times 10^7 - 10^{12}$ kg), corresponding to PBHs that have already lost a significant fraction of their mass through evaporation, these are the primary peak energy and the "valley" energy, the latter corresponding to the point where the secondary and primary emission spectra become comparable. Using both these energy values, one can partially disentangle the effects of the PBH mass and spin, allowing for an accurate measurement of both quantities with a detector with sufficient energy resolution. We generically find that an energy resolution of at least a few percent may allow for distinguishing a non-spinning PBH ($\tilde{a} \ll 1$) from one that is spinning with $\tilde{a} \gtrsim 0.2$. This methodology fails only in the intermediate PBH mass range ($2.5 \times 10^{10} - 5 \times 10^{11}$ kg) where neutral pion decays significantly change the shape of the spectrum, but even in this case, we were able to identify spectral features that at least allow one to place lower and upper bounds on the PBH mass and spin.

As the proposed methods rely on energy values rather than photon emission rates, they are independent of the Earth-PBH distance, d. Once M and $\tilde{a}$ are known, one can then predict the expected photon flux by dividing the theoretical emission rate $d^2N_\gamma/dtdE_\gamma$ by $4\pi d^2$, such that the observed photon counts can be used to infer the distance d. If the PBH is close enough for d to also be accurately determined through parallax measurements, this can be used to check the validity of the evaporating PBH hypothesis and also the consistency of the mass and spin determination.

We should note, however, that it may be challenging to, in practice, implement our proposed methodology since it relies on the shape of the spectrum close to the primary emission peak, where emission rates are considerably lower than for the low-energy tail of the secondary spectrum (see i.e. Fig. 9.14). If PBHs in this mass range do exist, they are much more likely to be found through the latter part of the spectrum, and only after detector sensitivities can be improved by a few orders of magnitude will it be possible to study spectral features close to the primary emission peak. For example, the pro-

posed AMEGO-X [233–235] and All-Sky-ASTROGAM missions [236, 237] are expected to have sensitivities down to $\sim 10^{-6}$ MeVcm^{-2}s^{-1} for photon energies $E_\gamma \sim 1$ MeV $- 1$ GeV (and energy resolution $< 10\%$), which can be recast as a lower bound on the PBH emission rate

$$\frac{d^2 N_\gamma}{dt dE_\gamma} \gtrsim 10^{24} \left(\frac{0.1 \text{ GeV}}{E_\gamma}\right)^2 \left(\frac{d}{100 \text{ AU}}\right)^2 \text{GeV}^{-1}\text{s}^{-1} \ . \tag{9.3}$$

This is above the primary peak emission rate for the PBH mass range considered except for PBHs within only a few AU of the Earth, which we would have to be extremely lucky to detect. Note also that only for the heaviest PBHs with $E_P \lesssim 1$ GeV could the primary spectrum be within the reach of such detectors. The ongoing Fermi-LAT instrument has a comparable sensitivity at higher energies, and PBH searches with this instrument have already been performed, albeit so far with null results [204]. The proposed MAST mission [239], with a large effective area, could improve upon Fermi-LAT's state-of-the-art sensitivity for high-energy gamma-rays (100 MeV - 1 TeV) by one order of magnitude, with an energy resolution possibly down to 6%-10% above 10 GeV. This may potentially enable the detection of primary Hawking emission for PBHs with $M \lesssim 10^{10}$ kg and the implementation of our mass and spin determination methods. PBH detection in the neutrino channel has also been proposed in the literature [243–247], and we envisage that the neutrino Hawking spectrum may, in principle, provide additional information for mass and spin determination, as we will see in the next chapter.

Our results show that it may be possible in the near future to not only detect Hawking radiation from small PBHs but also determine whether or not they rotate with moderately large spins, $\tilde{a} \gtrsim 0.2$. Evidence for the existence of such spinning PBHs could have a considerable impact in high-energy physics, given that PBHs lighter than 10^{12} kg should already have lost essentially all their angular momentum through Hawking emission of Standard Model particles and, to our knowledge, only the emission of a large number of light scalars (characteristic of scenarios such as the string axiverse) could justify finding $\tilde{a} \sim 0.1 - 0.5$.

9.2 High spin PBHs

It is well known that, if one assumes only the particle spectrum of the Standard Model (SM) of particle physics and a spin-2 massless graviton, with no yet undiscovered additional degrees of freedom, one finds that a BH loses angular momentum much faster than it loses mass. For instance, for $\tilde{a} \ll 1$ and a Hawking temperature above the electroweak scale ($M \lesssim 10^8$ kg) one obtains $\dot{J}/J \simeq 8\dot{M}/M$. In addition, within the standard paradigm for PBH formation, where the latter results from the gravitational collapse of large overdensities in the radiation-dominated era, PBHs are born with low spins, at or below the percent level [196, 197].

For these reasons, comparatively few works in the literature have so far considered the role of spin in the evolution and cosmological impact of PBHs [94, 202, 203, 212, 218, 221, 227, 251–255], although there are several models in which PBHs may be born or acquire a non-negligible spin parameter.

Firstly, there are cosmological scenarios where PBHs may exhibit large natal spins, even close to extremality ($\tilde{a} \sim 1$) if they are i.e. born in an early matter-dominated epoch [198][1] or result from the collapse of domain-walls [257] or scalar field fragmentation [258]. In this case $\dot{J}/J \simeq 2.6\dot{M}/M$ (within the SM), so one may hope to detect PBHs in the early stages of their evaporation process still exhibiting a substantial spin.

Secondly, in theoretically well-motivated scenarios with a large number of light scalar species such as the string axiverse [181], as we have discussed in previous chapters, PBHs may even develop spin parameters $\tilde{a} < 0.555$ through evaporation [11], since emission of scalar quanta with $l = 0$ does not change J while decreasing M, therefore increasing $\tilde{a}$ [90, 92]. Note that in the SM only the Higgs doublet fields (and pions below the QCD confinement temperature) exhibit this property, but their contribution is overwhelmed by the effects of all other particle species with non-zero spin (fermions and gauge bosons), which necessarily decrease a BH's angular momentum J[2]. Hence, depending on the number of light axion species and natal spin, light PBHs with $M \lesssim 10^{12}$ kg may thus exhibit a non-trivial mass-spin distribution that reflects the underlying particle physics (see also [12] for the potential effects of axion superradiant instabilities in this context).

[1] Note that in some scenarios accretion may decrease the PBH spin [256].

[2] Note that for a field of spin s emission occurs only in $l \geq s$ modes.

Devising methodologies to precisely determine a PBH mass and spin is thus an important goal in terms of particle physics, gravity, and cosmology. In our first paper on this topic [13], discussed in the previous section, we began this endeavor by showing that the energies and emission rates of particular features in the electromagnetic Hawking emission spectrum (including both primary and secondary components) can be used to infer both the PBH mass and spin independently of the distance between the latter and the Earth. We focused our discussion on PBHs with spin parameters $0.1 \lesssim \tilde{a} \lesssim 0.6$, since this is the range of spins developed by evaporating PBHs in the string axiverse scenario. In this second work, we now focus on PBHs with $\tilde{a} \gtrsim 0.6$, for which new features appear in the primary photon emission spectrum as a result of the enhanced angular momentum. As discussed above, values of $\tilde{a}$ in this range would correspond to PBHs born with large spins that are sufficiently heavy so as not to have lost a significant amount of angular momentum until the present day, assuming they were born in the early Universe (see i.e. [232] for possible scenarios of light BH formation at late times). Note that, even in the axiverse scenario with an arbitrarily large number of light scalar species, a PBH loses spin if it starts with $\tilde{a} > 0.555$, since in this regime scalar emission is dominated by non-spherical ($l \geq 1$) modes, which decrease the BH spin.
As in our previous work, our goal is to find observable quantities that are independent of the unknown PBH-Earth distance, although the latter could potentially be determined through parallax techniques if a PBH is sufficiently close [11]. This is the case of the energy of particular features in the emission spectrum and ratios between the corresponding emission rates. An objective is also to find observables depending exclusively on the PBH spin, or at least a methodology that can clearly disentangle the effects of the PBH mass and spin on the spectrum, such that both properties can be accurately measured. In our previous work the proposed method relied on features of both the primary and secondary photon emission spectrum, the latter corresponding to low energy photons emitted by charged particles in the primary Hawking spectrum as they propagate away from the BH horizon, as well as i.e. decay of primary particles like neutral pions. Although secondary photon emission is more intense than the more energetic primary emission (and hence easier to detect), it has in some regimes a non-trivial shape from which it is hard to extract the BH properties. The computation of the secondary spectrum also relies on high-energy physics numerical codes with a limited range of validity, so that

there is a non-negligible theoretical uncertainty.
As we will discuss, for large values of the PBH spin parameter $\tilde{a} \gtrsim 0.6$ the primary spectrum exhibits a multi-peak structure, each emission peak corresponding to photons emitted with $l = m = 1, 2, 3, \ldots$. Since the emission rate decreases with l, one may at least hope to detect the first two emission peaks, corresponding to the $l = m = 1$ and $l = m = 2$ modes. We will then show that the properties of these two emission peaks yield a robust method to determine the PBH spin and mass.
This section is organized as follows. In the next subsection, we review the main aspects of the computation of the primary Hawking emission spectrum. In subsection 9.2.2 we discuss our proposed methodology, first based on the total emission rates and later taking into account the effects of anisotropic emission. We summarize our results and discuss prospects for future work in subsection 9.2.3. Appendices B and C discuss a few technical aspects of our calculation, and in particular, validate our proposed methodology by taking into account the secondary component of the Hawking spectrum. This section is based on [14].

9.2.1 The Hawking spectrum

The differential Hawking emission rate for each particle species i of spin s is given by (5.36) [87, 88, 102].
The non-trivial part of determining the differential emission rate resides in computing the gray-body factors, which are determined by the solutions of the radial Teukolsky equation [37–40] - the master equation that governs the dynamics of (massless) test fields in the Kerr geometry, and which follows from the underlying curved spacetime field equations (Klein-Gordon, Dirac, Maxwell and perturbed Einstein equations). The transmission coefficient for each mode can then be computed by considering the associated wave scattering problem and solving the Teukolsky equation through numerical methods. We use a shooting method (see i.e. [39, 70] for details) to compute $\Gamma^s_{l,m}$ up to $l = 4$ for the $s = 1$ massless photons. Although the emission rate is formally an infinite sum over all angular modes, we find that this approximation is sufficiently good for our purposes, taking into account the computational time involved.
We have also explicitly computed the primary spectrum of other emitted par-

ticles in order to be able to determine the secondary photon spectrum, as discussed in the appendix. For fermions, we include modes up to $l = 7/2$ in our calculation, which is sufficiently accurate[3].

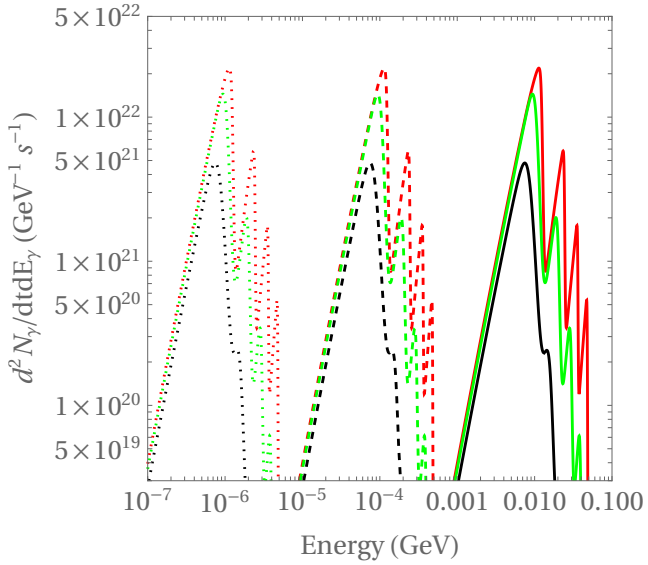

Figure 9.14: Primary photon spectrum for PBHs with $\tilde{a} = 0.6, 0.9, 0.99$ (black, green and red, respectively) and $M = 10^{13}, 10^{15}, 10^{17}$ kg (solid, dashed, and dotted curves, respectively), obtained using Eq. (5.36).

Fig. 9.14 shows examples of the primary Hawking spectrum for different values of the PBH mass and spin $\tilde{a} \geq 0.6$. As one can clearly see, the photon emission rate increases with the PBH spin, a characteristic feature of the emission of particles with non-zero spin, while the opposite behavior characterizes scalar emission (see i.e. Fig. 2 in [94]).
Independently on the PBH mass, if $\tilde{a} \gtrsim 0.6$ it is possible to identify in Fig. 9.14 a primary emission peak and a series of higher energy peaks of decreasing amplitude. As discussed in appendix B, the first peak receives the dominant contribution from the $l = m = 1$ mode, the second from the $l = m = 2$ mode, and so on. We will focus on the first two peaks since they yield the largest emission rates and hence are easier to detect. We also see that the second peak ($l = 2$) is barely discernible for $\tilde{a} = 0.6$, so it cannot be employed for PBH spin determination for smaller values of $\tilde{a}$, for which it is overwhelmed by the

[3]We have obtained a very good agreement between our results and those obtained in [259], the authors of which have kindly provided us their results for the massless spin-1 gray-body factors.

first peak ($l = 1$). In our analysis in the next section, we label the energy and differential emission rate at each peak as E_l and I_l, as illustrated in the example of Fig. 9.15.

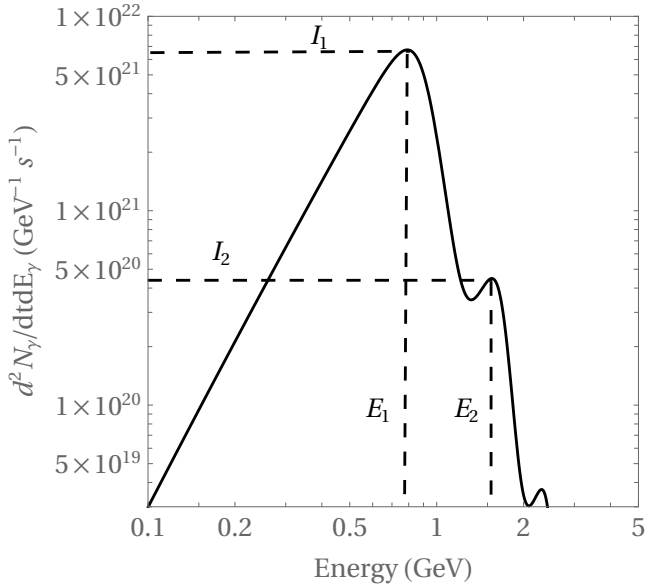

Figure 9.15: Primary photon spectrum for $M = 10^{11}$ kg and $\tilde{a} = 0.7$, illustrating the energies and emission rates of the first and second peaks used in our analysis.

In the next subsection, we study how these quantities depend on the BH mass and spin and devise a method to determine the latter by measuring these two peaks. Note that detection of the second peak already constitutes an indication of a PBH with $\tilde{a} \gtrsim 0.6$.

9.2.2 PBH mass and spin determination

In Fig. 9.16 we show our results for the dependence of the peak energies E_1 and E_2 on the PBH mass, for different values of dimensionless spin parameter $\tilde{a}$.

As this figure clearly illustrates, both peak energies are essentially inversely proportional to the PBH mass, $E_l \propto M^{-1}$, which is simply a consequence of the M^{-1} dependence of the Hawking temperature.

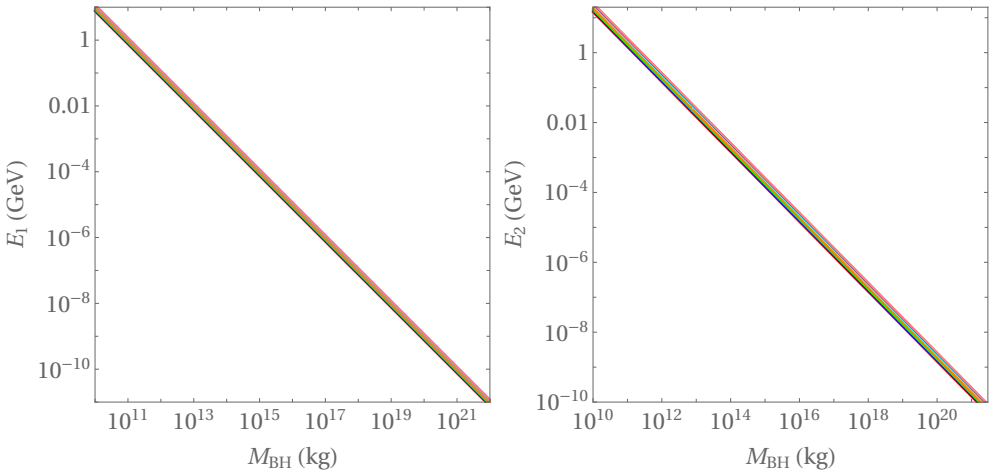

Figure 9.16: Energy of the first ($l = 1$, left) and second ($l = 2$, right) peaks as a function of the PBH mass for spin parameters $\tilde{a} = 0.6, 0.7, 0.8, 0.9, 0.99$ (red, blue, green, orange, and cyan, respectively).

The PBH spin dependence is, however, more involved since it is also due to the $\tilde{a}$-dependence of the gray-body factors. For $0.6 \leq \tilde{a} < 0.9999$, we obtain in particular:

$$E_1 = \frac{(7.463 - 11.640) \times 10^{10} \text{ kg}}{M} \text{ GeV} \ , \quad E_2 = \frac{(1.436 - 2.611) \times 10^{11} \text{ kg}}{M} \text{ GeV} \ , \tag{9.4}$$

where the largest numerical factors in the above expressions correspond to near-extremal PBHs. This suggests eliminating the PBH mass dependence by considering the ratio of the two peak energies, E_2/E_1, as presented in Fig. 9.17. This figure shows that this ratio is indeed only a function of the PBH spin, up to small numerical errors in the calculation, and is well described ($< 1\%$ deviations) by:

$$\frac{E_2}{E_1} \simeq 1.761 + 0.284\tilde{a} + \frac{0.000622\tilde{a}^2}{1 - 0.997\tilde{a}^2} \ , \tag{9.5}$$

The fact that this ratio takes values close to 2 is roughly related to the fact that the gray-body factors in Eq. (5.36), exhibit a "step-like" behavior, changing rapidly from 0 to 1 at a frequency/energy that grows with the mode's angular momentum l, as shown in Fig. 9.18. This is associated with the centrifugal potential barrier that wave modes have to tunnel through or overcome as they move away from the BH horizon. In the non-rotating limit (i.e. a Schwarzschild BH), this barrier has a height $V_{\rm max} = 4l(l+1)/27r_+^2$, and only modes with frequency $\omega^2 \gtrsim V_{\rm max}$ can be fully transmitted.

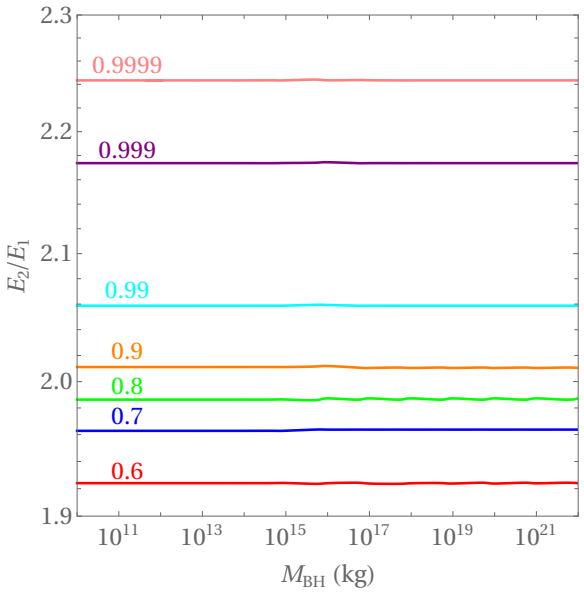

Figure 9.17: Ratio of peak energies E_2/E_1 as a function of the PBH mass for different values of the spin parameter $\tilde{a}$, as labeled.

Since the Bose-Einstein distribution in Eq. (5.36) is a strictly decreasing function in this limit, the above threshold frequency defines the energy of maximum emission for each mode. Hence, we expect $E_2/E_1 \simeq \sqrt{3} \simeq 1.73$ in the non-rotating case, which is close to our numerical fit in Eq. (9.5). Since the PBH spin affects both the gray-body factors and the Bose-Einstein distribution, it is not trivial to obtain an analytical expression for $\tilde{a} \neq 0$.

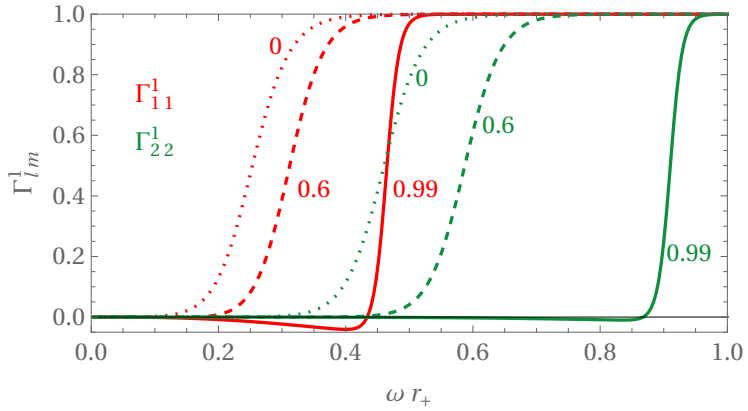

Figure 9.18: GBFs for the maximally co-rotating modes $l = m = 1$ (red) and $l = m = 2$ (green) of a massless spin-1 field for $\tilde{a} = 0$ (dotted), $\tilde{a} = 0.6$ (dashed) and $\tilde{a} = 0.99$ (solid).

Our numerical result shows, nevertheless, that the PBH spin can be determined from a measurement of the ratio between the energies of the second and first peaks of the photon Hawking spectrum. Away from extremality ($0.6 \lesssim \tilde{a} \lesssim 0.9$), this ratio has an approximately linear dependence on $\tilde{a}$, and one can easily see that i.e. a 10% change in the PBH spin changes the E_2/E_1 ratio by only 1-2%. This means that to determine the PBH spin with $\lesssim 10\%$ uncertainty one needs to measure the peak energies with resolution at or below the percent level. Prospects are better closer to extremal PBH spin values where the E_2/E_1 ratio exhibits a more pronounced growth with $\tilde{a}$.

A similar discussion applies to the ratio between the peak emission rates, I_2/I_1, since, as shown in Fig. 9.19, this is also BH mass-independent, being well described by ($< 4\%$):

$$\frac{I_2}{I_1} \simeq \frac{0.015 + 0.031\tilde{a}}{1 - 0.84\tilde{a}^2} + \frac{0.00241}{\sqrt{1 - 0.999\tilde{a}^2}} \,. \tag{9.6}$$

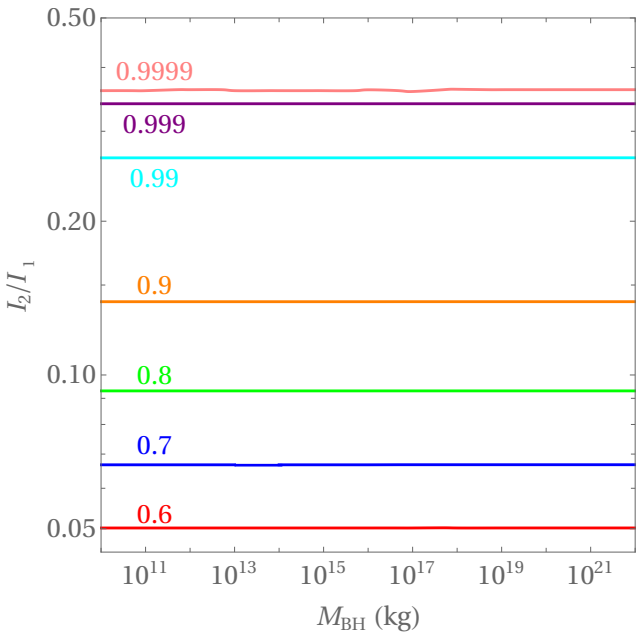

Figure 9.19: Ratio of the peak emission rates I_2/I_1 as a function of the PBH mass for different values of the spin parameter $\tilde{a}$, as labeled.

We note that this ratio is also independent of the Earth-PBH distance, even

though the observed fluxes are. In Fig. 9.20 we show how the two ratios vary with $\tilde{a}$.

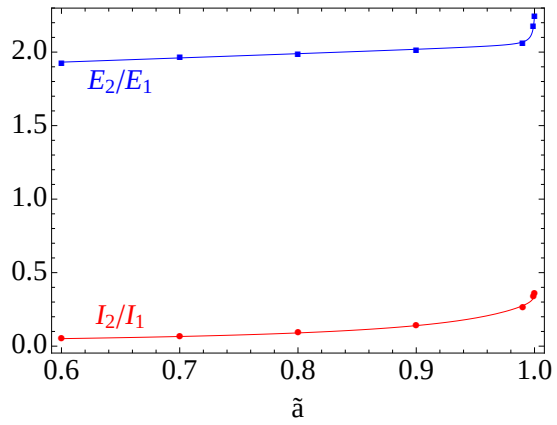

Figure 9.20: Ratios between the energies (blue) and the emission rates (red) of the $l = 1$ and $l = 2$ peaks in the primary Hawking spectrum as a function of the PBH spin parameter. The points correspond to numerically obtained values while the solid curves yield the approximate analytical expressions given in Eqs. (9.5) and (9.6).

In principle, we would thus have two observable quantities from which one could determine the PBH spin, and therefore a possible consistency check to validate the hypothesis that it corresponds to the Hawking spectrum of a Kerr PBH. However, one must take into account that we cannot really measure the total emission rate but only the flux emitted within a given solid angle along the line of sight. While for non-rotating BHs this is not a problem since the emission is isotropic, this is not the case for spinning Kerr BHs.
The angular differential emission rate is given by Eq. (5.37) [42, 103, 105–107, 260].
As mentioned earlier and shown more explicitly in the appendix, the peaks in the primary spectrum are dominated by the contribution of the maximally co-rotating modes $l = m = 1, 2, 3 \ldots$. This is illustrated in Fig. 9.21.
Hence, the energy of each peak is independent of the line-of-sight angle θ, since it corresponds essentially to maximizing the contribution to the spectrum of the corresponding $l = m$ mode. This implies that, on the one hand, the ratio E_2/E_1 is also independent of θ and can be used to determine the PBH spin as discussed above.

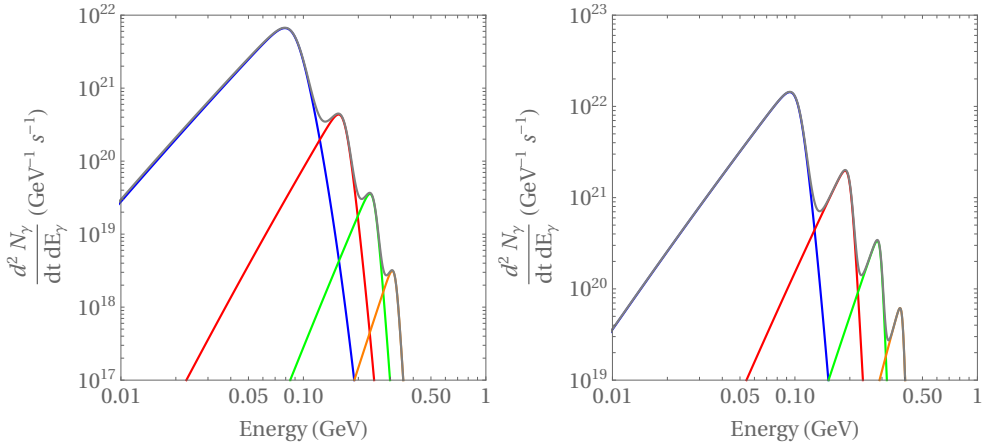

Figure 9.21: Superposition of the total primary photon spectrum (gray) and of the contributions of the maximally co-rotating modes $l = m = 1, 2, 3, 4$ (blue, red, green, and orange, respectively) for a BH of mass $M = 10^{12}$ kg and spin $\tilde{a} = 0.7$ (left) and $\tilde{a} = 0.9$ (right).

On the other hand, the intensity of each peak depends on the angle at which we observe the PBH. In particular, the ratio between the second and first peak photon emission fluxes is given by:

$$\frac{\mathcal{F}_2}{\mathcal{F}_1} = \frac{I_2}{I_1}\frac{|S^1_{2,2}(\theta)|^2}{|S^1_{1,1}(\theta)|^2} \simeq \frac{I_2}{I_1}\frac{|Y^1_{2,2}(\theta)|^2}{|Y^1_{1,1}(\theta)|^2} \simeq \frac{5}{3}\frac{I_2}{I_1}\sin^2\theta \ , \tag{9.7}$$

where in the last steps we have approximated the spin-1 spheroidal harmonic functions by their spherical counterparts, which holds away from extremality. Note that this implies that the $l = 2$ peak is suppressed relative to the $l = 1$ peak when the PBH is observed close to its poles at $\theta = 0, \pi$, and in these cases, our proposed methodology cannot be used.

Apart from these special configurations, we conclude that the ratio E_2/E_1 can be used to determine the spin of the PBH, while the corresponding flux ratio can be used to infer the inclination of its rotation axis relative to our line-of-sight, θ.

Optimistically, if a PBH is not too far from the Earth one could detect its proper motion, providing a change in the inclination angle θ with the characteristic sinusoidal modulation of the ratio of peak fluxes discussed above. For example, PBHs with $\sim 10^{12}$ kg, which have not yet evaporated significantly and may still exhibit large values of $\tilde{a}$, can make up a fraction $f \lesssim 10^{-7}$ of

the dark matter. The local dark matter density in our solar neighborhood is around $\rho_{DM} \simeq 0.4$ GeV/cm^3, which translates into a typical inter-PBH separation around ~ 100 AU so that we could realistically envisage finding PBHs with this mass less than ~ 50 AU from the Earth. Slightly heavier PBHs with 10^{14} kg may in fact make up all the dark matter density in the Universe, which could mean typical separations of just a few AUs, so they could in principle be much closer, as we discuss below. Taking the local velocity of the PBHs to be $\sim 200 - 300$ km/s relative to the Earth, this implies that each PBH travels a distance of $\sim 40 - 60$ AU per year, which may translate into an observable proper motion and, in general, to a significant change in inclination.

Measuring the sinusoidal modulation of the peak intensity ratio would then allow one to infer I_2/I_1, therefore allowing for a second (redundant) PBH spin determination. This could not only increase the precision of the spin measurement but also serve as a consistency check that the observed spectrum corresponds to an evaporating Kerr BH.

We should note, however, that detecting the primary Hawking emission from light PBHs may require technological advancements beyond the current state-of-the-art technology in terms of gamma-ray telescopes. We may consider the current bounds on the fraction of dark matter in PBHs with $10^{12} - 10^{14}$ kg from the contribution of Hawking radiation to the extra-galactic gamma-ray background (see i.e. [261] for a recent review):

$$f(M) < 2 \times 10^{-8} \left(\frac{M}{5 \times 10^{11} \text{ kg}} \right)^{3+\epsilon} , \tag{9.8}$$

where $\epsilon = 0.1 - 0.4$ and a monochromatic PBH mass spectrum is assumed. This then yields an upper bound on the number of PBHs of a given mass M that may come within a distance d from the Earth over i.e. $\Delta t \simeq 10$ yrs, which is a typical lifetime of an experiment:

$$N_{PBH} = \frac{f \rho_{DM}}{M} v \pi d^2 \Delta t < 1.6 \left(\frac{v}{250 \text{ km/s}} \right) \left(\frac{d}{100 \text{ AU}} \right)^2 \left(\frac{M}{5 \times 10^{11} \text{ kg}} \right)^{2+\epsilon} . \tag{9.9}$$

We may then optimistically assume that the dark matter bounds are saturated (i.e. that the extra-galactic gamma-ray background receives a significant contribution from PBH evaporation) and compute the distance d for which $N_{PBH} = 1$. We can then determine the corresponding photon energy

flux at the first peak ($l = 1$):

$$\Phi_1 \simeq \frac{E_1^2 I_1}{4\pi d^2} \ , \tag{9.10}$$

where we treat the emission as isotropic to estimate its magnitude, keeping in mind the anisotropic effects discussed above. Using our results for the peak energy E_1 given in Eq. (9.4) in the $\tilde{a}$ range of interest we then have:

$$\Phi_1 \lesssim (1.2-3)\times 10^{-8} \left(\frac{M}{5\times 10^{11}\ \text{kg}}\right)^{\epsilon} \left(\frac{I_1}{10^{22}\ \text{GeV}^{-1}\text{s}^{-1}}\right)\ \text{MeVcm}^{-2}\text{s}^{-1} \ , \tag{9.11}$$

where the spread in numerical factors is related to $\tilde{a}$-dependence of the peak energy E_1, with PBHs closer to extremality emitting a larger energy flux. This is maximized for PBHs with $M \sim 10^{14}$ kg that may account for the majority of dark matter and for which we may have $\Phi_1 \lesssim 10^{-7}\ \text{MeVcm}^{-2}\text{s}^{-1}$ (with a weak dependence on the PBH mass in the $10^{12} - 10^{14}$ kg mass range). Although this is still roughly an order of magnitude below the expected sensitivity of the planned AMEGO [233–235] and ASTROGAM missions [236,237] in the MeV-GeV range, it shows that detecting the primary emission from such PBHs may be possible in the not too distant future.

Note that, since we have found that $I_2/I_1 \simeq 0.05 - 0.4$ and $E_2/E_1 \simeq 1.9 - 2.2$ in our PBH spin range of interest, we expect $\Phi_2/\Phi_1 \simeq 0.2 - 1.8$. This means that the energy flux from the second peak ($l = 2$) may in fact be larger than that of the first peak for PBHs approaching extremality, being at most a factor 5 smaller than the latter for $\tilde{a} \simeq 0.6$.

9.2.3 Conclusion

In this work, we have proposed a new method to determine the mass and spin of PBHs from measurements of their primary Hawking radiation spectrum. We have shown, in particular, that the ratio between the energies of the $l = 2$ and $l = 1$ emission peaks is determined uniquely by the PBH spin parameter $\tilde{a}$, with both energies being inversely proportional to the PBH mass. This thus allows one to determine both Kerr parameters independently of the PBH-Earth distance. The ratio between the corresponding total emission rates is also only a function of $\tilde{a}$, which could yield an additional (redundant) observable to measure the latter. However, since the emission is anisotropic with a

distinct angular dependence near each peak, the ratio between the observed fluxes should exhibit a sinusoidal modulation with the line-of-sight. We argued that if a PBH passes sufficiently close to the Earth ($\lesssim 100$ AU), one may be able to detect this modulation from the PBH's proper motion relative to the Solar System.

Since the $l = 2$ peak only exceeds the tail of the $l = 1$ contribution for $\tilde{a} \gtrsim 0.6$, the proposed method is only applicable in this range. This thus complements the methodology that we have proposed in [13] for slowly rotating PBHs, $\tilde{a} \lesssim 0.6$, based on measurements of both the primary and secondary photon spectra. As we show in Appendix B, the secondary photon spectrum does not affect the methodology proposed in this work. We note that large spin parameters $\tilde{a} \gtrsim 0.6$ are only expected for PBHs that have not yet significantly evaporated, even within the context of the string axiverse where light scalar emission can significantly slow down a PBH's spin-down rate (or even spin it up if it is born with low spin values) [11]. We thus expect the methodology proposed in this work to be applicable to PBHs with $M \gtrsim 10^{12}$ kg. From current bounds on the PBH abundance, we showed that PBHs in the $10^{12} - 10^{14}$ kg mass range offer the best prospects for detection of primary Hawking emission in the future. We note that this should require at least an order of magnitude improvement in the sensitivity of gamma-ray telescopes compared to those currently being planned, and we hope that this work motivates further technological developments in gamma-ray detection to achieve this.

10 Evaporating Kerr black holes as probes of new physics

In this chapter, we discuss how, in the string axiverse scenario, PBHs can sustain non-negligible spin parameters as they evaporate. We show that tracking both the mass and spin evolution of a PBH in its final hour can yield a purely gravitational probe of new physics beyond the TeV scale, allowing one to determine the number of new scalars, fermions, vector bosons and spin-3/2 particles. Furthermore, we propose a multi-messenger approach to accurately measure the mass and spin of a PBH from its Hawking photon and neutrino primary emission spectra, which is independent of putative interactions between the new degrees of freedom and the Standard Model particles, as well as from the Earth-PBH distance. This chapter contains the main results of [15].
Several cosmological scenarios predict the formation of primordial black holes (PBHs) [1, 2, 153, 154, 154, 156, 194, 262–273] in the early Universe, typically within a very broad mass range. Although there is yet no concrete evidence for their existence, PBHs could be behind part of the gravitational wave signals observed by the LIGO-Virgo-Kagra detectors [3] or even the somewhat puzzling ultra-short microlensing events observed by OGLE [274].
This means that much lighter PBHs could also have been formed, in particular PBHs born with a mass $M \simeq 5 \times 10^{11}$ kg with a lifetime close to 14 Gyrs, which would now be in the final stages of their evaporation process through Hawking emission. Bounds on the abundance of these PBHs have been obtained from their contribution to the extra-galactic γ-ray background through Hawking emission, and they can account at most for a fraction $f < 2 \times 10^{-8}$ of the dark matter density [154, 202, 203, 238, 261, 275, 276]. Given the Solar System's velocity in the dark matter halo $\sim 200 - 300$ km/s ($\sim 10^{-4}$ pc/yr), this bound translates into a PBH flux $\lesssim 2 \times 10^5$ pc^{-2}yr^{-1}, implying that every

year there can be at most one "exploding" PBH passing within a milliparsec of the Earth. This means that one may still hope to observe PBHs in their final stages within the lifetime of existing γ-ray telescopes. Experiments such as H.E.S.S [277,278], Milagro [279], VERITAS [280], HAWC [281], and Fermi-LAT [204] have already performed dedicated searches for exploding PBHs in our vicinity, albeit so far no detections have been reported.

Detecting PBH Hawking radiation would be extremely important for probing the dynamics of quantum fields in curved spacetime, but it may also constitute a very interesting particle physics "laboratory" complementary to high-energy particle colliders. In [190, 191], in particular, it was shown that the existence of new particles beyond the TeV scale, predicted in several extensions of the Standard Model (SM) of particle physics, could significantly speed up a PBH's evaporation in its final fractions of a second when its Hawking temperature goes beyond the electroweak scale.

Since Hawking emission is a purely gravitational process, PBH evaporation depends only on the total number of particles with mass below the Hawking temperature, so this could yield at most limited information about the type of new particles involved, making it difficult to distinguish between different beyond the SM scenarios.

In this chapter, we take an important step further and show that a lot more information can be extracted from PBH evaporation if one can track not only the rate at which it loses mass but also the evolution of its spin parameter $\tilde{a} = JM_P^2/M^2$, where J denotes the PBH angular momentum ($0 \leq \tilde{a} < 1$).

10.1 BSM physics and Hawking evaporation

If a PBH can only emit the SM particle content, it will quickly spin down as it evaporates, since the majority of known particles have spin and thus carry away the PBH's angular momentum, as assumed in numerous studies (i.e. [246, 282–288]). Only scalar particles can be emitted as spherical waves ($l = 0$), as shown by Chambers, Hiscock, and Taylor [90–92] more than two decades ago. This is, in fact, the dominant scalar emission mode at low BH spin, such that each scalar quantum emitted reduces the BH mass but conserves J, therefore increasing $\tilde{a}$ and the BH's angular velocity, Ω_H.

While in the SM only Higgs doublet and pion emission can spin up a PBH, which is overwhelmed by quark, lepton and gauge boson emission, this picture

changes considerably in the context of string theory, the most promising framework for a quantum description of gravity alongside the other fundamental interactions. As argued in [181], string theory compactifications incorporating the Peccei-Quinn solution to the strong CP problem typically predict not just one but hundreds or even thousands of light axions. These scalar fields are the four-dimensional manifestation of the higher-dimensional gauge fields appearing in the closed and open string spectrum and of the intricate geometry of the six compact dimensions. Their mass is generated only by non-perturbative effects so they are typically very light.

In chapter 6 and [11], we have shown that the existence of $N_a \gtrsim 100$ axions lighter than a few MeV (the initial temperature of PBHs born with $M \sim 10^{12}$ kg) completely changes the evolution of the PBH spin so that even PBHs born with $\tilde{a} \lesssim 0.01$ in the radiation-dominated epoch [196, 197] can reach $\tilde{a} > 0.1$ throughout their evolution. In fact, for $N_a \gtrsim 400$ light axion emission dominates the evaporation process and the PBH spin tends to a constant value ($\tilde{a} = 0.555$ for $N_a \to \infty$ as found in [90–92]). This offers not only an opportunity to probe the *string axiverse* itself by measuring the present mass and spin distribution of PBH remnants but also, as we will now show, a novel way to probe particle physics beyond the TeV scale (see also i.e. [93, 94, 212, 252–255, 289–291] for some recent studies of the effect of spin on PBH evaporation).

The evolution of a PBH's mass and spin is determined by the dimensionless mass and angular momentum loss rates $\mathcal{F}(\tilde{a}) \equiv -(M^3/M_P^4)(\dot{M}/M)$ and $\mathcal{G}(\tilde{a}) \equiv -(M^3/M_P^4)(\dot{J}/J)$, which are given by [87–89] and defined in Eq. (5.45). As discussed in chapter 5, in our analysis [1], we include a massless graviton (assumed to be the only spin-2 particle), the SM degrees of freedom as T_H crosses the corresponding mass thresholds, an arbitrary number N_a of light axions and new particles at one or multiple mass thresholds above the electroweak scale. For the QCD degrees of freedom, we include pions for $m_\pi < T_H < \Lambda_{QCD}$ and free quarks and gluons according to the constituent masses given in [101,113–121] (the uncertainty in the exact values of the latter having no significant impact on our results). We consider new particles of spin $s = 0,\ 1/2$ and 1 typical of most SM extensions, as well as possibly a spin-

[1] Our computations were done using Mathematica and include field modes up to $l = 4$ ($l = 7/2$) for bosons (fermions), which is sufficiently accurate for our purposes. We have checked that our results for the loss functions agree with those obtained in [87–92].

3/2 gravitino arising in scenarios with spontaneously broken supersymmetry (SUSY), which is natural in the context of string compactifications. We note that in this framework spin-3/2 excitations of quarks and leptons may also be light enough to be relevant to our calculation [2] [292]. In practice we compute the contribution of generic massless spin-s particles to $\mathcal{F}$ and $\mathcal{G}$, specifying the particle content at each value of T_H by the number of real scalars n_0, the number of Weyl fermions $n_{1/2}$, the number of vector bosons n_1 and the number of gravitino-like particles $n_{3/2}$. For instance, the full axiverse-SM content at $T_H \simeq 200$ GeV corresponds to $(n_0, n_{1/2}, n_1, n_{3/2}) = (4 + N_a, 45, 12, 0)$.
The PBH evolution in the Regge plane can then be obtained according to (5.49) and (5.50) by integrating:

$$\frac{d\log\tilde{a}}{d\log M} = \frac{\mathcal{G} - 2\mathcal{F}}{\mathcal{F}} \ , \tag{10.1}$$

across the different particle mass thresholds. As examples of the resulting evolution, we show in Fig. 10.1 the PBH evolution with $N_a = 400$ light axions, the SM particles, and the graviton, alongside SM extensions where all new particles have a common mass threshold at 5 TeV, namely the Minimal Supersymmetric SM (MSSM) and a hidden sector (HS) that is a copy of the SM, inspired by heterotic string scenarios with gauge group $E_8 \times E_8$. These are not to be perceived as realistic scenarios, which may include multiple mass thresholds and potentially new massless particles like hidden photons or gluons, but only as simple examples that illustrate the competing effects of new particles with $s = 0$ and $s \neq 0$.
As one can see in Fig. 10.1, the PBH spins up as a result of axion emission until its final century, when the emission of free quarks and gluons starts spinning it down once more. The spin-down rate increases above the electroweak scale, mainly due to top quark emission. The new physics only has an effect in the very last second. In the MSSM example, the new scalars (squarks, sleptons and extra Higgs doublet) nearly balance the spin-down effect of the new fermions (Higgsinos, gauginos and gravitino), and the net result is only a slightly faster decrease in $\tilde{a}$ relative to the SM case.

[2] We note that SM extensions could include new particles with spin ≥ 2, i.e. the string excitations of SM gauge bosons or Kaluza-Klein graviton modes. Their inclusion in PBH evaporation would, however, require a detailed study of Hawking emission of such particles beyond the scope of this work, so our analysis is restricted to SM extensions with only $s \leq 3/2$ below ~ 100 TeV.

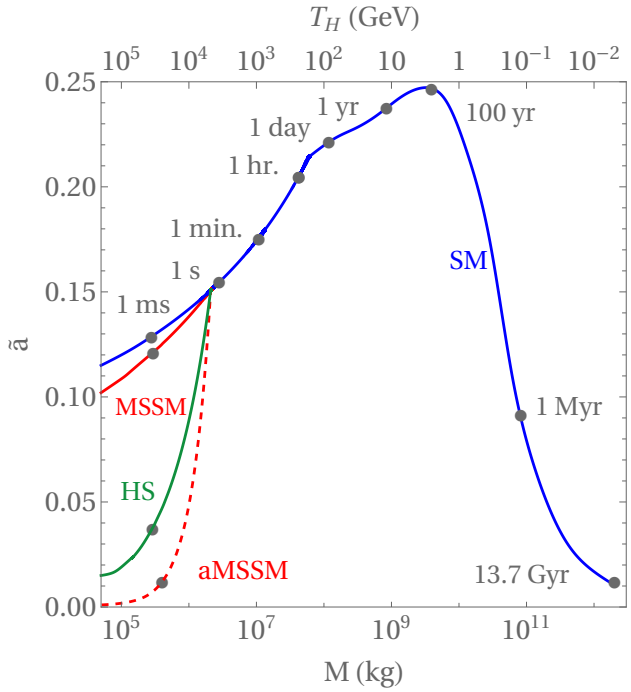

Figure 10.1: Evolution of a PBH born with $M_i = 2 \times 10^{12}$ kg and $\tilde{a}_i = 0.01$, considering $N_a = 400$ light axions and (i) the SM particles and the graviton (blue); (ii) the MSSM with $M_{SUSY} = 5$ TeV (solid red); (iii) the MSSM and axion superpartners (aMSSM) at the same SUSY breaking scale (dashed red); and a hidden sector copy of the SM (HS) also with a single mass threshold at 5 TeV (green). The labels indicate the remaining lifetime of the PBH and the upper horizontal axis gives the corresponding Hawking temperature for $\tilde{a} = 0$.

This changes drastically when one includes $N_a = 400$ TeV-scale axion superpartners, saxions ($s = 0$) and axinos ($s = 1/2$), where in particular axino emission quickly spins down the PBH. The effect is qualitatively similar for the HS scenario, albeit not so dramatic, since the number of new fermions and gauge bosons exceeds the number of new scalars.

These examples show that new physics may have a significant impact on the PBH's Regge trajectory, reflecting the competing effects of new $s = 0$ and $s \neq 0$ particles. The MSSM and HS scenarios also illustrate that SM extensions with a comparable number of new degrees of freedom, which is $\mathcal{O}(100)$ in both cases, can lead to very distinct PBH Regge trajectories. In Fig. 10.2 we plot the mass and angular momentum loss functions for these scenarios. Both

lead to sharp changes in $\mathcal{F}$ and $\mathcal{G}$ [3] that signal new particles being emitted by the PBH, but the MSSM particles lead to a sharper increase in $\mathcal{F}$, while the HS scenario has a more pronounced effect on $\mathcal{G}$.

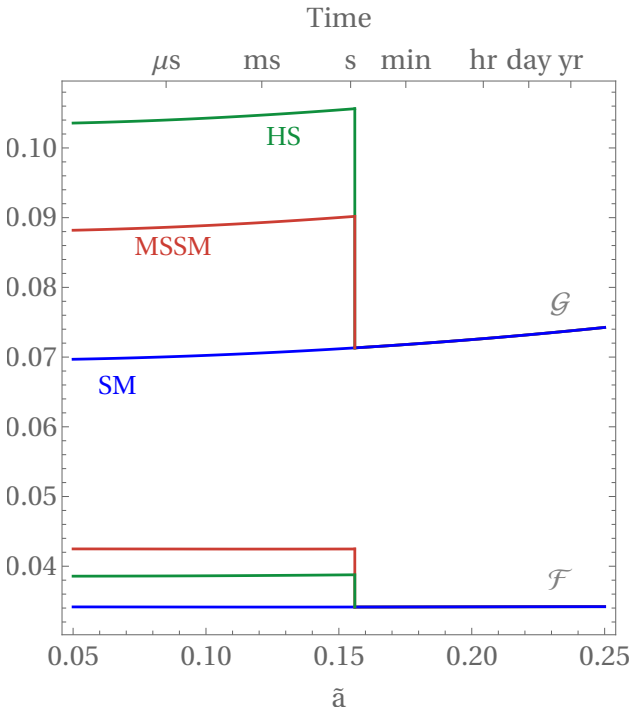

Figure 10.2: Mass and angular momentum loss functions for the SM (blue), MSSM (red), and HS scenarios (new particles with a common mass threshold of 5 TeV), considering the emission of $N_a = 400$ light axions.

The loss functions $\mathcal{F}(\tilde{a})$ and $\mathcal{G}(\tilde{a})$ may in principle be determined if one can measure a PBH's mass and spin as a function of time, as we discuss in more detail below. Accurate measurements of these functions may, in fact, provide crucial information about new physics, since they are linear in the number of particles of each spin, $\mathcal{F} = \sum_s f_s n_s$ and $\mathcal{G} = \sum_s g_s n_s$. This means that at each stage in the PBH evaporation, we may obtain two linearly independent relations between the particle numbers $(n_0, n_{1/2}, n_1, n_{3/2})$. If, in addition, one fits linear functions to the $\mathcal{F}$ and $\mathcal{G}$ data in small intervals around each value of $\tilde{a}$, we may determine their derivatives, $\mathcal{F}'(\tilde{a})$ and $\mathcal{G}'(\tilde{a})$. These would provide

[3] The loss functions should exhibit a smooth, albeit sharp, change across particle mass thresholds when the sub-leading finite mass effects are taken into account.

two further linearly independent relations between the particle numbers, thus fully determining the particle content at each point in the Regge trajectory (assuming no new particles with spin ≥ 2). This may then yield the number of particles in each spin representation with mass below the corresponding Hawking temperature.

Before the last second of a PBH's lifetime, this procedure can yield the number of light scalars in the spectrum, N_a, these being the only addition to the SM below the TeV scale that can counteract the PBH's otherwise inevitable spin down. In fact, finding even a single Kerr PBH that sustains $\tilde{a} \gtrsim 0.1$, as it evaporates, would constitute a smoking gun for a string axiverse.

We note that, in this context, the slope of the mass loss function $\mathcal{F}(\tilde{a})$ may, however, be too small to be accurately determined, as apparent in Fig. 9.15. This results from a partial cancellation between the contribution of scalar particles (namely the axions), since $\mathcal{F}'_0 < 0$ for $\tilde{a} < 0.62$, and of the remaining particles, since $\mathcal{F}'_s > 0$ for $s > 0$. In this case, a further linear relation between the particle numbers may be found from $\mathcal{G}''(\tilde{a})$, obtained i.e. by fitting the angular momentum loss function to a quadratic polynomial in $\tilde{a}$ within appropriate intervals.

10.1.1 Multi-messenger detection of evaporating PBHs

The picture just described could thus provide a powerful probe of new physics beyond the current reach of particle accelerators like the LHC, distinguishing different SM extensions. The PBH mass and spin could be determined from the photon primary Hawking emission spectrum if the distance to the PBH is known, which may be possible through parallax if it is sufficiently close to the Earth [11]. We have proposed in previous sections distance-independent methods to determine both Kerr parameters from the PBH spectrum, but these are either only applicable to large spin parameters $\tilde{a} > 0.6$ (as discussed in chapter 9 and for which the primary spectrum exhibits a multipolar peak structure) [14] or rely on the spectrum of secondary photons (those radiated by i.e. charged particles emitted by the PBH) [13]. The latter depends on whether the PBH emits new charged or unstable particles that can radiate secondary photons, so cannot be employed to probe new physics in a model-independent way.

Here we propose an alternative multi-messenger approach that relies on mea-

suring the primary emission spectra of both photons and neutrinos, requiring the simultaneous detection of an evaporating PBH with γ-ray and neutrino telescopes. These spectra are given by (5.37), as discussed in Chapter 4. We show in Fig. 10.3 examples of the photon and (single) neutrino spectra integrated over the solid angle Ω, for different values of $\tilde{a}$.

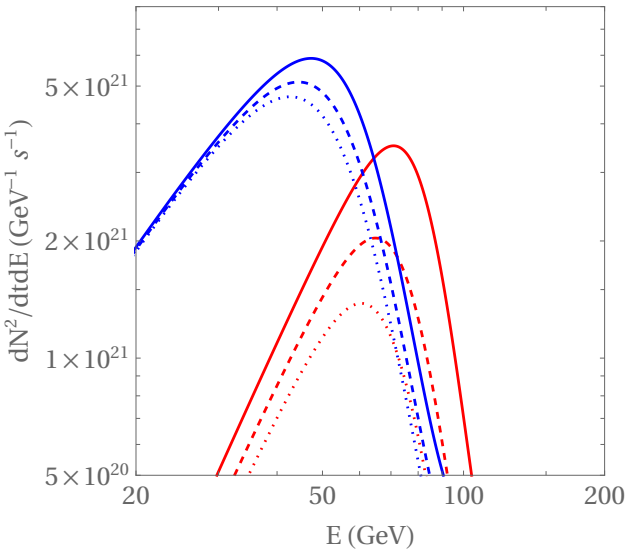

Figure 10.3: Primary photon (red) and single neutrino (blue) Hawking emission spectra for a PBH with $M = 10^9$ kg and $\tilde{a} = 0$ (dotted), $\tilde{a} = 0.2$ (dashed) and $\tilde{a} = 0.5$ (solid).

As one can see in this figure, the photon and neutrino emission peaks occur at different energies with distinct emission rates, which depend on the PBH spin. We also find that both peak energies $E_{\gamma,\nu} \propto T_H \propto M^{-1}$, while the maximum emission rates $I_{\gamma,\nu} = d\dot{N}_{\gamma,\nu}/dE(E_{\gamma,\nu})$ are independent of the PBH mass. This means that the ratios between these quantities for neutrinos and photons depend only on $\tilde{a}$, and numerically are well fitted by:

$$\frac{E_\nu}{E_\gamma} = 0.705 - \frac{0.559\tilde{a}^2}{1+5.18\tilde{a}}\,, \quad \frac{I_\nu}{I_\gamma} = 3.423 - \frac{31.05\tilde{a}^2}{1+7.05\tilde{a}}\,. \tag{10.2}$$

These ratios thus yield two independent ways of determining $\tilde{a}$, while the mass M can then be determined from the energies E_γ and E_ν. The ratio E_ν/E_γ only varies by $\sim 5\%$ for $0 < \tilde{a} < 0.5$, so that sub-percent energy resolution would be required to determine the PBH spin with $\Delta\tilde{a} \lesssim 0.1$ uncertainty,

beyond the capabilities of current technology. Fortunately, the ratio I_ν/I_γ is much more sensitive, so that measuring it with $\mathcal{O}(10\%)$ uncertainty would yield $\Delta\tilde{a} \lesssim 10^{-2}$, which would be required to probe scenarios like the MSSM example in Fig. 10.1.

We must, however, take into account the effects of anisotropic emission, since the measured fluxes depend on the unknown inclination of the PBH axis relative to our line of sight, θ, according to Eq. (5.36). For $0 < \tilde{a} \lesssim 0.5$ both the neutrino and photon spectra are dominated by the lowest $l = m = |s|$ modes and therefore the corresponding peak emission rates are θ-dependent. As proposed in [107], one may determine θ by measuring the asymmetry between the neutrino and anti-neutrino fluxes (the difference between the two terms in Eq. (5.36)) or the analogous photon polarization asymmetry (although current techniques for measuring photon polarization may be difficult to extend to high-energy γ-rays). We refer the reader to the discussion in [107] for further details.

An alternative way to measure the PBH inclination would be to use its proper motion since θ will vary if the PBH is sufficiently close to the Earth, and the corresponding signal modulation may then be used to infer the integrated I_ν/I_γ. In fact, one should note that axion emission greatly reduces a PBH's lifetime, so that PBHs presently in their final stages should have been born with a larger mass (and were hence colder) than assuming only SM particle emission, as in the example of Fig. 10.1 where the initial mass is 2×10^{12} kg. This means that they would have contributed significantly less to the extragalactic γ-ray background than in the standard scenario. We, therefore, expect that, in the string axiverse, such PBHs may be $\mathcal{O}(10 - 100)$ times more abundant than in the SM, i.e. that up to a few exploding PBHs may cross the Solar System within the typical lifetime of a detector.

Our proposal to determine a PBH's mass and spin does not require specially dedicated technology, since high-energy γ-ray and neutrino astronomy has a broad range of scientific goals that will surely motivate future improvements in sensitivity, energy and angular resolution of existing experiments like HAWC, Fermi-LAT, LHAASO [293–295] or IceCube. Several neutrino experiments like KM3Net [296], P-ONE [297], Trident [298] and Baikal-GVD [299] have already been proposed, alongside γ-ray telescopes with energy range beyond the TeV scale like CTA [300–302] and SWGO [303, 304] currently under development. We note that primary photons/neutrinos are more challenging to detect than

their secondary counterparts (not shown in Fig. 10.3 for clarity), which are more numerous albeit less energetic. To give an idea of the sensitivity required, peak primary emission for a PBH at a distance of 10^{-3} pc corresponds to an energy flux $\sim 10^{-7}(M/10^9 \text{ kg})^{-2}$ GeVs^{-1}cm^{-2}.

This work illustrates the enormous potential of multi-messenger astronomy to unveil new physics by accurately tracking Kerr PBH evaporation that we hope may further boost technological developments in this field. Even though at this stage we can only speculate about their existence, finding even just one of these compact objects in its last stages would allow us to probe fundamental aspects of an underlying string theory, from the expected large number of light scalars to new particles beyond the TeV scale, with PBH spin playing a key role.

11 Probing the metric structure using the Hawking emission

We study a regular rotating black hole evaporating under the Hawking emission of a single scalar field. The black hole is described by the Kerr-black-bounce metric with a nearly extremal regularizing parameter $\ell = 0.99 r_+$. We compare the results with a Kerr black hole evaporating under the same conditions. Firstly, we compute the gray-body factors and show that the Kerr-black-bounce evolves towards a non-Schwartzchild-like asymptotic state with $\tilde{a} \sim 0.47$, differently from a Kerr black hole whose asymptotic spin would be $\tilde{a} \sim 0.555$. We show that this result depends on the combined contributions of the changes in the gray-body factors and in the surface gravity introduced by the regularizing parameter. We also discuss how the surface gravity affects the temperature and the primary emissivity and decreases those quantities with respect to the Kerr black hole. Consequently, the regular black hole has a longer lifetime. Finally, we briefly comment on the possibility of investigating the beyond-the-horizon structure of a black hole by exploiting its Hawking emission. This chapter is based on [16].

11.1 Introduction

General Relativity (GR) has been tested for more than one century providing outstanding results in describing the Solar System and the Universe. Despite GR's successes, its lack in addressing many open problems remains and propels the idea that it may not be the ultimate theory of gravity. The origin of the cosmic acceleration and the nature of the dark contents of the Universe have been extensively studied using modified theories of gravity [305]. In recent years, the detection of Gravitational Waves (GW) from BH coalescence [3] by

the LIGO/Virgo Collaboration and the direct observation of the BH shadows at the center of the Milky Way [10] and M87 [4] by the Event Horizon Telescope (EHT) provided a new test bench capable of probing GR robustness in a strong-field regime [306–309]. The existence of singularities, namely portions of spacetime with an infinite curvature, is a hint that the classical framework of GR should break down or, at least, be incomplete at high energies. It is a commonly accepted idea that singularities just reveal our lack of knowledge in the high energy regime and the related problem may be cured by a quantum theory of gravity. Unfortunately, a theory of quantum gravity has not been yet developed despite the several proposals. Nevertheless, it is still possible to gain intuition by postulating the existence of regularized spacetimes inspired by quantum gravity arguments and studying whether these new metrics give rise to new signatures or modify preexisting characteristics. Since the 90s these motivations have led the research of regularized metrics mimicking the behavior of BH solutions [310]. Furthermore, in light of the new available high-energy regime tests, the field gained even more traction, and many studies about quasi-normal modes, superradiant regimes, and instabilities are regularly announced [311–327].

An interesting regular metric was proposed in [328] and further analyzed in [329]. This spacetime configuration, known as black-bounce, interpolates between the standard and regularized Schwarzschild BH and the Morris-Thorne traversable wormhole by introducing an additional parameter, ℓ. The black-bounce metric caused a fervent activity leading to many studies of its characteristics [330–337] and was recently extended in order to account for rotation [309, 338], and afterward rotation and charge [339]. The Kerr-black-bounce and Kerr-Newman-black-bounce have also been the subject of many studies [309, 340–345].

The main motivation of this part of my work is to further enlarge the analysis of the Kerr-black-bounce characteristics by considering its dynamical evolution due to Hawking evaporation driven by a single scalar field. Such characteristics are certainly irrelevant for BHs of the size we measure today but may become a powerful and handy tool in light of the possible future measurement of primordial BHs.

The lesson of this study is that under the same conditions, a Kerr-black-bounce is characterized by a dynamic behavior that differs from its singular counterpart. This work points out that tracking the evolution of a black hole spin and

its spectrum will provide information on the spacetime structure.
This chapter is organized as follows. Section 11.2 contains a brief review of the Kerr-black-bounce. Section 11.3 shows the equation governing the scalar perturbation of the Kerr-black-bounce metric, the evolution of the metric under a single scalar emission, and the numerical method used for calculating the Gray-Body Factors (GBFs). In section 11.4 the results are presented. Section 11.5 provides a summary in which future perspectives are considered.

11.2 Kerr-black-bounce metric

In this section, we briefly review the Kerr-black bounce metric [338]:

$$\begin{aligned} ds^2 = &- \left(1 - \frac{2M\sqrt{\tilde{r}^2+\ell^2}}{\Sigma}\right) dt^2 + \frac{\Sigma}{\Delta} d\tilde{r}^2 + \Sigma d\theta^2 \\ &+ \frac{A\sin^2\theta}{\Sigma} d\phi^2 - \frac{4Ma\sqrt{\tilde{r}^2+\ell^2}\sin^2\theta}{\Sigma} dt d\phi, \end{aligned} \tag{11.1}$$

where M, a, and ℓ are the parameters describing mass, spin, and the regularizing parameter of the metric, while

$$\begin{aligned} \Sigma &= \tilde{r}^2 + \ell^2 + a^2\cos^2\theta, \\ \Delta &= \tilde{r}^2 + \ell^2 + a^2 - 2M\sqrt{\tilde{r}^2\ell^2}, \\ A &= (\tilde{r}^2 + \ell^2 + a^2)^2 - \Delta a^2 \sin^2\theta. \end{aligned} \tag{11.2}$$

This is a generalization of the static and spherically symmetric metric proposed by Simpson and Visser [328, 329, 346]. It is a stationary, axially symmetric metric which, by introducing a positive parameter, $a < M$, describes the angular momentum of the black-bounce. This line element was recently further extended in order to describe a charged spacetime [339].
When the positive regularizing parameter $\ell \to 0$, the Kerr-black-bounce metric reduces to the singular Kerr solution, while for $\ell \neq 0$ the spacetime is regular and possesses a wormhole throat at $\tilde{r} = 0$. A coordinate singularity interpreted as an event horizon is present when $\Delta = 0$, or, equivalently, when

$$\tilde{r}_\pm = \sqrt{r_\pm^2 - \ell^2}, \tag{11.3}$$

where $r_\pm = M \pm \sqrt{M^2 - a^2}$.
Depending on the values of the regularizing parameter ℓ, the metric (11.1) describes a wormhole for $\ell > r_+$, for which no coordinate singularities are present on the manifold. If $\ell < r_+$ the metric (11.1) describes a BH which may have one or two coordinate singularities depending on $r_- < \ell < r_+$ or $\ell < r_-$, respectively. Finally, when $\ell = r_+$ the throat and the event horizon coincide.
To better visualize this interplay, it is convenient to define a new radial coordinate $r = \sqrt{\tilde{r}^2 + \ell^2}$ and pass from an extrinsic description of the manifold to an intrinsic one. It is easy to notice that $r \neq 0$ for all $\ell \neq 0$. In particular, the minimum value of r corresponds to the minimal radius of the throat. The coordinate r measures the areal radius. Given this new coordinate, the metric reads

$$\begin{aligned} ds^2 = &- \left(1 - \frac{2Mr^2}{\Sigma}\right) dt^2 + \frac{\Sigma}{\delta \Delta} dr^2 \\ &+ \Sigma d\theta^2 + \frac{A \sin^2\theta}{\Sigma} d\phi^2 - \frac{4Mar \sin^2\theta}{\Sigma} dt d\phi, \end{aligned} \tag{11.4}$$

and

$$\begin{aligned} \Sigma &= r^2 + a^2 \cos^2\theta, \\ \Delta &= r^2 + a^2 - 2Mr, \\ A &= (r^2 + a^2)^2 - \Delta a^2 \sin^2\theta, \\ \delta &= 1 - \frac{\ell^2}{r^2}. \end{aligned} \tag{11.5}$$

If $\ell \neq 0$, the curvature singularity at $r = 0$ is always prevented by the wormhole throat. When $\ell > r_+$ the wormhole throat is located at a larger radial value than the coordinate singularity of the event horizon. In this way, the presence of the horizon is prevented by the regular finite surface of the wormhole throat. If $0 \neq \ell < r_+$, the throat of the wormhole is enclosed by the event horizon and the metric describes a BH.
In the following part of this chapter, we focus on regular BHs avoiding coordinates singularities and inner horizons. The absence of the inner horizon is a desirable feature since it might avoid the problems related to mass inflation. Moreover, this choice allows a nearly maximal value of ℓ for which the metric (11.1) mostly differs from the Kerr BH and still describes a BH.
It has to be noticed that the metric (11.1) or, equivalently, (11.4), is inspired by

the reasonable quantum gravity argument of avoiding singularities and other pathology, and it is not a vacuum solution of GR.

11.3 Scalar perturbations and evolution

In this section, we derive the equation describing the scalar massless perturbations of the metric (11.1) and discuss the appropriate boundary conditions. The massless Klein-Gordon equation $\nabla^\mu \nabla_\mu \Phi = 0$ in curved spacetime reads

$$\frac{1}{\sqrt{-g}} \partial_\mu (\sqrt{-g} g^{\mu\nu} \partial_\nu) \Phi = 0. \tag{11.6}$$

Taking into account the decomposition $\Phi = R_{lm}(r) S_{lm}(\theta) e^{im\phi} e^{-i\omega t}$ where ω is the perturbation frequency, m is the azimutal quantum number, (11.6) separates into an angular equation

$$\frac{1}{\sin\theta} \frac{d}{d\theta} \left(\sin\theta \frac{d}{d\theta} S_{lm} \right) + \left(a^2 \omega^2 \cos^2\theta + A_{lm} - \frac{m^2}{\sin^2\theta} \right) S_{lm} = 0 \tag{11.7}$$

describing the spheroidal harmonics equation where A_{lm} are its eigenvalues, and a radial equation

$$\sqrt{\delta} \frac{d}{dr} \left(\sqrt{\delta} \Delta \frac{dR_{lm}}{dr} \right) + \left(\frac{K^2}{\Delta} + 2am\omega - a^2\omega^2 - A_{lm} \right) R_{lm} = 0, \tag{11.8}$$

where $K = (r^2 + a^2)\omega - am$.
The angular equation (11.7) is the spin-less case of the well-studied spin-weighted spheroidal harmonics equation [65, 67, 68]. To leading order $A_{lm} = -l(l+1) + \mathcal{O}(a\omega)$ and the $\mathcal{O}(a\omega)$ correction can be expressed as a power series in $a\omega \ll 1$, which is given in [68] and reported in (4.42). Besides, for our purposes, it is worth studying the radial equation (11.8) in two limits, near the horizon, and at spatial infinity. If the regularizing parameter satisfies $\ell < r_+$ and the Kerr-black bounce metric (11.1) describes a regular BH, then

the near-horizon solution reads [340],

$$\begin{aligned} R(r) &\sim (r-r_+)^{\pm i\sigma}, \\ \sigma &= \frac{am - 2M\omega r_+}{\gamma(r_+ - r_-)}, \\ \gamma &= \sqrt{1 - \frac{\ell^2}{r_+^2}}, \end{aligned} \tag{11.9}$$

while the far-away solution simply reads

$$R(r) \sim \frac{1}{r} e^{\pm i\omega r}. \tag{11.10}$$

To study a BH described by (11.1), evolving by the sole emission of scalar particles due to Hawking radiation, it is necessary to set up a scattering-like problem and take into account in-going and out-going boundary conditions at infinity, while at the event horizon, one must consider pure absorption. These asymptotic solutions and the conservation of energy fluxes, both at the horizon and at infinity, allow one to calculate the gray-body factor or transmission coefficients, defined as

$$T = \frac{dE_{hole}/dt}{dE_{in}/dt}. \tag{11.11}$$

We decided here to denote the gray-body factors with the letter T in order to underline their difference with respect to the previously computed ones. Nonetheless, they express the same concept of transmission coefficient filtering an otherwise black-body radiation and for $\ell \to 0$ it is valid $T \to \Gamma$. The gray-body factors depend on the modes, and, at a constant ℓ, are functions of both the BH spin parameter and frequency of the perturbation, $T = {}_\ell T^l_m(a, \omega)$. The gray-body factors emerge as a consequence of a geometrical potential in equation (11.8) which, acting as a barrier, partially shields the Hawking radiation from being totally emitted. This way the radiation emerging from the BH is not the one of a black body. The field quanta have energy and spin and their emission comes at the expense of both the BH mass and angular momentum. Following the path outlined in [88], the Kerr Black Bounce rates of mass and angular momentum loss are called f and g, respectively, and they read

$$\begin{pmatrix} f_0 \\ g_0 \end{pmatrix} = \sum_{i,l,m} \frac{1}{2\pi} \int_0^\infty dx \frac{{}_\ell T_{i,l,m}}{e^{2\pi k/\kappa} - 1} \begin{pmatrix} x \\ m\tilde{a}^{-1} \end{pmatrix}, \tag{11.12}$$

where the sum is taken over all particle species i, and l, m are the usual angular momentum quantum numbers. Here $x = \omega M$, $k = \omega - m\Omega$ and

$$\kappa = \sqrt{\frac{\tilde{r}_+^2}{\tilde{r}_+^2 + \ell^2}}\sqrt{1-\tilde{a}^2}/2r_+ \tag{11.13}$$

is the surface gravity of the BH [310, 339]. Since the choice of analyzing a singular Kerr BH $\ell = 0$ and the regular Kerr-black-bounce BH having $\ell = 0.99r_+$, the pre-factor $\sqrt{\tilde{r}_+^2/(\tilde{r}_+^2 + \ell^2)}$ takes just two values accordingly. To determine whether a BH spins up or down during its evolution it is necessary to calculate the mass to angular momentum loss rates as defined in 5.5

$$h_0 = \frac{g_0}{f_0} - 2. \tag{11.14}$$

A root of the function h, $\tilde{a}_*$, for which $h'(\tilde{a}_*) > 0$, represents a stable state towards which the BH evolves while evaporating. To investigate the time evolution of angular momentum and mass we followed the path outlined in section 5.5 and in [87–92] defining

$$y = -\ln a, \quad z = -\ln M/M_i, \quad \tau = -M_i^{-3}t, \tag{11.15}$$

where M_i is the initial mass of the BH. The evolution is then fully determined by the differential equations

$$\frac{d}{dy}z = \frac{1}{h}, \qquad \frac{d}{dy}\tau = \frac{e^{-3z(y)}}{hf}, \tag{11.16}$$

and the initial conditions $z(t = 0) = 0$ and $\tau(t = 0) = 0$. To estimate the primary spectrum of scalar particles we used the well-known formula (5.36) [11, 87, 88, 101, 113–121]:

$$\frac{d^2N}{dtdE} = \frac{1}{2\pi}\sum_{l,m}\frac{T_{l,m}(\omega)}{e^{2\pi k/\kappa} - 1}\ . \tag{11.17}$$

11.3.1 Numerical method

An explicit analytical calculation of the gray-body factors is possible only under stringent approximations and numerical methods are usually required to evaluate them. We implemented a code based on the so-called shooting method

which has been applied to solve similar problems, for example in [70, 82], and allows for the calculation of the gray-body factors with good accuracy.
The first step is to rewrite Eq.(11.8) in terms of the re-scaled coordinate

$$x = \frac{r - r_+}{r_+}, \tag{11.18}$$

such that:

$$\begin{aligned} &\delta x^2 (x+\tau)^2 \partial_x^2 R(x) \\ &+ 2x(x+\tau)\left(\frac{1}{2}(2x + \tau\delta + \frac{x(x+\tau)}{x+1}(1-\delta))\right)\partial_x R(x) \\ &+ V(\omega, x) R(x) = 0, \end{aligned} \tag{11.19}$$

where

$$V(\omega, x) = \mathcal{K}^2 - x(x+\tau)(A_{lm} + a^2\omega^2 - 2am\omega), \tag{11.20}$$

with $\tau = (r_+ - r_-)/r_+$, $\mathcal{K} = \varpi + x(x+2)\bar{\omega}$, $\varpi = (2-\tau)(\bar{\omega} - m\bar{\Omega}_+)$, where $\bar{\omega} = r_+\omega$, $\bar{\Omega}_+ = r_+\Omega_+$ and $\Omega_+ = a/2Mr_+$.
Setting purely in-going boundary conditions near the horizon, the solutions of Eq. (4.56) can be expressed in the form of the Taylor expansion [70, 82] of the form

$$R(x) = x^{-i\varpi/(\gamma\tau)} \sum_{n=0}^{\infty} a_n x^n. \tag{11.21}$$

The coefficients a_n can be determined by substituting (11.21) in (4.56) and solving iteratively the algebraic equations.
The near horizon solution is used to set the boundary conditions and numerically integrate the radial equation up to large distances, where the general form of the solution takes the form:

$$R(x) \to \frac{Y_{in}^{lm}}{r_+}\frac{e^{-i\bar{\omega}x}}{x} + \frac{Y_{out}^{lm}}{r_+}\frac{e^{i\bar{\omega}x}}{x}. \tag{11.22}$$

It is then possible to extract the coefficient $Y_{in}^{lm}(\omega)$ in order to evaluate the gray-body factor. The normalization of the scattering problem is set by requiring $a_0 = 1$, this way gray-body factors read

$$T^{lm}(\omega) = \frac{\varpi}{\bar{\omega}} |Y_{in}^{lm}(\omega)|^{-2}. \tag{11.23}$$

With this method, we computed the gray-body factors of a scalar perturbation on a regular BH described by the Kerr-black-bounce metric having a nearly extremal regularizing parameter ($\ell = 0.99 r_+$). Different values for the spin parameter of the BH spanning from $\tilde{a} = 0$ to $\tilde{a} = 0.99$ are considered and the gray-body factors are calculated up to $l = 4$.

11.4 Results

Let us compare the scalar perturbations of the Kerr BH and the ones of the nearly extremal Kerr-black-bounce BH.

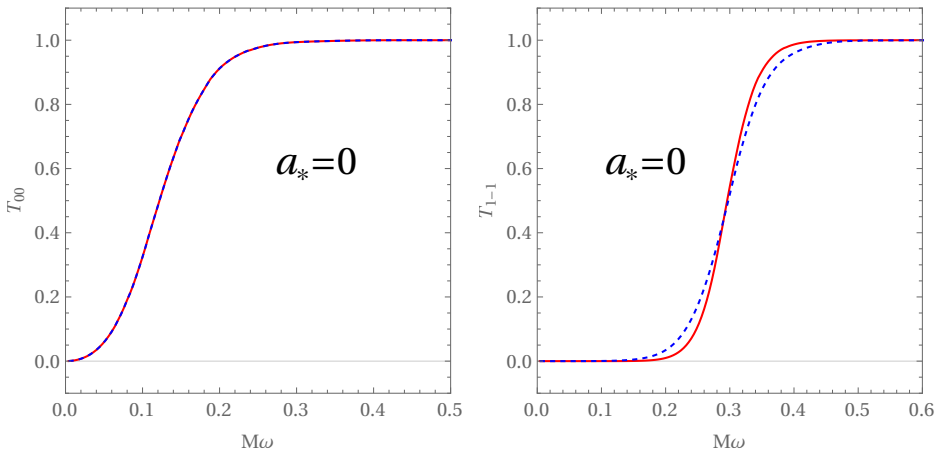

(a) (b)

Figure 11.1: (a) gray-body factors of the mode $l = m = 0$ of a BH rotating at $\tilde{a} = 0$ in the case $\ell = 0.99 r_+$ (solid red line) and $\ell = 0$ (blue dashed line). (b) gray-body factors of the mode $l = 1$, $m = -1$ of a BH rotating at $\tilde{a} = 0.99$ in the case $\ell = 0.99 r_+$ (solid red line) and $\ell = 0$ (blue dashed line).

These BHs share many characteristics such as the presence of a superradiant regime and a non-null asymptotic value of the spin parameter $\tilde{a}$. Nevertheless, for the two different metrics, the phenomenology changes and it is of great interest to analyze those differences.

The gray-body factors of the modes $l = m = 0$ are identical (as shown in Fig. 11.1 (a) for the non-rotating cases) and this equality is independent of the BH spin considered. The gray-body factors of the Kerr-black-bounce BH show a common behavior for the modes with $l \neq 0$. When they are compared with the Kerr BH ones, they grow faster for frequencies lower than the main

gray-body factors inflection point, on the contrary, they grow slower for higher frequencies (as shown in Fig. 11.1 (b) for the $l = 1$, $m = -1$ mode). Also, this behavior is independent of the spin of the BH.

The scalar perturbation of both metrics shows superradiant amplification if $\omega < m\Omega$. When this condition is met, both the gray-body factors have negative values, which are interpreted as wave amplification. Fig. 11.2 displays the comparison of the gray-body factors for the $l = m = 1$ modes at $\tilde{a} = 0.99$ highlighting the superradiant regime.

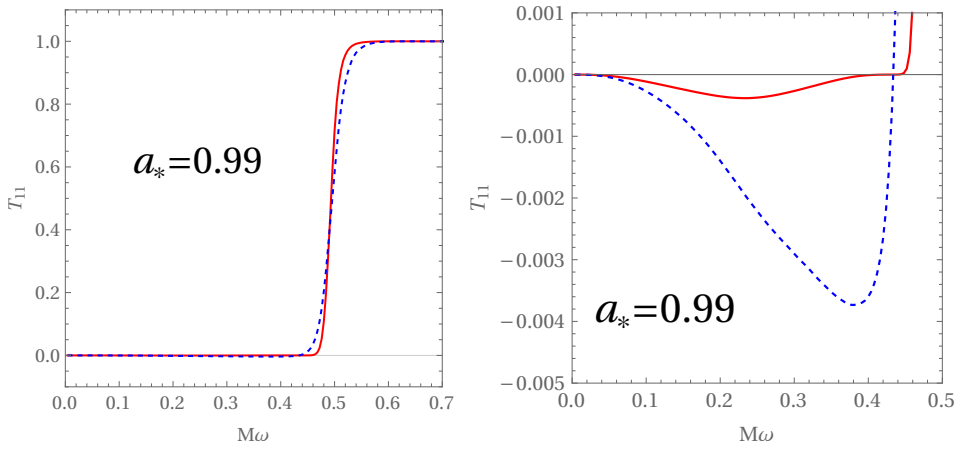

Figure 11.2: (a) Transmission coefficients of the mode $l = m = 1$ of a BH rotating at $\tilde{a} = 0.99$ in the case $\ell = 0.99r_+$ (solid red line) and $\ell = 0$ (blue dashed line). (b) Zoom of the superradiant regime of (a).

The Kerr-black-bounce gray-body factors show a less intense amplification and the shape of the superradiant regime peaks at lower frequencies. Also, the shape of the gray-body factors in the superradiant regime is different, being more symmetric than in the singular case. This result agrees with the tendency shown in the recent paper [340], which reports that increasing the parameter ℓ causes a decrease in the superradiant amplification factor. These are common features of all the superradiant modes. However, it has to be noticed that with an increasing azimuthal quantum number, the superradiant peak of the Kerr-black-bounce BH gray-body factors becomes smaller and smaller with respect to its singular counterpart.

The functions f and g are calculated through Eq. (11.12). The two BHs show

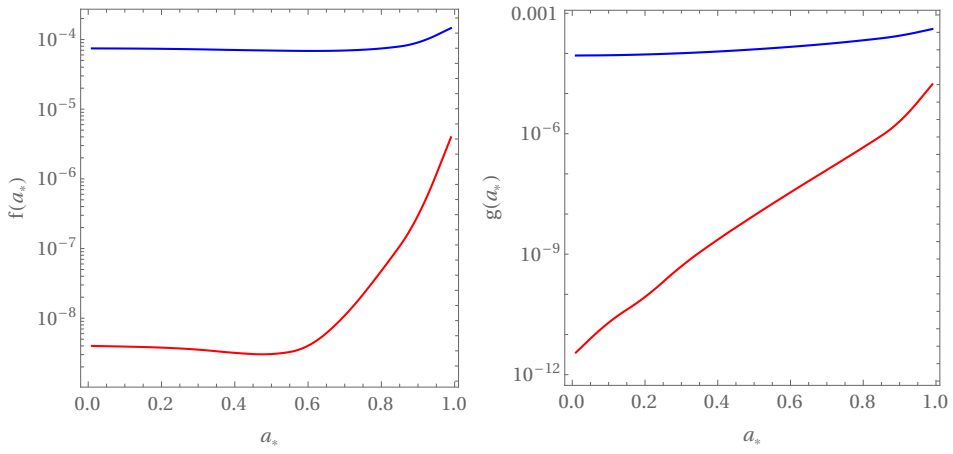

(a) (b)

Figure 11.3: Plot of functions f (a) and g (b) for different values of the BH spin parameter $\tilde{a}$. In the solid blue line is the Kerr BH, and in solid red the Kerr-black bounce

different values of these functions. These are due to the above-mentioned gray-body factor differences and in the different surface gravity (11.13), which plays a crucial role in the Bose-Einstein statistical factor in (11.12) selecting lower frequency if $\ell \neq 0$. For these reasons, the Kerr-black-bounce BH functions f and g for $\ell = 0.99 r_+$ are orders of magnitude smaller if compared with the singular case. Fig. 11.3 reports a comparison of those two cases.

For the same reasons, the functions h are also different. Fig.11.4 shows that the root of the Kerr BH is located at $\tilde{a}_* = 0.555$, while the one of the Kerr-black-bounce is at $\tilde{a}_* = 0.47$.

If the natal spin of both BHs is smaller than the respective root of h, the dominant emission mode is $l = 0$. In this case, the evaporation due to a single scalar field will cause both BHs to lose mass faster than angular momentum. As a result, the evaporating BH will increase its value of $\tilde{a}$ up to the respective asymptotic value $\tilde{a}_*$. Conversely, the evolution of highly spinning BHs is dominated by higher l modes decreasing the angular momentum of the BH and driving it toward its asymptotic values.

It is possible to speculate that the similar asymptotic value is due to the common origin of the gain/loss of dimensionless angular parameter. In fact, of the whole scalar modes emitted, $l = m = 0$ solely does not subtract angular momentum and as reported in Fig.11.1 the transmission coefficients for the two

analyzed BHs are the same for this mode. The differences are then related to the differences in the subdominant $l > 0$ transmission coefficients. The dependence of the asymptotic BH spin value on the regularizing parameter is mild but present since a variation in the regularizing parameter incurs variations in the $l > 0$ gray-body factors.

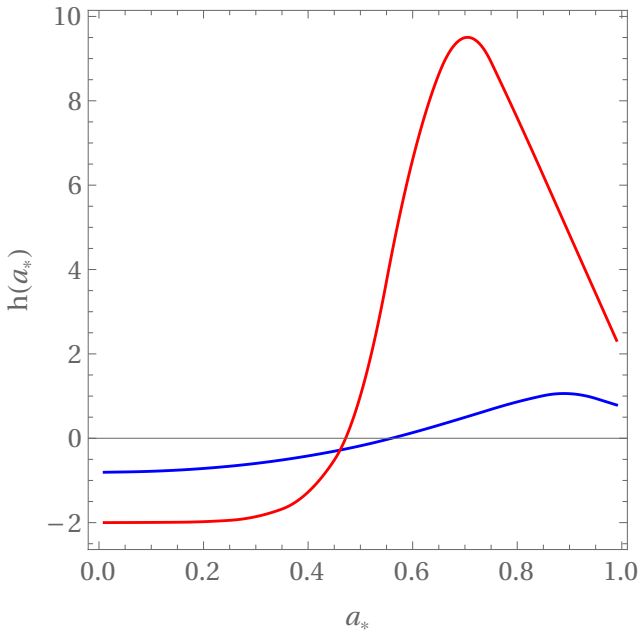

Figure 11.4: Plot of functions $h = g/f - 2$ at different values of the BH spin parameter $\tilde{a}$. In the solid blue line is the Kerr BH, and in solid red the Kerr-black bounce.

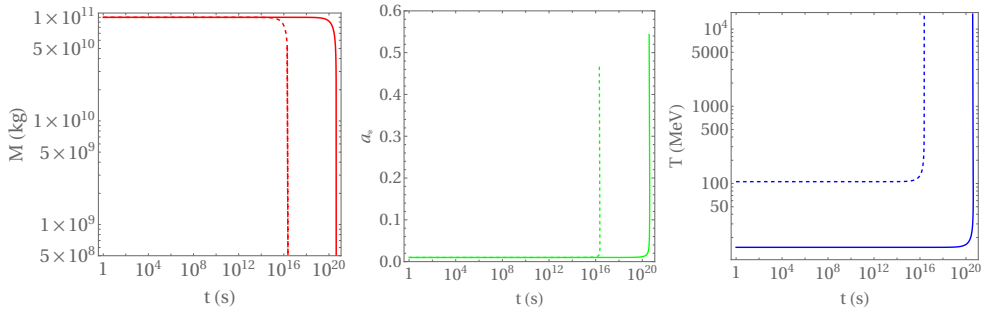

(a) (b) (c)

Figure 11.5: Plot of the mass (a), spin (b), and temperature (c) as functions of the time, of a Kerr-black bounce having $\ell = 0.99 r_+$ (solid lines) and a Kerr-black hole (dotted lines) of the same initial mass $M_K = 10^{11}$ kg, and spin parameter $a_{*iK} = 0,01$, evolving by the emission of a single type of scalar particle.

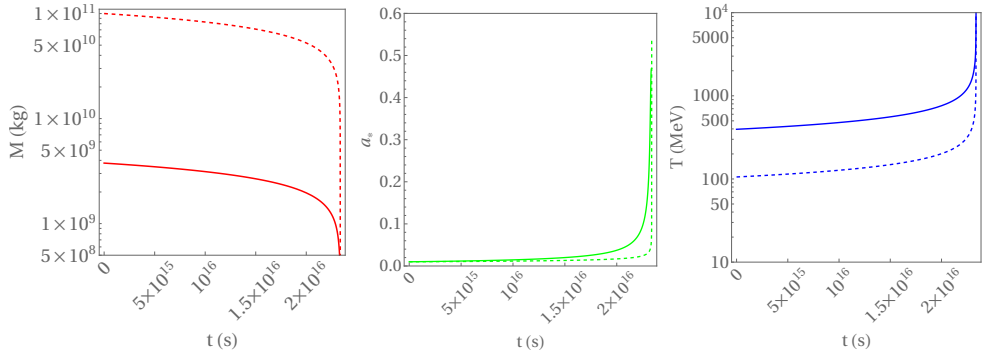

(a) (b) (c)

Figure 11.6: Plot of the mass (a), spin (b), and temperature (c) as functions of the time, of the Kerr-black bounce having $\ell = 0.99 r_+$ (solid lines) and the Kerr-black hole (dashed lines) of the same lifetime, evolving by the emission of a single type of scalar particle.

The regularizing parameter influencing the surface gravity plays a significant role in the dynamic evolution of the regular BH, which is much slower with respect to its singular counterpart. The lifetime of an isolated Kerr BH emitting only one scalar particle species and having natal mass and spin of $M_i = 10^{11}$ kg, and $a_{*i} = 0,01$, is $\sim 2.34 \times 10^{16}$ s, while a nearly extremal Kerr-black-bounce BH with the same initial conditions has a lifetime of $\sim 4.37 \times 10^{20}$ s. Fig. 11.5 reports mass, spin parameter, and temperature as a function of time

for such BHs. It is interesting to consider two BHs of the same life span and analyze their evolution. It is worth noticing that the time evolution of the spin parameters is different and the Kerr-black-bounce spin grows faster for most of the evolution as reported in Fig. 11.6.

Given its slower dynamical evolution, it is not surprising that the intensity peak of the primary emission for the regular BH is smaller than a Kerr BH with the same mass and spin. This situation is reported in Fig. 11.7 (a) where masses of $M = 3.5 \times 10^{10}$ kg and spin values of $\tilde{a} = 0, 0.9, 0.99$ are considered. This plot shows a reduction in the number of emitted scalars as well as a reduction in the energy at which they are emitted, in line with the previous comments. Finally, Fig. 11.7 (b) shows the primary emission rate for the same temperatures, namely, 301.93, 183.35, and 74.67 MeV for $\tilde{a} = 0, 0.9, 0.99$, respectively.

One may compare Fig. 11.7 with Fig. 2 of [94] which describes the primary emission of a Kerr BH for different field spins. Fig.2 of [94] highlights how the rotation in a Kerr BH reinforces the emission of $s \neq 0$ particles and decreases the emission of scalar particles. This is no longer valid for the Kerr-bounce BH. In fact its scalar particle emissivity peaks at higher values for values of the spin parameter close to extremality.

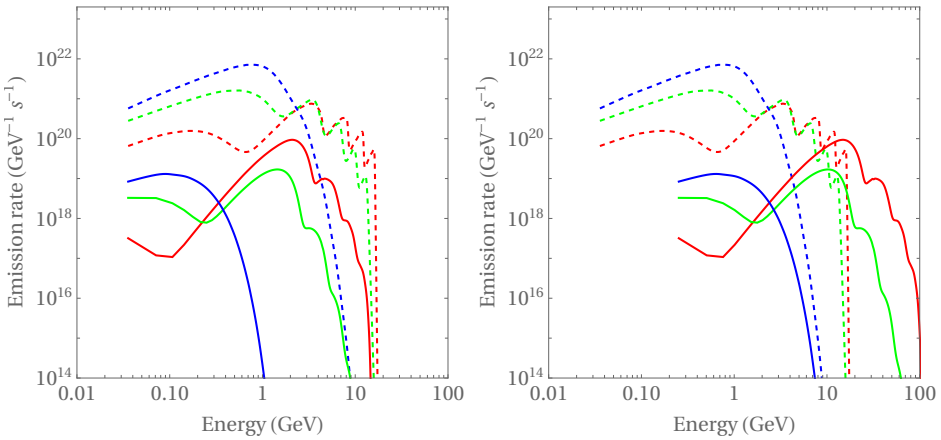

FIG. 11.7: (a) Primary emission rate for regular (solid) and singular (dashed) BHs in the case of same masses of $M = 3.5 \times 10^{10}$ kg for spin values of $\tilde{a} = 0, 0.9, 0.99$ in blue, green, and red, respectively. (b) Primary emission rate for the same BHs in the case of the same temperature, namely 301.93 MeV for $\tilde{a} = 0$ in blue, 183.35 MeV for $\tilde{a} = 0.9$ in green, and 74.67 MeV for $\tilde{a} = 0.99$ in red.

11.5 Conclusions

In this chapter, we studied the evolution, under the emission of scalar radiation via the Hawking process, of a rotating regular black hole described by the Kerr-black-bounce metric. The study is performed in the case of a nearly extremal value of the regularizing parameter ($\ell = 0.99 r_+$). The differences in the dynamics of the evaporation of such BH and a Kerr BH are outlined. Namely, the negative transmission coefficients regime, the asymptotic value of $\tilde{a}$, the emissivity, and the lifetime are discussed and compared.

The main lesson of this toy-model points towards a possible investigation of beyond-the-horizon features by analyzing the Hawking radiation. For example, by assuming a way to infer the BH mass and spin independently from the primary Hawking emission, it is possible by measuring the peak intensity to obtain an indirect measure of ℓ in the context of the Kerr-black-bounce solutions, and in general, would provide a measure of how much the BH solution differs from the Kerr one. We are more likely to observe the Hawking emission of photons than scalar particles, but, since the definition of f and g for spin-1 bosons is given by Eq. (11.12) with the appropriate gray-body factors, one can

expect that the differences between the Kerr solution and the regular one are still present. This work also suggests that tracking the time evolution of the spin parameter could provide information on the spacetime structure.
Such characteristics are certainly irrelevant for BHs of the size measured today but may become a powerful and handy tool in light of possible future PBH detection.
We leave gray-body factors calculation for spin 1/2, 1, and 2 fields and implementation of an accurate evaporation scenario for future studies.
In a standard evolution scenario, BHs clearly do not evaporate through the sole emission of a scalar field. Nevertheless, scenarios involving the conspicuous presence of scalar particles such as the string axiverse [11,181] may display similar characteristics. In fact, in the limit of many axion-like particles, the emission of scalar particles dominates the evolution which becomes similar, up to a normalization, to the single scalar case.

12 Conclusions

The contents of this PhD thesis are also discussed in the original papers [11–14,16] to which I contributed by realizing the vast majority of the calculations and plots, and are a part of my production which includes also [17–21]. Although we have already summarized the main conclusions of our results in each chapter, here we provide an overall summary of the research done for this dissertation.

Certainly, the detection of evaporating PBHs would per se be an extraordinary achievement, providing information about the early Universe and the nature of the semi-classical behavior of BHs. On top of that, our analysis shows that determining their evolution, Hawking emission spectrum and mass-spin distribution may provide unique probes of physics beyond the SM, and beyond vacuum solutions of GR. We identified different mechanisms leading to footprints of BSM Physics. The mass-spin distribution of PBHs of masses $5 \times 10^7 - 10^{12}$ kg provides information about the number of BSM light scalars. In the same range of masses, the presence of a heavy $(0.1 - 10$ GeV) scalar particle superradiantly amplified alters the very same mass-spin distribution, thus revealing a clear sign of its presence. If the heavy scalar has a decaying channel into photons it may provide an additional signal of its presence in the form of an emission line in the photon spectrum. Finally, the last stages of a PBH are characterized by a mass-spin distribution highly dependent on the particle physics beyond the TeV scale and may provide information on the particle degrees of freedom present at that energy. These results have motivated our search for methods to determine the mass and spin of PBHs in different mass and spin ranges in a distance-independent manner. We have proposed three distinct methods taking into account the features of the spectra in the analyzed ranges of mass and spin as well as the characteristics of the physics at the energies involved. In particular, we proposed a method for

PBHs of low spin ($0 \leq \tilde{a} \leq 0.5$) and masses $5 \times 10^7 - 10^{12}$ kg that relies on the primary and the secondary spectra. A second method applies in the case of high spin ($0.6 \leq \tilde{a} \leq 0.9999$) and in principle can be applied to a vast range of masses. In order to infer the mass-spin distributions at energies beyond the SM we proposed a multi-messenger approach that is independent of the putative coupling between the new heavy particles and the SM particles. Finally, considering the particular case of the Kerr Black-Bounce, we have shown how it is possible to investigate the beyond-the-horizon structure of a black hole by exploiting its Hawking spectrum and the time evolution of its parameters. The above-described results gain appeal in the light of the many experiments such as space telescopes, sky surveys, very large arrays, fast radio bursts observatories, MeV-GeV-TeV gamma-ray telescopes, Cherenkov telescopes, and neutrinos observatories, which although not designed for PBHs detection have nonetheless the capability to detect those that pass in the vicinity of the Solar System.

The examples discussed in this work demonstrate that PBHs can be fantastic laboratories for fundamental physics.

Appendices

A Double check using BlackHawk

To further validate our analysis of chapter 7 we used a modified version of BlackHawk code [93–96] to compute the evolution of a PBH of mass $M_0 = 10^{13}$ kg and $\tilde{a} = 0.01, 0.99$. The modification was implemented ad hoc by Dr. Jeremy Auffinger (creator of the BlackHawk code) to allow the BH spin parameter to grow during the BH evaporation. I am extremely thankful to Jeremy for his work. In fact, the original version of BlackHawk contains the file 'evolution.c' that is optimized to follow a standard evolution characterized by an ever-decreasing $\tilde{a}$. It is the file "evolution.c" that needs to be modified if one wants to reproduce our result.

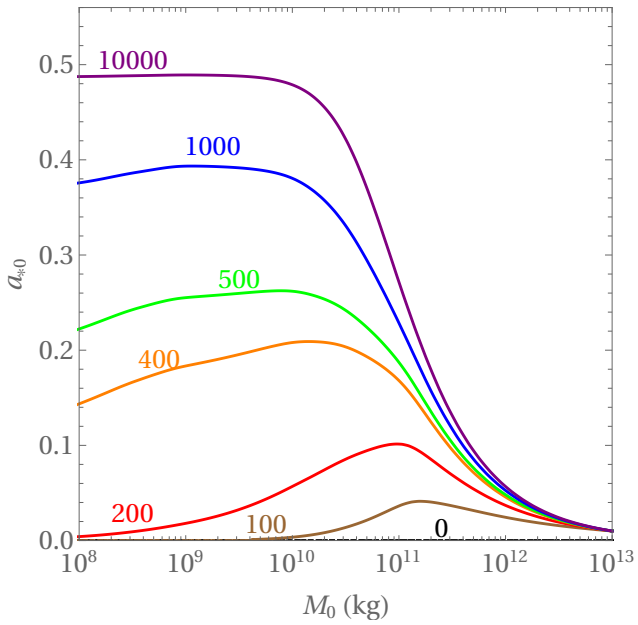

Figure A.1: PBH spin, $\tilde{a}_0$, as a function of the PBH mass, M_0, for an PBH with natal spin $\tilde{a} = 0.01$ and mass $M_* = 10^{13}$ kg. Curves are labeled by the number of light ALPs.

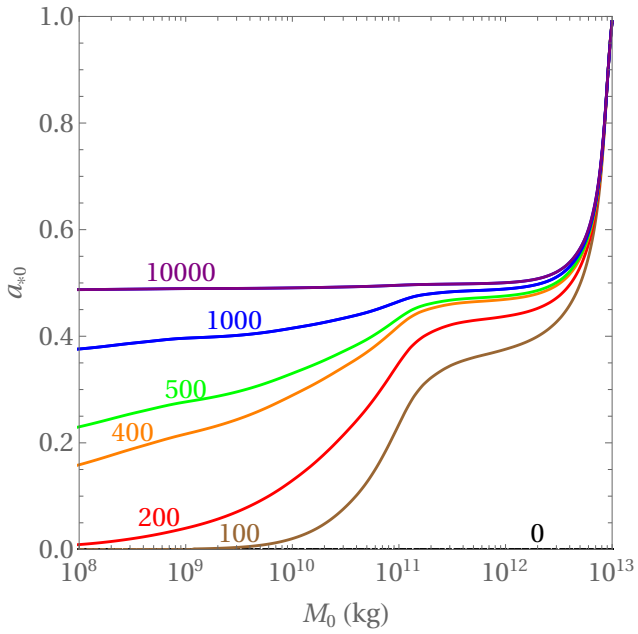

Figure A.2: PBH spin, $\tilde{a}_0$, as a function of the PBH mass, M_0, for an PBH with natal spin $\tilde{a} = 0.99$ and mass $M_* = 10^{13}$ kg. Curves are labeled by the number of light ALPs.

Fig. A.1 and A.2 show the evolution of a single PBH of natal mass 10^{13} kg and $\tilde{a} = 0.01, 0.99$ respectively, in the presence of a different number of light ALPs characterizing the underlining theory of particle physics.
We want to stress that Figs. A.1 and A.2 differ slightly for large values of the PBH masses with respect to Figs. 7.1 and 7.2. In fact, for each value of the number of ALPs, the curve in Figs. 7.1 and 7.2 are obtained by an initial population of PBHs of slightly different masses ($\sim 10^{13}$ kg) and the same natal $\tilde{a}$ evolved for a time given by the lifetime of the universe. The mass and spin of the remnant are then plotted and are the points constituting the curves. In this sense, 7.1 and 7.2 represent the mass and spin that it is expected to be measured today, a snapshot of the present distribution. On the other hand, the curve in Figs. A.1 and A.2 are obtained by following a single PBH of natal mass 10^{13} kg during its temporal evolution. This difference is obvious in the upper right portion of the plots A.2 and 7.2. In the first case, the lines converge to a single point, while in the second they do not. Basically, in these plots, we solve the same differential equations with marginal changes in the initial conditions. Such changes have an influence only in the rightmost part

of the plots. Anyway, since the changes in natal masses for obtaining (7.1) and (7.2) are infinitesimal and the plots look similar and the take-home message is the same: the ALPs modify the evolution of a PBH mass and spin and if their number is larger than 100 they can spin up or enhance the duration of a non-negligible spin for present masses of the PBH remnant $M < 10^{12}$ kg.
Increasing the number of ALPs in Fig. (A.1) and (A.2) does not lead to reaching the asymptotic value of $\tilde{a} = 0.555$ described in [90–92] with which we agree and which is reached when the evolution is dominated by ALPs (10000 ALPs) in Figs. (7.1) and (7.2). This is a flaw of pushing BlackHawk to do this kind of calculation. In fact, it is implemented in the framework of the SM where the scalar contribution comes only from the Higgs doublet and it is by large subdominant.

B Contribution of different modes to the Hawking spectrum

The peaks in the primary photon Hawking spectrum discussed in chapter 9 are, as mentioned in the text, dominated by the maximally co-rotating $l = m$ modes for $\tilde{a} > 0$. To better understand this, we show in Fig. B.1 the contribution of the lowest (l, m) modes, for both limits of a Schwarzschild and a near-extremal BH.

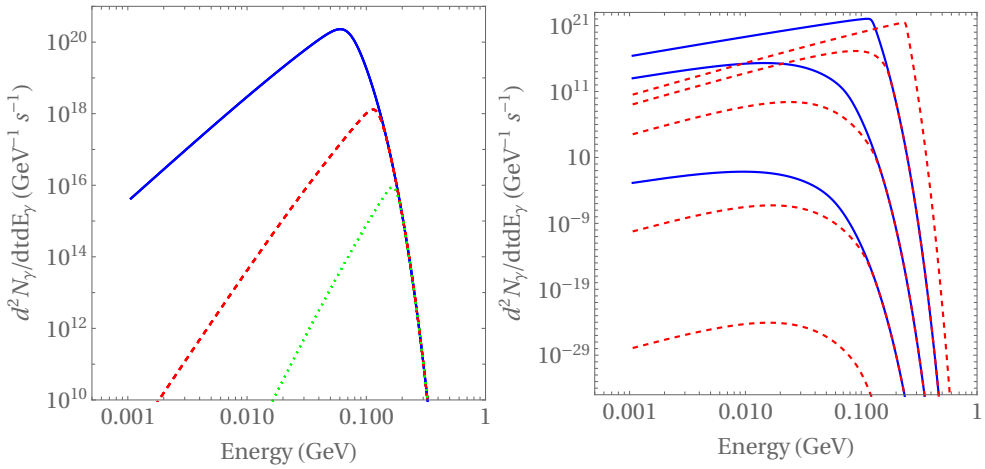

Figure B.1: Contribution of different (l, m) modes to the primary photon spectrum, for a PBH with $M = 10^{12}$ kg with $\tilde{a} = 0$ (left) and $\tilde{a} = 0.99$ (right). Solid blue/dashed red/dotted green curves correspond to $l = 1/2/3$ modes, respectively. In the Schwarzschild case modes with the same l are degenerate, while in the near-extremal PBH, the curves correspond to $m = -l, \ldots, +l$ from bottom to top.

As one can see in this figure, in the non-rotating (Schwarzschild) limit modes with the same l and different $m = -l, \ldots, +l$ yield degenerate contributions

to the Hawking emission rate, as should be expected from the spherical symmetry of the spacetime. One also sees that the contributions from $l > 1$ modes never exceed the dominant contribution from the dipolar ($l = 1$) modes. As discussed in the main body of this article, this is simply a consequence of higher-l modes having to cross a higher angular momentum barrier as they propagate away from the BH horizon, so that only modes with a larger energy, and hence a more Boltzmann-suppressed emission, are fully transmitted. This is why only PBHs with a non-zero spin exhibit the multi-peak structure in the primary Hawking spectrum required by our proposed methodology.

For $\tilde{a} > 0$, the m-degeneracy is broken, and maximally co-rotating modes with $l = m$ give the largest contributions to the spectrum. In fact, as illustrated in Fig. 9.9, the emission rate increases with m for a given value of l. Superradiant amplification plays a crucial role in breaking this degeneracy since it only occurs for co-rotating modes for which the superradiance condition $\omega < m\Omega$ can be satisfied at low energies/frequencies. For these modes, the exponential Boltzmann factor in Eq. (5.36) is below unity, $e^{2\pi(\omega - m\Omega)/\kappa} < 1$, and the transmission coefficient $\Gamma^1_{l,m} < 0$ (signaling mode amplification, see Fig. 9.18), so that both the numerator and denominator of the fraction determining the emission rate are negative. Furthermore, these modes are not Boltzmann-suppressed, therefore yielding significant contributions to the emission spectrum.

We also observe that the contributions from modes with $l \neq m$ are more suppressed for larger values of $\tilde{a}$, so that in the regime of interest to our spin determination method, $\tilde{a} \gtrsim 0.6$, an accurate expression for the spectrum can be obtained from adding the contributions from only the $l = m$ modes as shown in Fig. 9.8. Moreover, since we are mainly interested in the shape of the spectrum near the $l = 1$ and $l = 2$ peaks, it is sufficient to compute the contributions of modes up to $l = 4$ for the level of precision we are interested in[1].

[1] We note that for other applications such as computing scattering cross sections, one needs to include contributions from higher-l modes.

C Secondary photon emission spectrum

An evaporating PBH emits several differently charged particles that radiate photons as they travel away from the PBH. Photons also result from the decay of unstable particles, like neutral pions. These photons are naturally less energetic than those directly emitted but yield nevertheless a very significant contribution to the total photon spectrum at energies smaller than the one of the primary peak. The full spectrum can then be obtained by convoluting the primary emission rate in Eq. (5.36) with the number of photons radiated by each charged/unstable primary particle. This is, generically, a non-trivial procedure that has to be performed using numerical tools, particularly in the case of quarks and gluons that hadronize as they move away from the PBH, for Hawking temperatures roughly exceeding Λ_{QCD}. These reasons often motivate the adoption of toolkits such as BlackHawk [93–96] that employ the particle physics codes Hazma and PYTHIA to numerically compute the photon yield of each primary species.

However, since we are mainly interested in PBHs with $M \gtrsim 10^{12}$ kg that may presently exhibit large spin values, $\tilde{a} \gtrsim 0.6$, and for which $T_H \lesssim 10$ MeV, a good approximation to compute the secondary photon spectrum can be obtained by considering only the primary emission of electrons, muons and charged pions and the corresponding final state radiation (FSR), as well as the photon yield from neutral pion decay [100, 110]. The total photon spectrum is then given by (5.41), where the prime component is given by (5.36) while the second by (5.4.2), (5.42). The term (5.4.2) takes into account the convolution of the primary electron, muon and charged pion primary spectra as given in Eq. (5.36) with the Altarelli-Parisi splitting functions at leading order in the electromagnetic fine-structure constant α_{EM} [108, 109] where the

contributions from muons and charged pions are sub-leading and: The term (5.42) corresponds to the contribution from neutral pion decays into photon pairs.

In Fig. C.1 we show the total photon emission spectrum obtained using this method for a PBH with $M = 10^{12}$ kg and two limiting values of the spin parameter relevant to our proposed methodology, alongside the corresponding primary photon component.

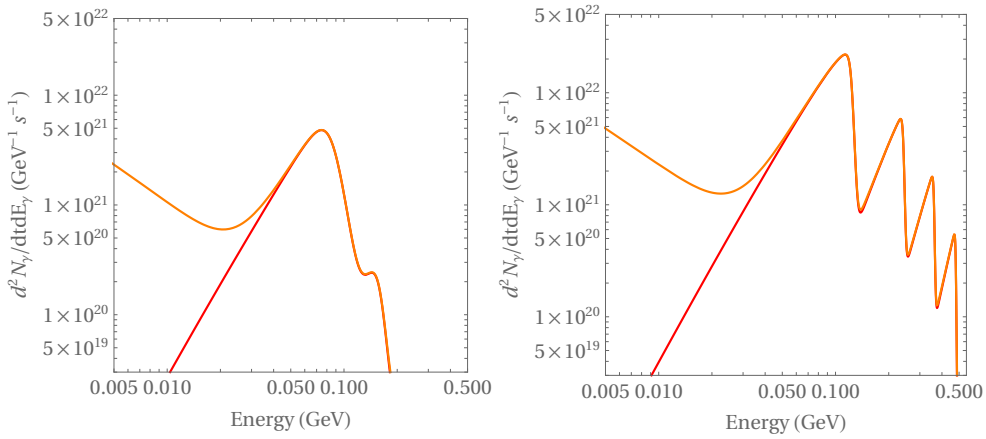

Figure C.1: Primary (red) and total (orange) photon emission spectrum of a PBH with $M = 10^{12}$ kg and (left) $\tilde{a} = 0.6$ and (right) $\tilde{a} = 0.99$.

This figure shows no substantial change in the shape of the spectrum near the primary emission peaks, particularly the $l = 1$ and $l = 2$ peaks relevant to our discussion, showing that our analysis of section 9.2 neglecting the secondary photon emission spectrum is robust. This should be expected since secondary photons carry only a fraction of the energy of their primary progenitors (electrons, muons, etc), with primary emission for all species peaking at comparable energies $\sim E_1$. Hence, in general, secondary emission is a significant component of the spectrum but only at energies well below the primary photon emission peaks.

Bibliography

[1] Y. B. Zel'dovich and I. D. Novikov, "The Hypothesis of Cores Retarded during Expansion and the Hot Cosmological Model," Soviet Astron. AJ (Engl. Transl.), **10** (1967), 602.

[2] S. Hawking, "Gravitationally collapsed objects of very low mass," Mon. Not. Roy. Astron. Soc. **152**, 75 (1971).

[3] B. P. Abbott *et al.* [LIGO Scientific and Virgo], "Observation of Gravitational Waves from a Binary Black Hole Merger," Phys. Rev. Lett. **116**, no.6, 061102 (2016) [arXiv:1602.03837 [gr-qc]].

[4] K. Akiyama *et al.* [Event Horizon Telescope], "First M87 Event Horizon Telescope Results. I. The Shadow of the Supermassive Black Hole," Astrophys. J. Lett. **875** (2019), L1 [arXiv:1906.11238 [astro-ph.GA]].

[5] K. Akiyama *et al.* [Event Horizon Telescope], "First M87 Event Horizon Telescope Results. II. Array and Instrumentation," Astrophys. J. Lett. **875** (2019) no.1, L2 [arXiv:1906.11239 [astro-ph.IM]].

[6] K. Akiyama *et al.* [Event Horizon Telescope], "First M87 Event Horizon Telescope Results. III. Data Processing and Calibration," Astrophys. J. Lett. **875** (2019) no.1, L3 [arXiv:1906.11240 [astro-ph.GA]].

[7] K. Akiyama *et al.* [Event Horizon Telescope], "First M87 Event Horizon Telescope Results. IV. Imaging the Central Supermassive Black Hole," Astrophys. J. Lett. **875** (2019) no.1, L4 [arXiv:1906.11241 [astro-ph.GA]].

[8] K. Akiyama *et al.* [Event Horizon Telescope], "First M87 Event Horizon Telescope Results. V. Physical Origin of the Asymmetric Ring," Astrophys. J. Lett. **875** (2019) no.1, L5 [arXiv:1906.11242 [astro-ph.GA]].

[9] K. Akiyama *et al.* [Event Horizon Telescope], "First M87 Event Horizon Telescope Results. VI. The Shadow and Mass of the Central Black Hole," Astrophys. J. Lett. **875** (2019) no.1, L6 [arXiv:1906.11243 [astro-ph.GA]].

[10] K. Akiyama *et al.* [Event Horizon Telescope], "First Sagittarius A* Event Horizon Telescope Results. I. The Shadow of the Supermassive Black Hole in the Center of the Milky Way," Astrophys. J. Lett. **930** (2022) no.2, L12 [arXiv:2311.08680 [astro-ph.HE]].

[11] M. Calzà, J. March-Russell and J. G. Rosa, "Evaporating primordial black holes, the string axiverse, and hot dark radiation," [arXiv:2110.13602 [astro-ph.CO]].

[12] M. Calzà, J. G. Rosa and F. Serrano, "Primordial black hole superradiance and evaporation in the string axiverse," [arXiv:2306.09430 [hep-ph]].

[13] M. Calzà and J. G. Rosa, "Determining the spin of light primordial black holes with Hawking radiation," JHEP **12**, 090 (2022) [arXiv:2210.06500 [gr-qc]].

[14] M. Calzà and J. G. Rosa, "Determining the spin of light primordial black holes with Hawking radiation II: high spin regime," [arXiv:2311.12930 [gr-qc]].

[15] M. Calzà and J. G. Rosa, "Evaporating Kerr black holes as probes of new physics," [arXiv:2312.09261 [hep-ph]].

[16] M. Calzá, "Evaporation of a Kerr-black-bounce by emission of scalar particles," Phys. Rev. D **107** (2023) no.4, 044067 [arXiv:2207.10467 [gr-qc]].

[17] M. Calzà, M. Rinaldi and L. Sebastiani, "A special class of solutions in $F(R)$-gravity," Eur. Phys. J. C **78** (2018) no.3, 178 [arXiv:1802.00329 [gr-qc]].

[18] M. Calzà, A. Casalino, O. Luongo and L. Sebastiani, "Kinematic reconstructions of extended theories of gravity at small and intermediate redshifts," Eur. Phys. J. Plus **135** (2020) no.1, 1 [arXiv:1910.04594 [gr-qc]].

[19] M. Calzá, A. Casalino and L. Sebastiani, "Local solutions of general relativity in the presence of the trace anomaly," Phys. Dark Univ. **37** (2022), 101066 [arXiv:2205.03329 [gr-qc]].

[20] M. Calzá and L. Sebastiani, "A class of static spherically symmetric solutions in f(Q)-gravity," Eur. Phys. J. C **83** (2023) no.3, 247 [arXiv:2208.13033 [gr-qc]].

[21] M. Calzá and L. Sebastiani, "A class of static spherically symmetric solutions in $f(T)$-gravity," [arXiv:2309.04536 [gr-qc]].

[22] N. S. Mankoc Borstnik, "How Clifford algebra can help understand second quantization of fermion and boson fields," [arXiv:2210.06256 [physics.gen-ph]].

[23] J. Jr. Vaz and R. Jr. da Rocha "An Introduction to Clifford Algebras and Spinors," Oxford University Press, 2016.

[24] Y. Q. Gu, "Clifford Algebra, Lorentz Transformation and Unified Field Theory," Adv. Appl. Clifford Algebras **28** (2018) no.2, 37

[25] R. Bott and L. W. Tu, Springer, 1982, ISBN 978-0-387-90613-3, 978-1-4419-2815-3, 978-1-4757-3951-0 doi:10.1007/978-1-4757-3951-0

[26] W. Graf, Ann. Inst. H. Poincare Phys. Theor. **29** (1978), 85-109

[27] Ian D. Lawrie. "A Unified Grand Tour of Theoretical Physics," Institute of Physics Publishing Bristol and Philadelphia, 2nd edition, 2002.

[28] General Relativity, Black Holes, and Cosmology Andrew J. S. Hamilton (2021)

[29] S. Weinberg, "The Quantum theory of fields. Vol. 1: Foundations," Cambridge University Press, 2005.

[30] S. Weinberg, "The quantum theory of fields. Vol. 2: Modern applications," Cambridge University Press, 2013.

[31] S. Weinberg, Cambridge University Press, 2013.

[32] E. Newman and R. Penrose, "An Approach to gravitational radiation by a method of spin coefficients," J. Math. Phys. **3** (1962), 566-578.

[33] A. Z. Petrov, "The Classification of spaces defining gravitational fields," Gen. Rel. Grav. **32** (2000), 1661-1663.

[34] W. M. Kinnersley, "Type D gravitational fields," CalTech Thesis, 1968.

[35] W. Kinnersley, "Type D Vacuum Metrics," J. Math. Phys. **10** (1969), 1195-1203.

[36] F. E. A. Pirani "Introduction to gravitational radiation theory," Brandeis summer institute in Theoretical Physics (1964) (notes by J. J. J. Marek).

[37] S. A. Teukolsky, "Rotating black holes - separable wave equations for gravitational and electromagnetic perturbations," Phys. Rev. Lett. **29** (1972), 1114-1118.

[38] S. A. Teukolsky, "Perturbations of a rotating black hole. 1. Fundamental equations for gravitational electromagnetic and neutrino field perturbations," Astrophys. J. **185**, 635-647 (1973).

[39] W. H. Press and S. A. Teukolsky, "Perturbations of a Rotating Black Hole. II. Dynamical Stability of the Kerr Metric," Astrophys. J. **185**, 649-674 (1973).

[40] S. A. Teukolsky and W. H. Press, "Perturbations of a rotating black hole. III - Interaction of the hole with gravitational and electromagnet ic radiation," Astrophys. J. **193**, 443-461 (1974).

[41] R- M. Wald, "On perturbations of a Kerr black hole," J. Math. Phys. **14** (1973), 1453.

[42] W. Unruh, "Separability of the Neutrino Equations in a Kerr Background," Phys. Rev. Lett. **31** (1973) no.20, 1265-1267.

[43] S. Chandrasekhar, "The Solution of Dirac's Equation in Kerr Geometry," Proc. Roy. Soc. Lond. A **349** (1976), 571-575.

[44] R. Gueven, "Wave Mechanics of Electrons in Kerr Geometry," Phys. Rev. D **16** (1977), 1706-1711.

[45] K. Düztaş, "Stability of event horizons against neutrino flux: The classical picture," Class. Quant. Grav. **32** (2015) no.7, 075003 [arXiv:1408.1735 [gr-qc]].

[46] K. Düztaş, "Is there a mode stability paradox for neutrino perturbations of Kerr black holes?," Phys. Rev. D **94** (2016) no.4, 044025 [arXiv:1503.05061 [gr-qc]].

[47] J. Wainwright, "Geometric properties of neutrino fields in curved space-time," J. Math. Phys. **12** (1971), 828-835.

[48] E. D. Fackerell and J. R. Ipser, "Weak electromagnetic fields around a rotating black hole," Phys. Rev. D **5** (1972), 2455-2458.

[49] S. L. Detweiler and J. R. Ipser, "Stability of scalar perturbations of a Kerr-metric black hole," Astrophys. J. **185** (1973), 675-683.

[50] S. L. Detweiler, "Klein-Gordon equation and rotating black holes," Phys. Rev. D **22** (1980), 2323-2326.

[51] S. Einstein and R. Finkelstein, "Solutions of the Rarita-schwinger Equation in the Kerr-Newman Space," J. Math. Phys. **20** (1979), 1972.

[52] R. Gueven, "Black holes have no superhair," Phys. Rev. D **22** (1980), 2327.

[53] N. Kamran "Separation of variables for the Rarita-Schwinger equation on all type D vacuum backgrounds," J. Math. Phys. **26** (1985), 1740.

[54] G. F. Torres Del Castillo, "Rarita-Schwinger fields in algebraically special vacuum space-times," J. Math. Phys. **30**, 446 (1989).

[55] G. F. Torres Del Castillo, "Spin-3/2 perturbations of algebraically special solutions of the Einstein-Maxwell equations," J. Math. Phys. **30** (1989), 2114-2119.

[56] G. F. Torres Del Castillo, "Debye Potentials for Rarita-schwinger Fields in Curved Space-times," J. Math. Phys. **30** (1989), 1323-1328.

[57] G. F. Torres del Castillo and G. Silva-Ortigoza, "Rarita-Schwinger fields in the Kerr geometry," Phys. Rev. D **42** (1990), 4082-4086.

[58] G. F. Torres del Castillo and G. Silva-Ortigoza, "Spin-3/2 perturbations of the Kerr-Newman solution," Phys. Rev. D **46** (1992), 5395-5398.

[59] C. H. Chen, H. T. Cho, A. S. Cornell, G. Harmsen and W. Naylor, "Gravitino fields in Schwarzschild black hole spacetimes," Chin. J. Phys. **53** (2015), 110101.

[60] S. Chandrasekhar, "The mathematical theory of black holes," Oxford University Press, 1983.

[61] J. A. H. Futterman, F. A. Handler, R. A. Matzner "Scattering from Black Holes," Cambridge University Press (1988).

[62] E. G. Kalnins, W.Jr. Miller, G. C. Williams, "Teukolsky-Starobinsky identities for arbitrary spin," J. Math. Phys. **30**, (1989), 2925.

[63] S. Chandrasekhar "The Teukolsky-Starobinsky constant for arbitrary spin," Royal Society, Volume 430, Issue 1879, (1990).

[64] E. G. Kalnins, W. Miller Jr,and G. C. Williams "Recent advances in the use of separation of variables methods in general relativity," Philosophical Transactions of the Royal Society of London. Series A: Physical and Engineering Sciences 340337-352 (1992).

[65] E. D. Fackerell and R. G. Crossman, "Spin-weighted angular spheroidal functions," J. Math. Phys. **18** (1977), 1849-1854.

[66] K. G. Suffern, "Eigenvalues of the Chandrasekhar-Page angular functions," J. Math. Phys. **24** (1983), 1350. [arXiv:math-ph/0402047 [math-ph]].

[67] E. Seidel, "A Comment on the Eigenvalues of Spin Weighted Spheroidal Functions," Class. Quant. Grav. **6** (1989), 1057.

[68] E. Berti, V. Cardoso and M. Casals, "Eigenvalues and eigenfunctions of spin-weighted spheroidal harmonics in four and higher dimensions," Phys. Rev. D **73** (2006), 024013 [erratum: Phys. Rev. D **73** (2006), 109902]. [arXiv:gr-qc/0511111 [gr-qc]].

[69] A. A. Starobinskii and S. M.Churilov, "Amplification of electromagnetic and gravitational waves scattered by a rotating black hole", Soviet Physics JETP, Vol. 38, p.1 (1973).

[70] J. G. Rosa, "Superradiance in the sky," Phys. Rev. D **95** (2017) no.6, 064017 [arXiv:1612.01826 [gr-qc]].

[71] S. Mano, H. Suzuki and E. Takasugi, "Analytic solutions of the Teukolsky equation and their low frequency expansions," Prog. Theor. Phys. **95** (1996), 1079-1096. [arXiv:gr-qc/9603020 [gr-qc]].

[72] S. Mano, H. Suzuki and E. Takasugi, "Analytic solutions of the Regge-Wheeler equation and the postMinkowskian expansion," Prog. Theor. Phys. **96** (1996), 549-566. [arXiv:gr-qc/9605057 [gr-qc]].

[73] S. Mano and E. Takasugi, "Analytic solutions of the Teukolsky equation and their properties," Prog. Theor. Phys. **97** (1997), 213-232. [arXiv:gr-qc/9611014 [gr-qc]].

[74] P. P. Fiziev, "Teukolsky-Starobinsky Identities: A Novel Derivation and Generalizations," Phys. Rev. D **80**, 124001 (2009) [arXiv:0906.5108 [gr-qc]].

[75] A. A. Starobinskii "Amplification of waves during reflection from a rotating black hole," ZhETF, Vol. 64, No. 1, p. 48, July 1973

[76] A. A. Starobinsky, "Amplification of waves reflected from a rotating "black hole".," Sov. Phys. JETP **37**, no.1, 28-32 (1973)

[77] H. Suzuki, E. Takasugi and H. Umetsu, "Perturbations of Kerr-de Sitter black hole and Heun's equations," Prog. Theor. Phys. **100** (1998), 491-505 [arXiv:gr-qc/9805064 [gr-qc]].

[78] H. Suzuki, E. Takasugi and H. Umetsu, "Analytic solutions of Teukolsky equation in Kerr-de Sitter and Kerr-Newman-de Sitter geometries," Prog. Theor. Phys. **102** (1999), 253-272 [arXiv:gr-qc/9905040 [gr-qc]].

[79] H. Suzuki, E. Takasugi and H. Umetsu, "Absorption rate of the Kerr-de Sitter black hole and the Kerr-Newman-de Sitter black hole," Prog. Theor. Phys. **103** (2000), 723-731 [arXiv:gr-qc/9911079 [gr-qc]].

[80] S. Creek, O. Efthimiou, P. Kanti and K. Tamvakis, "Greybody factors in a rotating black-hole background. II. Fermions and gauge bosons," Phys. Rev. D **76** (2007), 104013 [arXiv:0707.1768 [hep-th]].

[81] S. Chandrasekhar and S. L. Detweiler, "The quasi-normal modes of the Schwarzschild black hole," Proc. Roy. Soc. Lond. A **344** (1975), 441-452.

[82] J. G. Rosa, "Boosted black string bombs," JHEP **02** (2013), 014 [arXiv:1209.4211 [hep-th]].

[83] S. W. Hawking, "Black hole explosions," Nature **248** (1974), 30-31.

[84] S. W. Hawking, "Particle Creation by Black Holes," Commun. Math. Phys. **43** (1975), 199-220 [erratum: Commun. Math. Phys. **46** (1976), 206].

[85] W. T. Zaumen, "Upper bound on the electric charge of a black hole," Nature **240**, 530 (1974).

[86] G. W. Gibbons, "Vacuum Polarization and the Spontaneous Loss of Charge by Black Holes," Commun. Math. Phys. **44**, 245-264 (1975).

[87] D. N. Page, "Particle Emission Rates from a Black Hole: Massless Particles from an Uncharged, Nonrotating Hole," Phys. Rev. D **13** (1976), 198-206.

[88] D. N. Page, "Particle Emission Rates from a Black Hole. 2. Massless Particles from a Rotating Hole," Phys. Rev. D **14** (1976), 3260-3273.

[89] D. N. Page, "Particle Emission Rates from a Black Hole. 3. Charged Leptons from a Nonrotating Hole," Phys. Rev. D **16** (1977), 2402-2411.

[90] C. M. Chambers, W. A. Hiscock and B. Taylor, "Spinning down a black hole with scalar fields," Phys. Rev. Lett. **78** (1997), 3249-3251 [arXiv:gr-qc/9703018 [gr-qc]].

[91] C. M. Chambers, W. A. Hiscock and B. E. Taylor, "The 'Ups' and 'downs' of a spinning black hole," [arXiv:gr-qc/9710013 [gr-qc]].

[92] B. E. Taylor, C. M. Chambers and W. A. Hiscock, "Evaporation of a Kerr black hole by emission of scalar and higher spin particles," Phys. Rev. D **58** (1998), 044012 [arXiv:gr-qc/9801044 [gr-qc]].

[93] A. Arbey and J. Auffinger, "BlackHawk: A public code for calculating the Hawking evaporation spectra of any black hole distribution," Eur. Phys. J. C **79**, no.8, 693 (2019) [arXiv:1905.04268 [gr-qc]].

[94] A. Arbey, J. Auffinger and J. Silk, "Primordial Kerr Black Holes," PoS **ICHEP2020**, 585 (2021) [arXiv:2012.14767 [astro-ph.CO]].

[95] A. Arbey, J. Auffinger, M. Geiller, E. R. Livine and F. Sartini, "Hawking radiation by spherically-symmetric static black holes for all spins. II. Numerical emission rates, analytical limits, and new constraints," Phys. Rev. D **104**, no.8, 084016 (2021) [arXiv:2107.03293 [gr-qc]].

[96] A. Arbey and J. Auffinger, "Physics Beyond the Standard Model with BlackHawk v2.0," Eur. Phys. J. C **81**, 10 (2021) [arXiv:2108.02737 [gr-qc]].

[97] A. Coogan, L. Morrison and S. Profumo, "Hazma: A Python Toolkit for Studying Indirect Detection of Sub-GeV Dark Matter," JCAP **01**, 056 (2020) [arXiv:1907.11846 [hep-ph]].

[98] T. Sjostrand, S. Mrenna and P. Z. Skands, "A Brief Introduction to PYTHIA 8.1," Comput. Phys. Commun. **178**, 852-867 (2008) [arXiv:0710.3820 [hep-ph]].

[99] C. Bierlich, *et al.* "A comprehensive guide to the physics and usage of PYTHIA 8.3," [arXiv:2203.11601 [hep-ph]].

[100] A. Coogan, L. Morrison and S. Profumo, "Direct Detection of Hawking Radiation from Asteroid-Mass Primordial Black Holes," Phys. Rev. Lett. **126**, no.17, 171101 (2021) [arXiv:2010.04797 [astro-ph.CO]].

[101] T. N. Ukwatta, D. R. Stump, J. T. Linnemann, J. H. MacGibbon, S. S. Marinelli, T. Yapici and K. Tollefson, "Primordial Black Holes: Observational Characteristics of The Final Evaporation," Astropart. Phys. **80**, 90-114 (2016) [arXiv:1510.04372 [astro-ph.HE]].

[102] S.W. Hawking, "Particle creation by black holes," Comm. Math. Phys. 43 (1975) 199.

[103] A. Vilenkin, "Parity Nonconservation and Rotating Black Holes," Phys. Rev. Lett. **41** (1978), 1575-1577.

[104] D. A. Leahy and W. G. Unruh "Angular dependence of neutrino emission from rotating black holes," Phys. Rev. D 19, (1979).

[105] A. Vilenkin "Macroscopic parity-violating effects: Neutrino fluxes from rotating black holes and in rotating thermal radiation," Phys. Rev. D 20, 1807 (1979).

[106] M. Casals, S. R. Dolan, B. C. Nolan, A. C. Ottewill and E. Winstanley, "Quantization of fermions on Kerr space-time," Phys. Rev. D **87** (2013) no.6, 064027 [arXiv:1207.7089 [gr-qc]].

[107] Y. F. Perez-Gonzalez, "Identifying spin properties of evaporating black holes through asymmetric neutrino and photon emission," Phys. Rev. D **108** (2023) no.8, 083014 [arXiv:2307.14408 [astro-ph.HE]].

[108] G. Altarelli and G. Parisi, "Asymptotic Freedom in Parton Language," Nucl. Phys. B **126**, 298-318 (1977).

[109] J. Chen, T. Han and B. Tweedie, "Electroweak Splitting Functions and High Energy Showering," JHEP **11**, 093 (2017) [arXiv:1611.00788 [hep-ph]].

[110] K. Agashe, J. H. Chang, S. J. Clark, B. Dutta, Y. Tsai and T. Xu, "Correlating gravitational wave and gamma-ray signals from primordial black holes," Phys. Rev. D **105**, no.12, 123009 (2022) [arXiv:2202.04653 [astro-ph.CO]].

[111] https://pdg.lbl.gov/.

[112] W. M. Yao *et al.* [Particle Data Group], "Review of Particle Physics," J. Phys. G **33**, 1-1232 (2006).

[113] F. Halzen, E. Zas, J. H. MacGibbon and T. C. Weekes, "Search for gamma-rays from black holes," MAD-PH-575.

[114] F. Halzen, E. Zas, J. H. MacGibbon and T. C. Weekes, "Gamma-rays and energetic particles from primordial black holes," Nature **353**, 807-815 (1991).

[115] T. N. Ukwatta, *et al.*, "Spectral Lags of Gamma-Ray Bursts from Primordial Black Hole (PBH) Evaporations," AIP Conf. Proc. **1133**, no.1, 440-442 (2009) [arXiv:0901.0542 [astro-ph.HE]].

[116] J. H. MacGibbon, T. N. Ukwatta, J. T. Linnemann, S. S. Marinelli, D. Stump and K. Tollefson, "Primordial Black Holes," [arXiv:1503.01166 [astro-ph.HE]].

[117] J. H. MacGibbon, "Quark and gluon jet emission from primordial black holes. 2. The Lifetime emission," Phys. Rev. D **44**, 376-392 (1991).

[118] J. H. MacGibbon and B. J. Carr, "Cosmic rays from primordial black holes," Astrophys. J. **371**, 447-469 (1991).

[119] J. H. MacGibbon, B. J. Carr and D. N. Page, "Do Evaporating Black Holes Form Photospheres?," Phys. Rev. D **78**, 064043 (2008) [arXiv:0709.2380 [astro-ph]].

[120] J. H. MacGibbon, B. J. Carr and D. N. Page, "Do Evaporating 4D Black Holes Form Photospheres and/or Chromospheres?," [arXiv:1003.3901 [astro-ph.HE]].

[121] J. H. MacGibbon and B. R. Webber, "Quark and gluon jet emission from primordial black holes: The instantaneous spectra," Phys. Rev. D**41**, 3052-3079 (1990).

[122] T. Iritani, H. Suganuma and H. Iida, "Gluon-propagator functional form in the Landau gauge in SU(3) lattice QCD: Yukawa-type gluon propagator and anomalous gluon spectral function," Phys. Rev. D**80**, 114505 (2009). [arXiv:0908.1311 [hep-lat]].

[123] R. Brito, V. Cardoso and P. Pani, "Superradiance: New Frontiers in Black Hole Physics," Lect. Notes Phys. **906** (2015), pp.1-237 2020, [arXiv:1501.06570 [gr-qc]].

[124] Y. B. Zeldovich Pisma Zh. Eksp. Teor. Fiz. 14 (1971) 270 [JETP Lett. 14, 180 (1971)];Zh. Eksp. Teor. Fiz 62 (1972) 2076 [Sov.Phys. JETP 35, 1085 (1972)].

[125] W. H. Press and S. A. Teukolsky, "Floating Orbits, Superradiant Scattering and the Black-hole Bomb", Nature 238 (1972) 211-212.

[126] V. Cardoso, O. J. Dias, J. P. Lemos, and S. Yoshida, "The Black hole bomb and superradiant instabilities" , Phys.Rev. D70 (2004) 044039.

[127] S. Hawking and H. Reall, "Charged and rotating AdS black holes and their CFT duals", Phys.Rev. D61 (2000) 024014.

[128] V. Cardoso, O. J. Dias, and S. Yoshida, "Classical instability of Kerr-AdS black holes and the issue of final state", Phys.Rev. D74 (2006) 044008.

[129] N. Uchikata, S. Yoshida, and T. Futamase, "Scalar perturbations of Kerr-AdS black holes", Phys.Rev. D80 (2009) 084020.

[130] C. Burgess and C. Lutken, "Propagators and Effective Potentials in Anti-de Sitter Space," Phys.Lett. B153 (1985) 137.

[131] A. G. Sitenko, "Electromagnetic Fluctuations in Plasma. Academic", New York, 1976.

[132] R. Kulsrud and A. Loeb, "Dynamics and gravitational interaction of waves in nonuniform media", Phys.Rev. D45 (1992) 525-531.

[133] A. Dima and E. Barausse, "Numerical investigation of plasma-driven superradiant instabilities", arXiv:2001.11484 [gr-qc].

[134] S. A. Teukolsky, "Perturbations of a rotating black hole" PhD thesis, California Institute of Technology, 1973.

[135] M. H. P. M. Van Putten, Science 284 (1999) 115.

[136] A. N. Aguirre, "On the superradiance of spin 1 waves in an equatorial wedge around a Kerr hole", Astrophysical Journal 529 (2000) L9.

[137] V. P. Frolov, P. Krtous, and D. Kubiznak, "Separation of variables in Maxwell equations in Plebanski-Demianski spacetime", Phys. Rev. D97 (2018) no. 10, 101701.

[138] S. R. Dolan, "Instability of the Proca field on Kerr spacetime", Phys. Rev. D98 (2018) no. 10.

[139] M. Fierz and W. Pauli, "On relativistic wave equations for particles of arbitrary spin in an electromagnetic field", Proc.Roy.Soc.Lond. A173 (1939) 211-232.

[140] R. Brito, V. Cardoso and P. Pani, "Massive spin-2 fields on black hole spacetimes: Instability of the Schwarzschild and Kerr solutions and bounds on the graviton mass", Phys. Rev. D **88** (2013) no.2, 023514.

[141] H. Furuhashi and Y. Nambu, "Instability of massive scalar fields in Kerr-Newman space-time," Prog. Theor. Phys. **112**, 983-995 (2004) [arXiv:gr-qc/0402037 [gr-qc]].

[142] A. Arvanitaki, S. Dimopoulos, S. Dubovsky, N. Kaloper and J. March-Russell, "String Axiverse", Phys. Rev. D 81 (2010) 123530.

[143] T. J. M. Zouros and D. M. Eardley, "INSTABILITIES OF MASSIVE SCALAR PERTURBATIONS OF A ROTATING BLACK HOLE," Annals Phys. **118**, 139-155 (1979).

[144] P. Pani, V. Cardoso, L. Gualtieri, E. Berti and A. Ishibashi, "Perturbations of slowly rotating black holes: massive vector fields in the Kerr metric," Phys. Rev. D **86**, 104017 (2012) [arXiv:1209.0773 [gr-qc]].

[145] S. R. Dolan, "Instability of the massive Klein-Gordon field on the Kerr spacetime," Phys. Rev. D **76**, 084001 (2007) [arXiv:0705.2880 [gr-qc]].

[146] T. Damour, N. Deruelle and R. Ruffini, "On Quantum Resonances in Stationary Geometries," Lett. Nuovo Cim. **15**, 257-262 (1976).

[147] V. Cardoso and S. Yoshida, "Superradiant instabilities of rotating black branes and strings," JHEP **07**, 009 (2005) [arXiv:hep-th/0502206 [hep-th]].

[148] J. G. Rosa, "The Extremal black hole bomb," JHEP **06**, 015 (2010) [arXiv:0912.1780 [hep-th]].

[149] S. R. Dolan, "Superradiant instabilities of rotating black holes in the time domain," Phys. Rev. D **87**, no.12, 124026 (2013) [arXiv:1212.1477 [gr-qc]].

[150] W. E. East and F. Pretorius, "Superradiant Instability and Backreaction of Massive Vector Fields around Kerr Black Holes," Phys. Rev. Lett. **119**, no.4, 041101 (2017) [arXiv:1704.04791 [gr-qc]].

[151] W. E. East, "Superradiant instability of massive vector fields around spinning black holes in the relativistic regime," Phys. Rev. D **96**, no.2, 024004 (2017) [arXiv:1705.01544 [gr-qc]].

[152] S. R. Dolan, "Instability of the Proca field on Kerr spacetime," Phys. Rev. D **98**, no.10, 104006 (2018) [arXiv:1806.01604 [gr-qc]].

[153] B. J. Carr and S. W. Hawking, "Black holes in the early Universe," Mon. Not. Roy. Astron. Soc. **168**, 399 (1974).

[154] B. J. Carr, K. Kohri, Y. Sendouda and J. Yokoyama, "New cosmological constraints on primordial black holes," Phys. Rev. D**81**, 104019 (2010). [arXiv:0912.5297 [astro-ph.CO]].

[155] B. Carr, F. Kuhnel and M. Sandstad, "Primordial Black Holes as Dark Matter", Phys. Rev. D 94 (2016) no. 8, 083504.

[156] B. Carr and F. Kuhnel, "Primordial Black Holes as Dark Matter: Recent Developments," Ann. Rev. Nucl. Part. Sci. **70**, 355-394 (2020). [arXiv:2006.02838 [astro-ph.CO]].

[157] J. D. Lykken, "Introduction to Supersymmetry", arXiv:hep-th/9612114.

[158] S. P. Martin, "A Supersymmetry Primer", arXiv:hep-ph/9709356.

[159] A. Bilal, "Introduction to supersymmetry", arXiv:hep-th/0101055.

[160] J. Figueroa-O Farrill, "BUSSTEPP Lectures on Supersymmetry", arXiv:hep-th/0109172.

[161] J. Wess and J. Bagger, "Supersymmetry and supergravity", Princeton, USA: Univ. Pr. (1992) 259 p.

[162] P. C. West, "Introduction to supersymmetry and supergravity", Singapore: World Scientific (1990) 425 p.

[163] M. F. Sohnius, "Introducing Supersymmetry", Phys. Rep. 128 (1985).

[164] S.R. Coleman, J. Mandula,"All Possible Symmetries of the S Matrix". Phys. Rev. 159 (5): 1251-1256 (1967).

[165] R. Haag, J. T. Lopuszanski and M. Sohnius, "All Possible Generators of Supersymmetries of the s Matrix," Nucl. Phys. B **88** (1975), 257.

[166] G. Jungman, M. Kamionkowski and K. Griest, "Supersymmetric dark matter',' Phys. Rept. **267** (1996), 195-373.

[167] E. W. Kolb and R. Slansky, "Dimensional Reduction in the Early Universe: Where Have the Massive Particles Gone?", Phys. Lett. B **135** (1984), 378.

[168] G. Servant and T. Tait, M.P., "Is the lightest Kaluza-Klein particle a viable dark matter candidate?", Nucl. Phys. B **650** (2003), 391-419.

[169] G. Servant and T. Tait, M.P., "Elastic Scattering and Direct Detection of Kaluza-Klein Dark Matter", New J. Phys. **4** (2002), 99.

[170] Sidney Coleman, "The use of instantons".

[171] G. t Hooft, "Computation of the Quantum Effects Due to a Four-Dimensional Pseudoparticle", Phys.Rev. D14 (1976) 3432-3450.

[172] G. t Hooft, "How Instantons Solve the U(1) Problem", Phys.Rept. 142 (1986)357-387.

[173] C. A. Baker, D. D. Doyle, P. Geltenbort, K. Green, M. G. D. van der Grinten, P. G. Harris, P. Iaydjiev, S. N. Ivanov, D. J. R. May and J. M. Pendlebury, *et al.* "An Improved experimental limit on the electric dipole moment of the neutron," Phys. Rev. Lett. **97** (2006), 131801 [arXiv:hep-ex/0602020 [hep-ex]].

[174] R. D. Peccei and H. R. Quinn, "CP Conservation in the Presence of Instantons," Phys. Rev. Lett. **38**, 1440 (1977).

[175] R. Peccei and H. R. Quinn, "Constraints Imposed by CP Conservation in the Presence of Instantons", Phys.Rev. D16 (1977) 1791-1797.

[176] J. E. Kim, "Light Pseudoscalars, Particle Physics and Cosmology", Phys.Rept. 150 (1987) 1-177.

[177] David J. E. Marsh, "Axion Cosmology", "Axions and ALPs: a very short introduction".

[178] S. Weinberg, "A New Light Boson?," Phys. Rev. Lett. **40**, 223 (1978).

[179] F. Wilczek, "Problem of Strong p and t Invariance in the Presence of Instantons," Phys. Rev. Lett. **40**, 279 (1978).

[180] R. D. Peccei, Lect. Notes Phys. **741** (2008), 3-17 doi:10.1007/978-3-540-73518-2_1 [arXiv:hep-ph/0607268 [hep-ph]].

[181] A. Arvanitaki, S. Dimopoulos, S. Dubovsky, N. Kaloper and J. March-Russell, "String Axiverse," Phys. Rev. D**81** (2010), 123530. [arXiv:0905.4720 [hep-th]].

[182] I. Y. Kobzarev, L. B. Okun and I. Y. Pomeranchuk, "On the possibility of experimental observation of mirror particles," Sov. J. Nucl. Phys. **3** (1966) no.6, 837-841.

[183] S. I. Blinnikov and M. Y. Khlopov, "ON POSSIBLE EFFECTS OF 'MIRROR' PARTICLES," Sov. J. Nucl. Phys. **36** (1982), 472 ITEP-11-1982.

[184] R. Foot, H. Lew and R. R. Volkas, "A Model with fundamental improper space-time symmetries," Phys. Lett. B **272** (1991), 67-70.

[185] H. M. Hodges, "Mirror baryons as the dark matter," Phys. Rev. D **47** (1993), 456-459.

[186] Z. G. Berezhiani, A. D. Dolgov and R. N. Mohapatra, "Asymmetric inflationary reheating and the nature of mirror universe," Phys. Lett. B **375** (1996), 26-36 [arXiv:hep-ph/9511221 [hep-ph]].

[187] M. J. Strassler and K. M. Zurek, "Echoes of a hidden valley at hadron colliders," Phys. Lett. B **651** (2007), 374-379 [arXiv:hep-ph/0604261 [hep-ph]].

[188] M. Cvetic, J. Halverson and H. Piragua, "Stringy Hidden Valleys," JHEP **02** (2013), 005 [arXiv:1210.5245 [hep-ph]].

[189] R. Foot and S. Vagnozzi, "Dissipative hidden sector dark matter," Phys. Rev. D **91** (2015), 023512 [arXiv:1409.7174 [hep-ph]].

[190] M. J. Baker and A. Thamm, "Probing the particle spectrum of nature with evaporating black holes," SciPost Phys. **12** (2022) no.5, 150 [arXiv:2105.10506 [hep-ph]].

[191] M. J. Baker and A. Thamm, "Black Hole Evaporation Beyond the Standard Model of Particle Physics," [arXiv:2210.02805 [hep-ph]].

[192] P. Svrcek and E. Witten, "Axions In String Theory," JHEP **06** (2006), 051. [arXiv:hep-th/0605206 [hep-th]].

[193] A. Arvanitaki and S. Dubovsky, "Exploring the String Axiverse with Precision Black Hole Physics," Phys. Rev. D**83**, 044026 (2011). [arXiv:1004.3558 [hep-th]].

[194] B. J. Carr, "The Primordial black hole mass spectrum," Astrophys. J. **201**, 1 (1975).

[195] T. Chiba and S. Yokoyama, "Spin Distribution of Primordial Black Holes," PTEP **2017**, no. 8, 083E01 (2017) [arXiv:1704.06573 [gr-qc]].

[196] M. Mirbabayi, A. Gruzinov and J. Noreña, "Spin of Primordial Black Holes," JCAP **03**, 017 (2020) [arXiv:1901.05963 [astro-ph.CO]].

[197] V. De Luca, V. Desjacques, G. Franciolini, A. Malhotra and A. Riotto, "The initial spin probability distribution of primordial black holes," JCAP **1905**, 018 (2019) [arXiv:1903.01179 [astro-ph.CO]].

[198] T. Harada, C. M. Yoo, K. Kohri and K. I. Nakao, "Spins of primordial black holes formed in the matter-dominated phase of the Universe," Phys. Rev. D**96**, no. 8, 083517 (2017) Erratum: [Phys. Rev. D**99**, no. 6, 069904 (2019)] [arXiv:1707.03595 [gr-qc]].

[199] J. R. Rice and B. Zhang, "Cosmological evolution of primordial black holes," JHEAp **13-14**, 22-31 (2017) [arXiv:1702.08069 [astro-ph.HE]].

[200] Y. Ali-Hamoud and M. Kamionkowski, "Cosmic microwave background limits on accreting PBHs," Phys. Rev. D**95**, 043534 (2017) [arXiv:1612.05644 [astro-ph.CO]].

[201] M. Sasaki, T. Suyama, T. Tanaka and S. Yokoyama, "Primordial Black Hole Scenario for the Gravitational-Wave Event GW150914," Phys. Rev. Lett. **117** (2016) no.6, 061101 [erratum: Phys. Rev. Lett. **121** (2018) no.5, 059901] [arXiv:1603.08338 [astro-ph.CO]].

[202] A. Arbey, J. Auffinger and J. Silk, "Constraining primordial black hole masses with the isotropic gamma ray background," Phys. Rev. D**101**, no. 2, 023010 (2020) [arXiv:1906.04750 [astro-ph.CO]].

[203] P. B. Ferraz, T. W. Kephart and J. G. Rosa, "Superradiant pion clouds around primordial black holes," [arXiv:2004.11303 [gr-qc]].

[204] M. Ackermann *et al.* [Fermi-LAT], "Search for Gamma-Ray Emission from Local Primordial Black Holes with the Fermi Large Area Telescope," Astrophys. J. **857**, no.1, 49 (2018) [arXiv:1802.00100 [astro-ph.HE]].

[205] S. Mittal, A. Ray, G. Kulkarni and B. Dasgupta, "Constraining primordial black holes as dark matter using the global 21-cm signal with X-ray heating and excess radio background," [arXiv:2107.02190 [astro-ph.CO]].

[206] P. C. Argyres, S. Dimopoulos and J. March-Russell, "Black holes and submillimeter dimensions," Phys. Lett. B**441** (1998), 96-104 [arXiv:hep-th/9808138 [hep-th]].

[207] A. M. Green, "Supersymmetry and primordial black hole abundance constraints," Phys. Rev. D**60** (1999), 063516 [arXiv:astro-ph/9903484 [astro-ph]].

[208] G. Johnson, "Primordial Black Hole Constraints with Large Extra Dimensions," JCAP **09** (2020), 046 [arXiv:2005.07467 [astro-ph.CO]].

[209] T. Fujita, M. Kawasaki, K. Harigaya and R. Matsuda, "Baryon asymmetry, dark matter, and density perturbation from primordial black holes," Phys. Rev. D**89** (2014) no.10, 103501 [arXiv:1401.1909 [astro-ph.CO]].

[210] R. Allahverdi, J. Dent and J. Osinski, "Nonthermal production of dark matter from primordial black holes," Phys. Rev. D**97** (2018) no.5, 055013 [arXiv:1711.10511 [astro-ph.CO]].

[211] O. Lennon, J. March-Russell, R. Petrossian-Byrne and H. Tillim, "Black Hole Genesis of Dark Matter," JCAP **04** (2018), 009 [arXiv:1712.07664 [hep-ph]].

[212] D. Hooper, G. Krnjaic, J. March-Russell, S. D. McDermott and R. Petrossian-Byrne, "Hot Gravitons and Gravitational Waves From Kerr Black Holes in the Early Universe," [arXiv:2004.00618 [astro-ph.CO]].

[213] D. Hooper, G. Krnjaic and S. D. McDermott, "Dark Radiation and Superheavy Dark Matter from Black Hole Domination," JHEP **08** (2019), 001 [arXiv:1905.01301 [hep-ph]].

[214] J. Knödlseder, "The future of gamma-ray astronomy," Comptes Rendus Physique **17**, 663-678 (2016) [arXiv:1602.02728 [astro-ph.IM]].

[215] T. Flacke, B. Gripaios, J. March-Russell and D. Maybury, "Warped axions," JHEP **01** (2007), 061 [arXiv:hep-ph/0611278 [hep-ph]].

[216] M. Cicoli, M. Goodsell and A. Ringwald, "The type IIB string axiverse and its low-energy phenomenology," JHEP **10** (2012), 146 [arXiv:1206.0819 [hep-th]].

[217] L. A. Kofman, "Bound states in quantum evaporatin of black holes," Phys. Lett. A **87**, 281-284 (1982).

[218] J. March-Russell and J. G. Rosa, "Micro-Bose/Proca dark matter stars from black hole superradiance," [arXiv:2205.15277 [gr-qc]].

[219] A. Gruzinov, "Black Hole Spindown by Light Bosons," [arXiv:1604.06422 [astro-ph.HE]].

[220] M. Baryakhtar, M. Galanis, R. Lasenby and O. Simon, "Black hole superradiance of self-interacting scalar fields," Phys. Rev. D **103**, no.9, 095019 (2021) [arXiv:2011.11646 [hep-ph]].

[221] N. P. Branco, R. Z. Ferreira and J. G. Rosa, "Superradiant axion clouds around asteroid-mass primordial black holes," JCAP **04**, 003 (2023) [arXiv:2301.01780 [hep-ph]].

[222] H. Yoshino and H. Kodama, "Bosenova collapse of axion cloud around a rotating black hole," Prog. Theor. Phys. **128**, 153-190 (2012) [arXiv:1203.5070 [gr-qc]].

[223] H. Yoshino and H. Kodama, "The bosenova and axiverse," Class. Quant. Grav. **32**, no.21, 214001 (2015) [arXiv:1505.00714 [gr-qc]].

[224] H. Omiya, T. Takahashi and T. Tanaka, "Renormalization group analysis of superradiant growth of self-interacting axion cloud," PTEP **2021**, no.4, 043E02 (2021) [arXiv:2012.03473 [gr-qc]].

[225] H. Omiya, T. Takahashi, T. Tanaka and H. Yoshino, "Impact of multiple modes on the evolution of self-interacting axion condensate around rotating black holes," [arXiv:2211.01949 [gr-qc]].

[226] H. Omiya, T. Takahashi and T. Tanaka, "Adiabatic evolution of the self-interacting axion field around rotating black holes," PTEP **2022**, no.4, 043E03 (2022) [arXiv:2201.04382 [gr-qc]].

[227] J. G. Rosa and T. W. Kephart, "Stimulated Axion Decay in Superradiant Clouds around Primordial Black Holes," Phys. Rev. Lett. **120**, no.23, 231102 (2018) [arXiv:1709.06581 [gr-qc]].

[228] G. Grilli di Cortona, E. Hardy, J. Pardo Vega and G. Villadoro, "The QCD axion, precisely," JHEP **01**, 034 (2016) [arXiv:1511.02867 [hep-ph]].

[229] M. Bauer, M. Neubert and A. Thamm, "Collider Probes of Axion-Like Particles," JHEP **12**, 044 (2017) [arXiv:1708.00443 [hep-ph]].

[230] P. Agrawal, J. Fan and M. Reece, "Clockwork Axions in Cosmology: Is Chromonatural Inflation Chrononatural?," JHEP **10**, 193 (2018) [arXiv:1806.09621 [hep-th]].

[231] K. Langhoff, N. J. Outmezguine and N. L. Rodd, Phys. Rev. Lett. **129**, no.24, 241101 (2022) doi:10.1103/PhysRevLett.129.241101 [arXiv:2209.06216 [hep-ph]].

[232] Z. S. C. Picker and A. Kusenko, "Constraints on late-forming exploding black holes," [arXiv:2305.13429 [astro-ph.CO]].

[233] R. Caputo *et al.* [AMEGO], "All-sky Medium Energy Gamma-ray Observatory: Exploring the Extreme Multimessenger Universe," [arXiv:1907.07558 [astro-ph.IM]].

[234] A. Ray, R. Laha, J. B. Muñoz and R. Caputo, "Near future MeV telescopes can discover asteroid-mass primordial black hole dark matter," Phys. Rev. D **104**, no.2, 023516 (2021) [arXiv:2102.06714 [astro-ph.CO]].

[235] H. Fleischhack, "AMEGO-X: MeV gamma-ray Astronomy in the Multimessenger Era," PoS **ICRC2021**, 649 (2021) [arXiv:2108.02860 [astro-ph.IM]].

[236] A. De Angelis *et al.* [e-ASTROGAM], "The e-ASTROGAM mission," Exper. Astron. **44**, no.1, 25-82 (2017) [arXiv:1611.02232 [astro-ph.HE]].

[237] V. Tatischeff, *et al.* "All-Sky-ASTROGAM: The MeV Gamma-Ray Companion to Multimessenger Astronomy," Mem. Soc. Ast. It. **90**, no.1-2, 137-143 (2019) [arXiv:1905.07806 [astro-ph.HE]].

[238] B. Carr, K. Kohri, Y. Sendouda and J. Yokoyama, "Constraints on primordial black holes," Rept. Prog. Phys. **84**, no.11, 116902 (2021) [arXiv:2002.12778 [astro-ph.CO]].

[239] T. Dzhatdoev and E. Podlesnyi, "Massive Argon Space Telescope (MAST): A concept of heavy time projection chamber for γ-ray astronomy in the 100 MeV–1 TeV energy range," Astropart. Phys. **112**, 1-7 (2019) [arXiv:1902.01491 [astro-ph.HE]].

[240] N. Sanchis-Gual, F. Di Giovanni, M. Zilhão, C. Herdeiro, P. Cerdá-Durán, J. A. Font and E. Radu, "Nonlinear Dynamics of Spinning Bosonic Stars: Formation and Stability," Phys. Rev. Lett. **123**, no.22, 221101 (2019) [arXiv:1907.12565 [gr-qc]].

[241] F. Di Giovanni, N. Sanchis-Gual, P. Cerdá-Durán, M. Zilhão, C. Herdeiro, J. A. Font and E. Radu, "Dynamical bar-mode instability in spinning bosonic stars," Phys. Rev. D **102**, no.12, 124009 (2020) [arXiv:2010.05845 [gr-qc]].

[242] A. S. Dmitriev, D. G. Levkov, A. G. Panin, E. K. Pushnaya and I. I. Tkachev, "Instability of rotating Bose stars," Phys. Rev. D **104**, no.2, 023504 (2021) [arXiv:2104.00962 [gr-qc]].

[243] F. Halzen, B. Keszthelyi and E. Zas, "Neutrinos from primordial black holes," Phys. Rev. D **52**, 3239-3247 (1995) [arXiv:hep-ph/9502268 [hep-ph]].

[244] P. Dave *et al.* [IceCube], "Neutrinos from Primordial Black Hole Evaporation," PoS **ICRC2019**, 863 (2021) [arXiv:1908.05403 [astro-ph.HE]].

[245] A. Capanema, A. Esmaeili and A. Esmaili, "Evaporating primordial black holes in gamma ray and neutrino telescopes," JCAP **12**, no.12, 051 (2021) [arXiv:2110.05637 [hep-ph]].

[246] N. Bernal, V. Muñoz-Albornoz, S. Palomares-Ruiz and P. Villanueva-Domingo, "Current and future neutrino limits on the abundance of primordial black holes," [arXiv:2203.14979 [hep-ph]].

[247] B. Dasgupta, R. Laha and A. Ray, "Neutrino and positron constraints on spinning primordial black hole dark matter," Phys. Rev. Lett. **125**, no.10, 101101 (2020) [arXiv:1912.01014 [hep-ph]].

[248] X. D. Boluna, "Detection methods for discovering Evaporating Primordial Black Holes in modern Gamma-ray Telescopes,"

[249] C. Keith, D. Hooper, T. Linden and R. Liu, "Sensitivity of future gamma-ray telescopes to primordial black holes," Phys. Rev. D **106** (2022) no.4, 043003 [arXiv:2204.05337 [astro-ph.HE]].

[250] K. Agashe, J. H. Chang, S. J. Clark, B. Dutta, Y. Tsai and T. Xu, "Detecting axionlike particles with primordial black holes," Phys. Rev. D **108** (2023) no.2, 023014 [arXiv:2212.11980 [hep-ph]].

[251] N. Bernal, Y. F. Perez-Gonzalez and Y. Xu, "Superradiant production of heavy dark matter from primordial black holes," Phys. Rev. D **106**, no.1, 015020 (2022) [arXiv:2205.11522 [hep-ph]].

[252] A. Arbey, J. Auffinger and J. Silk, "Evolution of primordial black hole spin due to Hawking radiation," Mon. Not. Roy. Astron. Soc. **494**, no.1, 1257-1262 (2020) [arXiv:1906.04196 [astro-ph.CO]].

[253] A. Cheek, L. Heurtier, Y. F. Perez-Gonzalez and J. Turner, "Primordial black hole evaporation and dark matter production. I. Solely Hawking radiation," Phys. Rev. D **105**, no.1, 015022 (2022) [arXiv:2107.00013 [hep-ph]].

[254] A. Cheek, L. Heurtier, Y. F. Perez-Gonzalez and J. Turner, "Redshift effects in particle production from Kerr primordial black holes," Phys. Rev. D **106**, no.10, 103012 (2022) [arXiv:2207.09462 [astro-ph.CO]].

[255] A. Cheek, L. Heurtier, Y. F. Perez-Gonzalez and J. Turner, "Evaporation of primordial black holes in the early Universe: Mass and spin distributions," Phys. Rev. D **108**, no.1, 015005 (2023) [arXiv:2212.03878 [hep-ph]].

[256] E. de Jong, J. C. Aurrekoetxea, E. A. Lim and T. França, "Spinning primordial black holes formed during a matter-dominated era," [arXiv:2306.11810 [astro-ph.CO]].

[257] Y. N. Eroshenko, "Spin of primordial black holes in the model with collapsing domain walls," JCAP **12**, no.12, 041 (2021) [arXiv:2111.03403 [astro-ph.CO]].

[258] E. Cotner, A. Kusenko, M. Sasaki and V. Takhistov, "Analytic Description of Primordial Black Hole Formation from Scalar Field Fragmentation," JCAP **10**, 077 (2019) [arXiv:1907.10613 [astro-ph.CO]].

[259] R. Dong, W. H. Kinney and D. Stojkovic, "Gravitational wave production by Hawking radiation from rotating primordial black holes," JCAP **10**, 034 (2016) [arXiv:1511.05642 [astro-ph.CO]].

[260] D. A. Leahy and W. G. Unruh, "ANGULAR DEPENDENCE OF NEUTRINO EMISSION FROM ROTATING BLACK HOLES," Phys. Rev. D **19**, 3509-3515 (1979).

[261] A. Escrivà, F. Kuhnel and Y. Tada, "Primordial Black Holes," [arXiv:2211.05767 [astro-ph.CO]].

[262] B. Carr, T. Tenkanen and V. Vaskonen, "Primordial black holes from inflaton and spectator field perturbations in a matter-dominated era," Phys. Rev. D **96**, no.6, 063507 (2017) [arXiv:1706.03746 [astro-ph.CO]].

[263] J. Martin, T. Papanikolaou and V. Vennin, "Primordial black holes from the preheating instability in single-field inflation," JCAP **01**, 024 (2020) [arXiv:1907.04236 [astro-ph.CO]].

[264] M. Bastero-Gil and M. S. Díaz-Blanco, "Gravity waves and primordial black holes in scalar warm little inflation," JCAP **12**, no.12, 052 (2021) [arXiv:2105.08045 [hep-ph]].

[265] J. Garcia-Bellido, A. D. Linde and D. Wands, "Density perturbations and black hole formation in hybrid inflation," Phys. Rev. D **54**, 6040-6058 (1996) [arXiv:astro-ph/9605094 [astro-ph]].

[266] E. Bugaev and P. Klimai, "Formation of primordial black holes from non-Gaussian perturbations produced in a waterfall transition," Phys. Rev. D **85**, 103504 (2012) [arXiv:1112.5601 [astro-ph.CO]].

[267] J. Garcia-Bellido and E. Ruiz Morales, "Primordial black holes from single field models of inflation," Phys. Dark Univ. **18**, 47-54 (2017) [arXiv:1702.03901 [astro-ph.CO]].

[268] C. Germani and T. Prokopec, "On primordial black holes from an inflection point," Phys. Dark Univ. **18**, 6-10 (2017) [arXiv:1706.04226 [astro-ph.CO]].

[269] K. Kohri, C. M. Lin and T. Matsuda, "Primordial black holes from the inflating curvaton," Phys. Rev. D **87**, no.10, 103527 (2013) [arXiv:1211.2371 [hep-ph]].

[270] M. Kawasaki, N. Kitajima and T. T. Yanagida, "Primordial black hole formation from an axionlike curvaton model," Phys. Rev. D **87**, no.6, 063519 (2013) [arXiv:1207.2550 [hep-ph]].

[271] E. V. Bugaev and P. A. Klimai, "Primordial black hole constraints for curvaton models with predicted large non-Gaussianity," Int. J. Mod. Phys. D **22**, 1350034 (2013) [arXiv:1303.3146 [astro-ph.CO]].

[272] K. Jedamzik and J. C. Niemeyer, "Primordial black hole formation during first order phase transitions," Phys. Rev. D **59**, 124014 (1999) [arXiv:astro-ph/9901293 [astro-ph]].

[273] P. Meszaros, "Primeval black holes and galaxy formation," Astron. Astrophys. **38**, 5-13 (1975).

[274] H. Niikura, M. Takada, S. Yokoyama, T. Sumi and S. Masaki, "Constraints on Earth-mass primordial black holes from OGLE 5-year microlensing events," Phys. Rev. D **99**, no.8, 083503 (2019). [arXiv:1901.07120 [astro-ph.CO]].

[275] B. J. Carr, K. Kohri, Y. Sendouda and J. Yokoyama, "Constraints on primordial black holes from the Galactic gamma-ray background," Phys. Rev. D **94**, no.4, 044029 (2016) [arXiv:1604.05349 [astro-ph.CO]].

[276] J. Auffinger, "Primordial black hole constraints with Hawking radiation – a review," [arXiv:2206.02672 [astro-ph.CO]].

[277] J. F. Glicenstein *et al.* [H.E.S.S.], "Limits on Primordial Black Hole evaporation with the H.E.S.S. array of Cherenkov telescopes," [arXiv:1307.4898 [astro-ph.HE]].

[278] T. Tavernier, J. F. Glicenstein and F. Brun, "Search for Primordial Black Hole evaporations with H.E.S.S," PoS **ICRC2019**, 804 (2020) [arXiv:1909.01620 [astro-ph.HE]].

[279] A. A. Abdo, *et al.* "Milagro Limits and HAWC Sensitivity for the Rate-Density of Evaporating Primordial Black Holes," Astropart. Phys. **64**, 4-12 (2015) [arXiv:1407.1686 [astro-ph.HE]].

[280] S. Archambault [VERITAS], "Search for Primordial Black Hole Evaporation with VERITAS," PoS **ICRC2017**, 691 (2018) [arXiv:1709.00307 [astro-ph.HE]].

[281] A. Albert *et al.* [HAWC], "Constraining the Local Burst Rate Density of Primordial Black Holes with HAWC," JCAP **04**, 026 (2020) [arXiv:1911.04356 [astro-ph.HE]].

[282] Y. F. Perez-Gonzalez and J. Turner, "Assessing the tension between a black hole dominated early universe and leptogenesis," Phys. Rev. D **104** (2021) no.10, 103021 [arXiv:2010.03565 [hep-ph]].

[283] C. Yuan, R. Brito and V. Cardoso, "Evaporating black holes: Constraints on anomalous emission mechanisms," Phys. Rev. D **104** (2021) no.12, 124024 [arXiv:2107.14244 [gr-qc]].

[284] R. Calabrese, M. Chianese, D. F. G. Fiorillo and N. Saviano, "Direct detection of light dark matter from evaporating primordial black holes," Phys. Rev. D **105** (2022) no.2, L021302 [arXiv:2107.13001 [hep-ph]].

[285] A. Cheek, L. Heurtier, Y. F. Perez-Gonzalez and J. Turner, "Primordial black hole evaporation and dark matter production. II. Interplay with the freeze-in or freeze-out mechanism," Phys. Rev. D **105** (2022) no.1, 015023 [arXiv:2107.00016 [hep-ph]].

[286] N. Bernal, C. S. Fong, Y. F. Perez-Gonzalez and J. Turner, "Rescuing high-scale leptogenesis using primordial black holes," Phys. Rev. D **106** (2022) no.3, 035019 [arXiv:2203.08823 [hep-ph]].

[287] R. Calabrese, M. Chianese, D. F. G. Fiorillo and N. Saviano, "Electron scattering of light new particles from evaporating primordial black holes," Phys. Rev. D **105** (2022) no.10, 103024 [arXiv:2203.17093 [hep-ph]].

[288] R. Calabrese, M. Chianese, J. Gunn, G. Miele, S. Morisi and N. Saviano, "Limits on light primordial black holes from high-scale leptogenesis," Phys. Rev. D **107** (2023) no.12, 123537 [arXiv:2305.13369 [hep-ph]].

[289] I. Masina, "Dark Matter and Dark Radiation from Evaporating Kerr Primordial Black Holes," Grav. Cosmol. **27** (2021) no.4, 315-330 [arXiv:2103.13825 [gr-qc]].

[290] A. Arbey, J. Auffinger, P. Sandick, B. Shams Es Haghi and K. Sinha, "Precision calculation of dark radiation from spinning primordial black holes and early matter-dominated eras," Phys. Rev. D **103** (2021) no.12, 123549 [arXiv:2104.04051 [astro-ph.CO]].

[291] R. Gregory, I. G. Moss, N. Oshita and S. Patrick, "Black hole evaporation in de Sitter space," Class. Quant. Grav. **38** (2021) no.18, 185005 [arXiv:2103.09862 [gr-qc]].

[292] B. Hassanain, J. March-Russell and J. G. Rosa, "On the possibility of light string resonances at the LHC and Tevatron from Randall-Sundrum throats," JHEP **07**, 077 (2009) [arXiv:0904.4108 [hep-ph]].

[293] G. Di Sciascio [LHAASO], "The LHAASO experiment: from Gamma-Ray Astronomy to Cosmic Rays," Nucl. Part. Phys. Proc. **279-281**, 166-173 (2016) [arXiv:1602.07600 [astro-ph.HE]].

[294] A. Addazi *et al.* [LHAASO], "The Large High Altitude Air Shower Observatory (LHAASO) Science Book (2021 Edition)," Chin. Phys. C **46**, 035001-035007 (2022) [arXiv:1905.02773 [astro-ph.HE]].

[295] Z. Cao, S. Chen, R. Liu and R. Yang, "Ultra-High-Energy Gamma-Ray Astronomy," [arXiv:2310.01744 [astro-ph.HE]].

[296] S. Adrian-Martinez *et al.* [KM3Net], "Letter of intent for KM3NeT 2.0," J. Phys. G **43**, no.8, 084001 (2016) [arXiv:1601.07459 [astro-ph.IM]].

[297] M. Agostini *et al.* [P-ONE], "The Pacific Ocean Neutrino Experiment," Nature Astron. **4**, no.10, 913-915 (2020) [arXiv:2005.09493 [astro-ph.HE]].

[298] Z. P. Ye, F. Hu, W. Tian, Q. C. Chang, Y. L. Chang, Z. S. Cheng, J. Gao, T. Ge, G. H. Gong and J. Guo, *et al.* "Proposal for a neutrino telescope in South China Sea," [arXiv:2207.04519 [astro-ph.HE]].

[299] V. A. Allakhverdyan *et al.* [Baikal-GVD], "Diffuse neutrino flux measurements with the Baikal-GVD neutrino telescope," Phys. Rev. D **107**, no.4, 4 (2023) [arXiv:2211.09447 [astro-ph.HE]].

[300] B. S. Acharya *et al.* [CTA Consortium], "Science with the Cherenkov Telescope Array," WSP, 2018, ISBN 978-981-327-008-4 [arXiv:1709.07997 [astro-ph.IM]].

[301] O. Gueta [CTA Consortium and CTA Observatory], "The Cherenkov Telescope Array: layout, design and performance," PoS **ICRC2021**, 885 (2021) [arXiv:2108.04512 [astro-ph.IM]].

[302] W. Wild [CTA Observatory and CTA Consortium], "Cherenkov Telescope Array (CTA): building the world's largest ground-based gamma-ray observatory," Proc. SPIE Int. Soc. Opt. Eng. **10700**, 107000X (2018)

[303] P. Abreu, *et al.* "The Southern Wide-Field Gamma-Ray Observatory (SWGO): A Next-Generation Ground-Based Survey Instrument for VHE Gamma-Ray Astronomy," [arXiv:1907.07737 [astro-ph.IM]].

[304] G. La Mura, G. Chiaro, R. Conceição, A. De Angelis, M. Pimenta and B. Tomé, "Detection of very-high-energy gamma-ray transients with monitoring facilities," Mon. Not. Roy. Astron. Soc. **497**, no.3, 3142-3148 (2020) [arXiv:2001.04503 [astro-ph.IM]].

[305] S. Tsujikawa, "Modified gravity models of dark energy," Lect. Notes Phys. **800**, 99-145 (2010) [arXiv:1101.0191 [gr-qc]].

[306] I. Banerjee, S. Chakraborty and S. SenGupta, "Silhouette of M87*: A New Window to Peek into the World of Hidden Dimensions," Phys. Rev. D **101**, no.4, 041301 (2020) [arXiv:1909.09385 [gr-qc]].

[307] Z. Mark, A. Zimmerman, S. M. Du and Y. Chen, "A recipe for echoes from exotic compact objects," Phys. Rev. D **96**, no.8, 084002 (2017) [arXiv:1706.06155 [gr-qc]].

[308] P. Bueno, P. A. Cano, F. Goelen, T. Hertog and B. Vercnocke, "Echoes of Kerr-like wormholes," Phys. Rev. D **97**, no.2, 024040 (2018) [arXiv:1711.00391 [gr-qc]].

[309] H. C. D. Lima, Junior., L. C. B. Crispino, P. V. P. Cunha and C. A. R. Herdeiro, "Can different black holes cast the same shadow?," Phys. Rev. D **103** (2021) no.8, 084040 [arXiv:2102.07034 [gr-qc]].

[310] M. Visser, "Dirty black holes: Thermodynamics and horizon structure," Phys. Rev. D **46**, 2445-2451 (1992) [arXiv:hep-th/9203057 [hep-th]].

[311] A. Simpson and M. Visser, "The eye of the storm: a regular Kerr black hole," JCAP **03**, no.03, 011 (2022) [arXiv:2111.12329 [gr-qc]].

[312] A. Simpson and M. Visser, "Astrophysically viable Kerr-like spacetime," Phys. Rev. D **105**, no.6, 064065 (2022) [arXiv:2112.04647 [gr-qc]].

[313] R. G. Daghigh, M. D. Green, J. C. Morey and G. Kunstatter, "Scalar Perturbations of a Single-Horizon Regular Black Hole," Phys. Rev. D **102**, no.10, 104040 (2020) [arXiv:2009.02367 [gr-qc]].

[314] A. Ovgün and K. Jusufi, "Quasinormal Modes and Greybody Factors of $f(R)$ gravity minimally coupled to a cloud of strings in $2+1$ Dimensions," Annals Phys. **395**, 138-151 (2018) [arXiv:1801.02555 [gr-qc]].

[315] L. Sebastiani and S. Zerbini, "Some remarks on non-singular spherically symmetric space-times," [arXiv:2206.03814 [gr-qc]].

[316] Á. Rincón and G. Panotopoulos, "Quasinormal modes of scale dependent black holes in (1+2)-dimensional Einstein-power-Maxwell theory," Phys. Rev. D **97**, no.2, 024027 (2018) [arXiv:1801.03248 [hep-th]].

[317] G. Panotopoulos and Á. Rincón, "Quasinormal modes of regular black holes with non linear-Electrodynamical sources," Eur. Phys. J. Plus **134**, no.6, 300 (2019) [arXiv:1904.10847 [gr-qc]].

[318] G. Panotopoulos and Á. Rincón, "Quasinormal modes of five-dimensional black holes in non-commutative geometry," Eur. Phys. J. Plus **135**, no.1, 33 (2020) [arXiv:1910.08538 [gr-qc]].

[319] G. Panotopoulos and Á. Rincón, "Quasinormal spectra of scale-dependent Schwarzschild–de Sitter black holes," Phys. Dark Univ. **31**, 100743 (2021) [arXiv:2011.02860 [gr-qc]].

[320] P. A. González, Á. Rincón, J. Saavedra and Y. Vásquez, "Superradiant instability and charged scalar quasinormal modes for (2+1)-dimensional Coulomb-like AdS black holes from nonlinear electrodynamics," Phys. Rev. D **104**, no.8, 084047 (2021) [arXiv:2107.08611 [gr-qc]].

[321] M. Okyay and A. Övgün, "Nonlinear electrodynamics effects on the black hole shadow, deflection angle, quasinormal modes and greybody factors," JCAP **01**, no.01, 009 (2022) [arXiv:2108.07766 [gr-qc]].

[322] P. A. González, E. Papantonopoulos, J. Saavedra and Y. Vásquez, "Superradiant Instability of Near Extremal and Extremal Four-Dimensional Charged Hairy Black Hole in anti-de Sitter Spacetime," Phys. Rev. D **95**, no.6, 064046 (2017) [arXiv:1702.00439 [gr-qc]].

[323] S. Chinaglia and S. Zerbini, "A note on singular and non-singular black holes," Gen. Rel. Grav. **49**, no.6, 75 (2017) [arXiv:1704.08516 [gr-qc]].

[324] A. Colléaux, S. Chinaglia and S. Zerbini, "Nonpolynomial Lagrangian approach to regular black holes," Int. J. Mod. Phys. D **27**, no.03, 1830002 (2018) [arXiv:1712.03730 [gr-qc]].

[325] M. Bertipagani, M. Rinaldi, L. Sebastiani and S. Zerbini, "Non-singular black holes and mass inflation in modified gravity," Phys. Dark Univ. **33**, 100853 (2021) [arXiv:2012.15645 [gr-qc]].

[326] E. Babichev, C. Charmousis, A. Cisterna and M. Hassaine, "Regular black holes via the Kerr-Schild construction in DHOST theories," JCAP **06** (2020), 049 [arXiv:2004.00597 [hep-th]].

[327] A. Anabalon and A. Cisterna, "Asymptotically (anti) de Sitter Black Holes and Wormholes with a Self Interacting Scalar Field in Four Dimensions," Phys. Rev. D **85** (2012), 084035 [arXiv:1201.2008 [hep-th]].

[328] A. Simpson and M. Visser, "Black-bounce to traversable wormhole," JCAP **02**, 042 (2019) [arXiv:1812.07114 [gr-qc]].

[329] F. S. N. Lobo, M. E. Rodrigues, M. V. d. S. Silva, A. Simpson and M. Visser, "Novel black-bounce spacetimes: wormholes, regularity, energy conditions, and causal structure," Phys. Rev. D **103**, no.8, 084052 (2021) [arXiv:2009.12057 [gr-qc]].

[330] A. Övgün, "Weak Deflection Angle of Black-bounce Traversable Wormholes Using Gauss-Bonnet Theorem in the Dark Matter Medium," Turk. J. Phys. **44**, no.5, 465-471 (2020) [arXiv:2011.04423 [gr-qc]].

[331] J. R. Nascimento, A. Y. Petrov, P. J. Porfirio and A. R. Soares, "Gravitational lensing in black-bounce spacetimes," Phys. Rev. D **102**, no.4, 044021 (2020) [arXiv:2005.13096 [gr-qc]].

[332] F. S. N. Lobo, A. Simpson and M. Visser, "Dynamic thin-shell black-bounce traversable wormholes," Phys. Rev. D **101**, no.12, 124035 (2020) [arXiv:2003.09419 [gr-qc]].

[333] M. S. Churilova and Z. Stuchlik, "Ringing of the regular black-hole/wormhole transition," Class. Quant. Grav. **37**, no.7, 075014 (2020) [arXiv:1911.11823 [gr-qc]].

[334] N. Tsukamoto, "Gravitational lensing in the Simpson-Visser black-bounce spacetime in a strong deflection limit," Phys. Rev. D **103**, no.2, 024033 (2021) [arXiv:2011.03932 [gr-qc]].

[335] K. A. Bronnikov, R. A. Konoplya and T. D. Pappas, "General parametrization of wormhole spacetimes and its application to shadows and quasinormal modes," Phys. Rev. D **103**, no.12, 124062 (2021) [arXiv:2102.10679 [gr-qc]].

[336] H. C. D. Lima, C. L. Benone and L. C. B. Crispino, "Scalar absorption: Black holes versus wormholes," Phys. Rev. D **101**, no.12, 124009 (2020) [arXiv:2006.03967 [gr-qc]].

[337] J. Barrientos, A. Cisterna, N. Mora and A. Viganò, "AdS-Taub-NUT spacetimes and exact black bounces with scalar hair," Phys. Rev. D **106** (2022) no.2, 024038 [arXiv:2202.06706 [hep-th]].

[338] J. Mazza, E. Franzin and S. Liberati, "A novel family of rotating black hole mimickers," JCAP **04**, 082 (2021) [arXiv:2102.01105 [gr-qc]].

[339] E. Franzin, S. Liberati, J. Mazza, A. Simpson and M. Visser, "Charged black-bounce spacetimes," JCAP **07**, 036 (2021) [arXiv:2104.11376 [gr-qc]].

[340] E. Franzin, S. Liberati, J. Mazza, R. Dey and S. Chakraborty, "Scalar perturbations around rotating regular black holes and wormholes: Quasinormal modes, ergoregion instability, and superradiance," Phys. Rev. D **105**, no.12, 124051 (2022) [arXiv:2201.01650 [gr-qc]].

[341] Y. Yang, D. Liu, A. Övgün, Z. W. Long and Z. Xu, "Quasinormal modes of Kerr-like black bounce spacetime," [arXiv:2205.07530 [gr-qc]].

[342] M. Guerrero, G. J. Olmo, D. Rubiera-Garcia and D. S. C. Gómez, "Shadows and optical appearance of black bounces illuminated by a thin accretion disk," JCAP **08**, 036 (2021) [arXiv:2105.15073 [gr-qc]].

[343] Z. Xu and M. Tang, "Rotating spacetime: black-bounces and quantum deformed black hole," Eur. Phys. J. C **81**, no.10, 863 (2021) [arXiv:2109.13813 [gr-qc]].

[344] N. Tsukamoto, "Retrolensing by two photon spheres of a black-bounce spacetime," Phys. Rev. D **105**, no.8, 084036 (2022) [arXiv:2202.09641 [gr-qc]].

[345] M. Y. Ou, M. Y. Lai and H. Huang, "Echoes from asymmetric wormholes and black bounce," Eur. Phys. J. C **82**, no.5, 452 (2022) [arXiv:2111.13890 [gr-qc]].

[346] A. Simpson, P. Martin-Moruno and M. Visser, "Vaidya spacetimes, black-bounces, and traversable wormholes," Class. Quant. Grav. **36**, no.14, 145007 (2019) [arXiv:1902.04232 [gr-qc]].